51/1/2019
ISSN 1338–3523
ISSN 0369–2086

Mineralia Slovaca

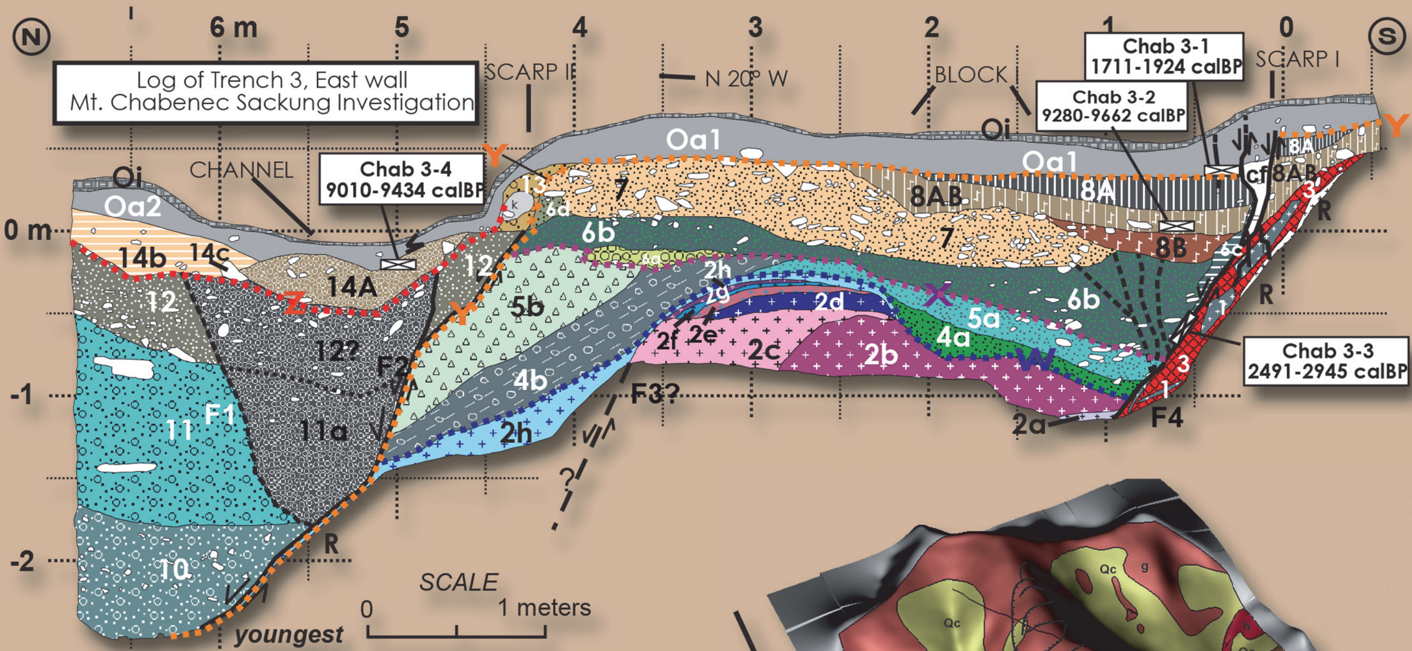

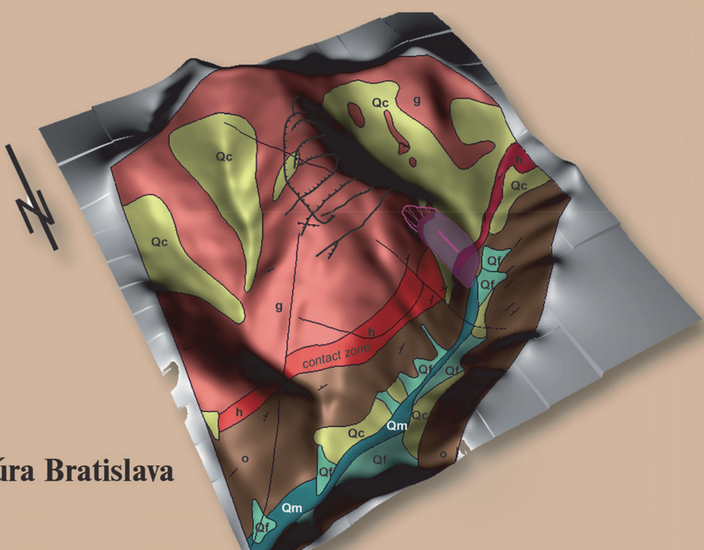

MENTE ET MALLEO
ŠTÁTNY GEOLOGICKÝ ÚSTAV DIONÝZA ŠTÚRA

Štátny geologický ústav Dionýza Štúra Bratislava

Mineralia Slovaca

Časopis pre regionálnu a environmentálnu geológiu
a aktivity Slovenskej geologickej spoločnosti a geologických asociácií

Mineralia Slovaca (Web ISSN 1338-3523, ISSN 0369-2086), EV 3534/09, vychádza dvakrát ročne. Vydavateľ a tlač: Štátny geologický ústav Dionýza Štúra, Mlynská dolina 1, 817 04 Bratislava, IČO 31 753 604. Dátum vydania čísla 51/1/2019: jún 2019. Predplatné v roku 2019 vrátane DPH, poštovného a balného pre jednotlivcov 18,70 €, pre členov SGS a geologických asociácií 17,60 €, pre organizácie v SR 24,20 €, pre organizácie v ČR 38,50 €. Cena jednotlivého čísla pri osobnom nákupe v predajniach ŠGÚDŠ v Bratislave a v Košiciach je 5,50 € vrátane DPH. Časopis možno objednať v redakcii a v knižnici regionálneho centra v Košiciach. Adresa redakcie: Štátny geologický ústav D. Štúra – RC Košice (Mineralia Slovaca), Jesenského 8, 040 01 Košice. Telefón: 055/625 00 43; fax: 055/625 00 44, e-mail: mineralia.slovaca@geology.sk, e-mail knižnica: secretary.ke@geology.sk

Mineralia Slovaca (Web ISSN 1338-3523, ISSN 0369-2086) is published twice a year by the State Geological Institute of Dionýz Štúr Bratislava, Slovak Republic. The date of issuing of the number 51/1/2019: June 2019.
Subscription for the whole 2019 calendar year (two numbers of the journal): 49.50 € (Europe), 60.50 € (besides Europe), including VAT, postage and packing cost. Claims for nonreceipt of any issue will be filled gratis.
Order of the Editorial Office: Štátny geologický ústav D. Štúra – RC Košice (Library), Jesenského 8, SK-040 01 Košice, Slovak Republic.
Phone: +421/55/625 00 43; fax: +421/55/625 00 44, e-mail: mineralia.slovaca@geology.sk, library: secretary.ke@geology.sk

www.geology.sk/mineralia

PÔVODNÉ ČLÁNKY – ORIGINAL PAPERS

OBÁLKA:

Hore: Fotografia rozsadliny 4, jz. pohľad, so sondážnou ryhou 3 vľavo a sondážnou ryhou 2 vpravo. Vzdialenosť medzi sondážnymi ryhami je 21 m. Skupina kopáčov sedí/stojí na bloku I.

V strede: Litologický profil na východnej stene sondážnej ryhy 3 s vyznačením odberu vzoriek na rádiokarbónové datovanie.

Dole: Geologická mapa jv. svahu Chabenca (Biely et al., 1992, upravená, na DMR zostavil P. Pauditš).

COVER:

Top: Photograph of Scarp 4 looking southwest, with Trench 3 (7.3 m long) at left and Trench 2 (5.2 m long) at right. Trenches are 21 m apart. A group of trench diggers sits/stands on Block I.

Centre: Log of the east wall of Trench 3, with indication of lithology and sampling for 14C radiocarbon dating.

Bottom: Geologic map of the southeastern slope of Mt. Chabenec (Biely et al., 1992, modified, on DMR compiled by P. Pauditš).

Mineralia Slovaca, Web ISSN 1338-3523, ISSN 0369-2086
51 (2019), 1 – 30,

Postglacial deformation history of sackungen on the southern slope of Mount Chabenec, Nízke Tatry Mts., Slovakia

JAMES P. McCALPIN[1], PAVEL LIŠČÁK[2*], ROBERT JELÍNEK[3], MOLLY O. ZORBA[4] and NURIA SANTACANA[5]

[1] GEO-HAZ Consulting, Crestone, Colorado, USA
[2] State Geological Institute of Dionýz Štúr, Bratislava, Slovak Republic: pavel.liscak@geology.sk,
* *Corresponding author*
[3] State Geological Institute of Dionýz Štúr, Banská Bystrica, Slovak Republic
[4] Apex Companies LLC, Thousand Oaks, California, USA
[5] Universitat Politècnica de Catalunya, Barcelona, Spain

Abstract: A series of distinct antislope scarps crosses the southern slope of the Mt. Chabenec in the Nízke Tatry Mountain range. Previous studies assumed that the deep-seated deformation with features of creep movement developed slowly towards the Lomnistá dolina Valley in the south-east direction. The field exploration comprised four exploration trenches across the antislope scarps, which have revealed conspicuous mylonite zones dipping at 50° towards the North. Trenches across the troughs adjacent to the antislope scarps all contained colluvial wedges, fissure fills, fault truncations, and angular unconformities. These structures and 20 ^{14}C-ages on trough sediments and buried soils indicate the scarps were formed by episodic displacements over the past 9.6 ka. The most recent displacement event (MRE) on all three scarps overlaps in age between 1,410 to 1,860 cal years BP (2-sigma range). The Nízke Tatry Mountains do have a historic record of earthquake shaking, so the MRE at Mount Chabenec could have been triggered by similar ground motions.

Key words: sackungen, slope stability, gravitational spreading, seismicity, Nízke Tatry Mts.,

Graphical abstract

Highlights

- Paleoseizmic trenching techniques were applied in four trenches dug in 1997 across three antislope scarps of deep seated slope deformation on the south ridge of Mount Chabenec, Nízke Tatry Mts.
- Structure and stratigraphy exposed in the trenches are consistent with episodic slip on the sackungen faults coupled with episodic deposition and soil formation in the adjacent troughs.
- Radiocarbon ages indicate that in all four trenches, there was a displacement event in the late Holocene (shortly after 1,410 to 1,860 cal yrs BP).

Introduction

Mt. Chabenec (48.94°N, 19.49°E; elevation 1,959 m) is situated in the Low Tatras (Nízke Tatry) Mountains, Central Slovakia (Fig. 1), in Nízke Tatry National Park. The marked feature of Mt. Chabenec is a series of parallel antislope scarps on its southern slope, which descends to the Lomnistá Valley floor (1,300 m elevation). These antislope scarps were described decades ago by Jahn (1964), Nemčok (1972), and Mahr and Nemčok (1977). The Chabenec deformation is part of a longer belt of similar deformations developed between Chopok and Prašivá Hills (a distance of 25 km) within the granitoid massifs forming the main ridge of the Low Tatras Mountains (Nemčok, 1982). Approximately 38 % of the mountain ridge is affected by such deformation. The scarps are easy to see because most of the ridge lies above the tree line at ~1,400 m.

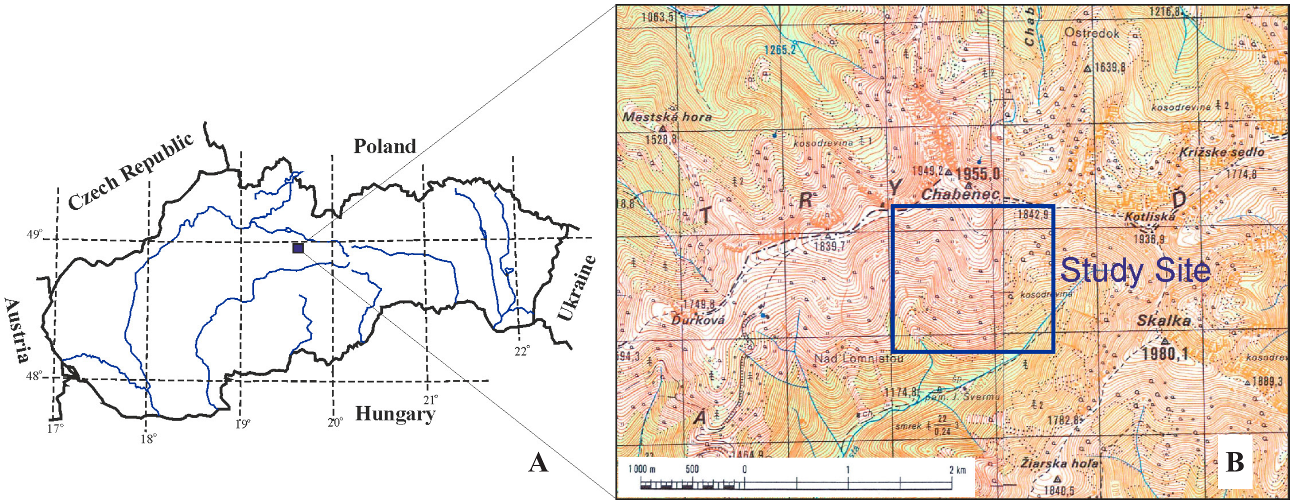

Fig. 1. Location map of the study site. A – shaded relief map of Slovak Republic and adjacent areas, dominated by the Carpathian Mountains. B – topographic map of the western part of the Nízke Tatry Mountains centered on Mt. Chabenec; thick contour interval is 50 m. Study site (box) occupies the southern slope of Mt. Chabenec.

This paper describes the results of a trenching study performed by the State Geological Institute of Dionýz Štúr (SGIDŠ) (formerly Geological Survey of the Slovak Republic), and the University of Colorado, USA. The study goal was to determine if paleoseismic trenching techniques could reconstruct the timing and rates of movements on these classic sackungen scarps. Prior to our 1997 field work few sackungen scarps had been trenched (e.g., Beget, 1985; McCalpin and Irvine, 1995; Thompson et al., 1997). However, in the past 20 years a steadily-increasing number of trenching investigations have been performed on sackungen (e.g., McCalpin and Hart, 2003; Tibaldi et al., 2004; Gutierrez et al., 2005, 2008; Agliardi et al., 2009; McCalpin et al., 2011; Pánek et al., 2011; Moro et al., 2012; Carbonel et al., 2013; Gori et al., 2014; Onida et al., 2016; Mariotto and Tibaldi, 2016) including in the Czech and Slovak Republics (Pánek et al., 2017).

Geological Setting

According to the geologic-geomorphologic division of Western Carpathians (Mazúr and Lukniš, 1980), Mt. Chabenec belongs to the Ďumbier part of the Nízke Tatry Mts. This mountain range represents a core mountain and is a part of the Tatricum Unit. This unit is built of crystalline basement rocks and Late Palaeozoic and Mesozoic cover sedimentary rocks.The Mt. Chabenec site is underlain by crystalline rocks. It consists of two parts (Fig. 2):

The northern part of the slope up to the peak is composed of medium-grained biotitic granodiorites to tonalites of the Ďumbier type. On the southern rim of this part a narrow contact zone is developed, in which hybrid granitoids, as well as remains of the mantle (the biotitic gneisses, mainly) can be observed. In the NE part of this zone relatively thin bodies of leucocratic granitoids crop out. According to the latest radiometric dating the intrusive activity took place at about the Devonian-Carboniferous boundary.

The southern part of the slope (the head of the Lomnistá Valley) is built of banded augengneisses with porphyroblasts of K-feldspars several cm in diameter. The orthogneiss with layers of paragneiss and amphibolites prevails. A re-markable feature of these rocks are ductile deformation structures (foliation, folds).

The contact of the gneiss complex and granitoids follows the direction of the main ridge. Its cropping out in the field is due to relatively extensive Quaternary cover rather indiscernible. We suppose that this is a tectonic contact, with the general strike E-W. The tectonic juxtaposition of both complexes likely took place in the Hercynian orogeny, but the important tectonic failures of the crystalline developed during the Alpine tectogenesis stage, mainly. In this stage mylonite zones originated, following older structures or new fault structures. They are mostly of the NE-SW direction with a medium to steep strike towards SE. In most cases they are overthrusts and strike-slip faults. The transversal brittle NW-SE and N-W faults, normal faults mostly, do not show large displacement amplitude.

Methods

Trenching: We excavated four trenches with picks and shovels across sackungen troughs in the central part of the southern slope, between 1,625 and 1,750 m elevation (Fig. 3). Trenches were roughly 60 cm wide, 4.5 to 7.3 m long, and 2.0 to 2.7 m deep. The eastern wall of each trench was cleaned and gridded with string, after which we drew a subjective field trench log on graph paper at a scale of 1:15 using the manual method (McCalpin, 2013). Those

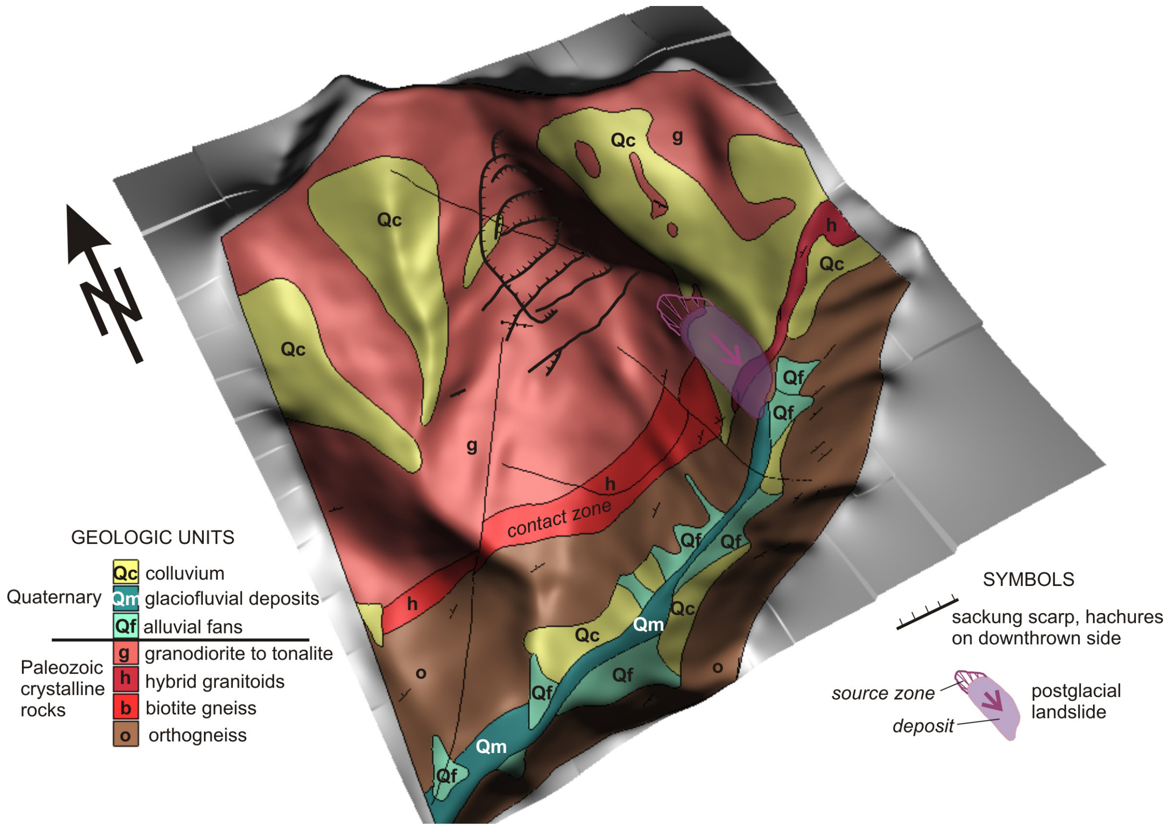

Fig. 2. Geologic map of the southeastern slope of Mt. Chabenec (Biely et al., 1992, modified, on DMR compiled by P. Pauditš). The antislope scarps are located relatively high on the southern slope of the mountain, on a subsidiary ridge flanked by two colluvium-filled valleys. Vertical relief between Mt. Chabenec and the Lomnistá dolina Valley is 660 m.

logs were then digitized for this paper. Unconsolidated stratigraphic units were defined based on color, texture, and sedimentary structures. Soil horizons developed on deposits (parent materials) were also identified and labeled according to the A/B/C horizon terminology used in the USA (e.g., Soil Survey Staff, 2014).

Geochronology: The three trenches were located in parts of sackungen troughs that were closed (or nearly closed) topographic depressions, in hopes that fine-grained trough sediments would contain organics amenable to radiocarbon dating. Each trench did contain both datable organics, and carbon from the finer-grained deposits (e.g., sag-pond silts and clays) yielded age sequences in correct stratigraphic order. However, carbon found in coarser-grained deposits, in scarp-derived colluvium, and in shear zones often yielded ages out of stratigraphic order, as described under Trenches 2, 3, and 4. All samples were dated by accelerator mass spectrometry (AMS) at the National Science Foundation Accelerator Dating Facility at the University of Arizona. The calibration curve of Reimer et al. (2013) was used to convert radiocarbon years to calendar years.

Results

Geomorphology of Slope Deformation

The antislope scarps on the upper southern slope of Mt. Chabenec run approximately parallel to contours and range from 300-600 m long. We numbered the most prominent scarps 1 (downslope) through 8 (upslope) and studied scarps 2, 4, 6, and 7 (Fig. 3), which have lengths of 600 m, 350 m, 300 m, and 300 m, respectively. The vertical surface offset of the hillslope across these major scarps varies from about 1 m to as much as 10 m (Fig. 4). Scarps 1-8 all lie downslope of an arcuate downslope-facing scarp (Scarp 9). Scarp 9 appears to be the head of a detached slab that contains all the antislope scarps. Scarp 9 can be traced easily down the west flank of Chabenec's south ridge to about Scarp 6. Between Scarps 6 and 4 the scarp becomes a faint vegetation lineament; below Scarp 4 it projects to a gully that appears structurally controlled. If Scarp 9 defines the western edge of the slab that slid downslope and gave rise to the antislope scarps, the slab may be significantly thinner than inferred by Mahr (1977). For example, Scarp 9 outcrops only 55 m below the ridge nose at Scarp 8, 65 m below the nose at Scarp 7, and 80 m below the nose at Scarp 6. If the slab has a planar bottom, then it is much thinner than the deep-seated gravitational slope deformation (DSGSD) mass inferred by Mahr (1977), which was inferred to be 135 m, 210 m, and 280 m thick at those same locations. If the slab is spoon-shaped then its thickness would be somewhat greater along its axis than at the edges. For example, given that the slab is only 600 m wide at Scarp 6, for its bottom to be 200 m deeper along its axis than at its edges only 300 m away would require the failure plane to be very deeply spoon-shaped in cross-section, sloping toward the axis at an average angle of 34°. An angle that steep would be more consistent with a wedge failure than with a slab failure.

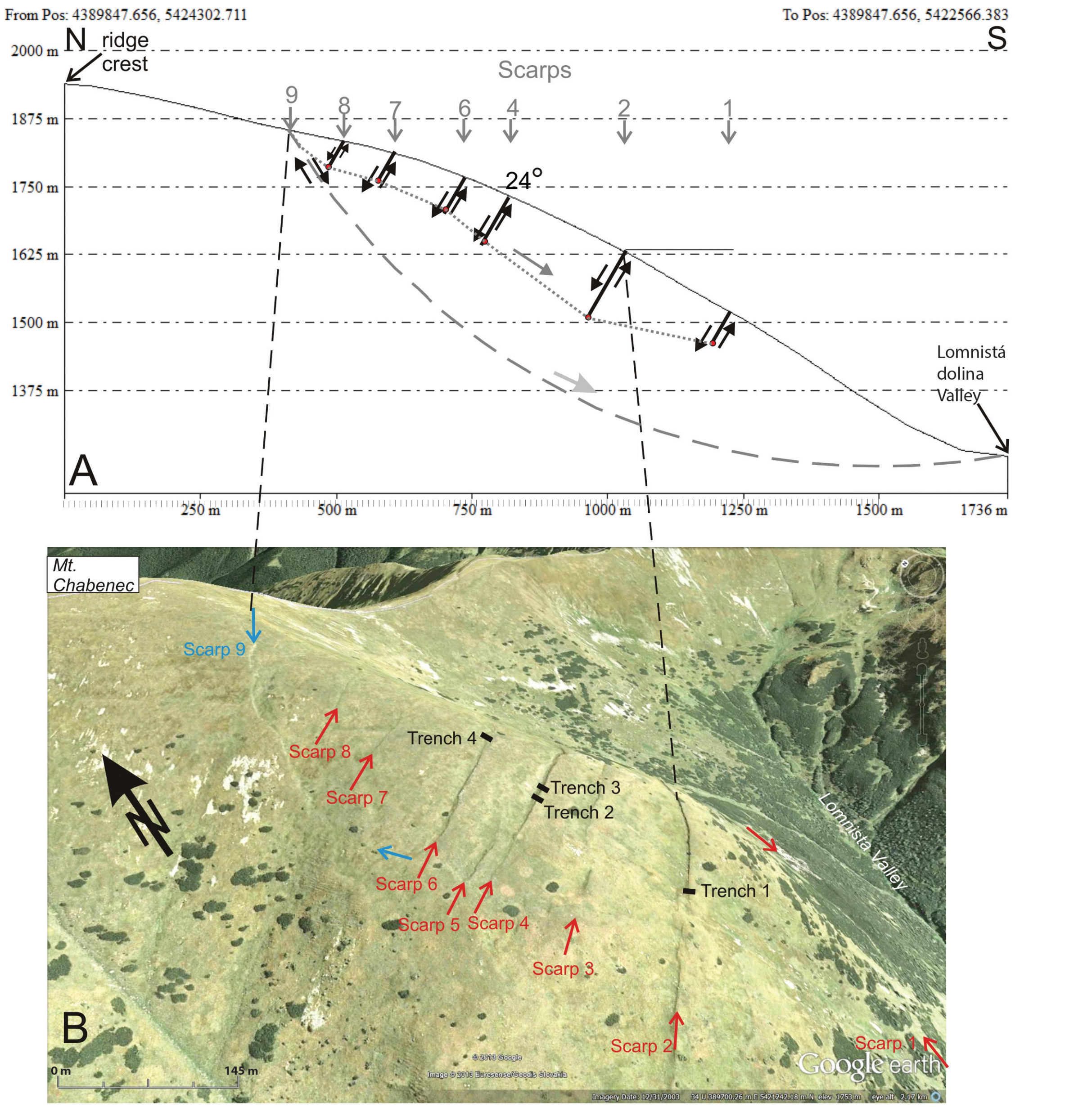

Fig. 3. Profile views of the southern slope of Mt. Chabenec. A – north-south topographic profile from the 30 m DEM (Shuttle Radar Topography Mission) that passes through scarps 1 - 9. No vertical exaggeration. The slope angle at Scarp 4 is 24°. The deep circular failure plane (dashed gray line, radius = 1,250 m) is that of Mahr, 1977 (see Discussion). The gray dotted line shows the elevation of Scarp 9 as it descends the west flank of the ridge, which forms a minimum depth estimate for the failed slab. B – oblique view from Google Earth (satellite imagery draped over the DEM) looking slightly north of east, showing antislope scarps 1 - 8, downslope-facing scarp 9, and the locations of our four trenches.

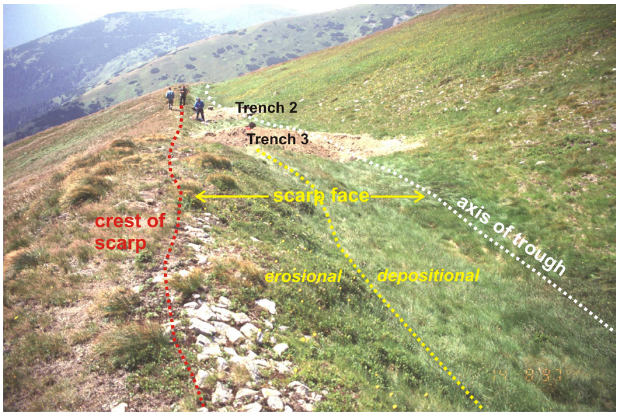

Fig. 4a. Photograph of the geomorphic components of a typical antislope scarp and its adjacent trough (Scarp 4, looking west). The slope uphill of the trough is mantled with normal residuum and colluvium, the latter of which is subject to downslope creep and slopewash erosion. Trenches 2 and 3 are visible in the middle ground; note people at Trench 2 for scale.

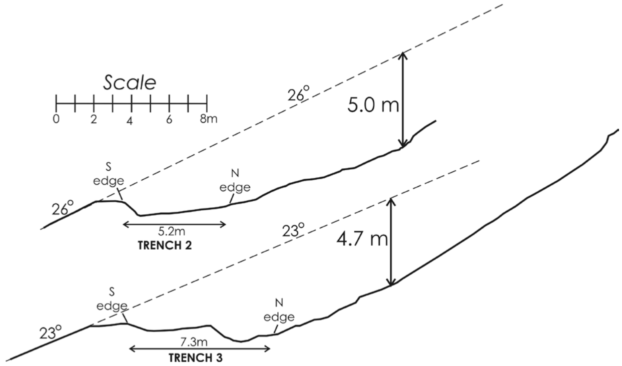

Fig. 4b. Topographic profiles across Scarp 4 at the locations of trenches 2 and 3. Dashed lines show the projection of the lower slope across the trough. Vertical surface offset across the antislope scarp ranges from 4.7-5.0 m, but is somewhat dependent on the slope angle projected and on exactly where the vertical offset is measured along the slope profile.

Trench 1 on Scarp 2

Scarp 2 is the longest (600 m) and tallest scarp at Mt. Chabenec (Figs. 3, 5). West of Trench 1 the trough has a low gradient to the west, with a near-horizontal depression at Trench 1. However, east of Trench 1 the scarp ascends diagonally upslope so the trough has a considerable westward gradient. Despite this gradient and the large slo-

Fig. 5. Photographs of Scarp 2 and Trench 1. *Above*, looking west down the scarp. Trench 1 is at center. Note persons at center standing above and below the scarp. *Above right*, close-up of the east wall of Trench 1 where it cuts into the scarp face. Note the steep angle of the scarp face. *Below right*, view of main fault zone on the east wall. String lines are 50 cm apart. Light area at right is the granodiorite footwall of the main fault. Overlying it is a 20-30 cm-thick shear zone of decomposed granodiorite and grayish-green, clayey fault gouge (units 2a and 2b on the trench log, Fig. 6). The shear zone dips 57°N.

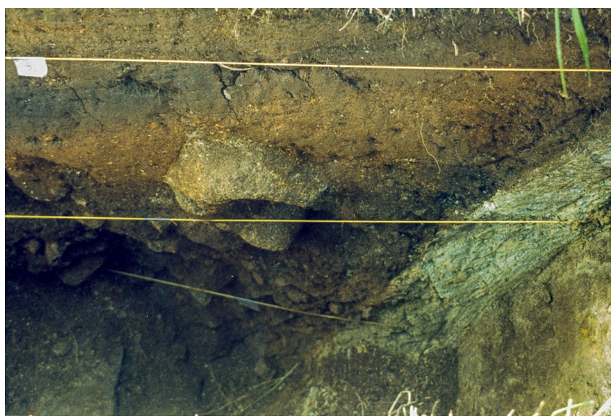

pe area that drains to the trough, there is no sign of erosion or channel development in the axis of the trough. We interpret this to mean that the scarp 4 is fairly young.

The scarp face is mantled with a tundra-like mat of turf grass, the top of which slopes 60 – 70° N at Trench 1. This slope angle is well above the angle of repose for unconsolidated deposits, so prior to trenching we assumed the grass was growing on a bedrock fault plane. However, no bedrock was exposed anywhere on the scarp face. Trenching later showed that the grass is growing on a fine-grained sag pond deposit that had been tilted up to 50° by drag on the fault.

Stratigraphy and Soils

On the east trench wall we define 9 major units which were further subdivided into 18 subunits (Fig. 6). Unit 1 is the non-weathered granodiorite of the main fault footwall, and units 2a and 2b are decomposed granodiorite and fault gouge in the main shear zone, respectively. The oldest unconsolidated deposit (unit 3a) appears in the fault zone as a fault-bounded sliver. It is a yellow-brown silty clay interpreted as a sag-pond deposit from a closed depression. Later faulting dragged part of the deposit upward into the fault zone from some stratigraphic position beneath the trench floor. The remainder of the unconsolidated deposits and soils (units 3b through Oi) form a vertical sequence of subhorizontal strata. Unit 3b is the oldest layer in this sequence and is a gravelly silty sand, and appears to be a coarser channel deposit related to unit 3a. Unconformably overlying unit 3b are a sequence of much coarser deposits (4a, 4b) containing angular clasts of fresh granodiorite. Clast long axes plunge away from the fault, suggesting they were deposited as colluvium shed from a bedrock free face. In the northern part of the trench a correlative unit (4c) has a similar texture. Units 4a and 4b are overlain by unit 5B, the most laterally extensive deposit in the trough. This unit is red-brown sandy clay interpreted as a soil textural B-horizon developed in a sag pond deposit. The B-horizon is overlain by an A-horizon (unit 6Ab1; black silt). The sequence 4a-4b-5B-6Ab1 appears to be a single fining-upward sequence ranging from a basal colluvium to fine sag pond deposits, then topped by a well-developed soil profile; it comprises 1.0 m of the 1.5 m-thick trough deposits exposed in the trench. The soil is unconformably overlain by unit 7, a brown silty sand with some gravel that we interpret as a channel deposited in the trough axis. Unit 7 is overlain by a thin organic soil composed of an A-horizon (unit Oa) and either a peat layer in the graben (unit Oc) or a grass mat on the scarp face (unit Oi).

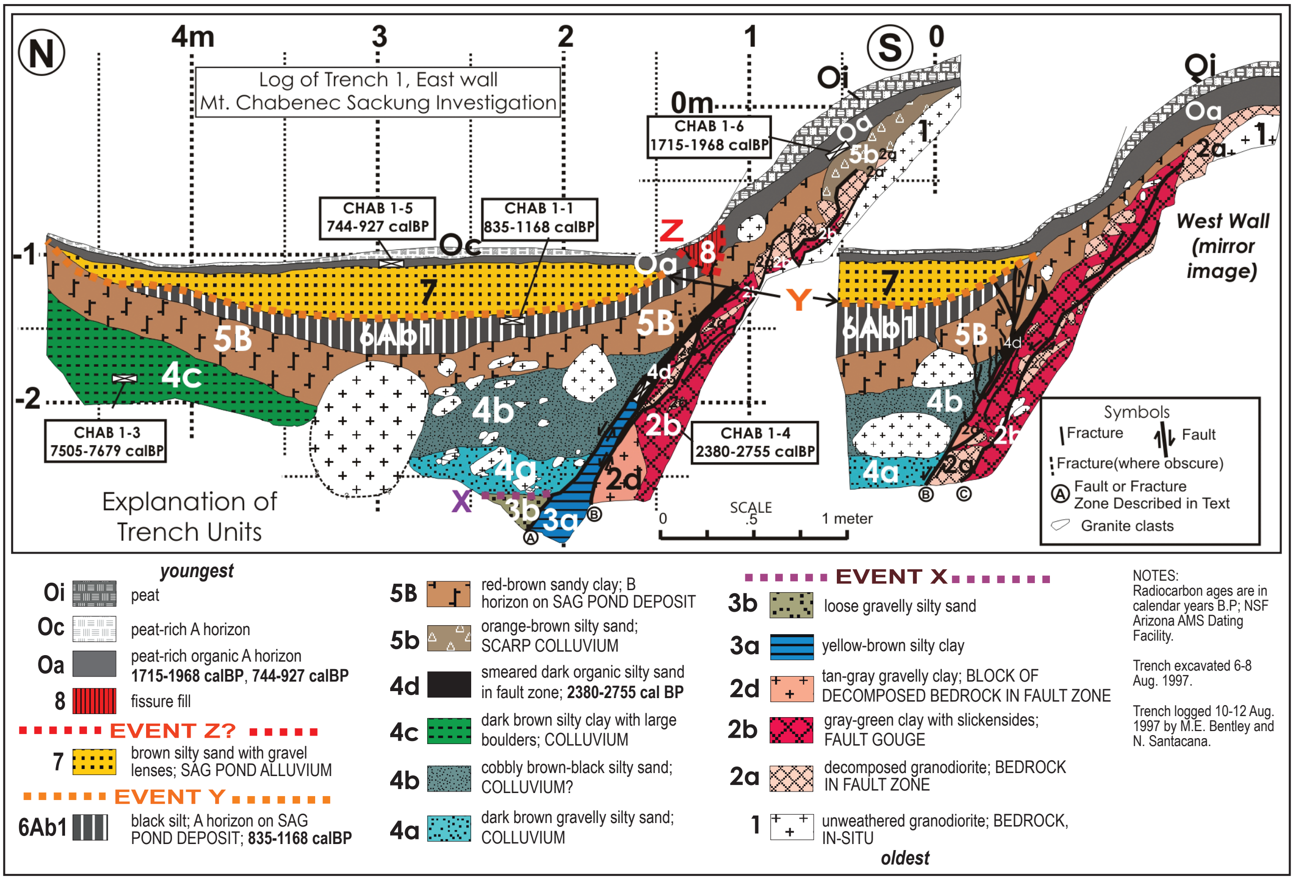

Fig. 6. Log of the east wall of Trench 1 (center and left) and a mirror image of the log of the west wall (at right).

Structure

The trench exposes only a single fault zone, a 25 cm thick bedrock shear zone that lies beneath the scarp face and extends to the bottom of the trench. The zone as a whole, and the individual fault planes within it, dip 55 – 60° N. The fault footwall is composed of non-weathered granodiorite. The shear zone is composed of fault- and fracture bounded blocks of two materials: (1) decomposed granodiorite, and (2) grayish-green clay containing slickensides (fault gouge). There are two major fault planes within the shear zone, one centered in the 25 cm-thick zone, and another at the northern boundary of the shear zone. The fault in the center is undulatory with a wavelength of 0.5 – 1 m and an amplitude of ~10 cm. The northern boundary fault is straighter. On the east wall the northern fault bounds a sliver of hanging wall unit 3a, an old sag pond silty clay. On the west wall the northern fault contains at least 8 short faults that splay off at steeper dips and displace hanging wall deposits. The highest of these splay faults also appears on the east wall, where it underlies the fissure filled with unit 8. This splay fault contains the only evidence for most recent displacement event (Event Z on Fig. 6). On the west trench wall the splay fault displaces units 5B and 6Ab1, but not unit 7 or soil horizon Oa. On the east wall the splay fault also displaces units 5B and 6Ab1, but the overlying fissure disrupts soil horizon Oa. However, there is no net vertical offset of horizon Oa across the fissure, so it looks like a block of soil may have been plucked out of Oa, possibly by man-made action.

The structural relationships of the trough deposits/soils (listed from oldest to youngest) can be summarized as follows:

– unit 3a is a fault sliver within the main fault zone, dragged upward from a stratigraphic level beneath the trench floor;

Tab 1.
Radiocarbon ages from trenches on Mt. Chabenec. Sample locations are shown on the trench logs (Figs. 6, 8, 10, and 12).

Trench No.	Sample No.	Lab No.[1]	Material	^{14}C Age (yr BP, 1 sigma)	Calendar Age (cal yr BP) intercept(s) in parentheses, 2 sigma range[2]
1	1	AA27851	Organic silt	1,065±45	835 (960) 1,168
1	3	AA27852	Silty clay	6,735±55	7,505 (7,540) 7,679
1	4	AA27853	Organic silt	2,530±60	2,380 (2,720) 2,755
1	5	AA27854	Organic silt	925±45	744 (830) 927
1	6	AA27855	Peaty silt	1,905±50	1,715 (1,860) 1,968
2	1	AA27856	Charcoal in black mud matrix of angular gravel[3]	485±50	335 (520) 640
2	3	AA27857	Organic silt	1,170±45	970 (1,060) 1,229
2	4	AA27858	Organic silt	4,215±55	4,577 (4,740) 4,864
2	5	AA27859	Organic silt	1,825±45	1,625 (1,720) 1,870
2	6	AA27860	Organic silt	467±50	331 (510) 631
2	8	AA27861	Mud coatings in black-stained gravel[3]	4,965±55	5,594 (5,670, 5,690, 5,710) 5,890
2	9	AA27862	Smeared black organic silt in *shear zone*[4]	3,320±50	3,446 (3,490, 3,510, 3,550) 3,690
3	1	AA27863	Organic silt	1,880±45	1,711 (1,820) 1,924
3	2	AA27864	Detrital charcoal in sandy channel deposit	8,485±90	9,280 (9,450) 9,662
3	3	AA27865	Charcoal in organic clay smeared in shear zone[4]	2,640±75	2,491 (2,750) 2,945
3	4	AA27866	Detrital charcoal in gravelly channel deposit[5]	8,230±90	9,010 (9,210) 9,434
4	1	AA27867	Detrital charcoal in gravelly channel deposit	7,600±140	8,049 (8,370) 8,725
4	3	AA27868	Organic silt	1,565±55	1,343 (1,410) 1,563
4	5	AA27869	Organic silt	1,225±50	1,009 (1,160) 1,279
4	6	AA27870	Organic silt	945±50	742 (840) 937

[1] All analyses were made at the NSF Arizona AMS Facility at the University of Arizona, Tucson.
[2] Calendar-year Calibration from OxCal 4.3 (2017), using the IntCal13 calibration data set; Reimer et al., 2013.
[3] Radiocarbon- & calendar-age is considered to be younger than the true age of the deposit, because the dated carbonaceous coatings on gravel clasts may have been transported downward by infiltrating water from higher, younger deposits.
[4] Radiocarbon samples from the main shear zone may include carbon from more than one stratigraphic unit that was dragged up and smeared along the shear zone. Thus, the radiocarbon age does not necessary date the age of a faulting event, but the weighted average age of the carbon-bearing deposits dragged up in the fault zone.
[5] Radiocarbon samples from scarp-derived colluvial wedges may contain significant carbon derived from the erosion of older deposits exposed in the scarp free face. In this case, the sample's radiocarbon age will not date the deposition of the colluvial wedge, but rather the age of carbon in the deposit exposed in the free face, which could be much older than the wedge.

- units 3b through 4b are in fault contact with the shear zone;
- units 5B and 6Ab1 are dragged upward onto the scarp face and faulted by the splay fault beneath the toe of the scarp;
- unit 7 is undeformed (i.e., post-dates sackungen movement).

The Petrography Laboratory at SGIDŠ described the shear zone material as follows:

"Clay gouge… distinct slickensides sloping to the North. The common accompanying features of these tectonic planes were well-developed mylonite zones with tectonic gouges. Tectonic gouges in the faults are known from civil engineering practice from various sites throughout Slovakia. ... with clayey fillings of fault zones consisting of illite-montmorillonite, with less kaolinite, palygorskite-sepiolite and carbonates….petrographical analysis of the tectonic gouge from the Chabenec site defined argillitized and weathered granodiorite. In the separated clayey fraction Dr. Žáková from SGIDS identified in 2001 the presence of illite and quartz, with admixture of highly dispersed feldspars using Roentgen Diffraction Analysis." Analytical data are reported in Appendix 1.

Geochronology

In the graben, the surface soil (unit Oa) dates at 744–927 cal BP and the underlying buried soil (6Ab1) dates slightly older at 835 to 1,168 cal BP (Table 1). However, horizon Oa on the scarp face dates older than either of the above ages at 1,715 to 1,968 cal BP, which presents a contradiction. Note that on the east wall horizons Oa and 6Ab1 merge at the toe of the scarp. This suggests that the A-horizon organic material (peat) on the scarp face must be time-equivalent to both A-horizons in the graben. That is, the scarp face A-horizon continued to develop and accumulate carbon during the deposition of multiple soils and deposits in the graben. The scarp-face soil would thus be a relict soil. The fact that the scarp face Oa sample yielded an age even older than 6Ab1 indicates it contains a mixture of even older carbon. Where could such older carbon have come from? One possible source is from older Holocene units deposited in the trough, which were then dragged up onto the footwall by faulting, and then eroded/redeposited on the scarp face directly beneath Oa, in a unit such as 5b. We know that carbon-bearing sediments have been dragged up the fault zone in the past because fault sliver 3a, dragged at least 1 m upward, contains carbon dated at 2,380 to 2,755 cal BP, which is even older than the age from scarp face Oa.

Interpretation

Based on stratigraphic superposition, cross-cutting relationships, and the occurrence of two paleosols, we interpret a sequence of at least three (possibly four) Holocene deformation events at Trench 1, with two more questionable events (Table 2). Age control for deformation events comes from radiocarbon dates of sediments deposited in structural depressions (Table 1). This approach to dating deformation events derives from paleoseismic studies of normal faults (e.g. McCalpin, 2009, Chapter 3).

Tab. 2.
Inferred sequence of depositional, pedogenic, and deformational events affecting Trench 1.

Event (oldest at bottom)	Evidence
8-Deformation EVENT Z?	A fracture forms at the scarp toe in soil horizon Oa and fills with fissure-fill unit 8. The fracture correlates with a similar splay fault on the west trench wall; however, there is no corresponding fissure on that wall. The fissure may possibly result from some human or animal disturbance, which plucked a root ball out of the ground.
7-Develop soil horizons Oa and Oi	Weak modern soil develops on unit 7 alluvium, with a possible loess component. Base of Oa horizon on scarp face **1,715 to 1,968 cal BP;** horizon Oa in graben, **744 to 927 cal BP**.
6-Deposit unit 7	Unit 7 deposited as alluvium in the newly-deepened trough.
5-Deformation EVENT Y	Unit 3a is faulted against units 3b, 4a, 4b; Units 5B and 6Ab1 are faulted and dragged up onto scarp face. Trough deepens by ~0.5 m.
4-Deposit units 4-5-6	Scarp-derived colluvium (units 4a, 4b) deposited from the south. Coeval slope colluvium (unit 4c) deposited from the north (**7,505 to 7,679 cal BP**). Over a long time, silt (aeolian?) washed into the trough, depositing unit 5 which fills in a broad trough. Soil horizons 5B and 6Ab1 then form (**soil top, 835 to 1,168 cal BP**).
3-Deformation EVENT X	Trough deepens due to faulting.
2-Deposit units 3a, 3b	Yellow-brown silty clay accumulates in standing water in a closed depression (unit 3a; **2,380 to 2,755 cal BP**). Later streamflow brings coarser alluvium into depression (unit 3b). Unit 3a now preserved only in a fault-bounded sliver.
1-Deformation EVENT W	Normal faulting creates the initial topographic trough.

Scarp 4 (Trenches 2 and 3)

Scarp 4 is 350 long with a vertical surface offset of ~5 m (Fig. 4). Scarp 4 is nearly parallel to contours, so the trough axis has a low gradient (Fig. 3). East of the trench site the scarp crest is composed of granodiorite of the sackungen footwall (Fig. 7, left). Elsewhere the scarp face is mantled with a tundra-like mat of turf grass, which slopes N at greater than 35 – 45°. We located Trenches 2 and 3 in the center of the scarp where the trough axis was nearly horizontal (Fig. 9). The scarp here was relatively low (vertical surface offset of 4.7 – 5 m), the trough axis was horizontal, the trough was a recent depocenter, and thus the lower part of the scarp had been buried by recent sedimentation (Fig. 7, right). We inferred that this site would have a thick record of post-sackungen sedimentation. Farther east (Fig. 7, left) the trough axis had a steeper gradient, was more erosional than depositional, so the scarp was accordingly higher and steeper. Although the scarp was more impressive there, we inferred it would have thinner or less complete records of trough sedimentation, making it less suitable for trenching.

A second feature of the trench site was complexity of the scarps. As shown in Fig. 7-right the trough contained a secondary scarp (Scarp 4B) parallel to the main scarp. At Trench 3 Scarp 4B is the higher of the two, but it becomes smaller westward and dies out between Trenches 2 and 3. The modern drainage follows the base of the Scarp 4B, but once Scarp 4B dies out the channel turns 45° and southward to the base of Scarp 4A. We felt that having two parallel sackungen faults bounding an intermediate structural block would permit better differentiating of displacement events via cross-cutting relationships. So we excavated Trench 3 across both scarps and Trench 2 across the main scarp past where the secondary fault had died out at the surface. The secondary fault was also exposed in Trench 2.

Trench 2, Stratigraphy and Soils

On the east trench wall 14 major units were defined which were further subdivided into 44 subunits (Fig. 8). Units 1-3 are bedrock and shear zone units and will be described in the next section. The oldest unconsolidated deposits (units 4, 4a) are sandy and silty gravels that overlie weathered granodiorite bedrock (unit 3). Unit 4 is overlain by unit 5a, a well-sorted fine gravel that is clearly alluvial, so it may have been deposited by runoff in the sackungen trough after trough formation (5,594 to 5,890 cal BP). It is unclear if the unit 4 – 4a gravel is a trough alluvium (postdates trough creation) or a slope colluvium that predates trough formation.

The log shows the former interpretation (i.e., the Event X horizon underlies units 4 and 4a). Units 6, 7, and 8 are well-sorted fine gravels interpreted as trough alluvium. On both sides of the main fault zone unit 8 is overlain by a lens-shaped body of colluvium (units 9a, 9b) which we interpret as scarp-derived colluvial wedges. Unit 10 is a 0.8 m-thick stack of talus deposits, solifluction deposits, and colluvium. The upper subunits (10d, 10e) thin toward the scarp, suggesting that they (and perhaps the rest of unit 10) were derived from the hillslope upslope of the trough. Unit 10 is overlain by a significant change in the type and pattern of sedimentation, to that of fine-grained (sag pond) deposits in the trough (units 11a, 11b, 12a) and small wedges of scarp-derived colluvium (unit 11c) on the trough margins. This rapid change suggests reactivated displacement on the sackungen scarp and deepening of the trough. Overlying unit 12 is unit 13 (composed of massive silts interpreted as loess) and well-sorted sands and fine gravels (alluvium). A soil A-horizon then developed

Fig. 7. Left – photograph of Scarp 4 about 50 m east of Trenches 2 and 3 (visible at far right center). Note outcrops of granodiorite along the scarp crest (center to left edge). Right – photograph of Scarp 4 looking southwest, with Trench 3 (7.3 m long) at left and Trench 2 (5.2 m long) at right. Trenches are 21 m apart. A group of trench diggers sits/stands on Block I. Lomnistá dolina Valley in background.

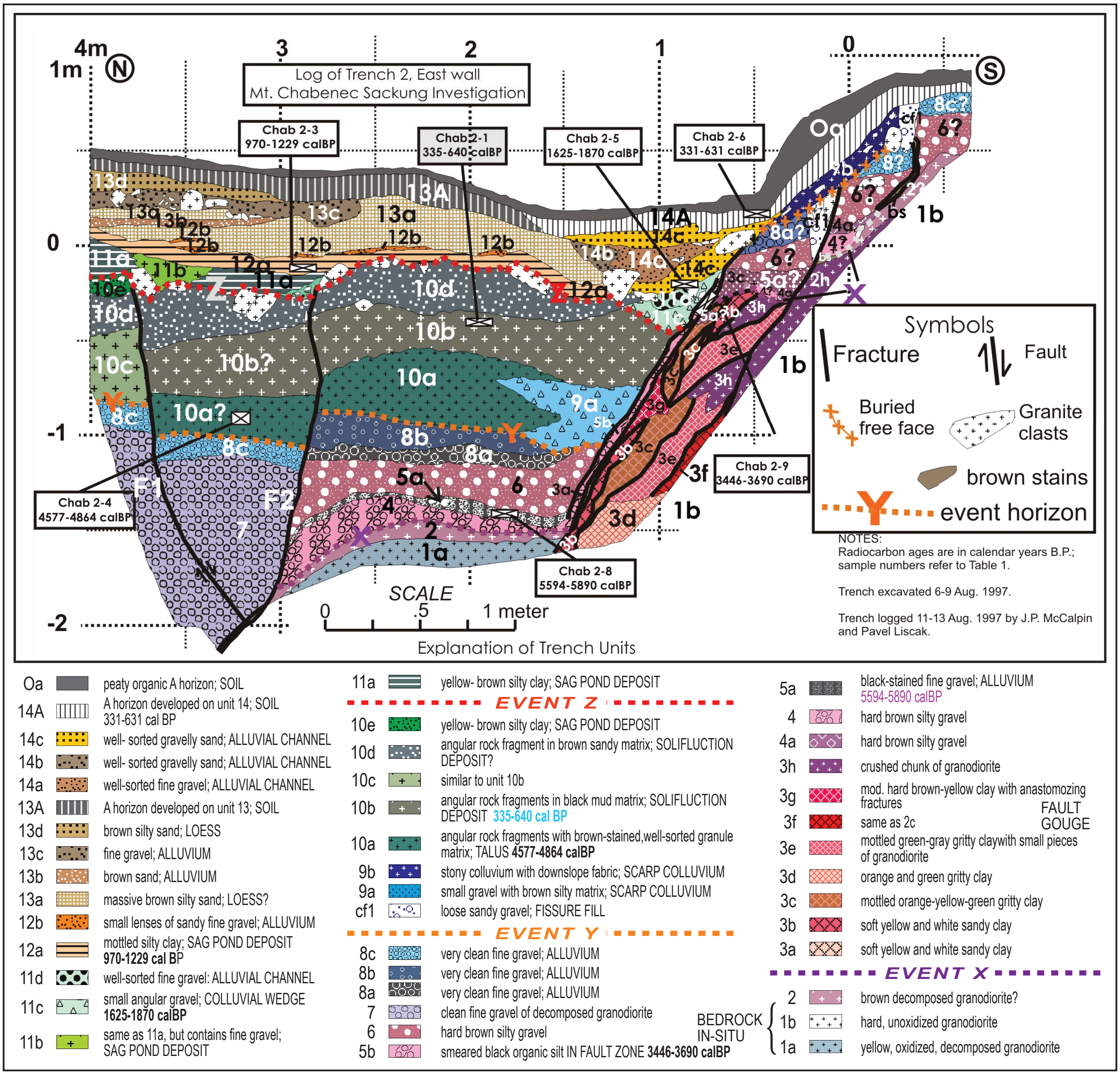

Fig. 8. Log of Trench 2. Three displacements events (from youngest to oldest, Events Z, Y, and X) are interpreted from colluvial wedges, upward fault terminations, and abrupt changes in sedimentology (see text for details). The graben structure at left does not reach the ground surface and has no topographic expression; it is probably the subsurface continuation of the fault beneath Scarp 4B (exposed in Trench 3).

on unit 13 (unit 13A). At the foot of the scarp units 13a and 13A have been eroded out by a younger channel containing units 14a-b-c. A younger A-horizon (unit 14A) then developed on unit 14, followed by the formation of a peaty organic soil horizon (unit Oa) over the entire scarp and trough.

Trench 2, Structure

The trench exposes two fault zones. The main fault zone is a 50 cm-thick shear zone in bedrock that lies beneath the Scarp 4A face and dips 55 – 60°N, and is exposed down ~1.5 m to the floor of the trench. The fault footwall is composed of granodiorite fractured by four joint sets (Fig. 9, left). Set 1 strikes perpendicular to the trench with fractures spaced 15 – 30 cm apart. Set 2 strikes parallel to the trench on a10 – 15 cm spacing. Sets 3 and 4 form a 30°/60° conjugate pattern on the plane of the footwall. The four joint sets break the footwall granodiorite into angular blocks 5 – 10 cm in diameter. There is oxidation along all joints but it does not penetrate the center of the joint-bounded blocks.

Fig. 9. Photographs of the main fault zone in Tench 2. Left – fractured granodiorite of the fault footwall at lower right. Shear zone is visible below lower string line. Right – closeup of shear zone. String lines are 50 cm apart.

The 50 cm-thick shear zone contains 5 to 6 discrete fault planes (Fig. 8). The outermost fault planes are long and relatively planar whereas the inner faults have a more anastomosing or en-echelon pattern. This pattern creates numerous fault-bounded slivers and lenses of contrasting color and texture (units 2a through 2h; see Fig. 12, right). All subunits are basically fault gouge with textures ranging from clay to sandy clay to gritty clay, and colors ranging from white, yellow, yellow-brown, orange, and green. The coarsest units (2c, 2e) contain visible angular pieces of unweathered granodiorite within the clay matrix, presumably ripped off the footwall and rolled into the gouge during rapid slip events. The northern margin fault has dragged up and smeared a thin layer of black organic silt into the fault zone (unit 5b). This disturbed layer appears to be derived from unit 5a and perhaps unit 4 in the trough sequence. The main shear zone does not extend to the ground surface, but is overlain on the upthrown side by a series of unconsolidated deposits. These beds resemble units 5a, 6, and 8a/8c on the downthrown side of the fault. If this correlation is correct, we can measure a vertical displacement of 2.0 m across the shear zone, based on the net offset of the base of unit 6. Faults in the shear zone displace units as young as 11d but do not displace unit 14.

A second fault zone is exposed 1.5 m north of the main shear zone, beneath the sackungen trough, composed of two subvertical faults (F1, F2) with a downdropped block between them. Fault F1 terminates into F2, indicating that F2 is the master fault. F2 also has evidence of greater vertical displacement, since it drops bedrock (units 1a, 3) and the older alluvial units (4, 5a, 6) down below the floor of the trench. The fault juxtaposes these units against a thick unit 7, which has no counterpart south of the fault. Higher on the F2 fault plane units 8 and 10 exist on both sides of the fault and are displaced about 10 cm down-to-the-north. From these relationships we can infer that: (1) F2 forms the northern margin of a structural block floored by bedrock, (2) F2 had large vertical displacement of units 1a through 6 prior to the deposition of unit 8, and (3) since deposition of unit 8 there has only been a minor 10 cm of reactivated movement on F2. The net vertical displacement across F1 and F2 since unit 8 time is negligible, indicating the faults mainly accommodate a small amount of horizontal extension. Faults F1 and F2 displace units as young as 10e, but are overlain by units 11a and younger.

Trench 2, Geochronology

Trench 2 yielded seven radiocarbon dates, the most from four trenches. Overall the dates indicate that trough sedimentation on the structural block began prior to 5.7 ka (unit 5a) and continued episodically through the latest Holocene. However, units 5a and 10a are matrix-free fine gravels where all the clasts are stained black or brown, and it is this stain (actually thin silt films on talus clasts) which was dated. It is not clear whether the black stains are primary depositional features, or younger illuviated components deposited by organic-rich groundwater. In other trenches, radiocarbon dates from these black-stained gravels have yielded anomalous ages compared to dates from less porous/permeable deposits. A second problem with the dates in Trench 2 is age reversals. For example, unit 10b yielded an abnormally young age (335 – 640 cal BP) compared to older ages from higher units. In fact, the date from unit 10b is nearly identical to that from the surface soil 14A (331 to 631 cal BP). The most likely explanation for this correspondence is that the carbon sampled in unit 10b was contaminated with intrusive carbon from unit 14A. The third-oldest date from the trench (3,446 to 3,690 cal BP) came from unit 5b in the shear zone. As in Trench 1, it is difficult to interpret this date, given the opportunities for physical mixing of carbon-bearing materials in the shear zone. The texture of unit 5b and its physical continuity with unit 5a near the bottom of the trench indicate it is mostly derived from units 4 and 5a. But unit 5b dates 2,200 years younger than in-situ unit 5a. To attain its present high position in the shear zone, the dated sample from unit 5b had to be dragged up the fault past units 6 through 10b. Notably, unit 10b contains very young carbon (as described above), so that is one possible source for mixing younger carbon into unit 5b.

Trench 2, Interpretation

We interpret a sequence of at least three (possibly four) Holocene deformation events at Trench 2 (Table 3). Age control comes from seven radiocarbon dates from sediments exposed in the trench walls (Table 1).

If this correlation of units 6 – 8 across the shear zone is correct, it implies that prior to deposition of unit 5a, erosion had removed all scarp relief at this site, as it has in the modern landscape where large swales cross the antislope scarps. Local alluviation then overfilled the trough and entirely buried the antislope scarp during unit 5 – 8 time. Later, during deformation Events Y and Z, the main fault reactivated, dropping units 5 – 8 two meters down in the trough.

Trench 3, Stratigraphy and Soils

On the east trench wall we define 14 major units which were further subdivided into 33 subunits (Fig. 10).

Units 1 – 3 are bedrock and shear zone units and will be described in the next section. The oldest unconsolidated deposits (unit 4a, 4b) are gravelly sand and silty sand that overlie weathered granodiorite bedrock (unit 2). Unit 4b is interpreted as a sag pond deposit, indicating it was deposited in an early sackungen depression. The overlying unit 5 coarsens upward, from gravelly sand (unit 5a, colluvium) to unit 5b (talus). Unit 5 is unconformably overlain by unit 6, which has a small alluvial channel fill (unit 6a) at its base but is mostly composed of unit 6b, a gravelly sand (colluvium). Unit 6b is overlain by a 40 – 50 cm-thick lobe of compact silty sand full of angular rock fragments (unit 7). Because this unit pinches out toward the Scarp 4A and contains rock fragments typical of the slope above the trough, we interpret it as a solifluction lobe. Overlying unit 7 near scarp 4A is unit 8, a finer alluvium that hosts three soil horizons (A, AB, and B). The B-horizon contains the most pedogenic development as judged by color (red-brown) and clay content, qualifying as a textural B-horizon. Unit 8 thins northward away from Scarp 4A. This geometry may reflect the original deposit shape, as a channel fill deposited against the scarp. Or it

Tab. 3.
Inferred sequence of depositional, pedogenic, and deformational events affecting Trench 2.

Event (oldest at bottom)	Evidence
8-Erode channel at toe of scarp and deposit unit 14	Streamflow down trough axis erodes a 0.4 m-deep channel at toe of scarp, followed by deposition of alluvial gravel and sand (units 14a-b-c). Soil 14A develops on unit 14 (**331 to 631 cal BP**). Later the entire trough floor is covered by a peaty organic A-horizon (unit Oa).
7-Deposit units 12a-13d	A thin sag pond deposit (12a; **970 to 1,229 cal BP**) is laid down over the whole trough floor, followed by thin alluviums (12b, 13b-13c) and two loesses (13a, 13d). A soil A-horizon forms on unit 13 (13A).
6-Deposit units 11a-11d	Unit 11c is a scarp-derived colluvial wedge (**1,625 to 1,870 cal BP**). Coeval trough axis facies (sag pond deposits 11a, 11b) are deposited.
5-Deformation EVENT Z	Units 1a through 8c? faulted on main shear zone ~1.2 m.
5-Deposit units 10c-10e	Continued alluviation in trough.
4-Deposit unit 9a	Scarp-derived colluvium (unit 9a) deposited in trough; possibly coeval colluvium 9b deposited on scarp face. Coeval alluvium (unit 10a) deposited in trench axis **(4,577 to 4,864 cal BP)**.
3-Deformation EVENT Y	Displacement on main shear zone of ~0.8 m.
2-Deposit units 5a through 8b	Alluvial units 5a **(5,594 to 5,890 cal BP)** through 8b are deposited in the sackungen trough.
1-Deformation EVENT X	Normal faulting creates the initial topographic trough; main fault displaces units 1 (bedrock) and possibly 4 (if it is the pre-faulting colluvium on the slope).

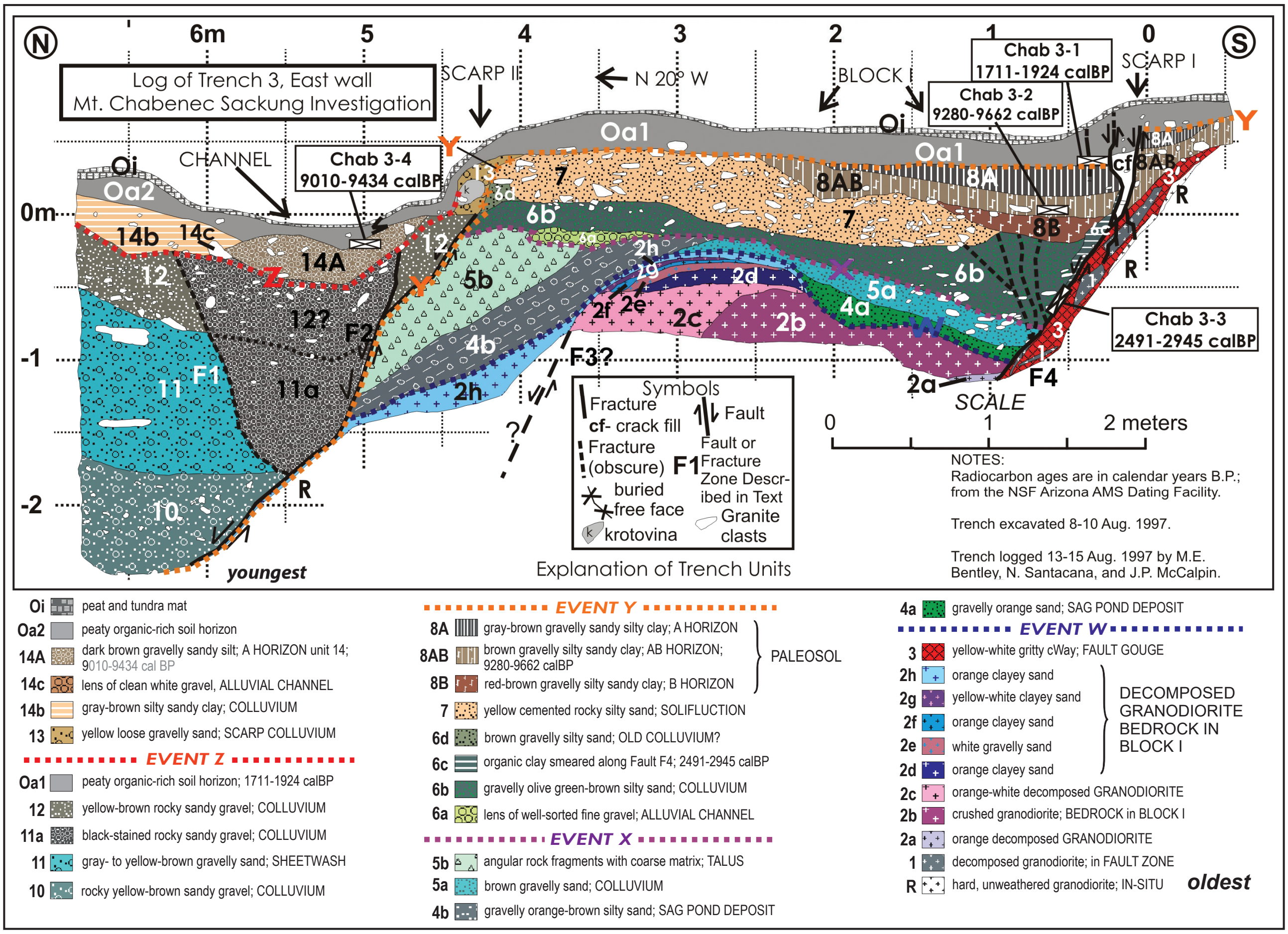

Fig. 10. Log of the east wall of Trench 3.

may represent erosion of a more laterally-extensive deposit that was tilted up-to-the-north by block faulting. Both units 7 and 8 are capped by a peaty, organic soil A-horizon (unit Oa1) that contains very rare clasts. This unit parallels the modern ground surface so is in angular unconformity with underlying tilted units 7 and 8. However, the horizon thins drastically as it goes over the face of Scarp 4B, as if it were stretched by faulting.

None of the trough deposits described above exist north of Scarp 4B and fault F2. Instead, the northern trough is underlain by much thicker, massive gravel deposits. Unit 10 is sandy gravel interpreted as colluvium, while unit 11 is finer (gravelly sand) interpreted as a slopewash deposit. Unit 12 is a yellow-brown rocky sandy gravel interpreted as colluvium sourced from the north. Between faults F1 and F2 all clasts in units 11 and 12 have been stained black. We infer this is some type of groundwater staining mechanism. Unit 12 is unconformably overlain by a clayey sag pond deposit (unit 14b), a small gravel channel (unit 14c), and an A-horizon developed on younger sandy silt (unit 14A). Unit 14 is overlain by peaty soil horizon Oa2, a thinner and younger version of unit Oa1.

In Trench 3, the Quaternary strata on Block 1 (units 4 through 8) represent only the early record of deposition in the trough, prior to the development of Scarp 4B. These four units comprise a 1.1 m-thick sequence of older trough sediments that overlie crystalline bedrock, and which correlate with the older half of the trough fill exposed in Trench 2 (units 4 through 10a, also ~1 m thick). After uplift of Block I in the mid-Holocene, trough deposition at Trench 3 shifted to the north of Block I and Scarp 4B, and units 10 – 14 were deposited. The correlative beds in Trench 2 are units 10b – 14A, which comprise the upper half of Quaternary deposits there.

4.3.6 Trench 3, Structure

Based on the sharpness of scarps at the surface (Scarp 4B younger than Scarp 4A), and on cross-cutting relationships in the trench wall, fault movement has generally progressed in time from the main shear zone (F4), to faults F3, then F2 and F1. For example, the oldest trough fill (unit 4a) lies against the main shear zone (F4), indicating that movement on F4 created the initial trough.

Those thin units (4a, 5a) are no longer horizontal but are backtilted strongly toward F4, which requires movement on another normal fault farther north (F3). Movement on F3 is also required to drag/tilt units 2h-4b-5b down-to-the-north. These tilted strata are truncated by F2; slip on F2 is also required to tilt units 6-7-8 down-to-the-south. So the progression of movement from F4 to F3 to F2 is well documented by cross-cutting. Fault F1 appears to be the youngest structure, being an antithetic fracture growing upward from F2 which has not yet accumulated significant vertical displacement.

Trench 3, Geochronology

At first glance the radiocarbon ages from Trench 3 seem too old and too inconsistent compared to those in nearby Trench 2. Two samples very close to the modern ground surface yielded anomalously old early Holocene ages (Chab 3 – 4, only 10 cm below the surface, 9,010 to 9,434 cal BP; Chab 3 – 2, 25 cm below the surface, 9,280 to 9,662 cal BP). By comparison, sample Chab 3 – 1 (15 cm below the surface, and only 10 cm higher than Chab 3 – 2) yielded an age of 1,711 to 1,924 cal BP. This age is reasonable compared to ages from Trench 2. One reason for this inconsistency is that there has been no trough sedimentation on Block I since faulting Event X (see Fig. 10). Since Block I was abandoned by active deposition, a moderately strong soil profile (8A-AB-B-horizons) has formed, which has subsequently been tilted south and the north halves removed by erosion. The soil development alone suggests that unit 8AB (site of the 9.4 ka sample Chab 3 – 2) is probably at least early Holocene in age. However, this line of reasoning cannot explain the early Holocene age of sample Chab 3 – 4 (9.2 ka), which is not on Block I and overlies much younger trough deposits. Our tentative interpretation is that the carbon sampled in sample Chab 3 – 4 was partly derived from erosion of units 8A or 8AB when they were exposed in a free face of Scarp 4B. If sample Chab 3 – 4 contained an intact colluvial chunk or block of horizon 8A, which was then overprinted by younger A-horizon 14A, it might have been difficult for trench loggers to distinguish the two A-horizons. Notably, sample Chab 3 – 4's age (9,010 to 9,434 cal BP) overlaps the age of in-situ unit 8AB (9,280 to 9,662 cal BP) at two sigma, suggesting they are related.

The late Holocene age of carbon in the main shear zone (Chab 3 – 3, 2,491 to 2,945 cal BP) is also problematic. Recall that in Trench 2 a similar shear-zone sample (Chab 2-9) yielded an age of 3,446 to 3,690 cal BP. That age was midway between radiocarbon ages at the bottom (5.6 ka) and top (1-1.8 ka) of the trough stratigraphic sequence, and we speculated that older and younger carbon had been smeared along the fault zone and physically mixed, yielding an intermediate age. That argument cannot apply to the sample from the Trench 3 shear zone, because all possible source beds for smeared-upward carbon (units 4a, 5a, 6b) are older than ~9.5 ka, so smearing them together should never yield an age of ~2.7 ka. The only way to explain such a young age is to argue that younger carbon was somehow introduced into the shear zone from above, from sources such as the crack fill at the top of fault F4 (labeled "cf" on Fig. 13). That fissure displaces carbon-bearing units 8A and Oa1, and could possibly have opened deep enough along the fault plane to allow some

Tab. 4.
Inferred sequence of depositional, pedogenic, and deformational events affecting Trench 3.

Event (oldest at bottom)	Evidence
Deposit unit 14	Unit 14 deposited in closed depression. Downwarped soil Oa1 continues to develop and accumulate carbon, but is slightly eroded by the modern drainage channel.
Deformation EVENT Z	Small displacement on F4 displaces units 8A and 8AB 25 cm down-to-north. Larger displacement (~0.5 m) occurs on F2, displaces soil Oa1. This movement also tilts unit 13 to near-vertical. Brings Scarp 4B to its present height.
Deposit units 10-13	Unit 13 deposited as a small scarp-derived colluvial wedge. Thick units 10 through 12 are deposited in the new trough created by faults F1 and F2 (~2.5 m thick). Soil horizon Oa1 forms across surface (basal age of **1,711 to 1,924 cal BP**).
Deformation EVENT Y	Much larger displacement occurs on F2 displacing units 4b through 7 down-to-the-north below the trench floor (minimum of 2.8 m). Units 4a through 8A are tilted more down-to-south, to their present dip angle. Later erosion planes off the northern halves of 8AB and 8A.
Deposit unit 6-8	Units 6, 7, and 8 are deposited. A strong soil profile (A-AB-B-horizons) develops on unit 8. Base of unit 8AB dates at **9,280 to 9,662 cal BP**.
Deformation EVENT X	Fault F3 develops, creating Block I. Block I deposits between F3 and F4 are tilted down-to-south by domino-style normal faulting, to roughly half their present dip. Movement on F3 also tilts and downdrops units 4b and 5b.
Deposit units 4 and 5	Units 4a and 5a were deposited in trough at base of main shear zone, sourced from the south; coeval units 4b and 5b have different lithology, so presumably sourced from north.
Deformation EVENT W	Initial sackungen displacement occurs on main shear zone (F4).

Fig. 11. Photographs of Trench 4 on Scarp 6. Left – looking southeast with Scarp 6 in the middle ground and the unnamed NW-trending scarp coming in from the lower left corner. Trench 4 is behind the light-colored spoil pile. Right – Trench 4 looking southwest.

late Holocene carbon to infiltrate down to the depth of sample Chab 3 – 3. In summary, half of the four samples collected yielded ages that cannot be reconciled with the physical stratigraphy, and must be explained away by some complicated movement/intrusion of younger or older carbon.

Trench 3, Interpretation

Based on stratigraphic superposition, cross-cutting relationships, and the existence of a strong paleosol, we interpret a sequence of four deformation events at Trench 3, the latest three of which are Holocene (Table 4).

Scarp 6 and Trench 4

Scarp 6 is roughly 300 m long and lies about 90 m north of and parallel to Scarp 4. The ambient slope of the ridge at Trench 4 is gentler than at Trenches 1 – 3 farther downslope (Fig. 11, left). The Trench 4 site is somewhat unique because it was sited where Scarp 6 was intersected by another antislope scarp coming in from the NW. The intersection of the two antislope scarps created a triple-junction occupied by a closed depression. The scarp faces here are relatively low and gentle, mantled with a tundra-like mat of turf grass.

Trench 4, Stratigraphy and Soils

On the west trench wall we define 10 major units further subdivided into 22 subunits (Fig. 12).

Unit 1 is in-situ crystalline bedrock of the main fault footwall, and unit 2 is the oldest Quaternary deposit (a sag-pond silt) overlying bedrock. The silt is exposed only on the footwall and is unconformably overlain by a series of thick talus deposits (units 3a, 4a; 1.4 m thick) which dip 10 – 15°S. This dip is similar to that of the slope gradient north of the trench, so we presume it is the original depositional dip. Similar thick talus units (4b, 4c, 4d; 1.4 m exposed thickness) exist on the hanging wall of the main fault. We tentatively correlate these talus units, acknowledging that: (1) the contact of talus (unit 4) over sag pond silt (unit 2) is not exposed on the hanging wall, (2) the stony character of unit 3a is not reproduced in units 4b or 4c, and (3) the 3a-4a contact is not recognized between hanging-wall units 4b-4d, possibly due to the black (groundwater) staining of unit 4c. The presence of thick talus on both sides of the main fault indicate that no sackungen scarp existed here when units 3 and 4 were deposited, even though a trough must have existed earlier (unit 2). Within the main shear zone, unit 3b appears to be a fault sliver derived from units 3a and 4a, whereas unit 4e appears to be a sliver derived from hanging wall units 4b-4d. Overlying unit 4 is a non-talus unit 5, interpreted as colluvium. Unit 5b abuts the main fault and has the shape of a colluvial wedge. Units 5c and 5d are fault slivers that share the texture of units 5a-5b and do not contain angular talus clasts, so are younger counterparts of fault slivers 4e and 3b. Unit 5a thins slightly away from the fault and does not exist on the footwall, thus appears to have been deposited only in a sackungen trough created by movement on the main fault zone.

The style of sedimentation changes after unit 5, to a series of thin trough channel and sag pond deposits. Units 6, 7a, and 7b were deposited in channels that flowed down the trough axis. Unit 7c is a scarp-derived colluvial wedge contemporaneous with unit 7b. Units 7b and 7c are overlain by sag pond silty clay (unit 8), indicating a closed depression. Deposits coarsen upward to unit 9, another channel deposit, upon which a modern soil horizon has developed (units 9A and 10).

Trench 4, Structure

Trench 4 exposes a series of about 12 north-dipping normal faults which we group into six fault groups. Faults F3 to F6 are individual faults in the main shear zone that

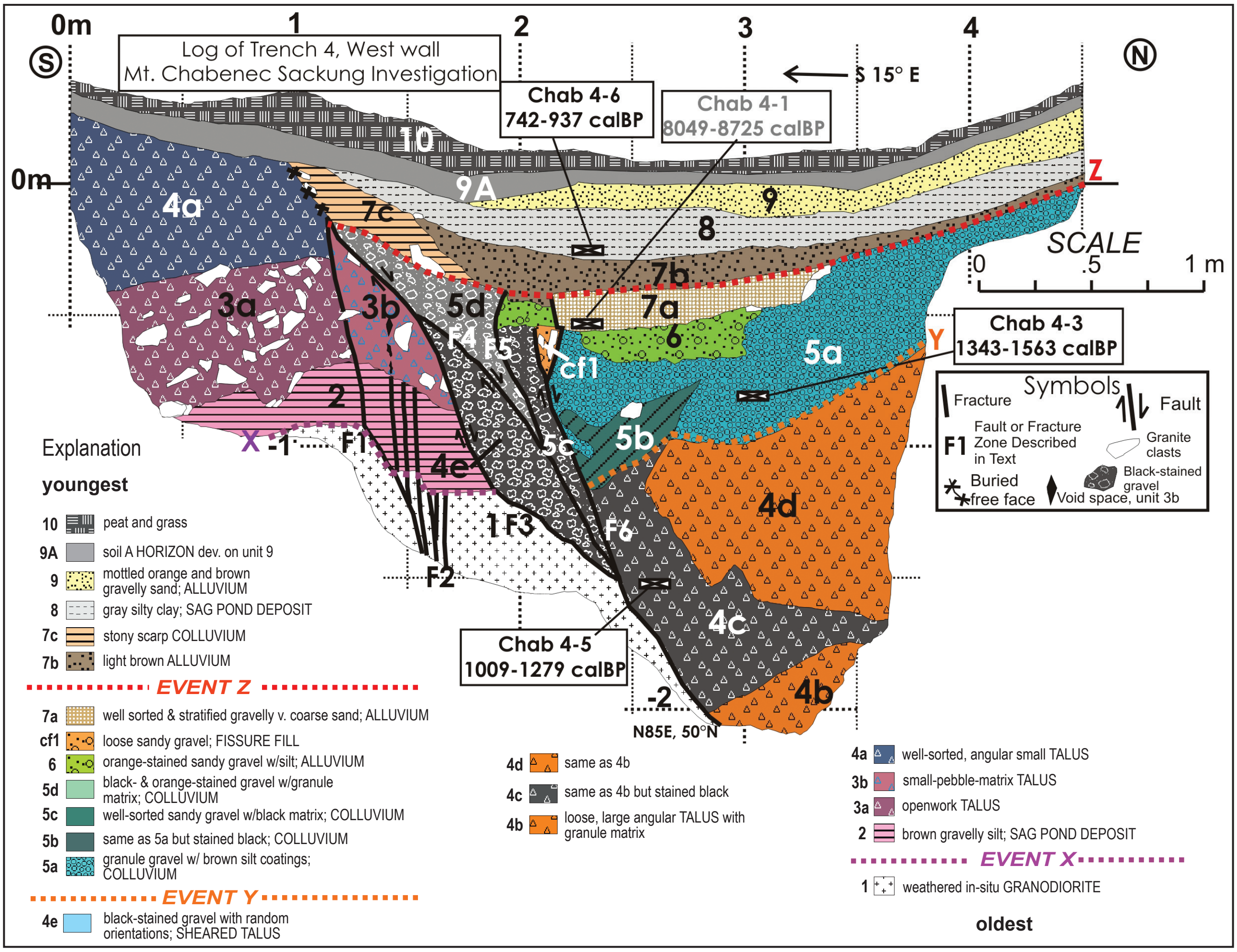

Fig. 12. Log of west wall of Trench 4.

underlies the surface scarp, whereas Faults F1 and F2 lie in the footwall of the main shear zone. On these faults we observe the same age progression of faulting as seen in other trenches. The earliest fault is not expressed in surface morphology, but must lie south of Trench 4, because even the upthrown side of the present scarp was a trough at that time (unit 2 deposition). Faults F1 and its secondary strands (F2) affect only the older units. For example, the three northern strands of F2 displace bedrock but not unit 2; the three southern strands displace unit 2 but not unit 3. F1 displaces units 2 – 4, but the total vertical displacement of unit 2 across F1 and F2 is only 30 cm.

Most of the displacement exposed in the trench has occurred on the main shear zone (faults F3 to F6). Faults F5 and F6 splay upward off Faults F3 and F4 and displace younger hanging-wall deposits. Units 6 and 7a are displaced by both F5 and F6, whereas unit 7b unconformably overlies both faults and is not displaced. This relationship, and the existence of scarp-derived colluvial wedge 7c, indicates the latest fault movement occurred after unit 7a but before unit 7b and 7c. An older event seems to be indicated by the fact that a fissure fill (unit cf1) was deposited near the top of fault F6, then was overlain by alluvial unit 6, after which unit 6 was faulted again.

Trench 4, Geochronology

Four radiocarbon samples were collected, two from the younger, well-stratified alluvial-sag pond section (units 7 – 8), and two from the older massive colluvium-talus deposits (units 4 and 5). The only age that appears reasonable, compared to those from other trenches, is that of the youngest sample (Chab 4 – 6 from sag pond unit 8), which dated at 742 to 937 cal BP. The next deepest sample (Chab 4 – 1) also comes from a thin stratified unit (alluvial unit 7a) but yields a much older age (8,049 to 8,725 cal BP). If this age was correct, then there would have to be a hiatus of 8,000 years between faulted unit 7a and unfaulted units 7b and 8. A comparable hiatus was exposed in Trench 3 (~7.7 ka), but there a well-developed soil profile consisting of an A, AB, and textural B-horizon had developed during the hiatus, as expected. In contrast, in Trench 4 there is no soil development whatsoever in the faulted units (7a and older), which would be an unlikely occurrence in a 8 ka hiatus. Sample Chab 4 – 1 was one of three detrital charcoal samples from gravelly alluvium in our set of 20 radiocarbon samples (Table 1). All three samples yielded anomalously old ages. Our tentative interpretation is that erosion somewhere upstream exposed old charcoal which was then transported down the trough axis and redeposited in the closed depression that we trenched. The underlying two radiocarbon ages are also problematic. Sample Chab 4-5 (unit 5a) lies nearly a meter below sample Chab 4 – 3 (unit 4c), yet yields a younger age (1,009 to 1,279 cal BP vs 1,343 to1,563 cal BP). In fact, unit 4c's radiocarbon age nearly overlaps at 2-sigma with unit 8's age, despite the fact that it is 1.5 m deeper in the section.

Trench 4, Interpretation

Based on stratigraphic superposition, cross-cutting relationships, and angular unconformities, we interpret a sequence of at least three deformation events at Trench 4 (Table 5 and Fig. 13).

Event Z has the best evidence of rapid vertical displacement and creation of a scarp free face (upward fault truncation at an angular unconformity, scarp-derived colluvial wedge). Its displacement is estimated as 20 cm on F6 (from the offset of unit 6) and 50 cm on F3 (twice the maximum thickness of colluvial wedge unit 7c; McCalpin, 2009). Event Y also has good evidence via the truncation of units 5a – 5b and their presence as deformed slivers in the main fault zone (units 5c – 5d). However, given Event Y's estimated net slip of 2 m, it should have generated a colluvial wedge deposit roughly 1 m thick. As shown in Stage 5 of Fig. 13, the most proximal part of units 5c and 5d may in fact be this colluvial wedge, shed from the Event Y free face, but later so sheared by displacement in Event Z (50 cm) that it became unrecognizable as a colluvial wedge.

Discussion

Due to the fine scale at which four trenches were logged, our observations on deposit sedimentology and soil formation are detailed enough to define several discrete depositional environments. In vertical section these depositional environments can change, sometimes rather abruptly. The most abrupt changes are usually associated with displacement events on the sackungen faults, recognized by the common indicators used in paleoseismic trenching (upward terminations of faults, colluvial wedges, angular unconformities, block tilting). Below a general model of sedimentation in sackungen troughs is described.

Sedimentation in Sackungen Troughs

Sackungen troughs are sediment traps affected by both climate changes and surface faulting. Due to the low axial slope of most troughs, minor changes in hillslope processes above the trough can change the style of sedimentation in the trough. For example, parts of the trough when initially formed may be closed depressions, filled by temporary ponds. Over time colluvial and slopewash sediments will selectively fill the closed depressions and eventually a through-flowing stream may develop in the trough. Such an evolution is represented in trough stratigraphy by fine-grained sag pond sediments directly overlying the bedrock, and grading upward into fluvial sediments. Conversely, if

Tab. 5.
Inferred sequence of depositional, pedogenic, and deformational events affecting Trench 4.

Event (oldest at bottom)	Evidence
Deposit units 7b-9, develop modern soil (horizons 9A, 10)	Alluvium (unit 7b) fills the deepened trough axis, while scarp-derived colluvium (unit 7c) covers the eroded F3-F4 free face. Thin colluvium (unit 8; **742-937 cal BP**) and more alluvium (unit 9) are deposited in trough. The modern soil A-horizon (unit 9A) and peat layer form.
Deformation EVENT Z	Renewed normal faulting on F3-F6 displaces units 5, 6, and 7a, and deepens the sackungen trough.
Deposit units 5-7a	Unit 5 is deposited as colluvium from the north. Then a small stream flows down the trough axis, depositing units 6 and 7a.
Deformation EVENT Y	Normal faulting on the main fault zone (F3-F6) displaces unit 4 at least 3 m down-to-north. Units on both footwall and hanging wall are rotated down-to-south from sub horizontal to 10-15° south dip. This suggests domino-style faulting.
Deposit units 2-4	Displacement creates a closed depression at the site of Trench 4, after which unit 2 is deposited in a shallow sag pond. Later, talus from upslope (north) fills the sag pond (units 3, 4). All units are subhorizontal.
Deformation EVENT X	Initial sackungen displacement occurs south of Trench 4.

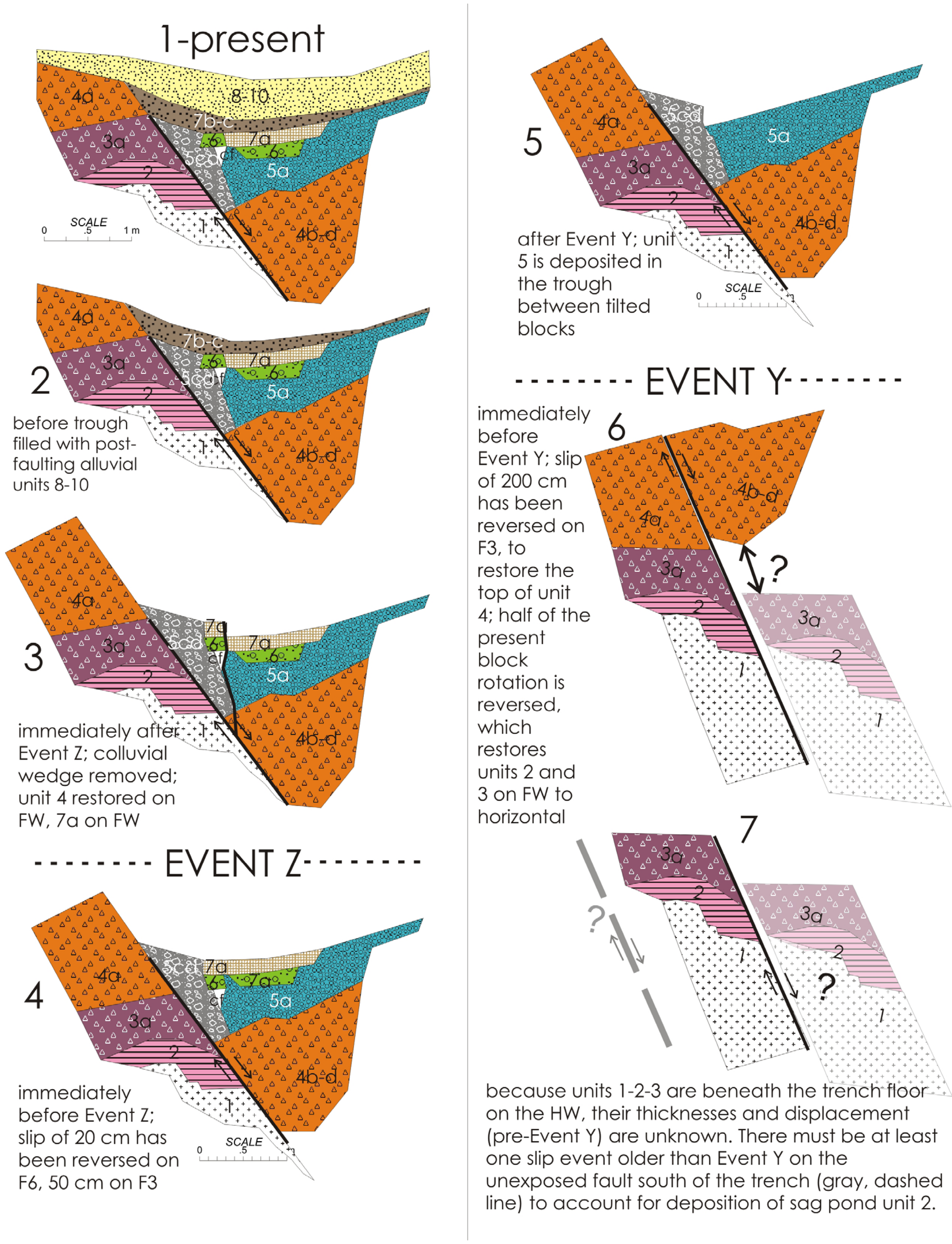

Fig. 13. Retro-deformation sequence of Trench 4. Stage 1 shows the present geometry of strata and structures on the trench wall. Preceding stages are drawn by removing any post-faulting strata (usually on the HW), restoring eroded parts of strata (on the FW), and then reversing the slip on the fault to re-align pre-faulting strata tops. This retro-deformation sequence cannot explicitly measure fault slip prior to deposition of unit 4, because the older units (1, 2, and 3 in Stages 6 and 7) are not exposed on both sides of the fault.

the axial slope of the trough is very low, increased colluvial deposition at any point can form a small dam in the trough, which also creates a closed depression. In such a depression the trough stratigraphy would show colluvium directly overlying the bedrock, and being overlain in turn by sag pond sediments.

A second cause of abrupt changes in trough sedimentation is renewed displacement on the sackungen fault, which creates (or deepens) closed depressions and exposes fresh bedrock on the scarp face. Trough stratigraphy will record the abrupt appearance of closed-depression facies (fine-grained sag pond deposits) in areas where previous deposition was colluvial or fluvial. As with tectonic normal faults, fault reactivation results in scarp-derived colluvial wedges near the fault. However, these wedges are smaller than those on tectonic fault scarps, for two reasons: (1) the exposed fault plane is usually bedrock which erodes slowly, compared to a free face in unconsolidated deposits, and (2) trough sediments are derived mainly from upslope or from upgradient in the trough axis, not from the scarp face. Accordingly, sackungen reactivation episodes are more commonly identified by: (1) upward termination of faults at different stratigraphic levels; (2) angular unconformities; (3) abrupt changes in the sedimentology of trough deposits; and (4) burial of soil profiles in the trough (developed during deposition hiatus) by renewed clastic sedimentation.

The climatic and 'tectonic' controls act independently yet synchronously on the scarp-trough system, making it challenging to determine which control is responsible for changes in trough sedimentation. Climate-driven deposition can range from slow and continuous, to episodic separated by hiatuses (soil formation). Likewise, surface displacement can range from slow creep to episodic surface-rupturing events. These two controls form four possible geometries for trough sediments (Fig. 14):

a) continuous deposition and continuous creep, which results in progressively more deformation down section in the trough sediments but a lack of paleosols,
b) continuous deposition combined with episodic fault displacement, which creates "packages" of trough strata bounded by angular unconformities, but without paleosols,
c) episodic deposition and continuous creep, which result in packages of strata bounded by angular unconformities, but each package is topped by a paleosol that represents a long hiatus during which creep continued to deform the underlying package,
d) episodic deposition combined with episodic displacement, which creates packages of strata and paleosols, but soils can appear anywhere within a package, because the two controls operate independently.

All of our trenches show evidence of episodic displacements, and most have buried soils in the trough sediments, so they correspond to Fig. 14d, as follows:

Trench 1: contains independent evidence of rapid displacements: (1) splay faulting cuts unit 5b and 6AB; (2) large granite clasts occur in colluvium (units 4a, 4b), in a much finer matrix, suggesting derivation from a scarp free face; and (3) there is a sudden change from soil formation (6AB) to sag pond conditions (unit 7). By itself the sudden change could be climatic (Fig. 14c), but since it coincides with an upward fault termination, it more likely represents episodic displacement (Fig. 14d).

Trench 2: shows a rapid change from coarse deposition (unit 10d, solifluction) to sag pond deposition (units 11a, 11b, 12). This disconformity could be caused by tectonic causes (i.e., reactivated faulting creates a closed depression) or by climatic causes. However, the disconformity also has a scarp-derived colluvial wedge sitting directly on it (unit 11c) at the main fault, and it forms the upward termination of two faults (F1, F2). Those two features cannot be created by climate changes.

Trench 3: contains structural indicators of episodic displacement. Between faults F2 and F3 units 2h, 4b, and 5b were rotated from subhorizontal (4b is a sag pond deposit) to a northward dip of 30°. All three units have

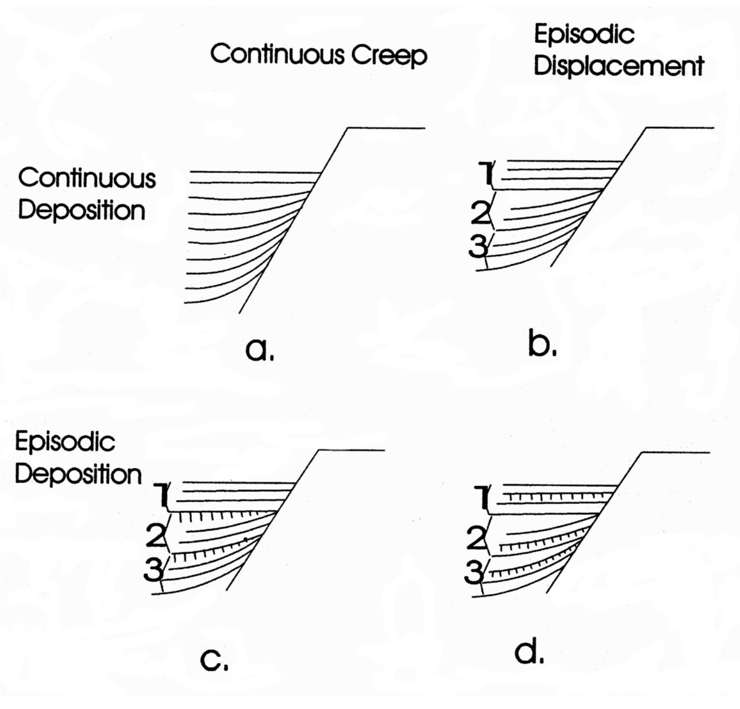

Fig. 14. Hypothetical cross-sections through a sediment-filled trough (at left) adjacent to a sackung scarp (at upper right). In the trough, thin lines indicate bedding, short vertical lines indicate soils. (a) Continuous creep and continuous deposition create a pattern of increasing folding (drag) with depth; no buried paleosols are present. (b) Episodic displacement and continuous deposition result several "packages" of strata bounded by angular unconformities; no buried paleosols are present. The angular unconformities are "event horizons" in the terminology used by paleoseismologists. (c) Continuous creep and episodic deposition yield several unconformity-bounded packages of strata. Each package is topped by a paleosol, the upper parts of which have been eroded nearest the sackung fault plane. The upper contact of each paleosol is an event horizon. (d) Episodic displacement and episodic deposition yield discrete unconformity-bounded packages of strata, but paleosols may be found at any position within the stratigraphic sequence. In this scenario, the angular unconformities are event horizons, which do not coincide with the paleosols. From McCalpin, 2003.

been rotated the same amount despite their difference in age, which is incompatible with creep displacement. The overlying units 5b and 6b are horizontal, forming a strong angular unconformity. There cannot be significant age difference between the youngest rotated stratum (5b) and the oldest unrotated stratum (6a), because closer to the main fault (F4) their correlatives (units 5a, 6b) lie conformably atop each other. Thus, the rotation of units 2h-4b-5b must have taken place in a very short time. There has been no movement on F3 since that time, which rules out fault creep.

Trench 4: has indicators of episodic displacement similar to Trench 2. There is a disconformity between units 5d-6-7a and units 7b-7c. Both units 7a and 7b are alluvium, so it could be argued that the disconformity was climatically induced. However, the disconformity also truncates faults F3, F4, F5, and F6 and has a colluvial wedge (unit 7c) sitting directly on it. Those features suggest the disconformity is tectonic.

Radiocarbon Dating of Sackungen

Table 1 (footnotes 3, 4, and 5) and the geochronology section for each trench describe some of the ambiguities in radiocarbon dating of sackungen trough sediments. We observed problems with three types of samples, described below.

Radiocarbon samples from shear zones

We dated carbon samples from shear zones in Trench 1 (Chab 1-4), Trench 2 (Chab 2-9), Trench 3 (Chab 3-3). This followed the practice from the early days of paleoseismic trenching, of dating any carbon found in a trench, especially near the fault. It was assumed then that all carbon in the fault zone had been dragged up (or fallen in) during the most recent displacement event (MRE), so its age would set a close maximum age constraint on the MRE. Sample Chab 1-4 dated at 2,380 to 2,755 cal BP, which was much older than the most recent movement in Trench 1. Sample Chab 2-9 dated at 3,446 to 3,690 cal BP, also older than the most recent event in Trench 2 (≥1.6-1.8 ka). Sample Chab 3-3 dated at 2,491 to 2,945 cal BP, compared to the youngest displacement even there of <1.7-1.9 ka. It then became obvious that the carbon in the shear zone could have one of two origins. First, it could represent surface soil carbon that fell into a crack or fissure at the time of a displacement event. In this case, the carbon would closely date a displacement event, but not necessarily the most recent one. This is especially likely for samples deep in the shear zone. Second, the carbon in trough deposits occurs as burn layers (charcoal) or as buried organic soil horizons. If this carbon is dragged up into the fault zone, its radiocarbon age reflects the age of sediment deposition or soil formation, not the age of the later displacement event that dragged it into the shear zone. We finally decided that most radiocarbon ages from shear-zones could not be associated with a specific displacement event, or interpreted as a minimum versus maximum age constraint.

Radiocarbon samples from thin silt films on talus clasts

Several of our trenches contained deposits composed angular pebble-sized rock fragments with no matrix (openwork texture) that we interpreted as talus (Trench 3, units 5b, 11a). If these deposits were located beneath the axis of the trough, the clasts were stained black, unlike all other units. The black stain was a thin coating of black silt/clay that could be rubbed off with the fingers. It is not clear whether the black stains are primary depositional features, or younger illuviated components deposited by organic-rich groundwater. Radiocarbon ages from these stains are anomalously young compared to the ages charcoal or soil organics in nearby stratigraphic units. We suspect that water standing in the trough infiltrated down through the A-horizon of the surface soil, entraining the black silt, and then carried it downward and redeposited it in the water-filled pore spaces of the openwork gravels.

Radiocarbon samples from scarp-face soils and scarp-derived colluvium

In the dynamic environment of sackungen scarps and troughs, old soils can be faulted upward, exposed at the top of a scarp free face, and then eroded and re-deposited into the colluvial wedge at the base of the free face. This process recycles old carbon from the faulted soil into the newly-deposited, post-faulting colluvial wedge, resulting in an anomalously old radiocarbon age for the wedge. That age is commonly older than the radiocarbon ages of the deposits underlying the colluvial wedge, such as occurs on Scarp 4B of Trench 3. There, soil 8A/8AB3 (9.3-9.6 ka) was upfaulted and tilted on Block I, eroded off the top of Scarp 4B, and redeposited into the much younger unit 14A, which on stratigraphic grounds is only slightly older than 1.7-1.9 ka. But the radiocarbon sample from 14A dated much older at 9.0-9.4 ka. In theory, a similar process could occur if the axial drainage in the trough undermined a soil-capped streambank, and pieces of an old organic soil fell into the alluvium.

Small-Scale Evolution of Sackungen Surface Deformation

Our two trenches on Scarp 4 revealed a complex evolution of structures over a small area, which contains two antislope scarps (4A, 4B) with an intervening structural

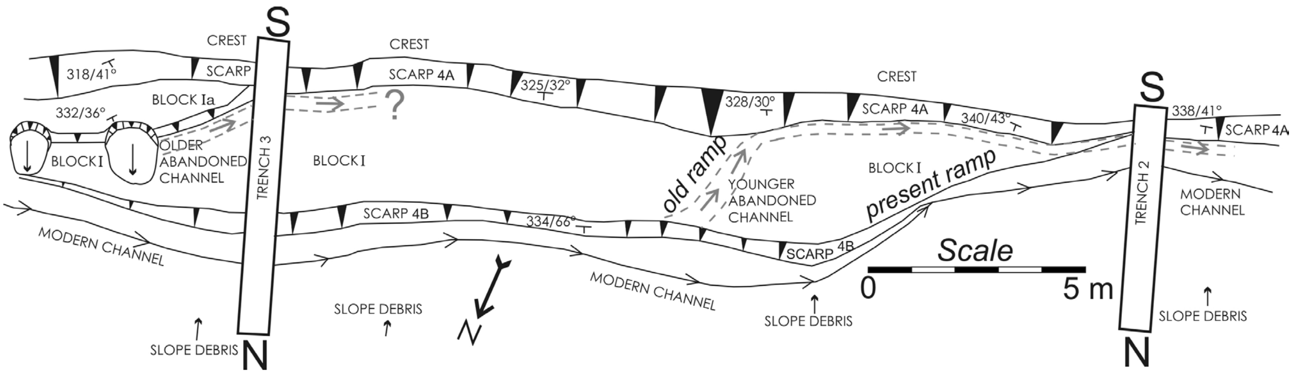

Fig. 15. Geomorphic sketch map of Scarp 4 in the vicinity of Trenches 2 and 3; north is toward bottom left. Triangles on scarp faces point downslope; strike/dip symbol and labels reflect the orientation of the scarp face. Scarp 4A (the main scarp) and Scarp 4B (subsidiary scarp) bound a structural block that we call Block I. The top of Block I forms a ramp structure (present ramp) that dives beneath the trough floor east of Trench 2.

block (Block I; Fig. 15). The modern channel in the sackungen trough flows west along the toe of Scarp 4B. At the western end of Block I, Scarp 4B dies out and the surface of Block I plunges beneath the trough floor in a fault ramp. The modern channel then follows the end of this ramp on an oblique path to the toe of Scarp 4A.

The western part of Block I is crossed by an abandoned, partially infilled channel with the same width and oblique orientation as the modern channel. This channel has been uplifted and truncated by Scarp 4B, which caused its abandonment. We infer that this “younger abandoned channel” marks a former location where the Block I ramp (old ramp) once plunged beneath the trough floor, and the stream at that time followed the toe of that ramp. Subsequently Block I has risen and both Scarp 4B and Block I have grown westward. As Scarp 4B continues to grow westward, its will eventually defeat the oblique reach of the modern channel and force the channel northward, thus truncating the modern channel and creating another abandoned channel segment on Block I. Farther east at the toe of Block Ia there is an even older abandoned channel, which has no surface expression, but is exposed in Trench 3.

Deposits of both the modern and older abandoned channels are exposed in Trench 3, whereas Trench 2 exposes the modern and younger abandoned channels (Fig. 16). The basal deposits of the younger abandoned channel date at 1,625 to 1,870 cal BP and the soil A-horizon overlying the channel dates at 331 to 631 cal BP. Soil development is weak, consisting of only a organic A-horizon, which is consistent with the channel’s young geomorphic expression and radiocarbon ages. In contrast, deposits of the older abandoned channel in Trench 3 carry a well-developed soil profile consisting of A, AB, and textural B-horizons. The base of horizon 8AB yielded an age of 9,280 to 9,662 cal BP (early Holocene), which is consistent with the degree of soil formation, and with the fact this paleo-channel has no surface expression. Overall, trench exposures confirm the spatial/temporal scenario suggested by the surface geomorphology. We now see that, as fault blocks and ramps develop and grow laterally in a sackungen trough, their emergence forces the trough depocenter to migrate laterally, shifting the locus of sag pond deposition and fluvial facies. Likewise, on rising fault blocks sedimentation changes from sag pond to fluvial, and then to aeolian and soil formation once the block is abandoned by trough sedimentation.

Large-Scale Evolution of Sackungen Surface Deformation

Previous research on swarms of parallel sackungen have documented that scarps at higher elevations formed later (known as “onset age”). Hippolyte et al. (2009) concluded: “*This decrease of the age of the scarps with elevation much probably reflects the propagation of the deformation toward the crest (from elevation 2,190 m to 2,419 m)... This chronology agrees with the proposed mechanism of flexural toppling. The migration of the slope deformation from the valley flank to the crest also supports the model of glacial debuttressing for the origin of the Arcs sackungen*.” Pánek and Klimeš (2016) concluded “*In general, we observe a statistically significant correlation showing a progressive decrease of sackungen scarp* [onset] *ages with their increasing altitudinal position... Such a relationship might indicate linkage of (delayed) sackungen genesis to overall thinning and retreat of glaciers since the LGM… Therefore, slow upslope migration of stress release after glacier withdrawal… could partly explain substantial time lag of a number of sackungen scarps*.”

The younger displacement events in our Chabenec trenches do not show this trend. In Fig. 17 we compare the ages of displacement events amongst the trenches over the past 6 ka (older events have too few radiocarbon ages and

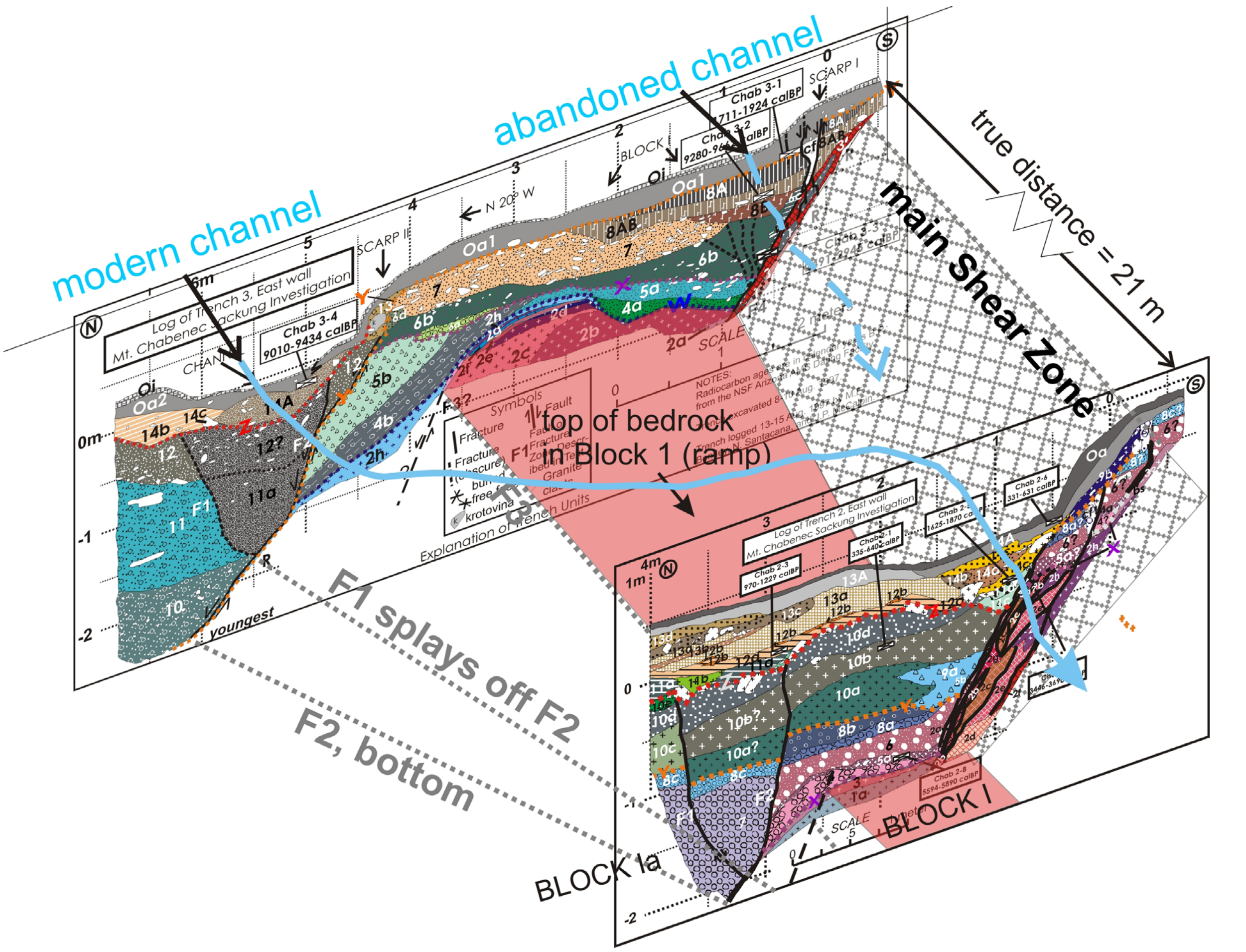

Fig. 16. Pseudo-isometric diagram of the Trenches 2 and 3, with distance between the trenches shortened from true scale. North is to the left. The top of bedrock in Block I is highlighted in red, plunging down to the west. Thick light blue lines indicate the modern and abandoned channel thalwegs.

are too affected by contamination processes; see section 5.2). The most striking pattern is that, in all four trenches, there is a displacement event between ca. 1 and 2 ka.

In paleoseismic trenches across normal faults, the maximum limiting radiocarbon age on a faulting event typically forms a closer age constraint than the minimum limiting age. This is because the dated carbon typically comes from a soil horizon that was rapidly buried by post-faulting deposition (McCalpin, 2009). Maximum limiting ages on events Y_1, Z_2, Z_3, and Z_4 are surprisingly similar (1,860 cal BP; 1,720 cal BP; 1,820 cal BP; and 1,410 cal BP, respectively).The ages are not strictly synchronous, but neither do they show a pattern of younger events at higher elevations. Therefore, a common trigger mechanism cannot not be ruled out.

Trigger Mechanism

Three trigger mechanisms are normally considered for episodic sackungen displacements, two exogenetic and one endogenetic: (1) seismic shaking, (2) extreme precipitation events, or (3) a slow uphill advance of tensional stress caused by glacial oversteepening of lower slopes (Pánek et al., 2015). Not surprisingly, workers in seismically-active regions prefer trigger 1 (e.g., Italy; Carpathian Mountains; Caucasus Mountains; New Zealand; California, USA), attributing sackung formation to either direct surface rupture or to seismic shaking (e.g., photographs in Khromovskikh, 1989; see also Zischinsky, 1966; Beck, 1968; Radbruch-Hall et al., 1976; Mahr, 1977). For example, Salvi and Nardi (1995, p. 107-108) state“... *strong ground shaking associated with earthquakes is one of the main triggering factors for the growth of ‘sackungen-like’ features*”. This contention is partly based on the appearance of new antislope scarps in hilly terrain after moderate-to-large-magnitude earthquakes (e.g., Dramis and Sorriso-Valvo, 1983; Morton and Sadler, 1989; Morton et al., 1989; Cotton et al., 1990; Ponti and Wells, 1991; Nolan and Weber, 1992; Blumetti, 1995; Jibson et al., 2004; Moro et al., 2007), and partly on a spatial association of sackungen

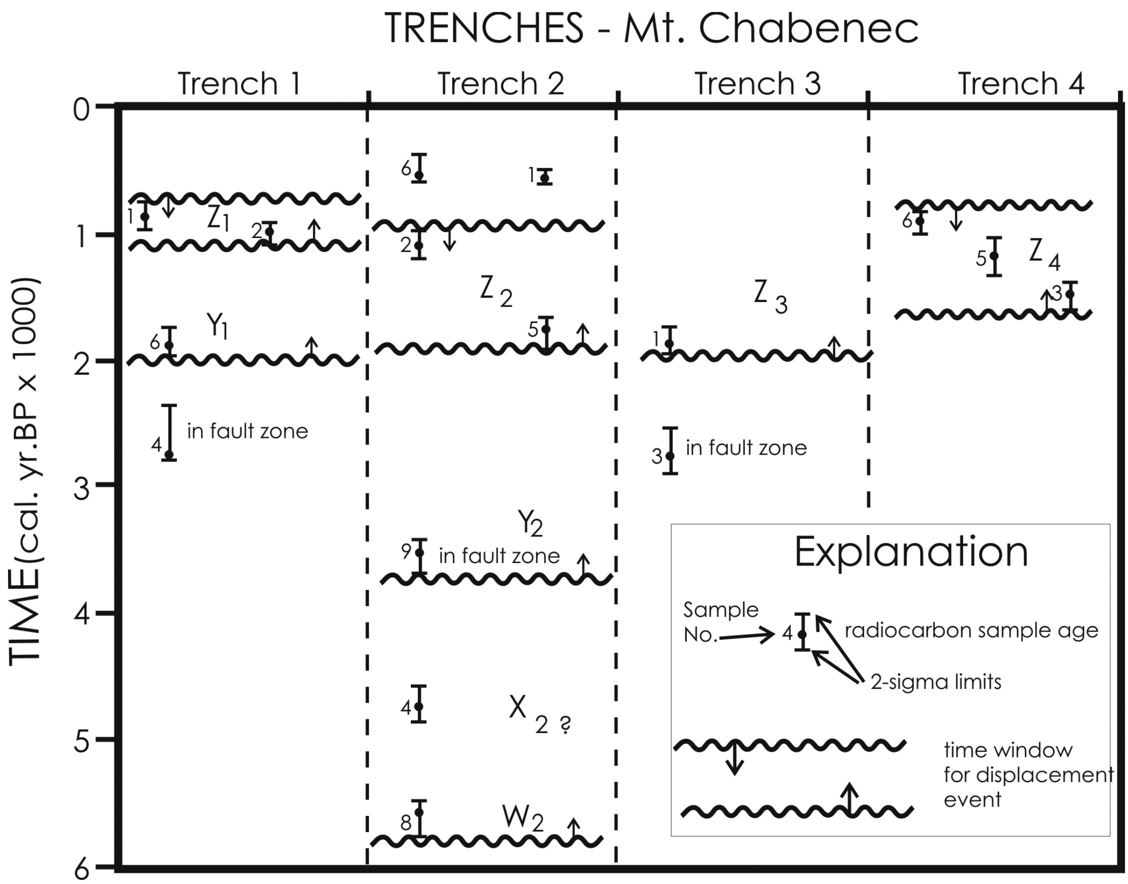

Fig. 17. Space-time diagram of displacement events observed in the four trenches. Z1 is the latest event in Trench 1; Y1, is the penultimate event in Trench 1, etc. Calendar-corrected ages are from Table 1.

with active fault traces. Criteria for testing possible trigger mechanisms are summarized by McCalpin (1999, 2003). In contrast, workers in glaciated mountains tend to favor trigger 3. An example is Pánek et al. (2017), who state that sackungen in the High Tatras are unlikely to be triggered by seismicity, given the low seismicity rates in the historic record. Instead, they conclude that: "*slow upslope migration of stress release after glacier withdrawal… could partly explain substantial time lag of a number of sackungen scarps*."

To assess the possibility of seismic triggering, we must consider the seismotectonic setting of Mount Chabenec. Our latest sackungen displacements date just younger than 1,410-1,860 cal yr BP (i.e., 140-590 A.D). Unfortunately, the earthquake history of northern Slovakia-southern Poland extends only back to 1259 A.D. (the 31-JAN-1259 earthquake; Io=7, Mw=5, at approx. 49.9N, 19.25W; Grunthal et al., 2009). The felt area in 1259 included "*Poland, Bohemia, Hungary, Russia, Leczyca, etc*." (Guterch and Kozak, 2015). The 1259 earthquake is hundreds of years too recent to be the trigger mechanism for the MRE displacements on Mount Chabenec, but it does demonstrate that seismic ground motions can occur at our study site, from moderate-magnitude regional earthquakes.

Mount Chabenec lies within the Čertovica seismotectonic zone (Fig. 18), one of four 'seismoactive zones' defined in Slovakia by Kováč et al. (2002), Hók et al. (2016). They describe the Čertovica line as follows: *"The Čertovica line is a surface projection of the thrust plane of the Veporic basement sheet over the Tatricum. Based on geological data, earthquake focal mechanisms (Pospíšil et al., 1992), geophysical data (Bezák et al., 1993, 1995; Šefara et al., 1998) and structural analyses (Hók et al., 1997, 1999, 2000) we consider this sector of the Čertovica Line as a recently active due to extensional collapse of the orogene. Earthquake events are released mostly on the Hron fault system of ENE-WSW direction... It is noteworthy that this system, like the Dobrá Voda system, is distinctive in the recent morphology and can be well traced by remote sensing methods (Janků et al., 1984)".* The active Hron fault system mentioned above extends within 10 km south of Chabenec's summit.

Historic earthquakes in the Čertovica zone have clustered at the western end near Banská Bystrica and at

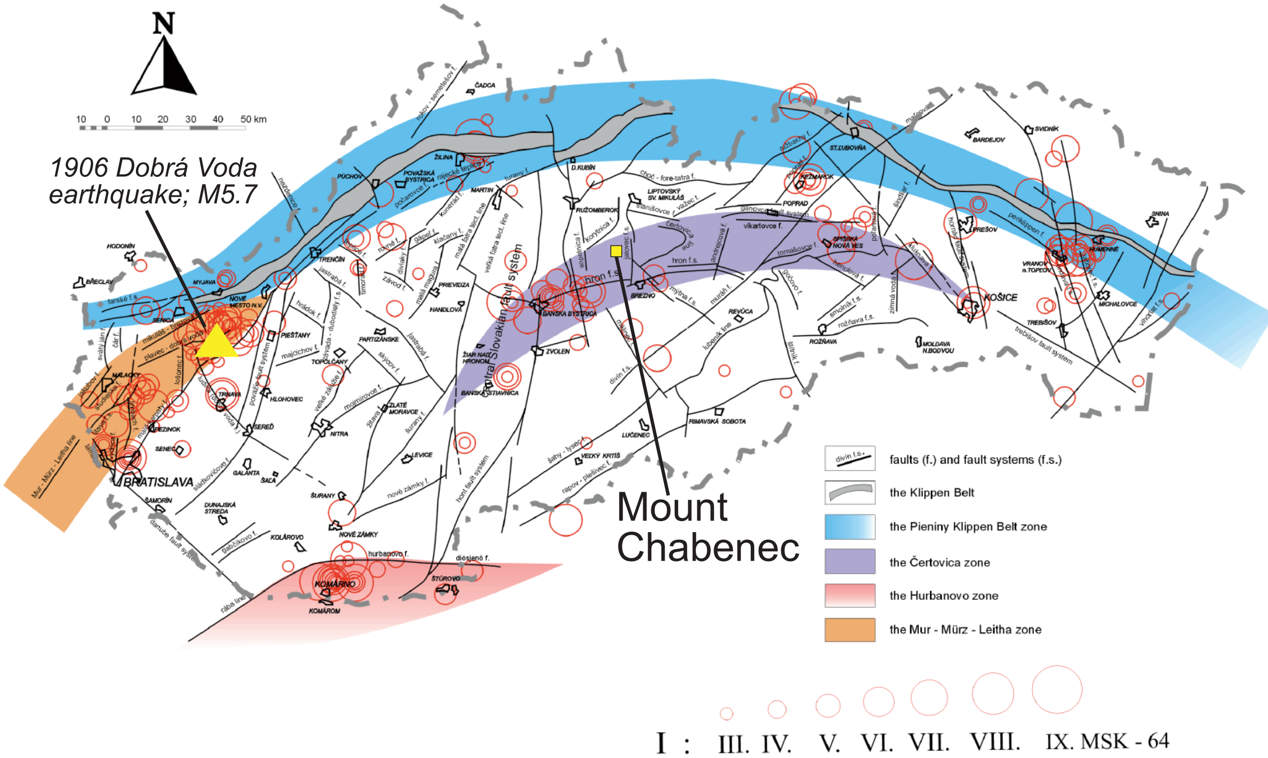

Fig. 18. Seismically active zones of the Western Carpathians with indicated epicenters of earthquakes for the period 1034–1990 and position of the seismotectonic zones. Mount Chabenec (yellow square) lies in the Čertovica seismotectonic zone, which contains the active Hron fault between Mount Chabenec and Banská Bystrica. The largest earthquake in the 20th century (1906 Dobrá Voda) is shown as a yellow triangle. Modified from Kováč et al., 2002.

the eastern end, with a "seismic gap" in the center. The former earthquakes include one of the largest instrumental events in the Slovakia (the M4.3 earthquake of 07-JUNE-1989; 48.779°N, 19.21°E) which occurred only 27 km southwest of Mount Chabenec. Recent neotectonic studies have discovered possible late Quaternary fault movements on the northern flank of the Nízke Tatry Mountains, not far NE of Chabenec. Vojtko et al. (2011) identified 130 ka alluvium apparently displaced by the 55 km-long Vikartovce fault, an E-W structure on the north side of the Nízke Tatry range. The west end of this south-dipping normal fault lies only 40 km NE of the Chabenec summit. Closer to Chabenec, Littva and Hók (2014) infer late Quaternary fault displacements in the NNE-trending Jánska dolina Valley, only 10 km NE of Chabenec. This trend, if projected southward, would approach even closer to the Chabenec sackungs. Neither of these studies included paleoseismic trenching or dating of individual paleoearthquakes, so there is currently no way to test if those faults moved between 1,410 to 1,860 cal yrs BP.

None of the neotectonic data above conclusively prove that seismic shaking triggered the sackungen reactivations between 1 and 2 ka. To test that hypothesis would require knowing if there had been active faulting events or strong shaking events in the vicinity of Chabenec in the 1 – 2 ka period. Such detailed data can only come from paleoseismic chronologies of regional active faults or of secondary shaking features such as liquefaction or lateral spreads, but such chronologies do not exist yet for northern Slovakia.

Conclusions

We applied paleoseismic trenching techniques to four trenches dug across three antislope scarps on the south ridge of Mount Chabenec. Beneath the scarps is a complex shear zone in granodiorite, 25 – 50 cm thick, dipping 55 – 60° N (into the slope). The shear zones contain multiple fault strands, gouge zones, and alteration zones suggestive of deep crustal shear rather than shallow extensional faulting. The implication is that ongoing deep-seated, gravitational toppling deformation is utilizing old pre-Quaternary fault zones. Structure and stratigraphy exposed in the trenches are consistent with episodic slip on the sackungen faults coupled with episodic deposition and soil formation in the adjacent troughs. Rapid changes in sedimentation style and cessation of soil formation correlate stratigraphically with episodes of displacement on the sackungen structures. Despite this correspondence of episodic displacement and sedimentation, we encountered difficulties in dating displacement events with radiocarbon. Five of our 20 samples yielded inverted ages, due either to recycling old carbon within the trough, or to contaminating porous old deposits with carbon from overlying, younger deposits. In hindsight, we should have supplemented radiocarbon dating with luminescence dating, which would have been possible because every trough contained one or more fine-grained, sag pond deposits.

Radiocarbon ages indicate that in all four trenches, there was a displacement event in the late Holocene (shortly after 1,410 to 1,860 cal yrs BP). The longest well-dated record in a single trench (Trench 2) contained four inferred displacement events in the past 6 ka, yielding a long-term average recurrence of ca. 1.5 ka. These four events have created an antislope scarp with ~5 m of vertical surface offset. The near-synchroneity of the late Holocene displacements stands in contrast to other dated sackungen sites, where displacements become younger with increasing elevation. Having near-synchronous displacement events at multiple elevations suggests an external trigger, either climatic or seismic. Unfortunately, there is no record of regional paleoearthquakes or meteorological events between 1 – 2 ka to further test that hypothesis.

Acknowledgements

Dating and travel support came from National Science Foundation grant EAR-9506371 to Principal Investigator Peter Birkeland at the University of Colorado, Boulder. Stan Novosad (Denver, CO) first told JPM about the classic sackungen at Mt. Chabenec and helped to plan our trenching campaign. PL and RJ coordinated all the field logistics. Thanks to our valiant trenching crew (Fig. 19) who ascended 600 m to the trench sites; dug the trenches; and descended back to base camp for 10 consecutive days.

References

Agliardi, F., Crosta, G. B., Zanchi, A. & Ravazzi, C., 2009: Onset and timing of deep-seatedgravitational slope deformations in the eastern Alps, Italy. *Geomorphol., 103, 113 – 129.*

Bagge, M. & Hampel, A., 2016: Three-dimensional finite-element modeling of coseismic Coulomb stress changes on intra-continental dip-slip faults. *Tectonophysics, 684, 52 – 62.*

Beck, A. C., 1968: Gravity faulting as a mechanism of topographic adjustment. *New Zealand J. Geol. Geophys., 11, 191 – 199.*

Beget, J. E., 1985: Tephrochronology of antislope scarps on an alpine ridge near Glacier Peak,Washington, USA. *Arct. Alpine Res., 17, 143 – 152.*

Fig. 19. Field team of the Chabenec trenching project. Red arrows indicate sackungen scarps on the southern slope of Mt. Chabenec. View to the east: 1 – Nuria Santacana, Tech. Univ. of Catalonia; 2 – Molly Bentley Zorba, Univ. of Colorado; 3 – Juraj Michalko, SGIDŠ; 4 – Stanislav Petruška†; 5 – ibor Vlník; 6 –Pavel Liščák, SGIDŠ; Not pictured: Robert Jelínek and Jozef Hók, SGIDŠ; Gustáv Gabauer†, J. P. McCalpin, GEO-HAZ Consulting (photographer). † indicates deceased.

Bezák, V., Hók, J., Kováč, P. & Madarás, J., 1993: Possibilities of tectonic interpretation of the seismic section 2T (in Slovak, English abstract), In: Rakús, M. and Vozár, J. (Eds.): Geodynamic model and deep structure of the western Carpathians. Konf., Symp., Sem. *Bratislava, Geol. Úst. D. Štúra, 287 – 290.*

Biely, A., Beňuška, P., Bezák, V., Bujnovský, A., Halouzka, R., Ivanička, A., Kohút, M., Klinec, A., Lukáčik, E., Maglay, J., Miko, O., Pulec, M., Putiš, M. & Vozár, J., 1992: Geological map of the Nízke Tatry Mountains 1 : 50,000. Bratislava, SGÚ – Geol. Úst. D. Štúra.

Blumetti, A. M., 1995: Neotectonic investigations and evidence of paleoseismicity in theepicentral area of the January – February 1703, central Italy, earthquakes. In: Serva, L. and Slemmons, D. B. (Eds.): Perspectives in Paleoseismology. *Assoc. Engin. Geol. Spec. Publ., 6, 83 – 100.*

Carbonel, D., Gutierrez, F., Linares, R., Roque, C., Zarroca, M., McCalpin, J. P., Guerrero, J. & Rodriguez, V., 2013: Differentiating between gravitational and tectonic faults by means of geomorphological mapping, trenching, and geophysical surveys; The case of the Zenzano fault (Iberian Chain, N Spain). *Geomorphol., 189, 93 – 108.*

Cotton, W. R., Fowler, W. L. & Van Velsor, J. E., 1990: Coseismic bedding plane faults and ground fissures associated with the Loma Prieta earthquake of 17 October 1989, In The Loma Prieta (Santa Cruz Mountains) California, earthquake of 17 October 1989. *Calif. Div. Mines Geol., Spec. Publ., 104, 95 – 103.*

Dramis, F. & Sorriso-Valvo, M., 1983: Two cases of earthquake-triggered gravitational spreading in Algeria and Italy. *Rendic. Soc. Geol. Italia, 6, 7 – 10.*

Gori, S., Falcucci, E., Dramis, F., Galadini, F., Galli, P., Giaccio, B., Messina, P., Pizzi, A., Sposato, A. & Cosentino, D., 2014: Deep-seated gravitational slope deformation, large-scale rock failure, and active normal faulting along Mt. Morrone (Sulmona basin, Central Italy); Geomorphological and paleoseismological analyses. *Geomorphol., 208, 88 – 101.*

Guterch, B. & Kozak, J. (Eds.), 2015: Studies of historical earthquakes in southern Poland. *Springer Publ., 179 p.*

Gutierrez, F., Acosta, E., Rios, S., Guerrero, J. & Lucha, P., 2005: Geomorphology and geochronology of sackungen features (uphill-facing scarps) in the Central Spanish Pyrenees. *Geomorphol., 69, 298 – 314.*

Gutierrez, F., Ortuno, M., Lucha, P., Guerrero, J., Acosta, E., Coratza, P., Piacentini, D. & Soldati, M., 2008: Late Quaternary episodic displacement on a sackungen scarp in the central Spanish Pyrenees; Secondary paleoseismic evidence? *Geodin. Acta, 21, 187 – 202.*

Hippolyte, J.-C., Bourlès, D., Braucher, R., Carcaillet, J., Léanni, L., Arnold, M. & Aumaitre, G., 2009: Cosmogenic ^{10}Be dating of a sackungen and its faulted rock glaciers, in the Alps of Savoy (France). *Geomorphol., 108, 312 – 320.*

Hók, J., Kováč, P., Madarás, J., Maglay, J., Kováč, M., Baráth, I., Sabol, I., Slávik, M. & Lukaj, M., 1997: Neotectonic and geomorphological evolution of the territory of Slovakia, part Geology (in Slovak). *Manuscript. Bratislava, archive St. Geol. Inst. D. Štúr, 1 – 77.*

Hók, J., Kováč, M., Kováč, P., Nagy, A. & Šujan, M., 1999: Geology and tectonics of the NE part of the Komjatice depression. *Slovak Geol. Mag., 5, 187 – 199.*

Hók, J., Bielik, M., Kováč, P. & Šujan, M., 2000: Neotectonic character of Slovakia (in Slovak, English summary). *Miner. Slov., 32, 459 – 470.*

Hók, J., Kysel, R., Kováč, M., Moczo, P., Kristek, J., Kristeková, M. & Šujan, M., 2016a: A seismic source zone model for the seismic hazard assessment of Slovakia. *Geol. Carpath., 67, 3, 273 – 288.*

Jahn, A., 1964: Slope morphological features resulting from gravitation. *Zeit. Geomorphol. Suppl. Bd., 5, 59 – 72.*

Janků, J., Pospíšil, L. & Vass, D., 1984: Contribution of remote sensing to the knowledge of West Carpathians structure (in Slovak, English summary). *Miner. Slov., 16, 121 – 137.*

Jibson, R. W., Harp, E. L., Schulz, W. & Keefer, D. K., 2004: Landslides triggered by the 2002 Denali Fault, Alaska, earthquake and the inferred nature of the strong shaking. *Earthquake Spectra, 20, 669 – 691.*

Khromovskikh, V. S., 1989: Determination of magnitudes of ancient earthquakes from dimensions of observed seismodislocations. *Tectonophysics, 166, 1 – 12.*

Kováč, M., Bielik, M., Hók, J., Kováč, P., Kronome, B., Labák, P., Moczo, P., Plašienka, D., Šefara, J. & Šujan, M., 2002: Seismic activity and neotectonic evolution of the Western Carpathians (Slovakia). *EGU Stephan Mueller Spec. Publ. Ser., 3, 167 – 184.*

Littva, J. & Hók, J., 2014: Neotectonics of the Inner Western Carpathians; Liptovský Ján area, case study (northern slopes of the Nízke Tatry Mts., Slovakia). *Acta Geol. Slov., 6, 2, 123 – 134.*

Mahr, T., 1977: Deep-reaching gravitational deformations of high mountain slopes. *Bull. Engr. Geol. Environ., 16, 121 – 127.*

Mahr, T. & Nemčok, A., 1977: Deep-seated creep deformations in the crystalline cores of the Tatry Mountains. *Bull. Engr. Geol. Environ., 16, 104 – 106.*

Mariotto, F. P. & Tibaldi, A., 2016: Inversion kinematics at deep-seated gravity slope deformations revealed by trenching techniques. *Nat. Haz. Earth Syst. Sci., 16, 663 – 674.*

Mazúr, E. & Lukniš, M., 1986: Regionálne geomorfologické členenie Slovenska 1 : 500 000 [Regional Geomorphological Division of Slovakia 1 : 500,000]. *Bratislava, Geogr. Úst. Slov. Akad. Vied.*

McCalpin, J. P., 1999: Criteria for determining the seismic significance of sackungen and other scarplike landforms in mountainous regions. In: Techniques for Identifying Faults and Determining Their Origins, U.S. Nuclear Regulatory Commission, Washington, DC, NUREG/CR-5503, A-122 – A-142.

McCalpin, J. P., 2003: Criteria for determining the seismic significance of sackungen and other scarplike landforms in mountainous regions. In: Hart, E.W. (Ed.): Ridge-Top Spreading in California; Contributions toward understanding a significant seismic hazard. *California Geol. Surv., CD 2003-05, 2 CD-ROMs.*

McCalpin, J. P., 2009: Paleoseismology of Extensional Tectonic Environments, Chapter 3. In: McCalpin, J. P. (ed.): Paleoseismology. 2nd Ed. *New York, Academic Press, 171 – 269.*

McCalpin, J. P., 2013: Trenching and Exposed Faces. In: Shroder, J. F., Switzer, A. D. and Kennedy, D. M. (Eds.): Treatise on Geomorphology, Vol. 14, Methods in Geomorphology. *San Diego, CA, Academic Press, 138 – 149.*

McCalpin, J. P., Bruhn, R. L., Pavlis, T. L., Gutierrez, F., Guerrero, J. & Lucha, P., 2011: Antislope scarps, gravitational spreading, and tectonic faulting in the western Yakutat microplate, south coastal Alaska. *Geosphere, 7, 5, 1 143 – 1 158.*

McCalpin, J. P. & Hart, E. W., 2003: Ridge-top spreading features and relationship to earthquakes, San Gabriel Mountains Region, Southern California – Part B: Paleoseismic investigations of ridge-top depressions. In: Hart, E. W. (Ed.): Ridge-Top Spreading in California; Contributions toward understanding a significant seismic hazard. *California Geol. Surv., CD 2003-05, 2 CD-ROMs.*

McCalpin, J. P. & Irvine, J. R., 1995: Sackungen at Aspen Highlands Ski Area, Pitkin County, Colorado. *Environ. Engin. Geosci., 1, 3, 277 – 290.*

Moro, M., Saroli, M., Gori, S., Falcucci, E., Galadini, F. & Messina, P., 2012: The interaction between active normal faulting and large scale gravitational mass movements revealed by paleoseismological techniques: A case study from central Italy. *Geomorphol., 151, 164 – 174.*

Moro, M., Saroli, M., Salvi, S., Stramondo, S. & Doumaz, F., 2007: The relationship between seismic deformation and deep-seated gravitational movements during the 1997 Umbria-Marche (central Italy) earthquakes. *Geomorphol., 89, 3 – 4, 297 – 307.*

Morton, D. M. & Sadler, P. M., 1989: The failings of the Pelona Schist; landslides and sackungen in the Lone Pine Canyon and Wrightwood areas of the eastern San Gabriel Mountains, southern California. In: Sadler, P. M. and Morton, D. M. (Eds.): Landslides in a semi-aridenvironment, with emphasis on the inland valleys of southern California. *Inland Geol. Soc., Publ., 2, 301 – 322.*

Morton, D. M., Campbell, R. H., Jibson, R. W., Wesson, R. L. & Nicholson, C., 1989: Ground fractures and landslides produced by the North Palm Springs, California, earthquake of July 8, 1986. In: Sadler, P. M. and Morton, D. M. (Eds.): Landslides in a semi-arid environment, withemphasis on the inland valleys of southern California. *Inland Geol. Soc., Publ., 2, 183 – 196.*

Nemčok, A., 1972: Gravitational slope deformation in high mountains. *Proc. 24th Int. Geol. Congress, 13, 132 – 141.*

Nemčok, A., 1982: Zosuvy v slovenských Karpatoch [Landslides in the Slovak Carpathians]. *Bratislava, VEDA, Slovak Acad. Sci. Publ., 318 p.*

Nolan, J. M. & Weber, G. E., 1992: Evaluation of ground cracking caused by the 1989 Loma Prieta earthquake, Santa Cruz County, California; case histories. In: Sharma, S. (Ed.): Proc. 28th Symp. Engin. Geol. Geotech. Engin. *Boise, Idaho, Boise State Univ., 272 – 286.*

Onida, M., Galadini, F. & Forcella, F., 2016: Application of paleoseismological techniques to the study of late Pleistocene-Holocene deep-seated gravitational movements at the Mortirolo Pass (central Alps, Italy). *Netherlands J. Geosci., 80, 209 – 227.*

Pánek, T. & Klimeš, J., 2016: Temporal behavior of deep-seated gravitational slope deformations. *A rev. Earth. Sci. Rev., 156, 14 – 38.*

Pánek, T., Mentlík, P., Ditchburn, B., Zondervan, A., Norton, K. & Hradecký, J., 2015: Are sackungen diagnostic features of (de)glaciated mountains? *Geomorphol., 248, 396 – 410.*

Pánek, T., Mentlík, P., Engel, Z., Braucher, R., Zondervan, A. & The Aster Team, 2017: Late Quaternary sackungen in the highest mountains of the Carpathians. *Quat. Sci. Rev., 159, 47 – 62.*

Pánek, T., Tábořík, P., Klimeš, J., Komárková, V., Hradecký, J. & Šťastný, M., 2011: Deep-seated gravitational slope deformations in the highest part of the Czech Flysch Carpathians; Evolutionary model based on kinematic analysis, electrical imaging, and trenching. *Geomorphol., 129, 92 – 112.*

Ponti, D. J. & Wells, R. E., 1991: Off- fault ground ruptures in the Santa Cruz Mountains, California – ridge-top spreading versus tectonic extension during the 1989 Loma Prieta Earthquake. *Bull. Seismol. Soc. Amer., 81, 1 480 – 1 510.*

Pospíšil, L., Buday, T. & Fusán, O., 1992: Neotectonic movements in the Western Carpathians (in Slovak, English summary). *Západ. Karpaty, Sér. Geol., 16, 65 – 84.*

Radbruch-Hall, D. H., Varnes, D. J. & Savage, W. Z., 1976: Gravitational spreading of steep-sided ridges ("sackungen") in western United States. *Bull. Int. Assoc. Engin. Geol., 14, 23 – 35.*

Reimer, P. J. & 27 others, 2013: IntCal13 and MARINE13 radiocarbon age calibration curves 0-50000 years cal BP. *Radiocarbon, 55, DOI: 10.2458/azu_js_rc.55.16947.*

Salvi, S. & Nardi, A., 1995: The Ovindoli fault; a segment of a longer, active fault zone in central Abruzzi, Italy. In: Serva, L. & Slemmons, D. B. (Eds.): Perspectives in Paleoseismology. *Assoc. Engin. Geol. Spec. Publ., 6, 101 – 113.*

Šefara, J., Kováč, M., Plašienka, D. & Šujan, M., 1998: Seismogenic zones in the Eastern Alpine-Western Carpathian-Pannonian Junction area. *Geol. Carpath., 49, 247 – 260.*

SGIDS, 2018: 1 : 50,000-scale geological maps of the Slovak Republic: State Geol. Inst of Dionýz Štúr, on-line map server at, accessed 13-Jan-2018.

Soil Survey Staff, 2014: Keys to Soil Taxonomy. *Washington, DC, US Dept. Agriculture-Natural Resources Conservation Service, 359 p.*

Thompson, S. C., Clague, J. J. & Evans, S. G., 1997: Holocene activity of the Mt. Currie scarp, Coast Mountains, British Columbia, and implications for its origin. *Environ. Eng. Geosci., 3, 329 – 348.*

Tibaldi, A., Rovida, A. & Corazzato, C., 2004: A giant deep-seated slope deformation in the Italian Alps studied by paleoseismological and morphometric techniques. *Geomorphol., 58, 27 – 47.*

Vojtko, R., Marko, F., Preusser, F., Madarás, J. & Kováčová, M., 2011: Late Quaternary fault activity in the Western Carpathians; evidence from the Vikartovce Fault (Slovakia). *Geol. Carpath., 62, 6, 563 – 574.*

Zischinsky, U., 1969: Über sackungen. *Rock Mechanics, 1, 30 – 52.*

APPENDIX 1- Petrographic and diffraction analyses of the fault gouge

Silicate analysis

Analyses results						
		01-004773	01-004774	01-004775	01-004776	01-004777
Component	**Unit**	**PB-1**	**PB-1F**	**PB-2**	**PB-3**	**PB-4**
$Si0_2$	%	60.71	53.38	61.37	61.35	61.06
Al_20_3	%	17.03	18.76	17.16	17.42	17.53
Fe_20_3	%	7.46	9.71	7.19	7.35	7.54
Ca0	%	1.07	1.01	1.09	1.15	1.47
Mg0	%	2.38	2.58	2.41	2.37	2.68
$Ti0_2$	%	0.917	1.073	0.922	0.906	0.912
Mn0	%	0.108	0.170	0.107	0.117	0.146
P_20_5	%	0.15	0.17	0.14	0.14	0.16
Na_20	%	2.87	1.1.98	2.70	2.42	2.77
K_20	%	2.96	2.93	3.17	3.09	3.14
Loss on ignition	%	4.09	8.00	3.52	3.44	2.33
H_20	%	1.27	2.89	1.57	0.99	0.48
Rb	ppm	97	115	106	99	101
Sb	ppm	141	122	136	144	182

X-ray phase analysis

Apparatus: URD-6	Radiation: Cu $K\alpha\lambda$ = 0,154178 nm	Goniometer shift: 0,1° 2Θ
37 kV/30 mA	Measuring range: 4 –70° 2 Θ	Frequency of scanning: 1 s

Archive number: **li040/01**	Sample designation: **PB-1**
Positive phases:	
Phases with larger content (dominant): Quartz, Illite, Chlorite, Albite,	Phases with minor content (minor):
Likely phases (or very low phases content): Hematite	
Archive number: **li041/01**	Sample designation: **PB-IF**
Positive phases:	
Phases with larger content (dominant): Quartz, Albite, Illite, Chlorite,	Phases with minor content (minor):
Likely phases (or very low phases content): Hematite	
Archive number: **li042/01**	Sample designation: **PB-2**
Positive phases:	
Phases with larger content (dominant): Quartz, Chlorite, Albite, Illite,	Phases with minor content (minor):
Likely phases (or very low phases content): Hematite	
Archive number: **li043/01**	Sample designation: **PB-3**
Positive phases:	
Phases with larger content (dominant): Quartz, Chlorite, Albite, Illite,	Phases with minor content (minor):
Likely phases (or very low phases content): Hematite	
Archive number: **li044/01**	Sample designation: **PB-4**
Positive phases:	
Phases with larger content (dominant): Quartz, Illite, Albite,	Phases with minor content (minor):
Likely phases (or very low phases content): Hematite	

Postglaciálna deformačná história hlboko založených svahových deformácií na južnom svahu Chabenca, Nízke Tatry, Slovensko

Južný svah Chabenca v Nízkych Tatrách je porušený systémom protiklonných rozsadlín, ktoré predstavujú povrchové prejavy hlboko založenej gravitačnej svahovej deformácie. Predchádzajúce štúdie predpokladali, že hlboko založená deformácia so znakmi tečenia sa pomaly vyvíjala smerom k Lomnistej doline v juhovýchodnom smere (Jahn, 1964; Nemčok, 1972; Mahr a Nemčok, 1977). Svahová deformácia Chabenec je súčasťou dlhšieho pruhu podobných gravitačných porúch vyvinutých medzi Chopkom a Prašivou (vzdialenosť 25 km) v granitoidnom masíve tvoriacom hlavný hrebeň Nízkych Tatier (Nemčok, 1982). Približne 38 % hlavného hrebeňa je tu postihnutých týmto typom svahových deformácií. Ich povrchové prejavy vo forme protiklonných rozsadlín sú dobre viditeľné, keďže väčšina z nich sa nachádza nad pásmom lesa v nadmorskej výške zhruba ≥ 1 400 m. V roku 1997 tu spoločný americko-španielsko-slovenský tím pod vedením prof. Jamesa McCalpina z Univerzity Boulder, Colorado, a Pavla Liščáka z ŠGÚDŠ uskutočnil paleoseizmický výskum, zameraný na zistenie mechanizmu vývoja svahovej deformácie a datovanie udalostí, ktoré viedli k vzniku uvedených rozsadlín. Prieskum v teréne zahŕňal výkopy sondážnych rýh vo vytypovaných rozsadlinách, detailný stratigrafický popis sedimentov zachytených v týchto „sedimentačných pasciach“, odber vzoriek na následné laboratórne petrografické zhodnotenie tektonických ílov, odber vzoriek a datovanie organických sedimentov pomocou metódy ^{14}C. Sondážne ryhy boli široké približne 0,6 m, dlhé 4,5 až 7,3 m a hlboké 2,0 až 2,7 m. Východná stena výkopu v každej sondážnej ryhe bola očistená a pomocou lanka bola vyznačená sieť 10 x 10 cm, ktorá slúžila na zhotovenie grafického záznamu o litologickom zložení a vzorkovaní na milimetrový papier v mierke 1 : 15. Odkryté stratigrafické jednotky boli definované na základe farby, textúry a sedimentárnych štruktúr. Pôdne horizonty na sedimentoch (substráte) boli taktiež identifikované a klasifikované v zmysle terminológie horizontov A/B/C používanej v USA. Petrografickú analýzu zabezpečila RNDr. Eva Žáková z ŠGÚDŠ, rádiokarbónové datovanie sa uskutočnilo v NSF (National Science Foundation), v laboratóriu atómovej hmotnostnej spektrometrie na urýchľovacom hmotnostnom spektrometri (Univerzita Arizona, Tucson, USA).

Protiklonné rozsadliny vo vrchných častiach južného svahu Chabenca (nad pásmom lesa) majú približne paralelný priebeh s vrstevnicami a dosahujú dĺžku 300 – 600 m. Celkovo sme identifikovali 9 rozsadlín od najspodnejšej, označenej 1, až po najvyššiu, označenú 9. Vlastný sondážny prieskum sme uskutočnili v protiklonných rozsadlinách 2, 4, 6 a 7, ktoré mali dĺžku 600 m, 350 m, 300 m a 300 m (v uvedenom poradí). Vertikálny povrchový skok v uvedených dominantných rozsadlinách varíroval v intervale od 1 až do 10 m.

Aplikovali sme paleoseizmickú metódu v štyroch sondážnych ryhách. Uvedenými sondážnymi ryhami realizovanými naprieč tromi protiklonnými trhlinami – rozsadlinami – na južnom hrebeni Chabenca bola odkrytá komplexná strižná zóna v granodiorite ďumbierskeho typu s mylonitmi hrubými 25 – 50 cm so smerom a sklonom 360/55 – 60° (do svahu). Strižné zóny obsahujú viacnásobné zlomové úseky, zóny tektonického ílu a alteračné zóny. Na základe toho je možné predpokladať, že prebiehajúca hlboko založená gravitačná deformácia využíva staré predkvartérne poruchové zóny. Štruktúra a stratigrafia odhalená sondážnymi ryhami sú v súlade s epizodickým sklzom pozdĺž porúch gravitačnej deformácie, spojených s následnou depozíciou a tvorbou pôdy v priľahlých rozsadlinách. Rýchle zmeny v sedimentačnom štýle a prerušenie tvorby pôdy stratigraficky korelujú s epizódami posunov na štruktúrach hlboko založenej gravitačnej deformácie. Napriek zjavnému chronologickému súladu medzi epizodickými pohybmi a tvorbou sedimentov sme sa stretli s ťažkosťami pri rádiokarbónovom datovaní pomocou metódy ^{14}C. Päť z našich 20 vzoriek prinieslo prevrátený vek, a to buď v dôsledku recyklácie starého uhlíka v rozsadlinách, alebo kontaminácie pórovitých starých sedimentov uhlíkom z prekrývajúcich, mladších sedimentov. Nie je vylúčené, že do depresií boli deponované sedimenty z povrchu v obrátenom poradí tak, ako boli erodované (najskôr mladšie a postupne staršie). Sedimenty si takýmto mechanizmom priniesli aj uhlíky a dnes vidíme obrátený vek. Keďže každá rozsadlina obsahovala jednu alebo viac preliačin, ktoré fungovali ako sedimentačné pasce, v spätnom pohľade by bolo vhodné rádiokarbónové datovanie doplniť luminiscenčným datovaním. V čase realizácie uvedených terénnych prác však táto metóda bola ešte len v plienkach a „projekt Chabenec“ s jej aplikáciou nepočítal.

Datovanie metódou ^{14}C vo všetkých štyroch sondážnych ryhách naznačuje, že v neskorom holocéne nastal posun (v období pred 1 410 až 1 860 rokmi). Najdlhší datovaný záznam v jednej sondážnej ryhe (ryha 2) obsahoval štyri odvodené udalosti posunu počas posledných 6 000 rokov, z čoho je zrejmé dlhodobé opakovanie udalosti s periódou v priemere zhruba 1,5 ka. Tieto štyri udalosti vytvorili protiklonnú rozsadlinu s približne 5 m vertikálnym povrchovým posunom. Kvázi synchrónnosť neskorých holocénnych posunov je v kontraste s inými vo svete známymi lokalitami starých, hlboko založených gravitačných svahových deformácií, kde s narastajúcou nadmorskou výškou sa posuny stávajú mladšími, zrejme v dôsledku relaxácie napätí po ústupe ľadovcov. Takmer synchrónne udalosti posunov vo viacerých nadmorských výškach naznačujú externý spúšťač, či už klimatický, alebo seizmický.

Doručené / Received: 29. 4. 2019
Prijaté na publikovanie / Accepted: 4. 6. 2019

Mineralia Slovaca, Web ISSN 1338-3523, ISSN 0369-2086
51 (2019), 31 – 60,

Outline of the geology of Slovakia (W. Carpathians)

JOZEF HÓK[1], ONDREJ PELECH[2], FRANTIŠEK TEŤÁK[2],
ZOLTÁN NÉMETH[2] and ALEXANDER NAGY[2]

[1]Comenius University in Bratislava, Department of Geology and Paleontology, Faculty of Natural Sciences,
Ilkovičova 6, SK-842 15 Bratislava, Slovakia; hok@fns.uniba.sk
[2] State Geological Institute of Dionýz Štúr, Mlynská dolina 1, SK-817 04 Bratislava, Slovakia

Abstract: The paper provides an overview of the main Alpine and earlier Hercynian (Variscan) tectonic units, as well as superimposed Cenozoic "post-nappe stacking" formations. Simplified localization maps of mentioned tectonic units, lithostratigraphic tables with emphasis on typical lithostratigraphic members and models of the assumed paleogeographical positions are included. References have been selected with an intention to provide more detailed information on a particular issue, resp. tectonic unit. Paper follows dual division of principal tectonic zones into the External (EWECA) and Internal Western Carpathians (IWECA), which reflects different rock composition as well as different time and mechanisms of their structuralization.

Key words: Western Carpathians, tectonics, lithostratigraphy, thrust belt

Graphical abstract

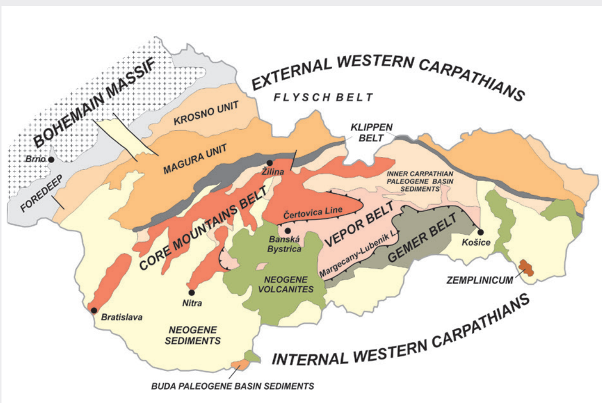

Highlights

- Dual division into External (EWECA) and Internal Western Carpatians (IWECA) is followed after earlier works
- The main Alpine tectonic units in Slovakia are described in the order: EWECA - Outer Group of Nappes (Krosno and Magura nappe systems and Oravicum), IWECA - Lower Group of Nappes (Vahicum and Tatricum), Middle Group of Nappes (Veporicum, Fatricum and Hronicum), Upper Group of Nappes (Gemericum, Turnaicum, Meliaticum and Silicicum), as well as the Zemplinicum with an exceptional status.
- The Upper Cretaceous–Cenozoic sequences are unconformably and transgressively overlying the nappe structures.

Introduction

Information about the geology of Slovakia was published by various authors (e.g. Andrusov, 1968; Maheľ & Buday, 1968; Maheľ, 1974, 1986; Mišík, 1997a; Plašienka et al., 1997; Kováč et al., 2003; Janočko et al., 2006; McCann, 2008; Bezák et al., 2011; Plašienka, 2018). Existing geological maps (Biely et al., 1996a, b; Lexa et al., 2000; Bezák et al., 2004, 2008, 2009; Geologická mapa Slovenska 1 : 50 000, 2013) mostly lack the relevant description of the geological structure of Slovak territory. This contribution provides concise information about tectonics and lithostratigraphy of the principal Alpine tectonic units of Slovakia in a comprehensible form to a foreign reader.

Principal tectonic units of the Western Carpathians – former division based on tectonic belts

The territory of Slovakia is formed by the Western Carpathians. Only southern regions of Slovakia represent a part of the Pannonian Basin system, which extends here from the area of Hungary. The present day geological structure of the W. Carpathians is generally a result of the Alpine orogenic stage, having preserved also remnants of earlier Hercynian (Variscan) evolution.

A tectonic unit is here considered as the three-dimensional rock body with defined borders, its own (unique) lithostratigraphic, metamorphic and structural content and defined tectonic evolution (Fig. 1). Since the second half of 20th century (Andrusov, 1973), the suffix -icum is used

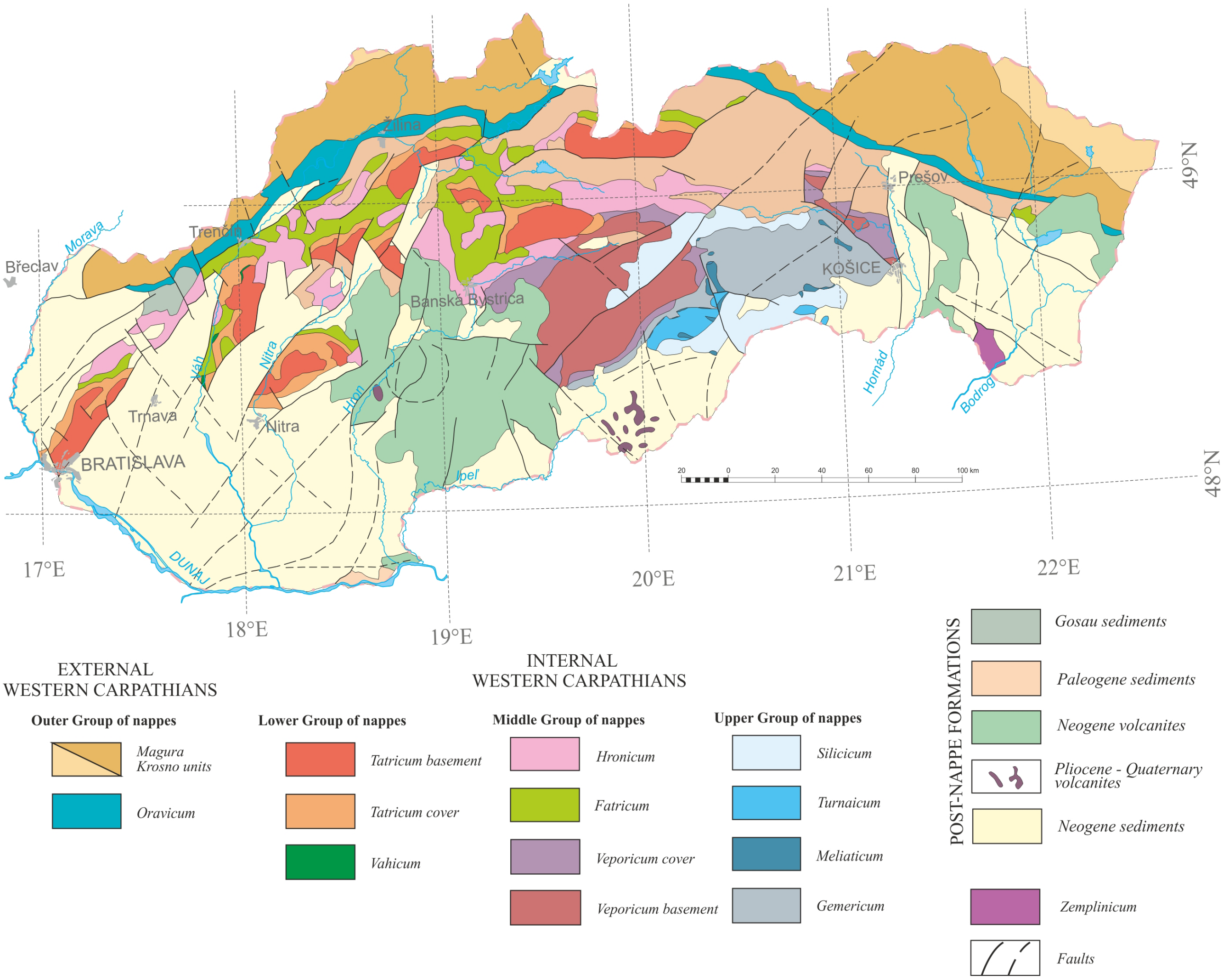

Fig. 1. Position of principal Alpine tectonic units and post-nappe formations in the territory of Slovakia (based on Hók et al., 2014).

for the names of the Western Carpathian Alpine tectonic units.

Tectonic units in the frame of the W. Carpathians are arranged in imbricated structures one above the other, generally thrust from the south to the north (i.e. having northern vergency; Fig. 2). The reason is that the Alpine orogenetic processes produced the horizontal crustal shortening and closed existing sedimentary basins. From the view of recent W. Carpathians it started in the southern – internal regions and proceeded generally to northern – external zones of W. Carpathian belt (Plašienka, 2018).

According to **timing and deformation mechanisms**, the orogenic zone of W. Carpathians is divided into **External Western Carpathians (EWECA)**, containing the Neo-Alpine (Miocene) nappes and the **Internal Western Carpathians (IWECA)** with Paleo-Alpine (Cretaceous) nappe stacking (Fig. 2). The boundary between them is represented by the Klippen Belt zone (Oravicum).

In the Alpine structure of the W. Carpathians, products of the **Hercynian (Variscan) orogenic phase** are preserved in relics, which either were not reworked by the Alpine deformation, or the degree of their Alpine overprint still allows to decipher older tectonic events. The Hercynian structural arrangement suggests the displacement of rock complexes generally from the north to south (or NNW to SSE; i.e. south-vergent). It means that Hercynian orogeny had generally opposite vergency than that of Alpine one (Bezák, 1994; Jacko et al., 1997; Németh, 2002). The main lithotectonic units of the Hercynian (Variscan) tectonic setting were formed due to the Meso-Hercynian lithospheric collision, which was accompanied with a thickening of the crust (380–340 Ma) and intrusion of granitic rocks. Later in the Neo-Hercynian stage (340–260 Ma) the compression was replaced by the extension (probably a post-orogenic relaxation), representing the second period of intrusions of granitic bodies (Broska et al., 2013; Uher et al., 2014). The oldest tectonic events, which for now can be reliably attributed to the Hercynian orogeny, took place during the Early Carboniferous (Mississippian; 360–330 Ma). On the contrary, the sediments of Late Carboniferous

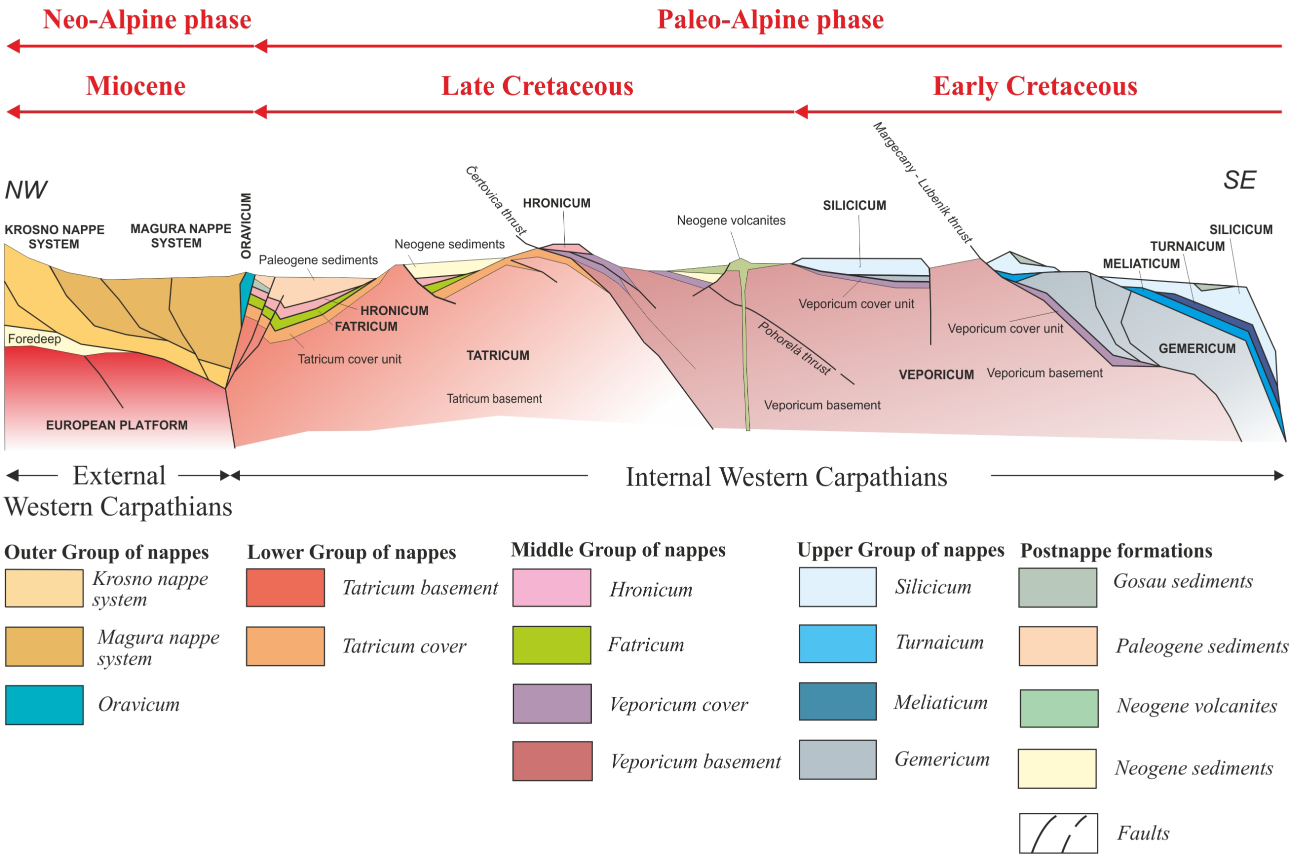

Fig. 2. Schematic cross-section showing the main tectonic units of the Western Carpathians in the territory of Slovakia with marked emplacement timing of particular group of nappes and the age of their tectonic individualization (based on Hók et al., 2014).

age (Pennsylvanian) represent the termination of the Hercynian orogeny in the territory of W. Carpathians. The degree of metamorphic transformation during the Hercynian orogeny can be generally considered to be higher (amphibolite-granulite facies) than during the Alpine tectono-metamorphic processes.

The **Alpine nappe emplacement** in the external zones of the W. Carpathians (EWECA) culminated during the **Neo-Alpine phase** in Neogene, resp. the Miocene. The EWECA include the Flysch Belt, consisting of the Krosno and Magura nappe systems (displaced Cretaceous and Paleogene sediments) as well as the independent Oravic (or Klippen Belt) tectonic units, built of Mesozoic sediments (Fig. 3).

The **Carpathian foredeep** is situated outside the territory of Slovakia (Fig. 3). It consists of autochthonous predominantly sandy and clayey sediments of the Neogene age, lying on their original basement – the European Platform (in their northern part) and Bohemian Massif (northwestern part). Assignment of the external Carpathian foredeep sediments into the W. Carpathian structure is disputable, because they represent autochthonous sedimentary cover of neighbouring basement units.

The **Flysch Belt** of EWECA represents massive accretionary wedge, a nappe stack composed of the Cretaceous and mainly the Paleogene formations in typical "flysch" development, with alternating clayey shales and sandstones, deposited in the deep-water environment by the gravity flows, mostly of the turbidity currents.

The Pieniny Klippen Belt (or the Klippen Belt, **Oravicum**) represents a narrow and intensively deformed belt. Name "Klippen Belt" is derived from their characteristic morphotectonic features – the steep cliffs – so-called klippen, towering above the surrounding soft relief. The "klippen" are composed of Jurassic and Early Cretaceous limestones that are more resistant to erosion than the surrounding Upper Cretaceous and Paleogene marlstones and clayey sediments.

The principal **Paleo-Alpine tectonic units**, internally (i.e. south) of the tectonic unit of Oravicum, are as follows: the Vahicum, Tatricum, Fatricum, Veporicum, Hronicum, Gemericum, Bôrka Nappe, Meliaticum, Turnaicum and Silicicum. These tectonic units, forming IWECA, are traditionally arranged in the higher order zones termed as "belts" (the Core mountains Belt, Vepor Belt and Gemer Belt, Fig. 3).

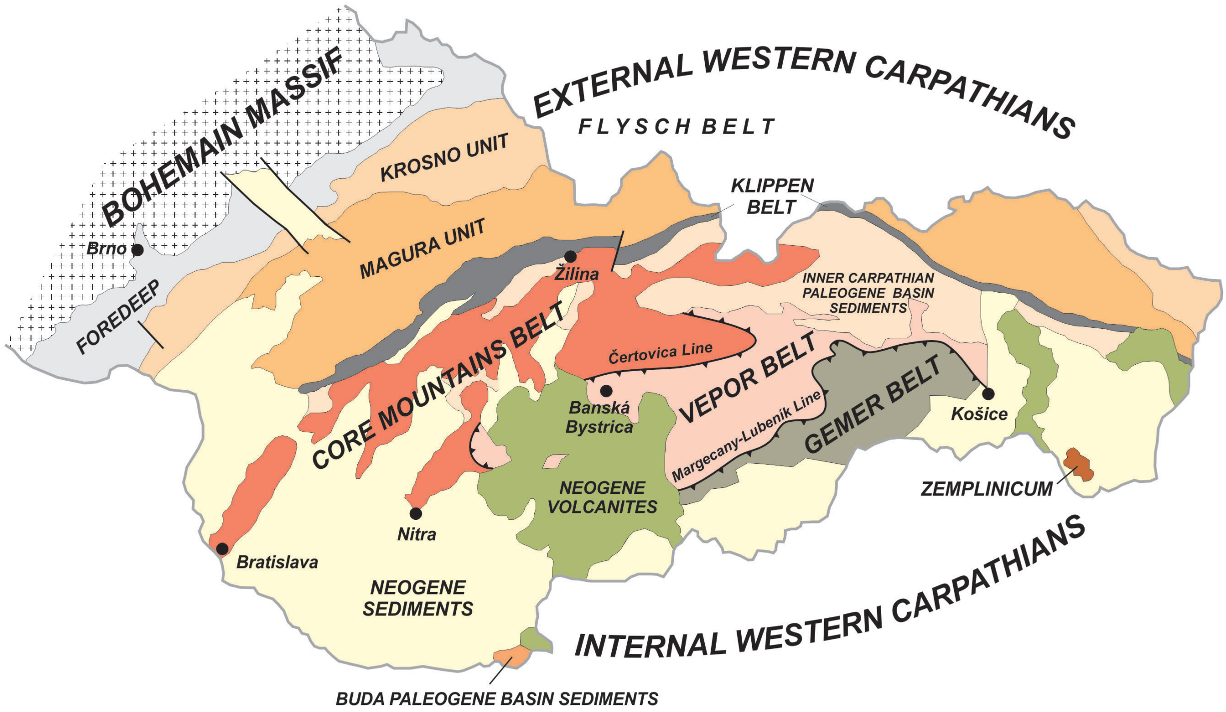

Fig. 3. Division of the Western Carpathians into separate sub-zones and belts (modified after Hók et al., 2001).

The **Core mountains Belt** represents northernmost and the most external tectonic unit of IWECA (Fig. 3). This belt is separated from the south located Vepor Belt by the Čertovica thrust on its southern (internal) margin. The Čertovica thrust is a product of Lower Cretaceous thrusting of Veporicum on Tatricum. The term *Core mountains* (originally Uhlig's (1903) *Kerngebirge*) is derived from the typical morphotectonic phenomenon, where the central part of the mountain range (core) is formed by the crystalline basement rocks (granites and crystalline schists) and these are overlain by the Late Paleozoic and mainly the Mesozoic sedimentary (cover) sequences, and often also directly by the Cenozoic sediments (e.g. in the Malé Karpaty Mts.). Besides Tatricum, tectonic units of the Vahicum, Fatricum and Hronicum are involved in the geological structure of the Core mountains. The Core mountains belt encompasses the Malé Karpaty Mts., Považský Inovec Mts., Žiar Mts., Strážovské vrchy Mts., Malá Fatra Mts., Veľká Fatra Mts., Tatry Mts., western part of the Nízke Tatry Mts. (so-called Ďumbierske Tatry Mts.) and the western part of the Tribeč Mts. (so-called Zobor part; Mazúr & Lukniš, 1986).

The largest part of the **Vepor Belt** is represented by the tectonic unit of Veporicum. Similarly as Tatricum, also the Veporicum is composed of Early Paleozoic crystalline basement and Late Paleozoic–Mesozoic sedimentary cover. Besides the Veporicum, other tectonic units participating in the structure of the Vepor Belt are represented by the Hronicum and Silicicum. The Vepor Belt is separated by the Čertovica thrust from the belt of Core mountains, located northwest, and the Margecany-Lubeník thrust divides it from the Gemer Belt, thrust above the Vepor Belt from the south (Fig. 3).

The Vepor Belt covers large areas of Central Slovakia (Fig. 5) - generally the Veporské vrchy Mts., Stolické vrchy Mts. and the Revúcka vrchovina Highland, eastern part of the Nízke Tatry Mts. (so-called Kráľovohoľské Tatry), northeastern part of the Tribeč Mts. (so-called Rázdiel Part), Kozie chrbty Mts., Branisko and Čierna hora Mts. Apart from the aforementioned regions, the Vepor Belt, or the Veporicum, crops out from below the Neogene volcanites (traditionally named neovolcanites) in the form of so-called "islands" or horsts. The largest horsts are the Sklené Teplice Horst between the towns of Sklené Teplice and Vyhne, the Pliešovce Horst exposed directly in the Pliešovce and the Lieskovec Horst east of the Zvolen town.

The **Gemer Belt** represents the most internal and structurally highest belt in the Alpine nappe structure of the W. Carpathians (Fig. 3). It is located in the Volovské vrchy Mts. and the Slovenský kras Mts. and includes tectonic units of Gemericum, Bôrka Nappe, Meliaticum, Turnaicum and Silicicum.

New tectonic division of the Western Carpathians – combination of tectonic belts and groups of nappes

It is obvious that division of W. Carpathians to External (EWECA) and Internal (IWECA) does not encounter any contradiction, because the tectonic individualization of **External W. Carpathians (EWECA)** took place during the **Neo-Alpine phase in Neogene**, i.e. later than that of IWECA (Paleo-Alpine phase; Cretaceous). EWECA includes Krosno and Magura nappe system and Oravicum. These units are built of Mesozoic to Paleogene sediments, and particularly the Krosno and Magura nappe systems are represented by the "flysch" character deep-water sediments deposited by the gravity flows (turbidity currents). Aforementioned units represent the **Outer group of nappes**, which is present only in **External W. Carpathians (EWECA)** (Fig. 2).

The situation is however more complex internally (south) of the Klippen Belt (Oravicum), where the individualization of **IWECA** took place earlier – in **Cretaceous.** The vertical division, however, raises the question how to lead the boundary between the particular belts in a way not split the same tectonic unit being encompassed in several belts (cf. Andrusov et al., 1973; Maheľ, 1983; Mišík et al., 1985; Plašienka, 1999). The tectonic division based on tectonic stacking of the main elements of the nappe structure, being separated (individualized) at different times on subhorizontal (usually overthrust) contacts, allows to allocate four main groups of nappes (Outer, Lower, Middle and Upper) with different mutual structural superposition and the age of tectonic individualization (Hók et al., 2014; Fig. 1). The subhorizontal division in this case is dominating over the vertical division into belts.

The **Lower group of nappes** of **Internal W. Carpathians** (IWECA) is represented by the tectonic unit of Tatricum, composed of crystalline basement rocks and Late Paleozoic/Mesozoic sedimentary cover, as well as tectonic unit of Vahicum. The Lower group of nappes was structuralized in the late Cretaceous to Paleogene (Figs. 1 and 2).

The **Tatricum** is generally regarded as the lowermost and sub-autochthonous unit of the IWECA. In tectonic superposition above Tatricum there are present several allochthonous tectonic units: the lower unit, or nappe, is called Fatricum, the structurally higher unit is represented by Hronicum. Both tectonic units, Fatricum and Hronicum are ranging here from to the Middle group of nappes, where they belong together with Veporicum.

The **Vahicum** is hypothetical tectonic and paleogeographic unit (Maheľ, 1981). The Belice Unit (Plašienka et al., 1994) in the Považský Inovec Mts. was considered as the main representative of the Vahicum in the present surface occurrences. Structural position of the Belice Unit is, however, in contradiction with previous interpretations (Pelech et al., 2016).

The **IWECA Middle group of nappes** was structuralized during the Late Cretaceous (Cenomanian–Campanian) and is formed by the tectonic units of Veporicum, Fatricum and Hronicum.

The **Veporicum** is predominantly composed of crystalline basement (granitoids, gneisses and mica schists). Based on lithostratigraphy of autochthonous Late Paleozoic and Mesozoic sediments, the Veporicum is divided into Northern and Southern Veporicum, separated by the Pohorelá thrust (Fig. 2).

The **Fatricum** is a tectonic unit of nappe character, transferred from the former position on the contact of the present Veporicum and Tatricum. Synonymously it is often referred as the **Krížna Nappe**. It occurs in allochthonous position in the Core mountains Belt and overlies the Tatricum. Stratigraphic range is very variable, especially in lower members. It is a result of closing of its former sedimentary basin and related decollement with movement of the Fatricum thrust sheet on its stratigraphic members with suitable rheology. Sedimentary sequence usually terminates with the earliest Upper Cretaceous (Cenomanian) "flysch"-like sediments (Poruba Fm.).

The **Hronicum** represents, similarly as the Fatricum, a stack of partial nappe bodies structuralized during Late Cretaceous from the facially subdivided sedimentary basin. Synonymously it is designated as the **Choč Nappe**. It occurs in the Core mountains Belt as well as in the Vepor Belt and overlies the Fatricum and Veporicum. Unlike the Fatricum, the original root area of the nappe is not known, although it is evident that it comes from southerly (more internal) paleogeographic zones than the Fatricum. The Hronicum sedimentary basin was formerly assumed between the Vepor Belt and Gemer Belt. Stratigraphic range of Hronicum is from Carboniferous to the Early Cretaceous. The complete sedimentary sequence is however nowhere preserved. The most typical sequences of Hronicum are composed mainly of Triassic carbonates (limestones and dolomites). Carboniferous and Permian volcanites and sediments represent very characteristic lithostratigraphic members of Hronicum, forming thick rock sequence of the Ipoltica Group.

The **IWECA Upper group of nappes** is located southernmost or most internal, representing tectonically the highest group of nappes of IWECA. It is composed of Paleozoic rock sequences of Gemericum and mostly Mesozoic complexes of the Bôrka Nappe, Meliaticum, Turnaicum and Silicicum as the Early Cretaceous nappe structures (Fig. 2).

The **Gemericum** is exposed in a largescale anticlinal dome – anticlinorium, which forms the region of Volovské vrchy Mts. (the Spišsko-gemerské rudohorie Mts., resp. Spiš-Gemer Ore Mts.). It substantially differs from the other basic W. Carpathian tectonic units by different rock composition, age and metamorphism. Unlike the Tatricum and Veporicum it is composed mainly of the low-grade metamorphic rocks with dominating Paleozoic age – the Early Paleozoic basement and its mostly Late Paleozoic sedimentary cover.

The **Bôrka Nappe** contains rock sequences of Permian to Middle Jurassic age. They are characterized by higher-grade metamorphic overprint, reaching in Mesozoic members the subduction related high-pressure and low-temperature (HP-LT) blueschists facies. The parallelization of the protolith of metamorphites with the cover sequences of southern Gemericum indicates that they are most probably derived from the zone between the Gemericum and Meliaticum (e.g. Németh, 1996, Fig. 4 ibid.).

The **Meliaticum** is a tectonic unit of nappe character, known in present day surface only in relics, cropping out from below the nappes of Turnaicum and Silicicum (Fig. 2). It represents a tectonic melange of Triassic carbonates, radiolarites and volcanites, occurring as blocks in the dark and black Jurassic shales and radiolarites. Sedimentary sequences indicate that it represents former zone of oceanic character. During the convergence, the Bôrka Nappe rocks were subducted and exhumed. Subduction of oceanic crust and the gradual closure of the Meliaticum basin caused the displacement of rock complexes originally deposited at the southern margin of this basin (in today's geographical coordinates) and forming the tectonic units of Turnaicum and Silicicum. Decollement and emplacement of the Meliaticum, Turnaicum and Silicicum nappe units represent the beginning of the shortening of the Internal W. Carpathians. Related thrusting and nappe displacements maintained its polarity from the south (internal areas) to the north since Early Cretaceous (in Gemer Belt) to the Late Cretaceous (in the Core mountains Belt).

The **Turnaicum** represents another nappe unit, cropping out from below the Silicicum (Fig. 2) and occurring in the southern part of the Gemer Belt, mainly in the Slovenský kras Karst plateau. Its Late Carboniferous to Late Triassic rock sequence bears characteristic metamorphic overprint. It differs from the Silicicum by the occurrence of the Triassic pelagic carbonate facies, by this way forming the transitional member between Meliaticum and Silicicum during the basin evolution.

The **Silicicum,** often referred as the **Silica nappe,** is structurally the highest tectonic unit of the IWECA Alpine nappe structure. It occurs as a relatively flat lying nappe body in the region of Slovenský kras Mts., Slovenský raj Mts., Galmus Mts. and Muránska planina Mts. (Fig. 2). The sedimentary sequence of the Silicicum ranges from the latest Permian–Early Triassic to the Late Jurassic (Callovian to Oxfordian). A substantial part of the Silicicum is built by the Middle and Upper Triassic shallow water limestones (e.g. Wetterstein limestones), often containing abundant fossil remains.

Description of the principal tectonic units

The **External Western Carpathians (EWECA)** encompass the Flysch Belt and Klippen Belt (Fig. 4). The sediments of the **Carpathian Foredeep** represent autochthonous Miocene–Pliocene sedimentary cover of the European Platform as well as Bohemian massif and are generally situated below the Krosno nappe system. Re-

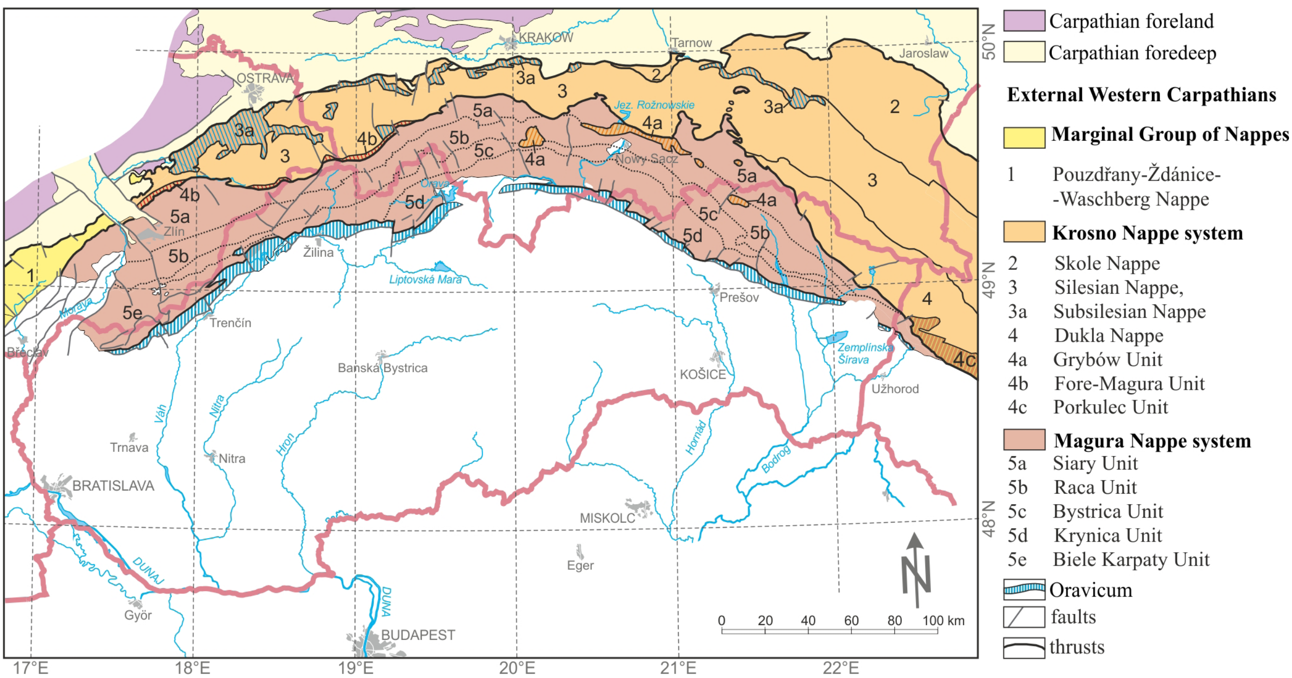

Fig. 4. Map of the External Western Carpathian nappes.

garding its position, the Carpathian foredeep should not to be assigned to the Carpathian system.

Flysch Belt – Krosno and Magura nappe system

EWECA are mostly formed by the Cretaceous to Paleogene deep-sea "flysch" deposits. Original flysch basins were bordered by continental crust ridges, which provided a clastic material to the basins. The Flysch Belt is one of the few zones being continuous across the whole Carpathian arc.

EWECA represents a system of rootless nappes amputated from their former basement and transported to the foreland represented by the European platform and the sediments of Carpathian foredeep.

Flysch Belt consists of several nappe systems arranged in imbricated style – the internal units are thrust over the external ones. Mostly the Magura nappe system occurs in Slovakia, and represents the southernmost part of the Flysch Belt. The underlying Krosno nappe system includes the Dukla, Silesian, Skole and other smaller nappes (see Fig. 4). The lithostratigraphic units within nappe systems are shown in Fig. 5. The Krosno nappe system is generally characterized by variegated claystones, the Magura nappe system by prevailing sandstones.

The sedimentary basins were situated in the area between the IWECA block and the European Platform. Similarly, as the area of the Carpathian foredeep, also the Magura Basin was connected to the west with the flysch foreland of the Eastern Alps (Rhenodanubian Flysch) and similarly to the north and east to the flysch nappes in present Poland and Ukraine (in the Eastern Carpathians). The oldest preserved EWECA sediments are represented by the Upper Jurassic limestones, marls and carbonate flysch. However, it can be assumed that the formation of future Flysch Belt basins is related to the regional extension period in the area of the W. Carpathians, which took place in the Middle Jurassic (Plašienka, 2018). The former sedimentary area of the EWECA was gradually closed since the end of middle Eocene (the Biele Karpaty Unit) up to the early Miocene (the Krosno nappe system). The youngest sediments are represented by the locally preserved Miocene deposits (Karpatian).

Marginal nappe system

The outermost (most external) EWECA unit is Pouzdřany-Ždánice-Waschberg Nappe, not reaching the territory of Slovakia (Fig. 4) and representing the allochthonous body (nappe) over the Bohemian Massif margin.

Krosno nappe system

Several tectono-lithofacial nappes (or units) north of the Magura nappe system form the Krosno nappe system. They are arranged from outer to inner as follows: Skole, Sub-Silesian, Silesian and Dukla (Grybów, Fore-Magura) nappes. Only Silesian and Dukla (Grybów) nappes reach the territory of Slovakia (Lexa et al., 2000).

The Skole Nappe is situated NE in the foreland of Sub-Silesian Nappe on Polish territory, not reaching the territory of Slovakia. The Sub-Silesian Nappe crops out as a thin body on the border of Skole and Silesian nappes. The Silesian Nappe is found in a limited extent in the northern Kysuce region (Potfaj et al., 2002, 2003), where only the Godula succession is present. Sandstone-rich Istebna Fm., Sub-Menilite Fm. with spherically disintegrating Ciężkowice sandstones, Menilite Fm. and Krosno Fm. are typical.

The Dukla Nappe reaches the NE edge of Slovakia. Its sedimentation area was initially associated with the Magura Basin. Younger deposits have affinity rather with the Silesian Nappe. To the west, Dukla Nappe passes into thin bodies of Grybów and Fore-Magura nappes, which underlie the Magura Nappe and crop out in the Smilno tectonic window.

The most characteristic for the Krosno nappe system are the menilite shales or Menilite Formation, composed of brown claystones with bodies of sandstones and black cherts which were formed from diatoms tests during the late Eocene to early Oligocene. Another very characteristic lithostratigraphic unit is the Sub-Menilite Formation of Eocene age, being composed of variegated (red, green and grey) claystones and sandstones. The menilite shales are known as the main oil-bearing horizon across the EWECA.

Magura nappe system

The Magura nappe system is the largest tectonic unit of the EWECA, and represents the main part of the EWECA on the Slovak territory (Cieszkowski, 1992; Lexa et al., 2000; Oszczypko et al., 2015; Kaczmarek et al., 2016). The Magura nappe system is divided into the partial tectono-lithofacial units. In ordering from the north (external units) to south (internal ones) these are the Siary, Rača, Bystrica, Krynica and Biele Karpaty units. Together with the Biele Karpaty Unit, which occurs only in the western part of the zone and has a special status, the Magura nappe system forms tectonically the highest part of EWECA. Moreover, the Krynica Unit was as well backthrust southward over the Klippen Belt (Oravicum) in the Orava region (Pešková et al., 2012).

The rocks of the Magura nappe system have deposited in a few hundred kilometers wide Magura Basin having 2,000 to 4,000 meters depth. The time, when the Magura Basin started to open, has not been reliably confirmed yet, because the nappe is completely detached from its substratum. There is assumed the Upper Jurassic time of its opening (Pícha et al., 2006; Hrouda et al., 2009; Golonka et al., 2013; Oszczypko et al., 2015). Pelagic claystones and thin-bedded "flysch" deposits (Ropianka Fm. and Beloveža Fm.) deposited in the deep-sea environment on the bottom formed probably by oceanic or distal continental crust. Along with thin-bedded deposits the red and green (variegated) claystones, mudstones or marls have deposited especially during the Upper Cretaceous and lower Eocene (Cebula Fm., Ondrášovec Mb. and Lower Beloveža Mb.). Sandy fans and lobes penetrated into the basin and partly also on the slopes of the basin. Clastic turbidity sedimentation dominated since Maastrichtian. Each fan deposited hundreds of meters of sandstones (less conglomerates).

According to petrographic and sedimentological properties, we can distinguish several major types of sandstones in the Magura nappe system: Soláň (Mutne), Szczawina, quartz-carbonate, Riečky, Skawce, glauconitic and Magura type sandstones. The petrographic composition of the sandstones reflects the nature of the source area (ridges/cordilleras). Its sedimentary structures are determined by the nature of the current transport, global temperature and sea-level changes. The Malcov Fm. represents the fill of smaller piggy-back sub-basins. The north-vergent thrusting by the end of Oligocene and in early Miocene until Badenian caused the spatial reduction and the origin of the fold and thrust setting. The boundary of the Krosno and Magura nappe systems in the Moravia is characterized by the occurrence of Jurassic limestones (olistoliths, formerly known as the so-called External Klippen Belt). Dozens of lithostratigraphic units have been determined by the combination of mentioned lithotypes and lithofacies (Fig. 5).

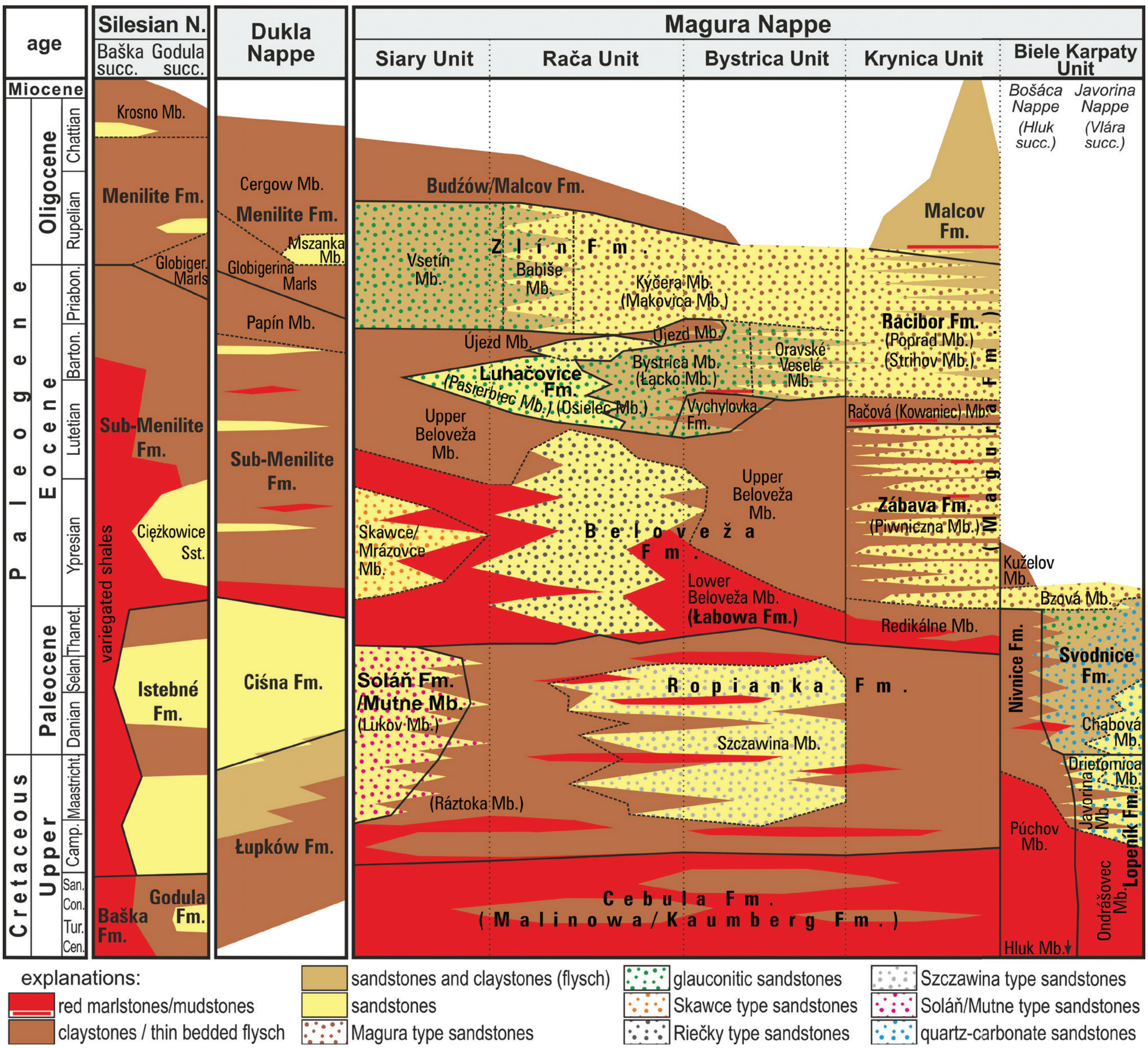

Fig. 5. Simplified lithostratigraphic scheme of the Flysch Belt in the Slovak territory (modified after Potfaj, 1993; Lexa et al., 2000; Teťák et al., 2016).

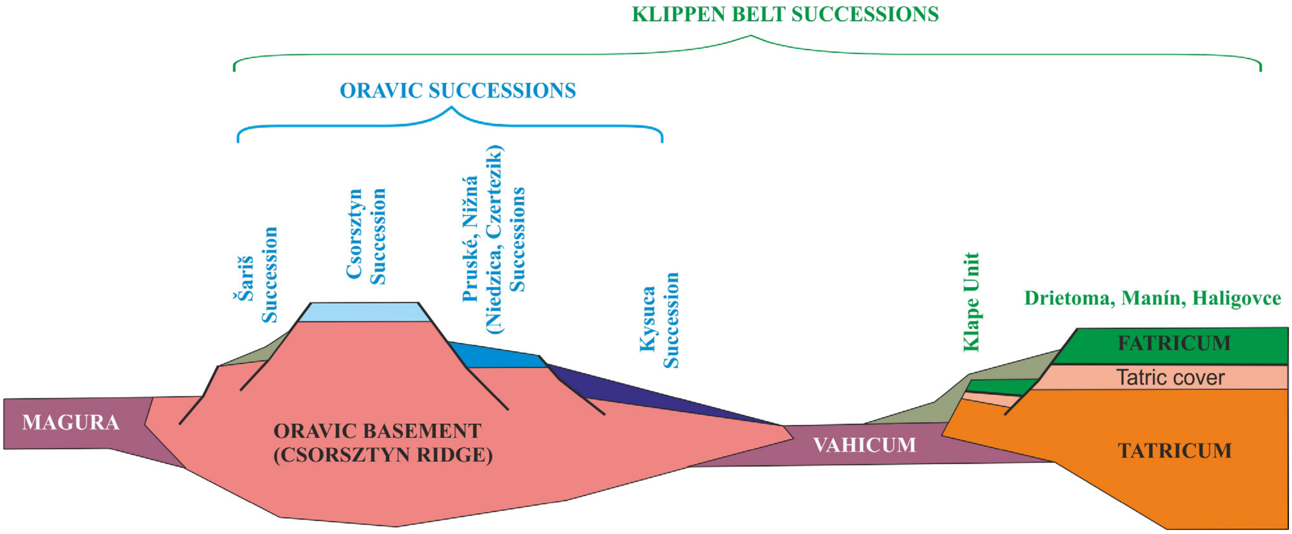

Fig. 6. Supposed paleogeographic position of the Oravic and Klippen Belt sensu lato successions during Jurassic period.

Klippen Belt – Oravicum

The Klippen Belt represents narrow (max. 15 km wide) and more than 600 km long morphotectonic structure on the boundary between the Internal and External W. Carpathians (Figs. 1 and 4). The Klippen Belt contains the Oravic rock successions as well as successions derived from the IWECA (Fig. 5).

The exceptional tectonic complexity and numerous identified rock successions (Mišík, 1997b) and formations (e.g. Birkenmajer, 1977) of the Klippen Belt are related to the fact that it suffered multiphase deformation: for the first time together with the Internal Western Carpathians and for the second time after the Paleogene with the Flysch Belt. Structure was additionally complicated by the strike-slip faults longitudinally segmenting its units. The essential segmentation of sedimentary basins of the future Klippen Belt, similarly as in the case of other W. Carpathian tectonic units, occurred in the Jurassic.

The Oravic units were during the Jurrasic situated in the paleogeographical position surrounding the hypothetical continental ribbon known as the Czorsztyn ridge (Fig. 6). The Czorstyn ridge was separated from the European platform by the oceanic domain of the Northern Penninicum or the Magura ocean in the north, and from the Internal Western Carpathian block by the oceanic domain of the Southern Pennicum or the Vahicum (Plašienka, 2012; Plašienka & Soták, 2015). According to its different facial character, resulting from differing paleogeographic areas, several sedimentary successions were distinguished, incl. the Czorsztyn and Kysuca, as well as the Niedzica/Pruské and Czertezik successions termed as the **Oravicum**.

The most widespread are the Czorsztyn and Kysuca (also Kysuca-Pieniny) successions. They are tectonically amputated and displaced from their former substratum, therefore their sedimentary sequence starts with Lower Jurassic rocks.

The Czorsztyn succession is characterized by generally shallow water sediments. The most typical member is represented by the Czorstyn Limestones (Middle to Late Jurassic) – the red nodular limestones with abundant fossils, especially ammonites. Another typical member is a sandy-crinoidal limestone (Middle Jurassic). The Czorsztyn sequence occurs in the outer – northern margin of the Oravicum/Klippen Belt and represents most externally located sequence among the Klippen Belt units.

The Kysuca succession is typical by Jurassic deep-water sediments – the Allgäu Formation, green and red radiolarites and Pieniny Limestone.

The Czorsztyn and Kysuca successions are typical with variegated (red, green and grey) marlstones (or calcareous claystones) and marly limestones mostly of the Late Cretaceous age. They are known under various local names (e.g. Púchov Marls) and often collectively they are referred as the “Couches Rouges”.

The Klape Unit is present in the Považie (Middle Váh Valley) and Orava regions in the frame of Klippen Belt. The most typical is the flysch formation predominantly of the Late Cretaceous age, containing several characteristic members with exotic material (Orlové Sandstone, Spherosiderite Beds, Upohlav Conglomerates). The Klape sequence is folded together with Klippen Belt main sequences (Czorstyn and Kysuca) and in the majority of occurrences the strata are in an overturned position.

The Manín Unit, known only in the Middle Váh Valley (name is derived from the Manínska tiesňava Gorge), is most internal sequence of the Klippen Belt. The paleogeographic position of the former sedimentary basin is problematic and placed on the northern margin of the Tatricum, as well as on the northern margin of the Fatricum (i.e. southern edge of Tatricum). The most characteristic part of this Early Jurassic to Middle Cretaceous sequence is the Urgonian Limestone (Manín Fm.) – the organodetritic limestone with abundant macrofossils (algae, corals, rudists). With the Manín Unit in the eastern part of the Klippen Belt **the Haligovce Unit** is correlated (Mišík, 1997b).

The Drietoma Unit is a structural element derived from the Fatric nappe system incorporated into the western segment of the Klippen Belt. Typical lithostratigraphic members of the Upper Triassic (Norian) – Lower Cretaceous (Berriasian) Drietoma Unit are the Carpathian Keuper and Allgäu Fm.

The **Internal Western Carpathians (IWECA)** encompass following tectonic units, individualized in the Cretaceous: Vahicum, Tatricum, Fatricum, Hronicum, Veporicum, Gemericum, Bôrka Nappe, Meliaticum, Turnaicum and Silicicum. These units are present in the Core mountains Belt, Vepor Belt as well as the Gemer Belt (Figs. 1 and 3). In the subhorizontal division of W. Carpathians into the separate Alpine groups of nappes, the Vahicum and Tatricum represent the Lower Group of Nappes, the Fatricum, Hronicum and Veporicum represent the Middle Group of Nappes and the Gemericum, Bôrka Nappe, Meliaticum, Turnaicum and Silicicum represent the Upper Group of Nappes (Fig. 1).

The Lower Group of Nappes

The rock complexes of the Lower Group of Nappes (Vahicum and Tatricum), crop out mainly in the Core mountains Belt (Figs. 2 and 7).

Vahicum

The Vahicum is a hypothetical tectonic unit paleogeographicaly situated in the frontal part of the IWECA (Fig. 6) and considered as an equivalent of the Alpine Penninicum (Maheľ, 1981). Supposed oceanic crust of the Vahicum is unknown from the surface presence. Some authors parallelize Vahicum with occurrences of Upper Cretaceous Horné Belice Group (Belice Unit) in the Považský Inovec Mts. (Plašienka et al., 1994). Substantial part of the Horné Belice Group is represented by the Late Cretaceous (Turonian–Maastrichtian) turbidites (“flysch”), with occurrences of olistoliths of crystalline basement, and Early Triassic to Upper Cretaceous sediments (Rakús in Ivanička et al., 2011; Pelech et al., 2016). Similar formations also occur in the borehole SBM-1 Soblahov east of Trenčín (Maheľ, 1985), as well as above Tatric sedimentary cover east of Piešťany (Pelech et al., 2017). The sediments of the Horné Belice Group in the Považský Inovec Mts. are therefore of unclear tectonic affiliation and probably represent a remnant of larger sedimentary wedge-top basin adjacent to the IWECA area (Pelech et al., 2016).

Tatricum

Tectonic unit of Tatricum contains Hercynian crystalline basement rocks (granitoids, gneisses and mica schists), covered by the Late Paleozoic (rarely Carboniferous, more often Permian) and Mesozoic rocks, deposited directly on the basement.

The crystalline basement rocks of the Tatricum were formed by the Hercynian magmatic and tectono-metamorphic processes. Concerning the Hercynian structure, it is not possible to distinguish between the Tatricum and Veporicum crystalline basements, forming during Hercynian orogeny the uniform stabilized unit, later overlapped by cover sequences. The Hercynian tectonics

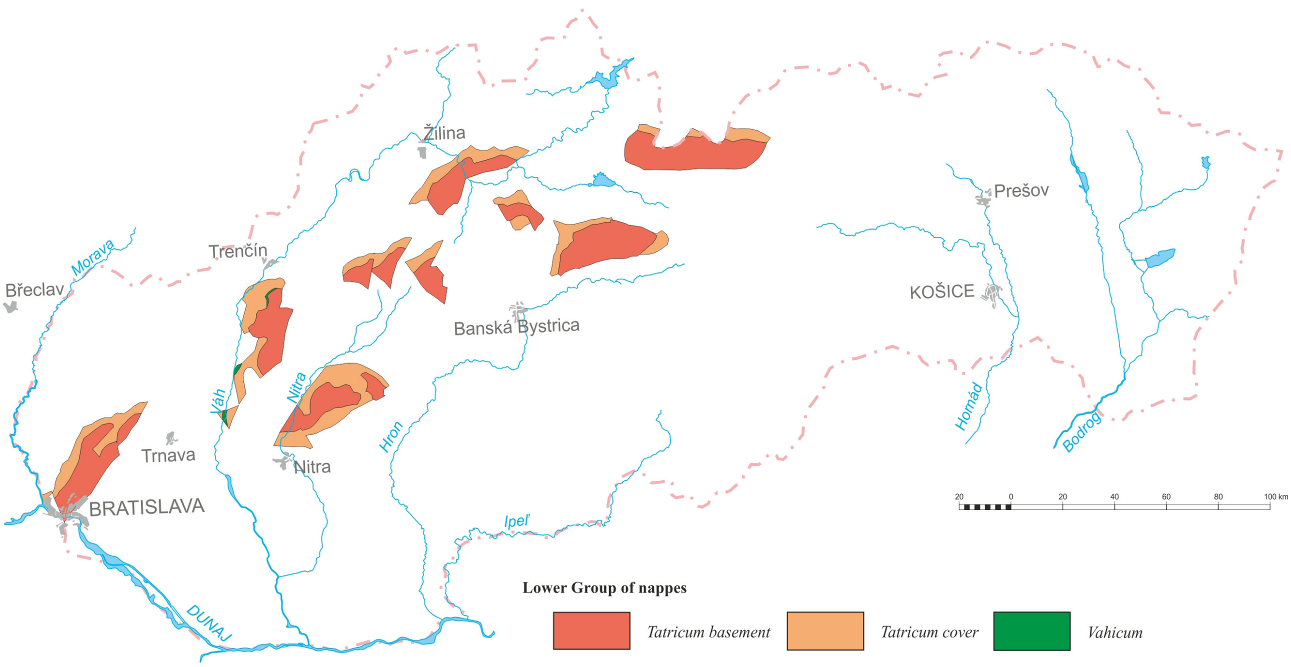

Fig. 7. Position of rock complexes of tectonic units of Vahicum and Tatricum of the Lower Group of Nappes (based on Hók et al., 2014).

had the opposite polarity (south-vergent) than the Alpine one – so being thrust generally from the north to south, the high grade metamorphic rocks were structurally the highest and their relics are today found in the northernmost (most external) part of this unit and *vice versa* – the low grade metamorphic rocks are the lowest and their relics are preserved in the south (Bezák, 1994). The Alpine north-vergent nappes overprinted the pre-existing structure, making the reconstruction of the original position of the Hercynian tectonic units rather complicated (Hrouda et al., 2002). Based on the present state of knowledge, it is possible to reconstruct the Hercynian structure into the following three units (Bezák, 1994):

Upper Lithotectonic Unit (ULU) – composed of high-grade metamorphic rocks (gneisses, migmatites, granitoids and amphibolites) it is present predominantly in the Core mountains;

Middle Lithotectonic Unit (MLU) – forms the substantial part of the Veporicum crystalline basement and consists of gneisses, mica schists and relicts of low-grade metamorphic rocks;

Lower Lithotectonic Unit (LLU) – is present in southernmost zones of the Veporicum and consists of low grade metamorphic crystalline schists.

Lithological composition of the aforementioned units is even more complicated in detail. Lower-grade metamorphic sequences occur within each lithotectonic unit and paragneisses are intruded by granitoid rocks of different ages (Bezák et al., 2004). The Upper Lithotectonic Unit is overlain by a separate complex with characteristic low-grade metamorphic rocks known as the Upper Epizonal Complex (e.g. the Pernek Group in the Malé Karpaty Mts.).

Upper Lithotectonic Unit

Protolith of the ULU metamorphites was represented mainly by greywackes with smaller proportion of sandstones and basic volcanic rocks. These complexes were partly intruded by granitoids, later transformed to orthogneisses.

The reconstruction of the tectonic relationships indicates that these complexes in the highest position are usually overlying the medium-grade metamorphic rocks. It is best seen in the Západné Tatry Mts. (Janák, 1994) and in the eastern Nízke Tatry Mts. The ULU occurs mainly in the Core mountains Belt (Tatry, Nízke Tatry, Branisko a Čierna hora, Malá Fatra, Strážovské vrchy and Považský Inovec Mts.).

The ULU contains also probably Early Paleozoic low-grade metamorphic complexes (greenschist facies; so-called upper epizonal complexes) occurring in isolated occurrences within the higher metamorphic crystalline basement rocks of the Tatricum and Veporicum, having local names according their regional distribution. Locally they overlie the older granites (Klinisko Phyllites on the northern slopes of the Ďumbierske Tatry Mts), or they are affected by the contact metamorphism of nearby granitoids (i.e. being metamorphosed by the heat rising from the granite magma, e.g. Harmónia Series or Pezinok Group in the Malé Karpaty Mts). Other occurrences encompass the metasediments in the Bukovecká dolina Valley on the southern slopes of the Ďumbierske Tatry Mts. and occurrences in the Veporicum crystalline basement – the Jánov grúň Complex, Predná hoľa Complex and the Kraklová Fm.

Middle Lithotectonic Unit

The Middle Lithotectonic Unit is known mainly from the Veporicum (Putiš et al., 1997), however occurs also in several Core mountains as the Malé Karpaty Mts., Považský Inovec Mts. and Tribeč Mts. MLU is built of mica schist to gneiss complexes with amphibolites, locally orthogneisses and minor metaquartzites, graphitic gneisses and metamorphosed sedimentary Fe-ores. Several complexes of the MLU are described from the Northern Veporicum (Hron, Čierny Balog and Kráľova hoľa complexes).

Lower Lithotectonic Unit

The low-grade metamorphic complexes with variegated lithology, assigned to the LLU, occur in the Southern Veporicum (e.g. Ostrá, Klenovec and Sinec complexes), as well as within the Pezinok-Pernek Series (Pernek Group) in the Malé Karpaty Mts.

The vast majority of the Tatricum granitoid rocks are Carboniferous in age. The youngest granitoid rocks are known in the area of Rochovce (Rochovce granite). They are however known only in the sub-surface position, originally due to their contact metamorphism of the surrounding rocks. The 80 Ma age of intrusion was based on radiometric dating (Hraško et al., 1999).

Tatricum sedimentary cover sequences

The crystalline basement was deeply eroded after the end of the Hercynian tectogenesis and the evolving depressions were gradually filled with the Late Paleozoic continental sediments. Carboniferous sediments are known only in the northern Považský Inovec Mts. (Novianska dolina Fm.). The Permian sediments occur in a limited extent in the Malé Karpaty Mts. (Devín Fm.), Považský Inovec Mts. (Kálnica Group), Tribeč Mts. (Skýcov Fm. and Slopňa Fm.), Malá Fatra Mts. (Stráňanský potok Fm.), Tatry Mts. (Meďodoly Fm.) and Ďumbier part of the Nízke Tatry Mts. (Vážna Fm.). They consist of greywackes, arkoses, sandstones and shales of generally variegated colours (red, purple, green). The composition of the sediments and their weak sorting reflects the proximity of the source area (consisting of granites and crystalline schists clasts) and generally short transport (Vozárová & Vozár, 1988).

The Mesozoic sedimentary sequence starts in the Early Triassic and continues with several gaps up to the Late Cretaceous (Cenomanian) with exception of the

Považský Inovec Mts. (Campanian), Tatry and Veľká Fatra Mts., where the sedimentary record ends in the middle Turonian (Pelech et al., 2017 and references herein). The Lower Triassic rocks in the whole Tatricum region are characterized by the quartzites and shales (Lúžna Fm.), which are discordantly overlying the Permian rocks or more often directly the crystalline basement. The quartzites represent the continental sedimentation, being in the Middle Triassic replaced by the marine carbonate sedimentation (Gutenstein Limestone and Ramsau Dolomite). During the Late Triassic the sedimentation continued in shallower lagoonar and continental (terrestrial) conditions. Succession of versicolour sediments (red, violet, yellow sandstones, shales and dolomites) is referred to as the Carpathian Keuper. The latest Triassic (Rhaetian) in the Tatricum region is characterized by a discontinuity in sedimentation. The continental sediments of the Late Triassic are preserved in the Tichá dolina Valley in the Tatry Mts. (Tomanová Fm.), where the footprints of dinosaur were found (see Niedźwiedzki, 2011). Non-deposition and often a significant erosion occurred in the Early Jurassic due to major paleogeographyc changes in the Tethyan region (Plašienka, 2018). In the Middle Jurassic the sedimentation in the Tatricum was divided into two contrasting facies – the deep-water type facies (Fatra type or synonymously Šiprúň type), containing a Middle Jurassic radiolarites, radiolarian limestones and

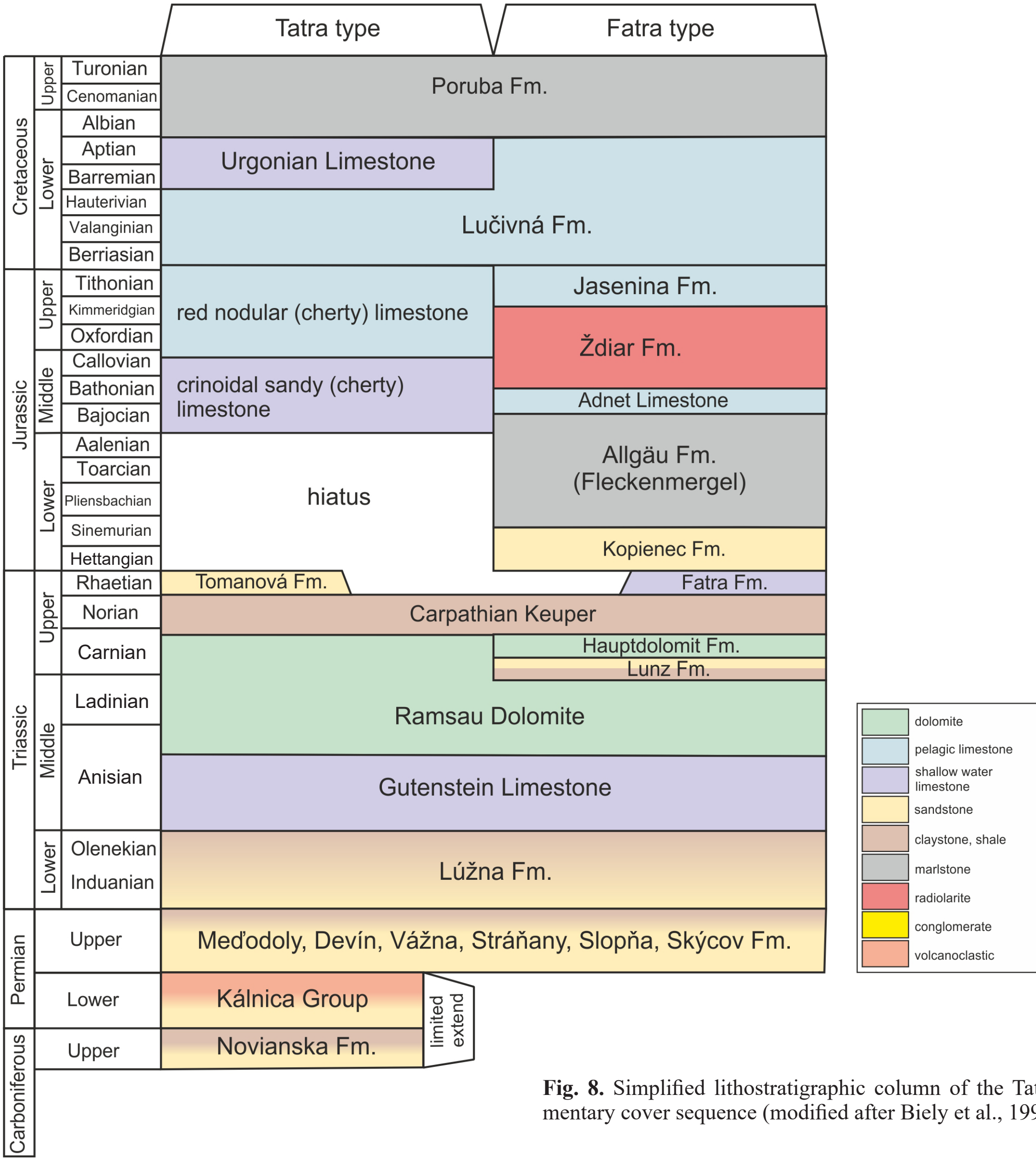

Fig. 8. Simplified lithostratigraphic column of the Tatric sedimentary cover sequence (modified after Biely et al., 1996a).

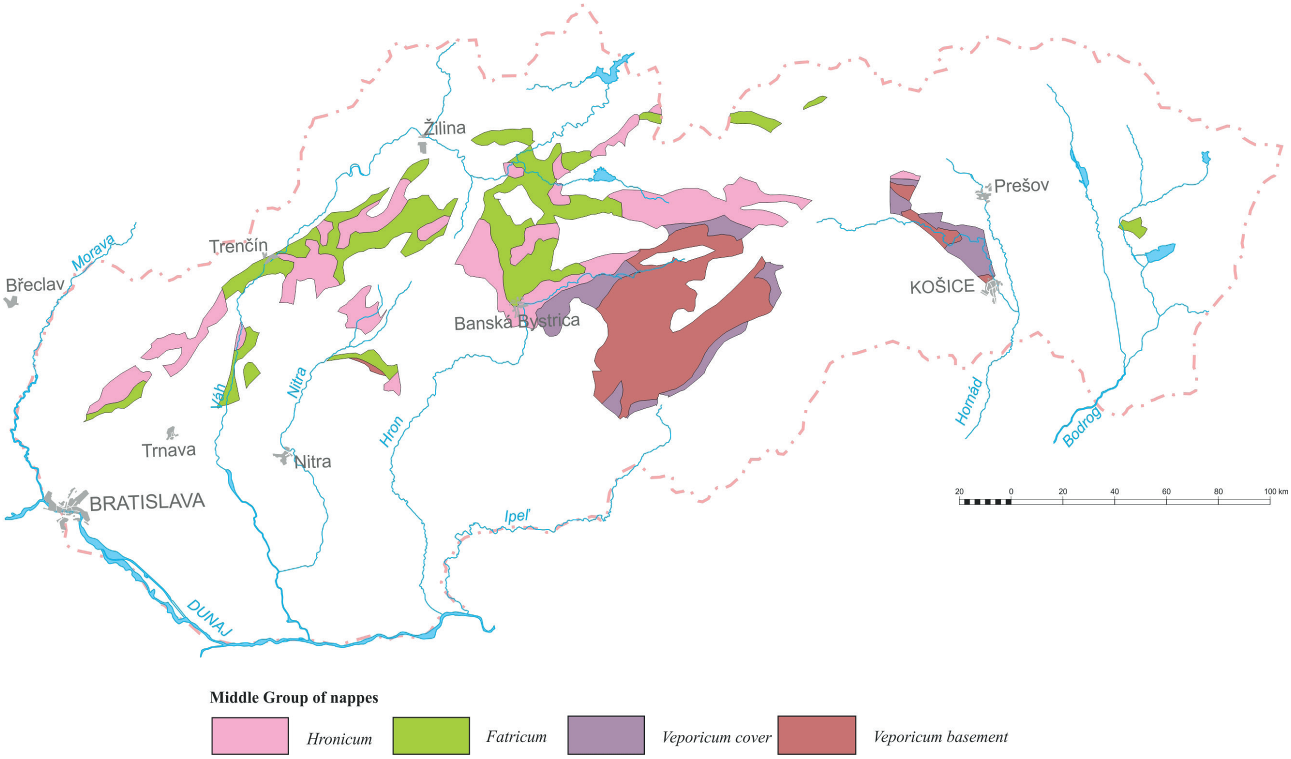

Fig. 9. Position of the tectonic units of Middle Group of Nappes (based on Hók et al., 2014). Dark-red colour indicates position of Veporicum, depicted in Fig. 10 below.

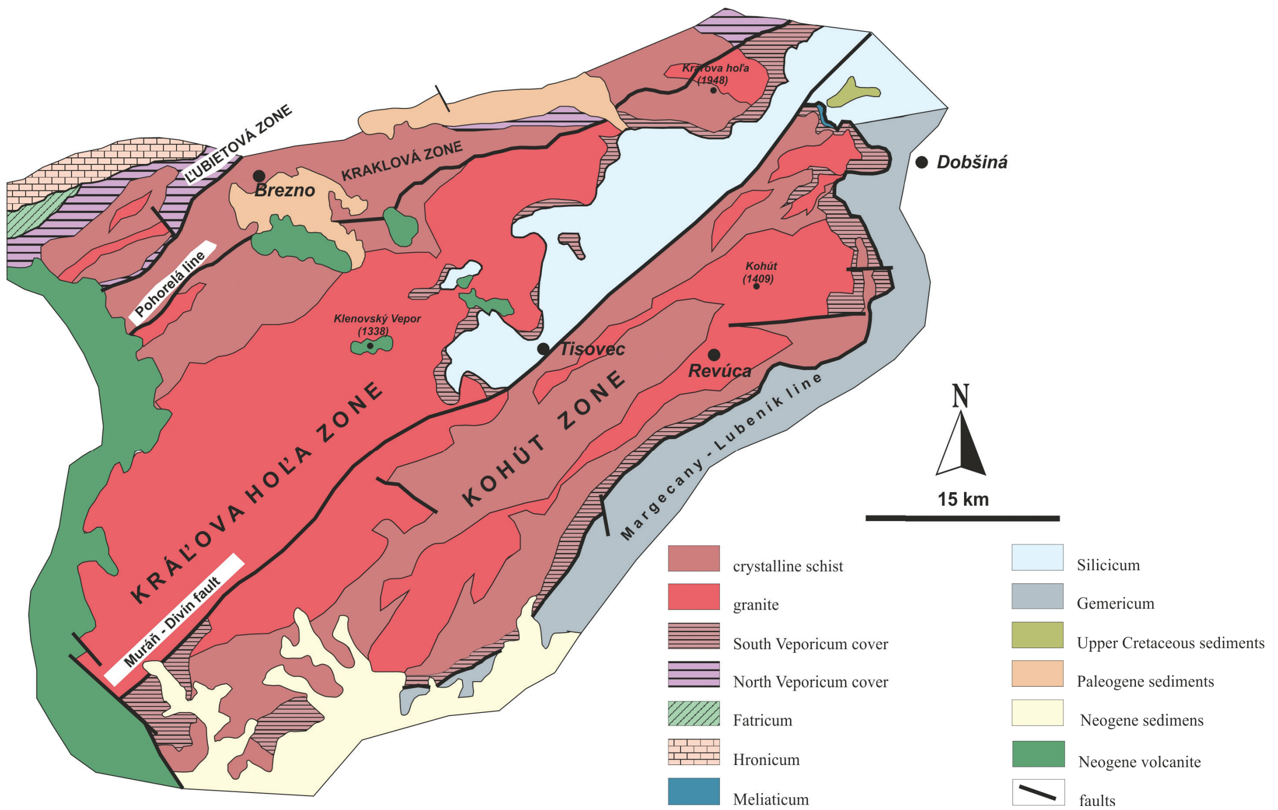

Fig. 10. Tectonic scheme of essential portion of the Veporicum, present in the Veporské vrchy Mts., Stolické vrchy Mts. and Revúcka vrchovina Mts. (modified after Hók et al., 2001).

spotted marly limestones and shales ("Fleckenmergel" – Allgäu Fm.), and the shallow water facies (Tatra type), characterized by the crinoid and sandy limestones (Hierlatz Limestone).

The **Fatra type** of the sedimentary cover sequences occurs in the Veľká Fatra Mts., Malá Fatra Mts., Považský Inovec Mts. and Strážovské vrchy Mts. The **Tatra type** occurs in the Tatry, Nízke Tatry Mts. and Tribeč Mts. Beside the aforementioned basic facial types a number of specific successions occurs in the particular Core mountains. Typical example represent the cover sequences in the Malé Karpaty Mts., among which the Borinka succession exhibits a contrasting difference from all other sedimentary cover sequences (Plašienka, 2012).

The Tatricum was considered structurally as the lowermost tectonic unit in the frame of Alpine setting of Internal Western Carpathians, which is overridden by other tectonic units, forming large-scale nappe structures. The internal structure of the Tatricum itself is however considerably complicated with a wide range of partial thrusts, duplexes in the sedimentary cover sequences, as well as crystalline basement, e.g. fold of Giewont and Červené vrchy in the Tatry Mts., fold of Tlstá in the Nízke Tatry Mts., Žibrica duplex in the Tribeč Mts. The allochthonity (nappe position) of the granitoid rocks forming the Bratislava and Modra bodies was documented in the Malé Karpaty Mts. The granitoid bodies are thrust over the Borinka cover succession. The Borinka sequence is due to its facial difference and the allochthonous position of granitoids considered to be even lower tectonic element than Tatricum (i.e. Infratatricum; Plašienka et al., 1997).

Middle Group of Nappes

The Middle Group of Nappes is represented by Veporicum (crystalline basement and sedimentary cover sequences), which occurs in the Vepor Belt (Fig. 9) and thin-skinned nappes of Fatricum and Hronicum that overlie tectonic units of Tatricum and Veporicum in the Core mountains Belt and the Vepor Belt (Fig. 1).

Veporicum

Veporicum covers significant part of Central Slovakia (Figs. 1, 9 and 10). The Vepor Belt is divided from the Core mountains Belt (Tatricum) by the **Čertovica thrust** and from the Gemer Belt (Gemericum) by the **Margecany-Lubeník thrust**. The Gemer Belt is thrust over the Vepor Belt. The largest part of the Vepor Belt is built by the Veporicum. Other tectonic units involved in the geological structure of the Vepor Belt are represented by the Silicicum and Hronicum. As in the case of the Tatricum, the Veporicum is composed of a crystalline basement and sedimentary cover sequences of the late Paleozoic to Mesozoic age.

Veporicum crystalline basement

The crystalline basement of Veporicum is predominantly composed of specific types of granitic rocks (e.g. Vepor type, Sihla type, Hrončok granite, Čierťaž granite, etc.) and various grade metamorphic rocks (migmatites, gneisses, mica schists and phyllites), which similarly as granites, are designated by local names (Muráň orthogneiss, Klenovec gneiss, Brezina mica schist, etc.). The Veporicum crystalline basement contains relatively well-preserved relics of Hercynian structure. The prevailing part of the crystalline basement is composed of the Middle lithotectonic unit and, contrary to the Tatricum, also the Lower lithotectonic unit with the lower grade metamorphic rocks is present. The geological and tectonic structure of the crystalline basement is very complicated. It is mainly due to the considerable share of Hercynian tectonics and its subsequent significant Alpine overprint. This fact has led in the past to various interpretations of the geological setting, reflecting different levels of knowledge and geological information about the region. Differing interpretations are still widely used today.

Vertical division of the Veporicum was based upon the differing proportion of the individual types of the crystalline rocks and sedimentary cover sequences (Zoubek, 1957). According to this principle the Veporicum was divided (from the south to the north) to the Kohút Zone, Kráľova hoľa Zone, Kraklová Zone and Ľubietová Zone (Fig. 10). The individual zones were thrust above each other or separated by the subvertical faults (e.g. Muráň-Divín Fault, Pohorelá Line). Later on (Klinec, 1966, 1971), revealing the Alpine nappe position of the crystalline complexes, a horizontal division into the Kráľova hoľa and Hron complexes became predominant. The **Kráľová hoľa Complex,** composed predominantly of granitic rocks and high-grade metamorphic rocks (migmatites, gneisses and amphibolites) is lying in the nappe position above the **Hron Complex,** consisting of lower grade metamorphic rocks (mica schists, phyllites).

Veporicum sedimentary cover sequences

It is possible to divide the sedimentary sequences of Veporicum into two distinct successions: the Southern Veporicum sedimentary cover unit (Federáta Unit) and the Northern Veporicum sedimentary cover unit (Veľký bok Unit). The Federáta Unit is present in the Kohút and Kráľova hoľa zones. It covers the southeastern margin of the Veporicum and dips under the Gemericum along the Lubeník thrust and at the same time it forms the substratum of the Muráň Nappe (Silicicum) in the Muránska planina Plateau. The contact zone with corresponding kinematics (thrusting and subsequent unroofing) was proved also in the eastern margin of the Gemer Belt – along the Margecany part of the Lubeník-Margecany thrust zone, forming the mutual contact of the Spiš-Gemer Ore Mts. and Čierna hora Mts. (cf. Németh et al., 2012). The Veľký bok Unit is present mainly in the Kráľovohoľské Tatry (eastern part of the Nízke Tatry Mts.).

The **Federáta Unit** represents complicated system of thrust slices affected by the low-grade metamorphic overprint. The Mesozoic sedimentary sequence ranges from the Lower to Upper Triassic. However, also the Upper Carboniferous and Permian rocks (Revúca Group) are its integral part, often representing tectonically independent thrust slice. The dolomites of the Late Triassic age (Norian) represent the youngest lithostratigraphic member, substituting the rocks of Carpathian Keuper, which represents the most significant difference with regard to the sedimentary sequence of the Northern Veporicum.

The **Veľký bok Unit** is characterized by close linkage to the crystalline basement, lithostratigraphic and tectonic affinity to the Fatricum and sedimentary sequence ranging from Permian to the earliest Lower Cretaceous (Albian). Tectonic position of the Veľký bok Unit, confined to the Fatricum, similarly as paleogeographic location relates to southern margin of former sedimentary basin of Fatricum. During Alpine tectogenesis it was displaced, together with the underlying Veporic crystalline basement above the Tatricum. Its autochthonous position above the northern zones of Veporicum (as the sedimentary cover) was preserved. The Veľký bok Unit is exposed in the zone of direct contact of Tatricum and Veporicum (so-called *root zones of the Krížna Nappe*), for example in the Nízke Tatry Mts. (the Veľký bok sequence), Branisko Mts., Čierna hora Mts. and Tribeč Mts. (Veľké Pole sequence).

Fatricum

The Fatricum (other names: Krížna Nappe, Krížna sequence/series) is an (allochthonous) nappe unit present in the Core mountains Belt above the Tatricum and below the Hronicum nappe. The Fatricum, unlike other thin-skinned nappes, is well identifiable from its root zones to its foreland. The westernmost surface occurrences of the

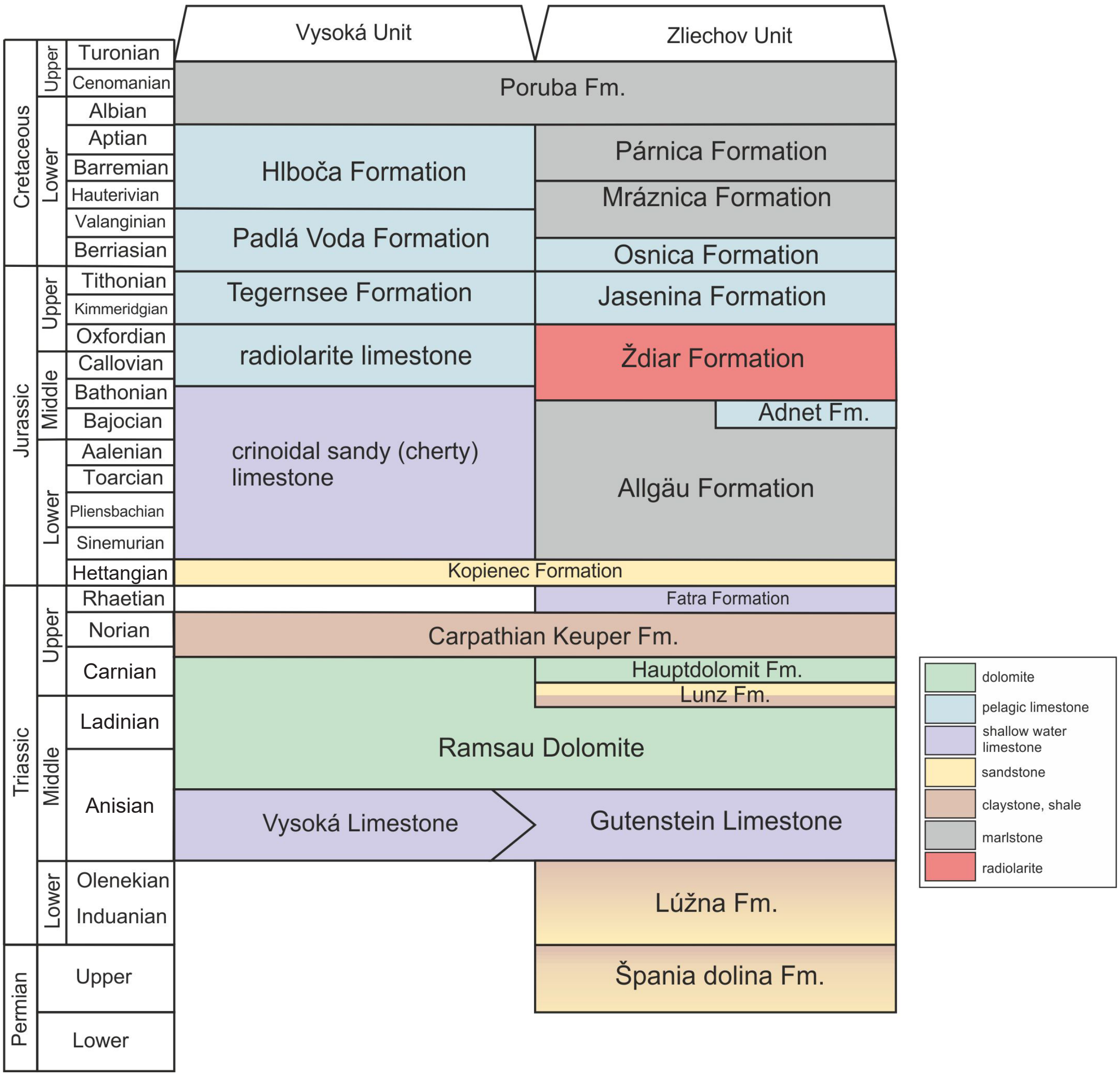

Fig. 11. Simplified lithostratigraphic column of the Fatricum (modified after Biely et al., 1996a).

Fatricum are known from the northern part of the Malé Karpaty Mts., the easternmost ones are known from the Humenské vrchy Mts. Hinterland (internal or southern) zones of the nappe are exposed in the Kráľovohoľské Tatry (eastern part of the Nízke Tatry Mts.), Starohorské vrchy and Tribeč Mts. In this context, often an obsolete term "Sub-Tatric" nappes for the Krížna and Choč Nappes is also still in use (e.g. Jurewicz, 2005; Wolska et al., 2016).

The former sedimentary basin of Fatricum was situated south (internally) of the Tatricum approximately in the area of present tectonically compressed boundary between the Veporicum and Tatricum. Recently, e.g. the Veľký bok Unit is situated in this area.

The rock complexes of Fatricum are composed almost exclusively of sedimentary rocks because the crystalline basement was separated during the nappe emplacement, except the Veľký bok Unit in the Nízke Tatry Mts., Veľké Pole Unit in the Tribeč Mts. and tectonic slices of the Fatricum in the Starohorské vrchy Mts.

Stratigraphic range of Fatricum is from the Lower Triassic to earliest Upper Cretaceous (Albian–Cenomanian). The older Permian rocks are known only from few locations close to the root zone of the nappe. Lithostratigraphy of the Fatricum is entirely similar to that of the Tatricum cover (Figs. 8 and 11). Therefore, characteristic phenomenon with repeating sedimentary successions arises in the Core mountains Belt. The Fatricum is however characterized by the presence of thicker sequences of the Jurassic and Cretaceous age, which are not so well developed in the Tatricum and Hronicum. Another typical sign represents the locally up to 500 m thick formation of Albian–Cenomanian flysch known as the Poruba Formation, which forms the uppermost and at the same time the youngest member of the Fatricum sedimentary sequence. It is usually overlied by the Hronicum.

The Fatricum is usually tectonically divided into two units, distinguished mainly by the lithofacial character of the Jurassic part of the sedimentary sequence.

The **Zliechov Unit**, sometimes referred to as the Krížna Unit s.s. represents deep-water sequence. It is characterized by the presence of the Jurassic spotted limestones and marlstones (Allgäu Formation) and radiolarites (Ždiar Fm.). It represents the spatially dominant part of the Fatricum, usually located above the Vysoká Unit.

The **Vysoká Unit** and its equivalents (Beckov, Belá, Ďurčiná and Iľanovo units) represent shallow-water sequence characterized by the presence of Jurassic crinoidal and sandy-crinoidal limestones (Hierlatz Formation).

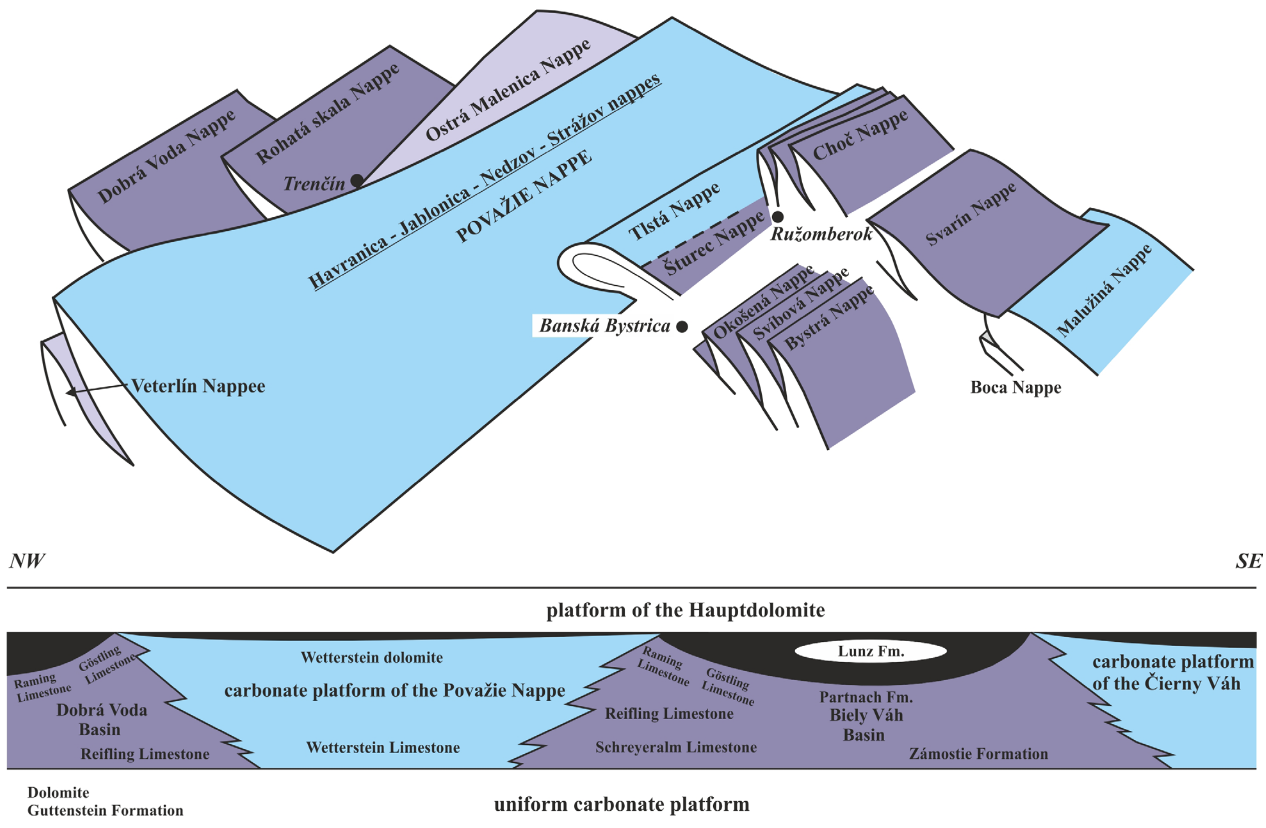

Fig. 12. Schematic cross-section showing position of the Triassic sediments arranged in partial nappes system across the sedimentary basin of the Hronicum (according to Havrila, 2011, simplified).

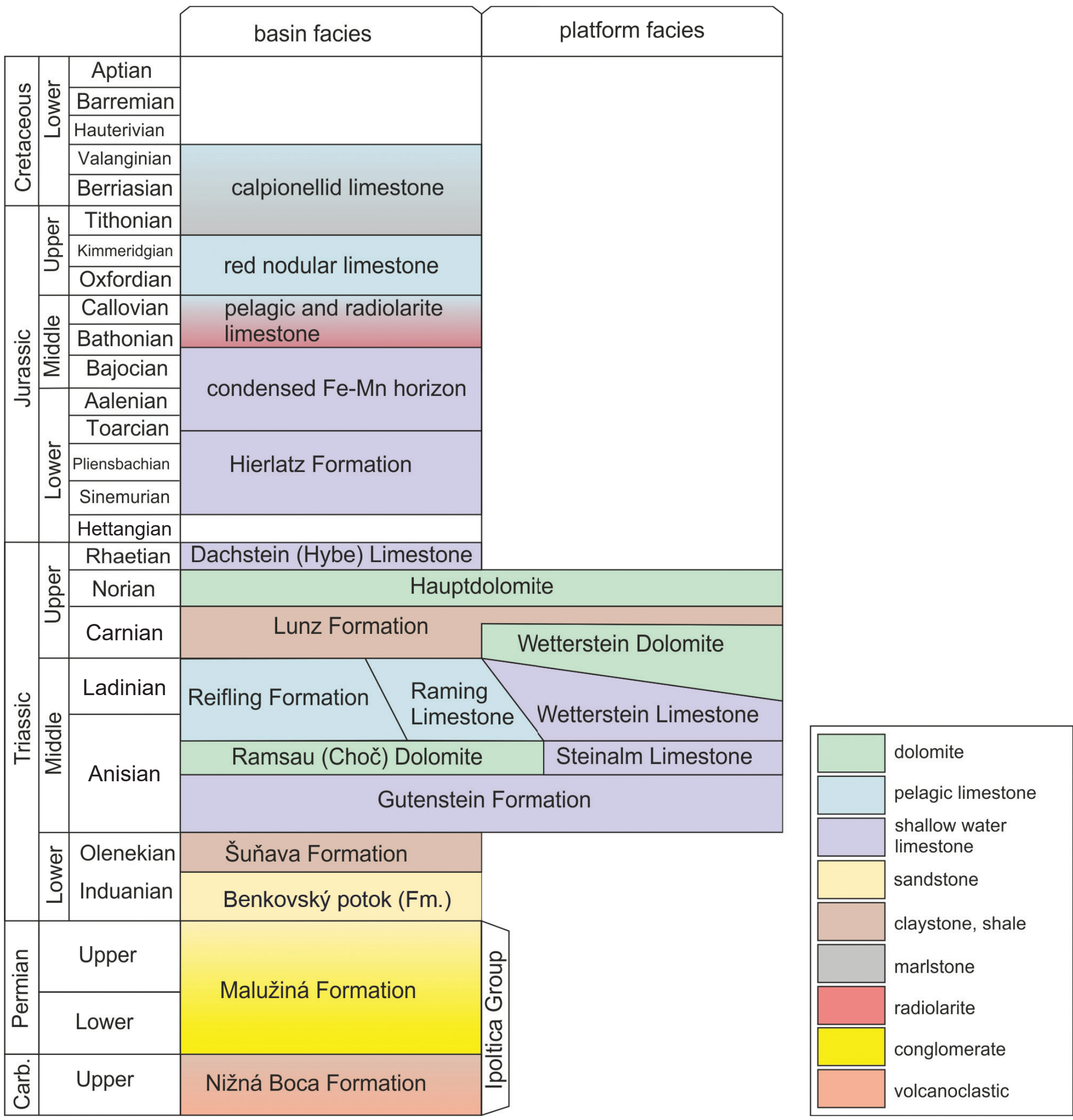

nplified lithostra-
ın of the Hronicum
Biely et al., 1996a).

Fatricum shallow-water units are spatially less significant than in the Zliechov Unit and are usually located in its footwall.

Hronicum

The Hronicum (syn. Choč nappe, formerly Upper Sub-Tatric nappe) represents structurally the highest nappe in the Middle Group of Nappes located above the Fatricum and Veporicum. Occurrences of the Hronicum are limited to the Core mountains and Vepor belts. It crops out in the Malé Karpaty Mts., Považský Inovec Mts., Tribeč Mts., Strážovské vrchy Mts., Žiar Mts., Malá Fatra Mts., Chočské vrchy Mts., Veľká Fatra Mts., Vysoké Tatry Mts., Nízke Tatry Mts., Branisko Mts. and Čierna hora Mts. Presence of the Hronicum was proven in deep boreholes of the northeastern part of the Slovak sector of the Vienna Basin under the sediments of the Neogene age. In several areas of the internal Western Carpathians, the Hronicum is tectonically imbricated into the system of partial nappes (Fig. 12).

Hronicum rock complexes stratigraphically range from Late Carboniferous to Early Cretaceous. Jurassic and Cretaceous sediments are, however, eroded and occur only in the Brezovské Karpaty and Čachtické Karpaty Mts., Strážovské vrchy Mts. and on the northern slopes of the Nízke Tatry Mts.

Characteristic feature of the Hronicum is the presence of Late Carboniferous and Permian volcano-sedimentary formations included in the **Ipoltica Group**, formerly known also as the Melaphyre Series (Vozárová & Vozár, 1979). It forms basal part of the nappe that is present predominantly across the more internal (southern) zones of the Hronicum occurrence. In the north, the Hronicum sequence usually starts with the Triassic carbonates.

Another characteristic feature is the alteration of shallow water and deep water lithofacies during the Middle

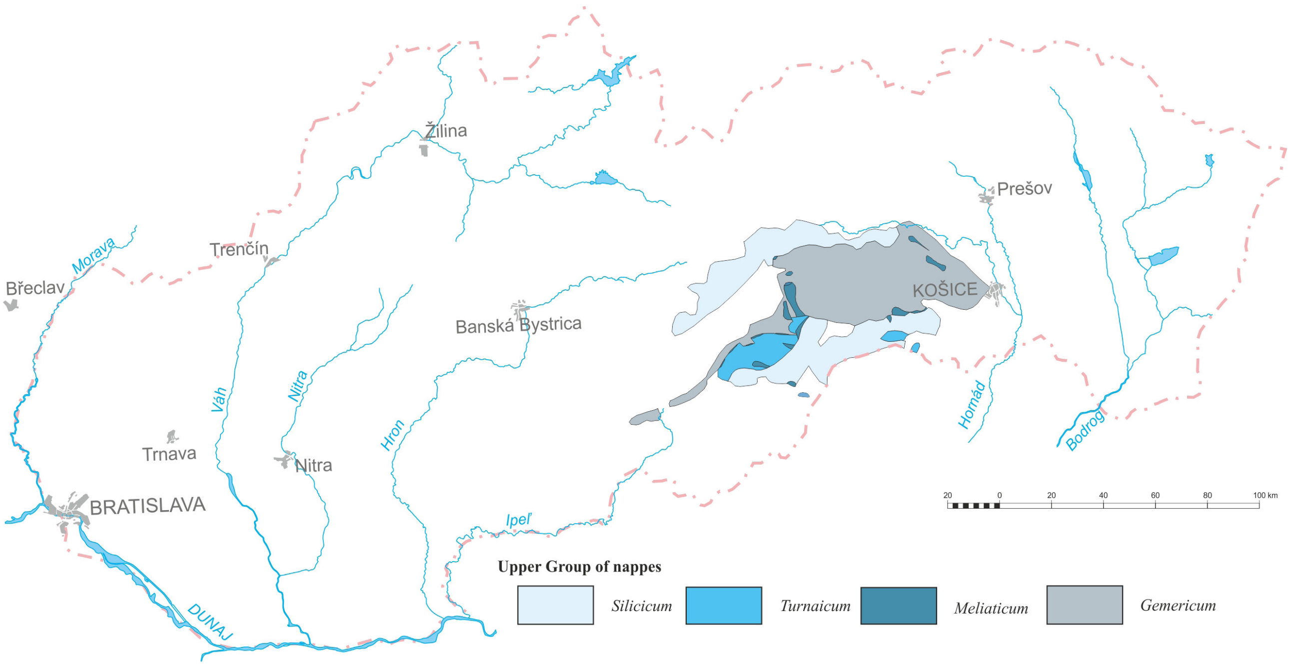

Fig. 14. Position of the Upper Group of Nappes (based on Hók et al., 2014).

Triassic (Fig. 12). The shallow water, reefal and lagoonal facies are represented by Wetterstein limestones and dolomites, which build Mojtín-Harmanec and Čierny Váh carbonate platforms. The deep-water facies are represented by Zámostie, Reifling and Schreyeralm limestones, forming Dobrá Voda and Biely Váh intra-platform basins. The Upper Triassic of Hronicum is characterized by levelling of basins and carbonate platforms and deposition of the Lunz Formation (Fig. 13), which thickness is much greater above the regions with basinal facies (Dobrá Voda and Biely Váh) than above the former platform areas. The Lunz Beds are overlain by thick Main Dolomite (Norian) – another characteristic and widespread lithostratigraphic member of the Hronicum.

Structuralization of the Hronicum occurred during the early Cretaceous and continued during the late Cretaceous and Paleocene, as it is confirmed by the boreholes in the Vienna Basin (boreholes of the Lakšárska Nová Ves series). The Triassic lithostratigraphy of the Hronic nappes system is in most of members similar to the Tirolic and Bajuvaric nappe system in the Northern Calcareous Alps (Janoschek & Matura, 1980; Piller et al., 2004).

Upper Group of Nappes

The Upper Group of Nappes is represented by the tectonic units of Gemericum (low grade metamorphic rocks and cover sequences), Meliaticum and Turnaicum nappes, that are occurring in the Gemer Belt and Silicicum nappe which is found in Vepor and Gemer belts (Figs. 1 and 14). The tectonic units of the Upper Group of Nappes occur in regions of Volovské vrchy Mts., Slovenský kras Plateau, Spišsko-gemerský kras Plateau (Muránska planina Plateau and Slovenský raj Mts.) and eastern part of the Revúcka vrchovina Mts. The Upper Group of Nappes is tectonically superimposed above the Middle Group of Nappes, in particularly over the Veporicum unit. It represents the highest structural element of the Alpine structure of the Internal Western Carpathians, being structuralized already during the Jurassic–Early Cretaceous transition (Fig. 2).

Gemericum

The Gemericum forms an extensive anticlinorium (Fig. 1) of the Volovské vrchy Mts. It differs from the rest of the W. Carpathian main tectonic units due to its rock composition, age and metamorphism (Grecula, 1982; Vozárová & Vozár, 1988; Vozárová, 1993). In contrast to the Tatricum and Veporicum the Gemeric Hercynian (Variscan) basement is on the surface composed by the low-grade metamorphic rocks mostly of Early Paleozoic age, with locally present Permian granitic rocks (Radvanec et al., 2009), volumetrically representing an important part of the tectonic unit according to the geophysical investigation (Šefara et al., 2017). Granitic rocks were during Alpine tectogenesis thrust northward as rigid blocks together with their surrounding lithology. The granites reach surface in Betliar, Hnilec, Poproč and Zlatá Idka localities.The Gemeric basement consists of three principal groups differing in lithology and metamorphic grade. The amphibolite facies metamorphic conditions are reported from the **Klátov Group** (Faryad, 1990), representing Variscan dismembered metaophiolite suite (Radvanec et al., 2017) and recently occurring in tectonic slices and fragments along the eastern and northern boundary of the low-grade Early Paleozoic complexes of Gemericum. The

Rakovec Group (formerly also "Phyllite-diabase Series") is in contrast composed of mafic rocks and their derivatives, mostly metabasalts, tuffs and tuffites, present mainly in the northern Gemericum (Fig. 15). Other sedimentary rocks are less common (Ivan, 1994). The age of the Rakovec Group is probably Devonian to Early Carboniferous, as the overlying Late Carboniferous sediments contain clasts of Rakovec Group rocks. Basalts are related to sub-marine volcanism and the occurrence of pillow-lavas was interpreted by Hovorka et al. (1988). According to other interpretation (Radvanec & Németh, 2018) some of them represent exhumed metagabbros, present along the axis of Variscan suture zone, which is evidenced also by structural and petrological findings, as well as occurrences of exhumed blocks of Variscan ultra-high pressure metamorphic rocks. The suture character of Rakovec Group is a product of collisional closure of the basin in Westphalian (Pennsylvanian: Kasimovian; Late Carboniferous; Németh, 2002; Radvanec & Németh, 2018). **The Gelnica Group** builds a substantial part of the Gemericum (Fig. 15) and morphologically occupies vast part of the Volovské vrchy Mts. The lower part of this unit consists of a thick turbiditic sequence of Ordovician-Early Devonian age with interbeds of bimodal volcanic rocks, gradually passing into volcanosedimentary sequence accompanied by products of massive rhyolite-dacite volcanism of the Late Devonian age (Grecula, 1982; Ivanička et al., 1989; Grecula & Kobulský, eds., 2011). On the basis of lithofacial and lithostratigraphic analysis, three formations were defined within the Gelnica Group from the bottom upwards: the Vlachovo Fm., Bystrý potok Fm., and Drnava Fm. (Ivanička et al., 1989). According to lithostratigraphy by Grecula (1982 and following works), reflecting the revealed Early Paleozoic riftogenesis within the pre--Hercynian (pre-Variscan) continental crust, the Betliar Fm., Smolník Fm. and Hnilec Fm. were distinguished.

More recent concept divides the Gemericum according to character of the sedimentary cover sequences into Northern Gemericum and Southern Gemericum (Vozárová & Vozár, 1988).

The Northern Gemericum is composed of **Rakovec** and **Klátov groups**. Their sedimentary cover is composed of numerous formations with their specific evolution, position and age. The Early Carboniferous sequences are represented by the **Ochtiná Group** of Gemericum with **Črmeľ Formation** in its eastern side (Vozárová, 1996).

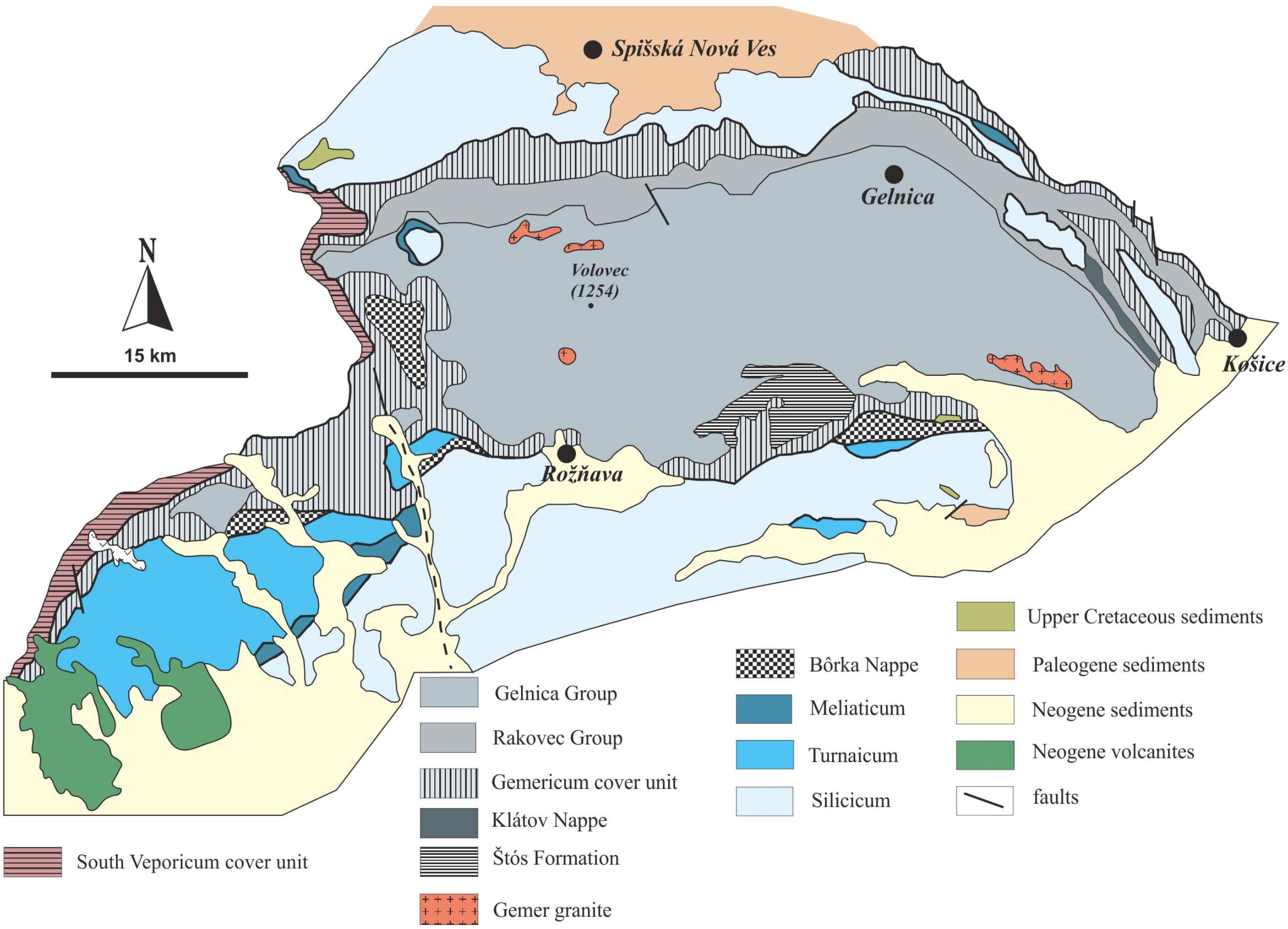

Fig. 15. Simplified tectonic scheme of the Gemericum and surroundings (modified after Hók et al., 2001).

They both represent volcano-sedimentary units with important deposits of magnesite (so called "*Magnesite-bearing Carboniferous"*). The cover Permian rocks of the **Krompachy Group** are typical by the presence of coarse-grained conglomerate material, sandstones and variegated shales (Knola and Petrova hora fms.). Conglomerate composition suggests that the source area was in the former Gemericum. The late Permian–early Triassic overlying sequences were deposited in lagoonal environment – evaporites and shales of the Novoveská Huta Fm. **The Southern Gemericum** is composed of Gelnica Group rocks and Štós Fm. The **Štós Formation** (Fig. 15) is mostly represented by the metamorphosed sandstones, phyllites (formerly probably shales), rarely also bodies of metabasalts. The pre-Permian age of the Štós Fm. is proved by geological data and the occurrences of the Štós Fm. rock fragments in Early Permian conglomerates (Vozárová et al., 2014). The cover of the Southern Gemericum is represented by the **Gočaltovo Group**.

Besides two generations of thrust systems (Variscan and Alpine), double unroofings (Permian and Late Cretacesous; Németh et al., 2016), the spectacular tectonic structure, overprinting the pre-Mesozoic metamorphic fabric of the Gelnica Group as well as in its NE margin also Rakovec Group, is the Gemericum Cleavage Fan. The cleavage forms an asymmetric positive fan structure developed transversally across the entire length of the Gemeric unit (Lexa et al., 2003). As recent investigations manifest, this cleavage fan trending NE-SW is a product of sinistral transpressional shearing (Transgemeric shear zone), and representing a conjugate system to dextral shear zones trending NW-SE (Grecula et al., 1990; Németh et al., 2012, Fig. 3 ibid).

Bôrka Nappe

The Bôrka Nappe was formerly considered as a part of Meliaticum. At present it is distinguished as a separate tectonic unit (however, not without doubts). It includes rock sequences of Permian to Jurassic age characterized mainly by the subduction-type higher metamorphic overprint (HP-LT) in comparison to other surrounding tectonic units. The Bôrka Nappe rock complexes are typical with the crystalline limestones (marbles) with volcanogenic admixture (Dúbrava Fm.) with evidences of blueschists facies metamorphism (Mello et al., 1998).

Meliaticum

The Meliaticum is a tectonic unit (mélange) of nappe character, known also from the territory of Austria (Kozur & Mostler, 1992). It occurs in relics emerging from below the Turnaicum and Silicicum nappes in the present-day surface (Fig. 15). Occurrences of Meliaticum are represented by the tectonic mélange of the Triassic carbonates, radiolarites and volcanic rocks, found within the grey shales and radiolarite beds of Jurassic age (Mock et al., 1998). Oceanic domain of former Meliaticum was closed during late Jurassic and early Cretaceous. Subduction of the oceanic crust and gradual closure of the sedimentary basin resulted in the north-vergent tectonic transport of rock complexes, originally deposited at the southern margin of this oceanic realm. According to present knowledge, north-vergently displaced rock complexes were later transformed into the Turnaicum and Silicicum nappes. Simultanously, the rock sequences of the future Bôrka Nappe, probably located between the Gemericum and Meliaticum, were pulled into the subduction zone. The detachment of Meliaticum, Turnaicum and Silicicum started the shortening of Internal Western Carpathians while preserving the polarity of the tectonic transport from the south (from the inside) to the north during the Early Cretaceous (the Upper Group of Nappes) to the Late Cretaceous (the Lower Group of Nappes).

Turnaicum

The Turnaicum is tectonic unit of nappe character exposed from below the Silicicum (Lačný et al., 2016). It occurs in the southern part of the Gemer Belt, mainly in the Slovenský kras Mts. The Late Carboniferous-Late Triassic sedimentary sequence of Turnaicum is characterized by metamorphic overprint and deep-water Triassic carbonate facies, distinguishing it from the Silicicum. The most characteristic member are the Upper Triassic (Carnian–Norian) grey nodular limestones (Pötschen Limestone) and grey shales with intercalations of volcanic rocks and sandstones of Middle Triassic age (Dvorníky Formation).

Silicicum

The Silicicum is structurally the highest tectonic unit of the Alpine nappe structure of the Internal Western Carpathians (Mello, 1979). It is exposed as relatively flat-lying nappe body in the Slovenský kras Mts., Slovenský raj Mts., Galmus and Muránska planina Mts. Similarly, as the Hronicum unit, also Silicicum was formerly divided into several partial nappes (the Silica, Muráň and Besník nappes). Now they are considered as erosional relics of one larger nappe – Silicicum (often called as the Silica Nappe *sensu lato*). Sedimentary sequence of Silicicum starts in uppermost Permian or lowermost Triassic and continues up to Upper Jurassic (Callovian–Oxfordian). The Lower Triassic has similar development as in the Turnaicum and is represented by the sandstones and shales (Fig. 16). Major part of the Silicicum is formed by the Middle–Upper Triassic shallow-water carbonates (mainly Wetterstein Limestones). The sparsely preserved Jurassic deposits form the youngest part of sedimentary sequence and characterize the deeper water environment. The vergence or sense of nappe displacement of Silicicum is still a matter of debate. Former concept presumed that Silicicum was transported together with the Hronicum from the present-day Margecany-Lubeník zone, whereby the Hronicum was transported to the north and Silicicum to the south (Mišík et al., 1985). Present model prefers an

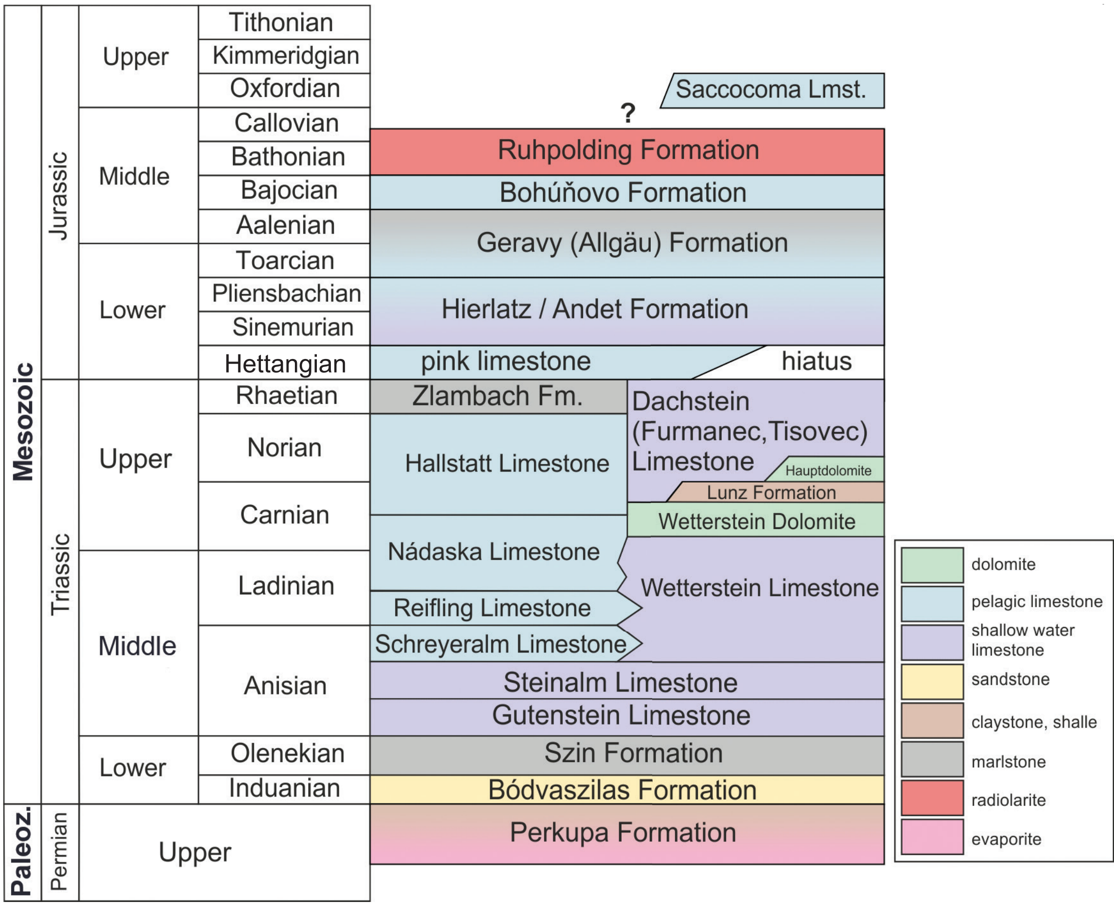

nplified lithostra-
um of the Silici-
ed after Biely et
l Rakús & Sýkora,

interpretation that the tectonic transport of the Silicicum was northward from the South Gemeric zone (Plašienka, 2018). Silicicum is overlain by the locally preserved Upper Cretaceous ("Senonian") Gosau type sediments. Principal Triassic lithostratigraphic members of the Silicicum are resembling Juvavic nappe system.

Zemplinicum

Zemplinicum represents a tectonic unit occurring in the Zemplínske vrchy Mts. in the southeastern Slovakia (Slávik, 1976; Fig. 1). Its tectonic assignment is not satisfactorily resolved (Vozárová & Vozár, 1988; Grecula & Együd, 1977; Plašienka et al., 1997). The Zemplinicum is composed of high-grade Hercynian basement overlain by continental sediments of Carboniferous with coal seams and by Permian continental clastic red beds with acid volcanics. Overlying formations are represented by Lower Triassic quartzites and Middle Triassic carbonates. Correlation of the Zemplinicum with surrounding units is intricate, due to thick Neogene sedimentary cover as well as the nature of the East Slovak Basin pre-Neogene basement. Deep boreholes reaching the pre-Neogene basement suggest the presence of metamorphosed Jurassic to Paleogene succession (so called Iňačovce-Kričevo Unit). The Iňačovce-Kričevo Unit was correlated with the Belice Unit of the Považský Inovec Mts. (i.e. Vahicum, Plašienka et al., 1995) and both were together considered as equivalent of the Penninicum. Later (Plašienka & Soták, 2015), there was inferred that the Iňačovce-Kričevo and related units continue from the subsurface of the East Slovak Basin to the Pannonian Basin basement along the Mid-Hungarian fault zone (Sava-Szolnok Belt) to the Dinaridic Sava Zone (see also Schmid et al., 2008). Due to the presence of the Iňačovce-Kričevo Unit, the tectonic affiliation of the Zemplinicum becomes even the more obscure and complicated.

Post-nappe stacking formations of the Western Carpathians

All rock formations of the Late Cretaceous (Coniacian–Maastrichtian) and Cenozoic age are in the Internal Western Carpathians traditionally considered as the "post-nappe stacking" formations. They are unconformably and transgressively overlying the nappe structures. Later research, however, points to fact that mainly in the external parts of the Internal Western Carpathians the sediments of Late Cretaceous and Paleogene age are folded together with their substratum (Hók et al., 2016; Pelech et al., 2017; Plašienka, 2018). This means that the rock complexes of the Middle Group of Nappes in this part of the Western

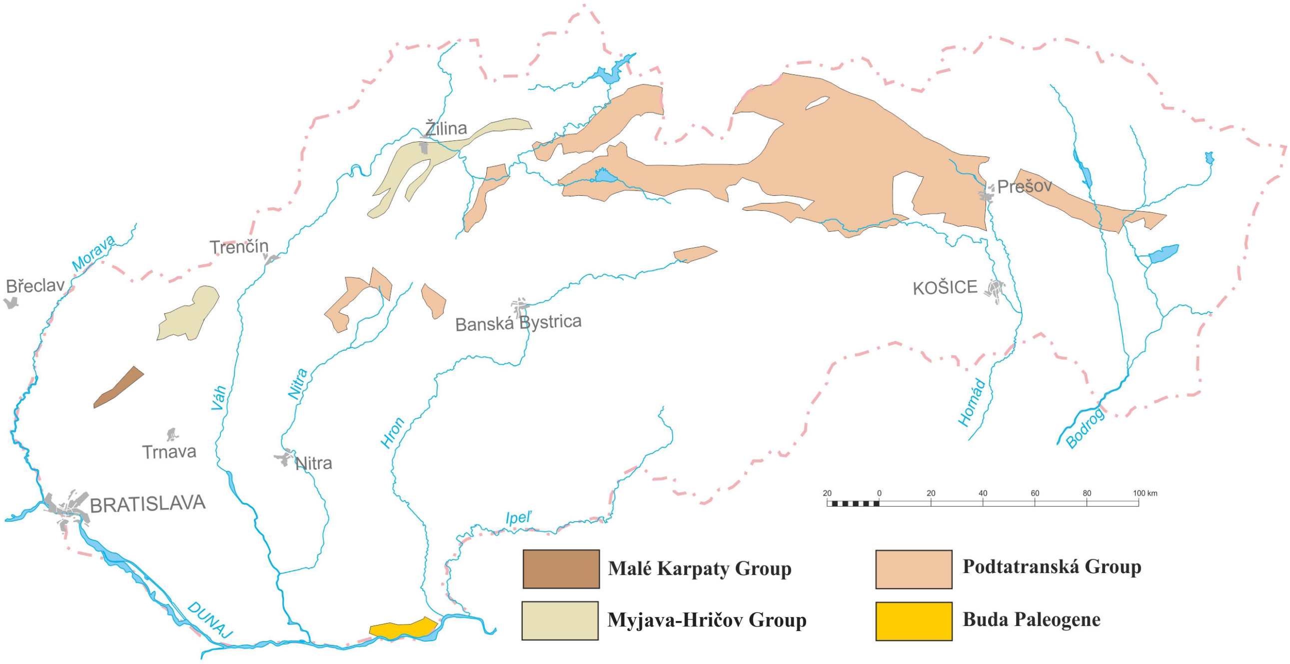

Fig. 17. Position of the Paleogene sediments in the Internal Western Carpathians (based on Hók et al., 2014).

Carpathians were displaced in the late Cretaceous–Eocene period, in contrast to the Upper Group of Nappes, where the Late Cretaceous sediments cover discordantly and transgressively their basement, represented by the Silicic nappes. The outer edge of the Internal Western Carpathian block was during the early Miocene affected by the back-thrusting (south-vergent), which is related to the Neo-Alpine phase of mountain building (e.g. Pelech & Olšavský, 2018).

Upper Cretaceous ("Senonian") sediments (Coniacian-Maastrichtian)

The Upper Cretaceous sediments were preserved only sporadically on few localities (the Miglinc Valley west of Moldava nad Bodvou; Dobšinská ľadová jaskyňa Cave; Šumiac; Myjavská pahorkatina Upland; Brezovské Karpaty and Čachtické Karpaty Mts.). Deep drillings confirmed the presence of Upper Cretaceous rocks also in the area of Krupina and Rimavská Sobota (Čierna Lúka Fm., Vass et al., 2001) in Central Slovakia and from the pre-Neogene basement of the Vienna Basin. Oldest (lowermost) parts of these sedimentary sequences, correlated with Gosau Group, were deposited mostly in freshwater environment. The higher parts are represented by marine, often deep-water sediments.

The Upper Cretaceous rock occurrences could be divided into two groups. The first one is covering solely the Silicic nappes, representing the highest structural element of the Upper Group of Nappes (Miglinc Valley; Dobšinská ľadová jaskyňa Cave; Šumiac and Čierna Lúka Fm. occurrences). Among them, the most widespread and lithologically most complete are the occurrences in the wider area of the Dobšinská ľadová jaskyňa Cave, which are represented by two lithologically different formations. The "lower formation" of ?early Santonian to early Campanian age contains freshwater limestones and brown-grey to grey shales with coal interbeds. It was formed in the freshwater to the brackish environment, with its highest parts being formed in the marine environment. The "upper formation" of probably Maastrichtian to Paleocene age is represented by variegated conglomerates with interbeds of red and green shales with planktonic foraminifers pointing to marine environment (Mello et al., 2000; Pipík et al., 2009; Hók & Littva, 2018).

The second group of the Upper Cretaceous rock occurrences is located atop of Hronicum, which represents highest structural element of the Upper Group of Nappes (Myjavská pahorkatina Upland, Brezovské Karpaty and Čachtické Karpaty Mts. and pre-Neogene basement of the Vienna Basin). The most widespread occurrences are located in the Myjavská pahorkatina Upland and are represented by the Brezová Group (Coniacian – Maastrichtian, Salaj et al., 1987). Lower part of the Brezová Group is due to its lithological and facial content similar to the Upper Cretaceous rocks of the Eastern Alps (Wagreich & Marschalko, 1995). The basal part is composed of conglomerates and sandstones. The upper part, which is clearly of marine origin is composed of "flysch-like" sediments, red marlstones and limestones. The occurrences of the Brezová Group rocks continue also into the basement of the Vienna Basin Neogene sedimentary infill.

Paleogene sediments

The Paleogene sediments (Fig. 17) are divided into several lithostratigraphic (lithofacial) groups which are at the same time localized in the particular areas: Central Carpathian Paleogene Basin (or Podtatranská Group sensu Gross et al., 1984; Gross, 2008), Myjava-Hričov Group, Malé Karpaty Group and so-called Buda Paleogene (North Hungarian Paleogene Basin). Paleogene sediments are deposited transgressively and discordantly above pre-Cenozoic rocks. During the early Paleogene (Paleocene) most of the Internal Western Carpathians territory was probably sub-aerially exposed land. The Paleocene sediments are mostly located only along the Pieniny Klippen Belt (Myjava-Hričov Group).

Podtatranská Group

The Podtatranská Group (sensu Gross et al., 1984; also termed as the Inner Carpathain Paleogene or fill of Central Carpathian Paleogene Basin) represents prevailing part of the Paleogene rocks in the Internal Western Carpathians (Fig. 17). Sediments of Podtatranská Group morphologically form the mountainous regions of Skorušinské vrchy, Spišská Magura, Levočské vrchy, Bachureň and Šarišská vrchovina, but mainly the Tertiary intramountain basins of Žilinská kotlina, Turčianska kotlina, Hornonitrianska kotlina, Podtatranská kotlina, Hornádska kotlina and Horehronské podolie. Stratigraphic range of the Podtatranská Group sediments is from Eocene to Oligocene (in the Hornonitrianska kotlina Basin up to early Miocene). The rock sequence starts with transgressive basal breccias and conglomerates (Borové Fm.). The transgression has progressed generally from W to E and was diachronous in time. The basal formation is overlain by the packet of claystones (Huty Fm.) and typical mass transport deposits ("flysch" sandstones and claystones, Zuberec Fm.). The sedimentary sequence was terminated by the deposition of predominantly sandy gravity flow deposits (Biely Potok Fm.).

Malé Karpaty Group

The Malé Karpaty Group represents the westernmost occurrence of the Paleogene sediments within the Western Carpathians (Fig. 17). The rock sequence represents only a relic of a larger basin transgressively and discordantly overlying various litostratigraphic units of the Hronicum (Buček in Polák et al., 2012). Age of the Malé Karpaty Group sediments – conglomerates, breccia, sandstones and claystones – is early to middle Eocene, though the sedimentation continued after hiatus in the early Oligocene. Sediments differ from those in the Podtatranská Group.

Myjava-Hričov Group

The Myjava-Hričov Group contains a lithologically diverse "flysch"-type rock sequence, mainly sandstones, claystones, limestones and conglomerates (Súľov Conglomerates). It is located along the inner edge of the western part of the Pieniny Klippen Belt (Fig. 17). The sediments are predominantly transgressively overlying its footwall, manifesting hiatus during the early Paleocene. However, the Paleocene sediments of the Polianka Fm. were exceptionally deposited continuously since Late Cretaceous. The stratigraphic record of the Myjava-Hričov Group ends in the late Eocene (Buček in Mello et al., 2011; Plašienka & Soták, 2015).

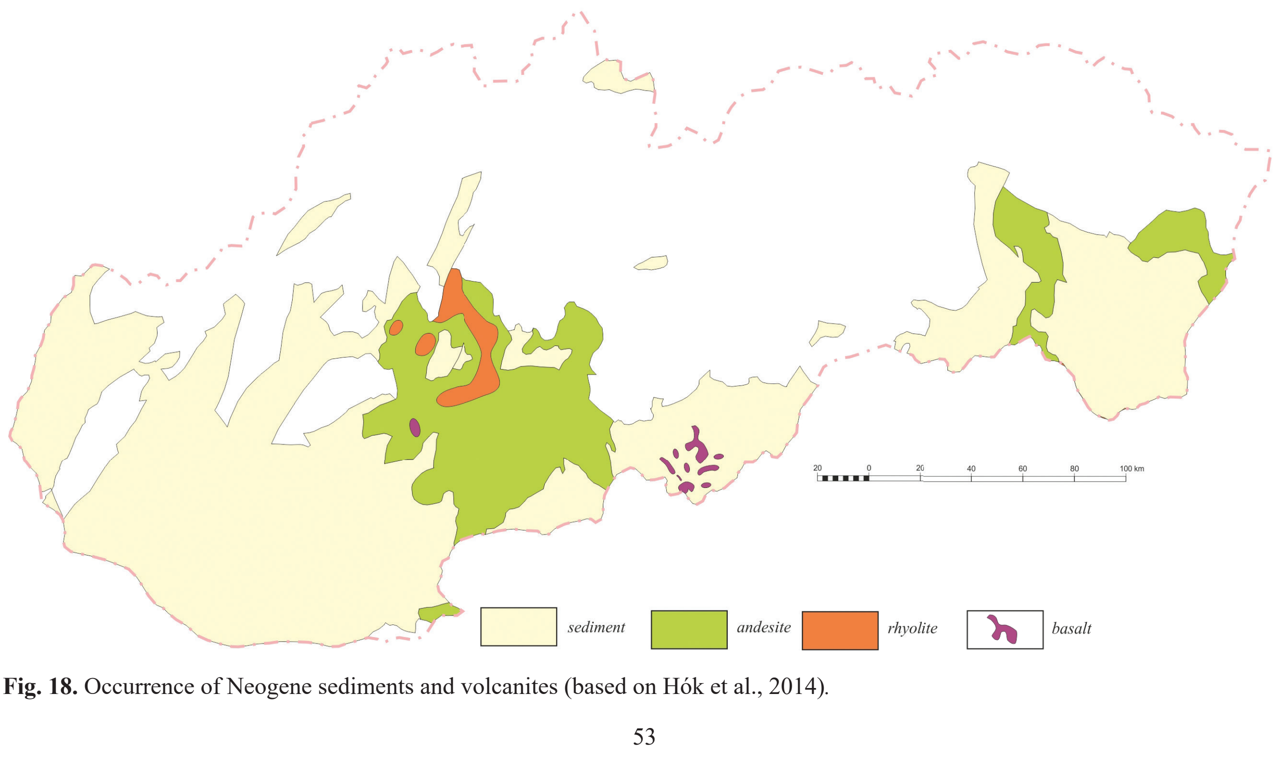

Fig. 18. Occurrence of Neogene sediments and volcanites (based on Hók et al., 2014).

Buda Paleogene

The Buda Paleogene sequence (late Eocene–early Oligocene) occurs only in southern Slovakia (mainly in the area of the Štúrovo town and the South Slovak Basin). In the region of Štúrovo the Buda Paleogene sediments are not exposed on the surface but were revealed by boreholes. The Buda Paleogene sequence is not an integral part of the W. Carpathians. Overlying the tectonic units of Hungarian Transdanubian range, they are lithofacially closer to units of Southern Alps. The sediments of the Buda Paleogene are characterized by the alternation of the brackish (mixed marine and freshwater environments) and the marine sedimentation, and in particular the occurrence of the coal seams (Vass, 2002).

Neogene sediments

The Neogene sedimentary basins and intermontane depressions (in Slovak usually termed *kotlina;* Fig. 18), together with the Core mountains represent the most characteristic morpho-tectonic features of the W. Carpathians. Regarding the common origin and evolution, the Neogene sedimentary basins cannot be separated from Carpathian Neogene volcanic province (Konečný et al., 2002) occurring in Central and Eastern Slovakia, and at the same time, they must be understood in the context of the whole Pannonian Basin System and wider Paratethys region (Royden & Horváth, 1988; Kováč, 2000; Haas et al., 2013).

The Neogene basins in the Slovak territory are represented by complex and extensive Vienna, Danube, South Slovak and East Slovak (Transcarpathian) basins. The intramontane depressions have usually thinner and structurally less complicated Neogene infill and are often situated between the (Core) mountains. The northern embayments of the Danube Basin – the Blatné, Rišňovce and Komjatice depressions (formerly known as the Piešťany, Topoľčany and Zlaté Moravce embayments) are included among the intermontane depressions since their evolution is closely related to surrounding mountains. The smaller Neogene intermontane basins include Trenčín, Ilava, Orava, Bánovce, Horná Nitra, Turiec, Žiar, Zvolen and Rožňava basins. The intermontane depressions are bounded by normal faults, delimiting them from the surrounding areas. The sediment thickness often reaches several kilometers and Neogene rocks unconformably and transgressively overlie dismembered basement of various ages and tectonic affiliation. The Neogene rocks are characterized by great diversity and many local names (e.g. Vass, 2002, Fig. 19).

The evolution of the Neogene basins and intermontane depressions was coeval with subduction-accretion processes in the Outer Western Carpathians. Since the Oligocene, the subduction and collision of the Flysch Belt with Bohemian Massif and North European platform took place. The subduction was diachronous and proceeded continually from the west (Eggenburgian) to the east (end of Neogene). Gradual consumption of the Flysch Belt basement resulted in contraction of the area between fixed and consolidated European Platform and the Internal Western Carpathian (ALCAPA) block. The Internal Western Carpathian block was due to the subduction roll-back effect generally moving to the north and rotated counter clockwise at the same time. The rotation was controlled by actually active segments of subduction (Jiříček, 1979; Márton et al., 2016). The aforementioned processes in the Internal W. Carpathian regions resulted in stress regime that enabled strike-slips and normal faulting. The Neogene evolution of W. Carpathian sedimentary basins can be divided into several stages (Kováč et al., 2018, Fig. 19):

Pre-rift stage of Early Miocene (Eggenburgian–early Badenian) can be characterized by transtensional regime. Early Miocene marine sediments (e.g. Čausa, Bánovce, Lakšárska Nová Ves and Rakša fms.) were deposited in the northern part of the Danube Basin (Blatné, Bánovce, Horná Nitra and Turiec depressions), as well as in the Vienna, East Slovak and South Slovak basins.

Syn-rift stage of the middle Miocene (Badenian–Sarmatian) is characterized by the marine sedimentation and regional extension that reached maximum during this time in the whole Internal W. Carpathians. The onset of the main rift phase is marked by regional unconformity, where the middle Miocene sediments often overlap the pre-Cenozoic basement. Considerable amount of sediments has accumulated in relatively short time (nearly 3 000 m of sediments during Badenian in the Blatné Depression). Extension to transtension was diachronously moving to the SE (Hók et al., 2016). Typical horst and graben structure of the Core mountains belt was formed during this stage and accompanied by considerable tilting of several hanging wall blocks. Clays, marls and sandstone at the beginning of marine environment (e.g. Špačince and Báhoň fms.) were later replaced by deltaic to brackish sedimentation (Vráble Fm.). This stage was terminated by regional unconformity at the end of Sarmatian.

Post-rift stage represented the thermal collapse of the Pannonian Basin lithosphere. It was accompanied by wide rift normal faulting, which dominated in the evolution of the sedimentary basins during the late Miocene (Pannonian) to Quaternary. Main depocenters were located in Rišňovce, Komjatice and Gabčíkovo depressions. The sedimentary sequences were changing from brackish to freshwater (Ivanka Fm.), deltaic (Beladice Fm.) to alluvial sedimentation (Volkovce Fm. and Kolárovo Fm.). Important unconformity and hiatus occurred during the Pontian–Dacian due to basin inversion.

Neogene–Quaternary volcanic rocks

The Neogene volcanic activity was geotectonically tightly bound to the processes of subduction in the External Western Carpathians (Konečný et al., 2002). The petrographic and geochemical character of volcanic rocks

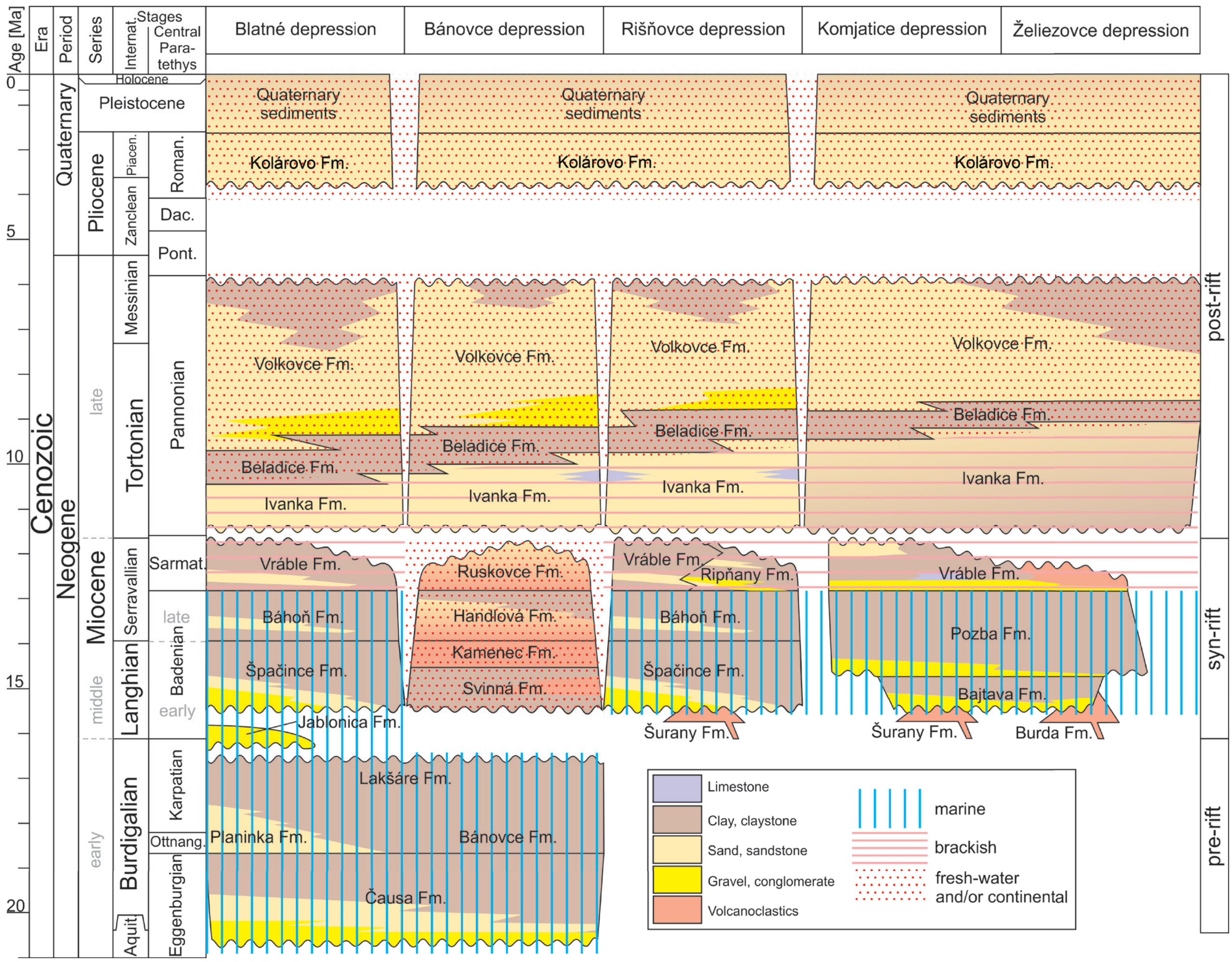

Fig. 19. Lithostratigraphy of the Slovak part of the Danube Basin (based on Vass, 2002, and Kováč et al., 2018).

is directly limited by the nature of the subduced plate as well as the upper mantle (Biely et al., 1996b). Regarding the geotectonic evolution, succession of volcanotectonic events, different petrological and volcanological types and forms, it is not possible to separate Neogene and Quaternary volcanic activity, having following individual stages (Lexa et al., 1993):

Acid calc-alkaline areal volcanism is represented mainly by rhyolites, rhyodacites and their products of two periods: (1) The **early Miocene** (Eggenburgian–early Badenian) restricted only to marginal facies – tuffs, recorded in the South Slovak basin and the East Slovak basin. Geodynamically, they can be parallelized with the pre-rift stage of the Neogene extension. (2) The **late Miocene** (Sarmatian–Panonian) volcanism can be parallelized with processes of the post-rift stage. Volcanic products are more widespread and occur together with andesite volcanoes, especially in the Central Slovakia region.

Intermediate calc-alkaline areal volcanism represented mainly by the middle Miocene (Badenian–Sarmatian) granodiorites, andesites, dacites and their volcaniclastic products. It represents the lowest part of the large Štiavnica, Javorie and Poľana stratovolcanoes. Geodynamically, they can be parallelized to the syn-rift stage (maximum back-arc extension).

Intermediate calc-alkaline arc volcanism mainly of basaltic andesites, rare dacites and their products is documented in particular during the middle Miocene (Sarmatian). The occurrence is mainly connected to the region of Eastern Slovakia (the volcanoes of Slánske vrchy Hills and Vihorlatské vrchy Mts.). Petrological character of rocks reflects the processes of active subduction.

Alkali basalt volcanism (besides basalts also nepheline basanite) is found only in the central Slovak region – predominantly in the Cerová vrchovina Upland and represents the final stage of late Miocene–Quaternary volcanic activity. The youngest products (nepheline basanites) with documented age of 100 000–140 000 years BP, were found near Nová Baňa (Putikov vŕšok; Šimon & Maglay, 2005).

Summary

The territory of Slovakia is formed by the north convex-bent arch of the Western Carpathian mountain range and the northern margin of the Pannonian Basin. The geological/tectonic structure of the W. Carpathians was formed by the north-vergent Alpine orogenic processes. The deformation advanced generally from internal (southern) to the external (northern) parts of the present-day arc. The Internal W. Carpathians (IWECA) were tectonically transformed to the present structure during the Cretaceous period and the External W. Carpathians (EWECA) during the Neogene period. The main tectonic units are from north to south and from bottom to top as follows: The Flysch Belt composed of Krosno and Magura nappe systems. The border between the EWECA and IWECA is the Klippen Belt containing the Oravic tectonic units. IWECA is built by the Lower, Middle and the Upper Group of Nappes. The Vahicum and Tatricum tectonic units form the Lower Group of Nappes. The Veporicum, Fatricum and Hronicum are present in the Middle Group of Nappes and finally the Gemericum, Meliaticum, Turnaicum and Silicicum represent the Upper Group of Nappes. The Tatricum, Veporicum and Gemericum can be considered as the thick-skinned units involving the Paleozoic crystalline basement. Other tectonic units represent cover nappes containing mostly Mesozoic carbonate sediments. Rock formations of the Late Cretaceous (Coniacian–Maastrichtian) and Cenozoic age are in the IWECA traditionally considered as the “post-nappe stacking”, however, in the external parts of the IWECA the sediments of late Cretaceous and Paleogene age are tectonized together with their basement. The most characteristic Cenozoic elements in the IWECA include: (1) the Paleogene sediments of the Podtatranská Group transgressively overlapping IWECA nappes and reaching thickness of several thousand m in the central and eastern Slovakia; (2) horst and graben system of the Core mountains, representing the transitional zone between the IWECA and northern part of the Miocene Danube/ Pannonian Basin; (3) Miocene to Pliocene rhyolitic, andesitic and later basaltic volcanism (Neovolcanism) particularly extensive in central and eastern Slovakia.

Acknowledgement

The work was financially supported by the VEGA grant No. 1/0115/18and the Slovak Research and Development Agency under the contracts No. APVV-17--0170, APVV–16–0121 and APVV–16–0146. Authors are thankful for constructive comments and suggestions of Ján Madarás and anonymous reviewer, who improved the quality of the paper.

References

Andrusov, D., 1968: Grundriss der Tektonik der Nördlichen Karpaten. *Bratislava, 1 – 188.*

Andrusov, D., Bystrický, J. & Fusán, O., 1973: Outline of the Structure of the West Carpathians. X. Congres of Carpathian-Balkan Association. *Bratislava,Geol. Úst. D. Štúra, Vyd. Slov. Akad. Vied, 1 – 44.*

Bezák, V., 1994: Návrh nového členenia kryštalinika Západných Karpát na základe rekonštrukcie hercýnskej tektonickej stavby. *Miner. Slov., 26, 1, 1 – 6. (In Slovak with English summary.)*

Bezák, V., Broska, I., Ivanička, J., Reichwalder, P., Vozár, J., Polák, M., Havrila, M., Mello, J., Biely, A., Plašienka, D., Potfaj, M., Konečný, V., Lexa, J., Kaličiak, M., Žec, B., Vass, D., Elečko, M., Janočko, J., Pereszlényi, M., Marko, F., Maglay, J. & Pristaš, J., 2004: Tektonická mapa Slovenskej republiky 1 : 500 000. *Bratislava, Minister. život. prostr. Slov. rep., Št. Geol. Úst. D. Štúra.*

Bezák, V., Elečko, M., Fordinál, K., Ivanička, J., Kaličiak, M., Konečný, V., Kováčik, M., Maglay, J., Mello, J., Nagy, A., Polák, M. & Potfaj, M. (eds.), 2008: Prehľadná geologická mapa Slovenskej republiky 1 : 200 000. *Bratislava, Št. Geol. Úst. D. Štúra.*

Bezák, V. (ed.), Elečko, M., Fordinál, K., Ivanička, J., Kaličiak, M., Konečný, V., Maglay, J., Mello, J., Nagy, A., Polák, M., Potfaj, M., Šimon, L., Biely, A., Broska, I., Buček, S., Filo, I., Grecula, P., Hraško, Ľ., Jacko, S., Kobulský, J., Kohút, M., Kováčik, M., Lexa, J., Olšavský, M., Plašienka, D., Pristaš, J., Teťák, F., Vass, D. & Vozárová, A., 2009: Vysvetlivky k prehľadnej geologickej mape Slovenskej republiky 1 : 200 000. *Bratislava, Št. Geol. Úst. D. Štúra, 534 p.*

Bezák, V., Biely, A., Elečko, M., Konečný, V., Mello, J., Polák, M. & Potfaj, M., 2011: A new synthesis of the geological structure of Slovakia – the general geological map at 1 : 200 000 scale. *Geol. Quart., 55, 1, 1 – 8.*

Biely, A. (ed.), Bezák, V., Elečko, M., Gross, P., Kaličiak, M., Konečný, V., Lexa, J., Mello, J., Nemčok, J., Potfaj, M., Rakús, M., Vass, D., Vozár, J. & Vozárová, A., 1996a: Explanation to geological map of Slovakia 1 : 500,000. *Bratislava, GS SR, Vyd. D. Štúra, 77 p.*

Biely, A., Bezák, V., Elečko, M., Kaličiak, M., Konečný, V., Lexa, J., Mello, J., Nemčok, J., Potfaj, M., Rakús, M., Vass, D., Vozár, J. & Vozárová, A., 1996b: Geologická mapa Slovenskej republiky 1 : 500 000. *Bratislava, Minister. život. prostr. Slov. rep., GS SR.*

Birkenmajer, K., 1977: Jurrassic and Cretaceous lithostratigraphic units of the Pieniny Klippen Belt, Carpathians, Poland. *Stud. geol. polon., 45, 101 – 121.*

Broska, I., Petrík, I., Beeri-Shlevin, Y., Majka, J. & Bezák, V., 2013: Devonian/ Mississippian I-type granitoids in the Western Carpathians: A subduction related hybrid magmatism. *Lithos, 162 – 163, 27 – 36.*

Cieszkowski, M., 1992: Marine Miocene deposits near Nowy Targ, Magura Nappe, Flysch Carpathians (South Poland). *Geol. Carpath., 43, 339 – 346.*

Faryad, S. W., 1990: Rulovo-amfibolitový komplex gemerika. *Miner. Slov., 22, 303 – 318. (In Slovak with English summary.)*

Geologická mapa Slovenska M 1 : 50 000, 2013: *Bratislava, Št. Geol. Úst. D. Štúra. Available on web:: http://apl.geology.sk/gm50js.*

Golonka, J., Ślączka, A., Waśkowska, A., Krobicki, M. & Cieszkowski, M., 2013: Budowa geologiczna zachodniej części polskich Karpat zewnętrznych. In: Krobicki, M., Feldman-Olszewska, A. (eds.): Głębokomorska sedymentacja fliszowa: sedymentologiczne aspekty historii basenów karpackich: V Polska Konferencja Sedymentologiczna POKOS 5' 2013. *Żywiec: abstrakty referatów i posterów oraz artykuły: przewodnik do wycieczek, 11 – 61. (In Polish.)*

Grecula, P. & Együd, K., 1977: Pozícia zemplínskeho ostrova v tektonickom pláne Karpát. *Miner. Slov., 9, 6, 449 – 462. (In Slovak with English summary.)*

Grecula, P., 1982: Gemerikum – segment riftogénneho bazénu Paleotetýdy. *Bratislava, Alfa, 1 – 263. (In Slovak with English summary.)*

Grecula, P., Návesňák, D., Bartalský, B., Gazdačko, Ľ., Németh, Z., Ištván, J. & Vrbatovič, P., 1990: Shear zones and arc structure of Gemericum, the Western Carpathians. *Miner. Slov., 22, 2, 97 – 110.*

Grecula, P. & Kobulský, J. (eds.), Gazdačko, Ľ., Németh, Z., Hraško, Ľ., Novotný, L., Maglay, J., Pramuka, S., Radvanec, M., Kucharič, Ľ., Bajtoš, P. & Záhorová, Ľ., 2011: Vysvetlivky ku geologickej mape Spišsko-gemerského rudohoria 1 : 50 000. *Bratislava, Št. Geol. Úst. D. Štúra, 1 – 308 (In Slovak with English summary.)*

Gross, P., 2008: Litostratigrafia Západných Karpát: Paleogén – podtatranská skupina. *Bratislava, Št. Geol. Úst. D. Štúra, 1 – 78. (In Slovak with English summary.)*

Gross, P., Köhler, E. & Samuel, O., 1984: Nové litostratigrafické členenie vnútrokarpatského paleogénu. *Geol. Práce, Spr., 81, 103 – 117. (In Slovak with English summary.)*

Haas, J. (ed.), Hámor, G., Jámbor, A., Kovács, S., Nagymarosy, A. & Szederkényi, T., 2013: Geology of Hungary. *Heidelberg, Springer Verlag, 244 p.*

Havrila, M., 2011: Hronikum: paleogeografia a stratigrafia (vrchný pelsón – tuval), štrukturalizácia a stavba. Geol. Práce, Spr., 117, 7 – 103. (In Slovak, English summary).

Hók, J., Kahan, Š. & Aubrecht, R., 2001: Geológia Slovenska. *Bratislava, Univerzita Komenského, 1 – 47. (In Slovak.)*

Hók, J., Kováč, M., Pelech, O., Pešková, I., Vojtko, R. & Králiková, S., 2016: The Alpine tectonic evolution of the Danube Basin and its northern periphery (southwestern Slovakia). *Geol. Carpath., 67, 5, 495 – 505.*

Hók, J., Šujan, M. & Šipka, F., 2014: Tektonické členenie Západných Karpát – prehľad názorov a nový prístup. *Acta Geol. Slov., 6, 2, 135 – 143. (In Slovak with English summary.)*

Hók, J. & Littva, J., 2018: Chtelnické súvrstvie – nová litostratigrafická jednotka sladkovodných vápencov vrchnej kriedy v Brezovských Karpatoch a Čachtických Karpatoch (západné Slovensko). *Geol. Práce, Spr., 132, 53 – 58. (In Slovak with English summary.)*

Hraško, Ľ., Határ, J., Huhma, H., Mäntäri, I., Michalko, J. & Vaasjoki, M., 1999: U/Pb zircon dating of the Upper Cretaceous granite (Rochovce type) in the Western Carpathians. *Krystalin., 25, 163 – 171.*

Hrouda, F., Putiš, M. & Madarás, J., 2002: The Alpine overprints of the magnetic fabrics in the basement and cover rocks of the Veporic Unit (Western Carpathians, Slovakia). *Tectonophysics, 359, 271 – 288.*

Hrouda, F., Krejčí, O., Potfaj, M. & Stráník, Z., 2009: Magnetic fabric and weak deformation in sandstones of accretionary prisms of the Flysch and Klippen Belts of the Western Carpathians: Mostly offscraping indicated. *Tectonophysics, 479, 254 – 270.*

Ivan, P., 1994: Early Paleozoic of the Gemeric Unit (Inner Western Carpathians): Geodynamic setting as inferred from metabasalt geochemistry data. *Mitt. Österr. geol. Gesell., 86, 23 – 31.*

Ivanička, J. & Kohút, M. (eds.), Havrila, M., Olšavský, M., Hók, J., Kováčik, M., Madarás, J., Polák, M., Rakús, M., Filo, I., Elečko, M., Fordinál, K., Maglay, J., Pristaš, J., Buček, S., Šimon, L., Kubeš, P., Scherer, S., Zuberec, J., Dananaj, I. & Klukanová, A., 2011: Vysvetlivky ku geologickej mape Považského Inovca a jv. časti Trenčianskej kotliny. *Bratislava, Št. Geol. Úst. D. Štúra, 7 – 389.*

Ivanička, J., Snopko, L., Snopková, P. & Vozárová, A., 1989: Gelnica Group – lower unit of the Spišsko-gemerské rudohorie Mts. (West Carpathians) Early Paleozoic. *Geol. Zbor. Geol. carpath., 40, 4, 483 – 501.*

Jacko, S., Hók, J. & Madarás, J., 1997: Pre- and syn-granitoid deformations of the Western Carpathian metamorphic complexes. In: Grecula, P., Hovorka, D., Putiš, M. (Eds.): Geological evolution of the Western Carpathians. *Bratislava, Miner. Slov. – Monogr., 359 – 370.*

Janák, M., 1994: Variscan uplift of the crystalline basement, Tatra Mts., Central Western Carpathians: Evidence from $^{40}Ar/^{39}Ar$ laser probe dating of biotite and P-T-t paths. *Geol. Carpath., 45, 5, 293 – 300.*

Janočko, J., Pereszlényi, M., Vass, D., Bezák, V., Jacko, S., Jr., Jacko, S., Kohút, M., Polák, M. & Mello, J., 2006: Geology and hydrocarbon resources of the Inner Western Carpathians, Slovakia, and Poland. In: Golonka, J. & Picha, F. J. (eds.): The Carpathians and their foreland: Geology and hydrocarbon resources. *Memoir (Amer. Assoc. Petrol. Geol.), 84, 569 – 603.*

Janoschek, W. R. & Matura, A., 1980: Outline of the geology of Austria. *Abh. Geol. Bundesanst., 34, 7 – 98.*

Jiříček, R., 1979: Tektogenetický vývoj karpatského oblouku během oligocénu a neogénu. In: Maheľ, M. (ed.): Tektonické profily Západných Karpát. *Bratislava, Geol. Úst. D. Štúra, 203 – 213. (In Czech with English summary.)*

Jurewicz, E., 2005: Geodynamic evolution of the Tatra Mts. and the Pieniny Klippen Belt (Western Carpathians): problems and comments. *Acta geol. polon., 55, 3, 295 – 338.*

Kaczmarek, A., Oszczypko-Clowes, M. & Cieszkowski, M., 2016: Early Miocene age of Stare Bystre Formation (Magura Nappe, Outer Carpathians, Poland) indicated by the calcareous nannoplankton. *Geol. Quart., 60, 341 – 354.*

Klinec, A., 1966: Zum Bau und Bildung des Veporiden-Kristallin. *Sbor. geol. Vied, Západ. Karpaty, 6, 7 – 28. (In Slovak with German summary.)*

Klinec, A., 1971: Hlavné tektonické elementy východných veporíd. *Geol. Práce, Spr., 57, 105 – 109. (In Slovak with English summary.)*

Konečný, V., Kováč, M., Lexa, J. & Šefara, J., 2002: Neogene evolution of the Carpatho-Pannonian region: an interplay of subduction and back-arc diapiric uprise in the mantle. *EGU Stephan Mueller Spec. Publ. . 1, 105 – 123.*

Kováč, M., 2000: Geodynamický, paleogeografický a štruktúrny vývoj karpatsko-panónskeho regiónu v miocéne: Nový pohľad na neogénne panvy Slovenska. *Bratislava, Veda, 202 p. (In Slovak, English summary).*

Kováč, M., Plašienka, D., Aubrecht, R., Halouzka, R., Krejčí, O., Kronome, B., Nagymarosy, A., Přichystal, A. & Wagreich, M., 2003: Geological structure of the Alpine-Carpathian-Pannonian junction and neighbouring slopes of the Bohemian Massif. *Bratislava, Univerzita Komenského, 1 – 88.*

Kováč, M., Rybár, S., Halásová, E., Hudáčková, N., Šarinová, K., Šujan, M., Baranyi, V., Kováčová, M., Ruman, A., Klučiar, T. & Zlinská, A., 2018: Changes in Cenozoic depositional environment and sediment provenance in the Danube Basin. *Bas. Res., 30, 97 – 131.*

Kozur, H. & Mostler, H., 1992: Erster paläontologischer nachweis von Meliaticum und Süd-Rudabanyaicum in den Nördlichen Kalkalpen (Österreich) und ihre beziehungen zu den abfolgen in den Westkarpaten. *Geol. Paläont. Mitt. Innsbruck, 18, 87 – 129.*

Lačný, A., Plašienka, D. & Vojtko, R., 2016: Structural evolution of the Turňa Unit constrained by fold and cleavage analyses and its consequences for the regional tectonic models of the Western Carpathians. *Geol. Carpath., 67, 2, 177 – 193.*

Lexa, J., Bezák, V., Elečko, M., Mello, J., Polák, M., Potfaj, M. & Vozár, J. (eds.), 2000: Geological map of the Western Carpathians and adjacent areas 1 : 500 000. *Bratislava, Ministry Environ. Slovak Rep., Geol. Surv. Slovak Rep.*

Lexa, J., Konečný, V., Kaličiak, M. & Hojstričová, V., 1993: Distribúcia vulkanitov karpatsko-panónskeho regiónu v priestore a čase. In: Rakús, M. & Vozár, J. (eds.): Geodynamický model a hlbinná stavba Západných Karpát. *Bratislava, Geol. Úst. D. Štúra, 57 – 69. (In Slovak.)*

Lexa, O., Schulmann, K. & Ježek, J., 2003: Cretaceous collision and indentation in the West Carpathians: View based on structural analysis and numerical modeling. *Tecton., 22, 6, 1 066.*

Maheľ, M., 1981: Penninikum v Západných Karpatoch z pohľadu globálnej tektoniky. *Miner. Slov., 13, 4, 289 – 306. (In Slovak with English summary.)*

Maheľ, M. (ed.), 1974: Tectonics of the Carpathian Balkan Regions. Explanations to the tectonic map of the Carpathian-Balkan regions and their foreland. *Bratislava, Geol. Institutute D. Štúr, 1 – 453.*

Maheľ, M., 1983: Návrh na novú tektonickú nomenklatúru základných tektonických elementov Západných Karpát. *Miner. Slov., 15, 6, 559 – 565. (In Slovak with English summary.)*

Maheľ, M., 1985: Geologická stavba Strážovských vrchov. *Bratislava, Geol. Úst. D. Štúra, 222 p. (In Slovak with English summary.)*

Maheľ, M., 1986: Geologická stavba československých Karpát. Paleoalpínske jednotky 1. *Bratislava, Veda, 1 – 510. (In Slovak.)*

Maheľ, M. & Buday, T. (eds), 1968: Regional Geology of Czechoslovakia. Part II. The West Carpathians. *Praha, Geol. Surv. Czechosl., Academia, 1 – 723.*

Márton, E., Grabowski, J., Tokarski, A. K. &Túnyi, I., 2016: Palaeomagnetic results from the fold and thrust belt of the Western Carpathians: an overview. In: Pueyo, E. L., Cifelli, F., Sussman, A. J. & Oliva-Urcia, B. (eds.): Palaeomagnetism in Fold and Thrust Belts: New Perspectives. *London, Geol. Soc., Spec.Publ., 425, 7 – 36.*

Mazúr, E. & Lukniš, M., 1986: Geomorfologické členenie SSR a ČSSR. Časť Slovensko. *Bratislava, Slov. kartografia. (In Slovak.)*

Mello, J., 1979: Sú tzv. vyššie subtatranské príkrovy a silický príkrov súčasťou gemerika? *Miner. Slov., 11, 3, 279 – 281. (In Slovak.)*

Mello, J., Boorová, D., Buček, S., Filo, I., Fordinál, K., Havrila, M., Iglárová, Ľ., Kubeš, P., Liščák, P., Maglay, J., Marcin, D., Nagy, A., Potfaj, M., Rakús, M., Rapant, S., Remšík, A., Salaj, J., Siráňová, Z., Teťák, F., Zuberec, J., Zlinská, A. & Žecová, K., 2011: Vysvetlivky ku geologickej mape Stredného Považia 1 : 50 000. *Bratislava, Št. Geol. Úst. D. Štúra, 377 p. (In Slovak with English summary.)*

Mello, J., Filo, I., Havrila, M., Ivan, P., Ivanička, J., Madarás, J., Németh, Z., Polák, M., Pristaš, J., Vozár, J., Vozárová, A., Liščák, P., Kubeš, P., Scherer, S., Siráňová, Z., Szalaiová, V. a Žáková, E., 2000: Vysvetlivky ku geologickej mape Slovenského raja, Galmusu a Hornádskej kotliny 1 : 50 000. *Bratislava, Št. Geol. Úst. D. Štúra, 299 p. (In Slovak with English summary.)*

Mello, J., Reichwalder, P. & Vozárová, A., 1998: Bôrka Nappe: high-pressure relic from the subduction-accretion prism of the Meliata ocean (Inner Western Carpathians, Slovakia). *Slovak Geol. Mag., 4, 4, 261 – 273.*

Mišík, M., Chlupáč, I. & Cicha, I., 1985: Stratigrafická a historická geológia. *Bratislava, Slov. Pedag. Nakl., 570 p. (In Slovak.)*

Mišík, M., 1997a: Slovakia. In: Moores, E. M. & Fairbridge, R. W. (eds.): Encyclopedia of European and Asian Regional Geology. *Dodrecht, Springer Publishers, 656 – 664.*

Mišík, M., 1997b: The Slovak part of the Pieniny Klippen Belt after pioneering works of D. Andrusov. *Geol. Carpath., 48, 4, 209 – 220.*

McCann, T. (ed.), 2008: The Geology of Central Europe: Mesozioc and Cenozoic. *London, Geol. Soc. Publ. House, 1 500 p.*

Mock, R., Sýkora, M., Aubrecht, R., Ožvoldová, L., Kronome, B., Reichwalder, P. & Jablonský, J., 1998: Petrology and stratigraphy of the Meliaticum near the Meliata and Jaklovce Villages, Slovakia. *Slovak Geol. Mag., 4, 4, 223 – 260.*

Niedźwiedzki, G., 2011: A Late Triassic dinosaur−dominated ichnofauna from the Tomanová Formation of the Tatra Mountains, Central Europe. *Acta palaeont. pol., 56, 2, 291 – 300.*

Németh, Z., 1996: Prvé zistenie príkrovu Bôrky vo východnej časti Spišsko-gemerského rudohoria. *Miner. Slov., 28, 3, 175 – 184. (In Slovak with extended English resume.)*

Németh, Z., 2002: Variscan suture zone in Gemericum: Contribution to reconstruction of geodynamic evolution and metallogenetic events of Inner Western Carpathians. *Slovak Geol. Mag., 8, 3 – 4, 247 – 257.*

Németh, Z., Radvanec, M., Gazdačko, Ľ. & Kobulský, J., 2012: Variscan tectonic setting vs. Alpine overprint in Gemericum (Inner Western Carpathians): Their role in the recent distribution of tectonic units in the eastern part of the territory as expressed in significant localities. *Miner. Slov., 44, 1, Geovestník, 8 – 15.*

Németh, Z., Putiš, M. & Hraško, Ľ., 2016: The relation of metallogeny to geodynamic processes - the natural prerequisite for the origin of mineral deposits of public importance (MDoPI): The case study in the Western Carpathians, Slovakia. *Miner. Slov., 48, 2, 119 – 134.*

Oszczypko, N., Ślączka, A., Oszczypko-Clowes, M. & Olszewska, B., 2015: Where was the Magura Ocean? *Acta geol. pol., 65, 3, 319 – 344.*

Pelech, O. & Olšavský, M., 2018: Post-early Eocene backthrusting in the northeastern Strážovské vrchy Mts. (Western Carpathians). *Miner. Slov., 50, 2, 149 – 158.*

Pelech, O., Hók, J. & Józsa, Š., 2017: Turonian – Santonian sediments in the Tatricum of the Považský Inovec Mts. (Internal Western Carpathians, Slovakia). *Aust. J. Earth Sci., 110, 1, 21 – 35.*

Pelech, O., Hók, J., Havrila, M. & Pešková, I., 2016: Structural position of the Upper Cretaceous sediments in the Považský Inovec Mts. (Western Carpathians). *Acta Geol. Slov., 8, 1, 43 – 58.*

Pešková, I., Hók, J., Potfaj, M. & Vojtko, R., 2012: Structural interpretation of the Varín and Orava segments of the Klippen Belt (in Slovak). *Geol. Práce, Spr., 120, 51 – 64. (In Slovak with English summary.)*

Pícha, F. J., Stráník, Z. & Krejčí, O., 2006: Geology and hydrocarbons resources of the Outer Carpathians and their foreland, Czech Republic. In: Golonka, J. & Pícha, F. J. (eds.): The Carpathians and their foreland: Geology and hydrocarbon resources. *Memoir (Amer. Assoc. Petrol. Geol.), 84, 49 – 175.*

Piller, W. E., Egger, H., Erhart, C. W., Gross, M., Harzhauser, M., Hubmann, B., Van Husen, D., Krenmayr, H.-G., Krystyn, L., Lein, R., Lukeneder, A., Mandl, G., Rögl, F., Roetzel, R., Rupp, C., Schnabel, W., Schönlaub, H. P., Summesberger, H., Wagreich, M. & Wessely, G., 2004: Die stratigraphische Tabelle von Österreich (sedimentäre Schichtfolgen). *Österr. Stratigraph. Kommission.*

Pipík, R., Sýkora, M., Colin, J. P. & Havrila, M., 2009: A new phytal limnic ostracod Rosacythere carpathica sp. nov. from the Upper Cretaceous of the Western Carpathians: implications for evolution of the Timiriaseviinae. *Cret. Res., 30, 465 – 476.*

Plašienka, D., 1999: Tektonochronológia a paleotektonický model jursko-kriedového vývoja centrálnych Západných Karpát. *Bratislava, Veda, Vyd. Slov. Akad. Vied, 1 – 125. (In Slovak with English summary.)*

Plašienka, D., 2012: Jurassic syn-rift and Cretaceous syn-orogenic, coarse-grained deposits related to opening and closure of the Vahic (South Penninic) Ocean in the Western Carpathians – an overview. *Geol. Quart., 56, 4, 601 – 628.*

Plašienka, D., 2018: Continuity and episodicity in the early Alpine tectonic evolution of the Western Carpathians: How large-scale processes are expressed by the orogenic architecture and rock record data. *Tecton., 37, 1 – 50.*

Plašienka, D., Marschalko, R., Soták, J., Peterčáková, M. & Uher, P., 1994: Pôvod a štruktúrna pozícia vrchnokriedových sedimentov v severnej časti Považského Inovca. Prvá časť: Litostratigrafia a sedimentológia. *Miner. Slov., 26, 311 – 334. (In Slovak with English summary.)*

Plašienka, D., Soták, J. & Spišiak, J., 1995: Penninic units of the Central Western Carpathians: lithological, structural and metamorphic signatures. Proceedings XV. Congress CBGA. *Geol. Soc. Greece, Spec. Publ., 4, 1, 80 – 85.*

Plašienka, D., Grecula, P., Putiš, M., Kováč, M., & Hovorka, D., 1997: Evolution and structure of the Western Carpathians: An overview. In: Grecula, P., Hovorka, D. & Putiš, M. (eds.): Geological evolution of the Western Carpathians. *Bratislava, Miner. Slov. – Monogr., 1 – 24i.*

Plašienka, D. & Soták, J., 2015: Evolution of late Cretaceous and Palaeogene synorogenic basins in the Pieniny Klippen Belt and adjacent zones (Western Carpathians, Slovakia): tectonic control over a growing orogenic wedge. *Ann. Soc. geol. Pol., 85, 43 – 76.*

Polák, M., Plašienka, D., Kohút, M., Putiš, M., Bezák, V., Maglay, J., Olšavský, M., Havrila, M., Buček, S., Elečko, M., Fordinál, K., Nagy, A., Hraško, Ľ., Németh, Z., Malík, P., Liščák, P., Madarás, J., Slavkay, M, Kubeš, P., Kucharič, Ľ., Boorová, D., Zlinská, A., Siráňová, Z. & Žecová, K., 2012: Vysvetlivky ku geologickej mape Malých Karpát 1 : 50 000. *Bratislava, Št. Geol. Úst. D. Štúra, 1 – 287. (In Slovak with English summary.)*

Potfaj, M., 1993: Postavenie bielokarpatskej jednotky v rámci flyšového pásma. *Geol. Práce, Spr., 98, 55 – 78. (In Slovak with English summary.)*

Potfaj, M. (ed.), Šlepecký, T., Maglay, J., Hanzel, V., Boorová, D., Žecová, K., Kohút, M., Nagy, A., Teťák, F., Vass, B., Sandanus, M., Buček, S., Sýkora, M., Köhler, E., Fejdiová, O., Kandera, K., Samuel, O., Bubík, M. & Beleš, F., 2003: Vysvetlivky ku geologickej mape regiónu Kysuce 1 : 50 000. *Bratislava, Št. Geol. Úst. D. Štúra, 1 – 193. (In Slovak with English summary.)*

Potfaj, M., Maglay, J., Šlepecký, T. & Teťák, F., 2002: Geologická mapa regiónu Kysúc 1 : 50 000. *Bratislava, Minister. život. prostr. Slovak. rep., Št. Geol. Úst. D. Štúra.*

Putiš, M., Filová, I., Korikovsky, S. P., Kotov, A. B. & Madarás, J., 1997: Layered metaigneous complex of the Veporic basement with features of the Variscan and Alpine thrust tectonics (the Western Carpathians). In: Grecula, P., Hovorka, D. & Putiš, M. (eds.): Geological evolution of the Western Carpathians. *Bratislava, Miner. Slov. – Monogr., 175 – 196.*

Radvanec, M., Konečný, P., Ondrejka, M., Putiš, M., Uher, P. & Németh, Z., 2009: The Gemeric granites as an indicator of the crustal extension above the Late-Variscan subduction zone and during the Early Alpine riftogenesis (Western Carpathians): An interpretation from the monazite and zircon ages dated by CHIME and SHRIMP methods. *Miner. Slov., 41, 4, 381 – 394.*

Radvanec, M., Németh, Z., Kráľ, J. & Pramuka, S., 2017: Variscan dismembered metaophiolite suite fragments of Paleo-Tethys in Gemeric unit, Western Carpathians. *Miner. Slov., 49, 1 – 48.*

Radvanec, M. & Németh, Z., 2018: Variscan epidote-eclogite, blueschists and pumpellyite-actinolite facies Cpx/Sr-rich epidote-metagabbro blocks exhumed in Carboniferous with Permian amphibolite facies overprint (Gemeric unit, Western Carpathians). *Miner. Slov., 50, 55 – 99.*

Rakús, M. & Sýkora, M., 2001: Jurassic of Silicicum. *Slovak Geol. Mag., 7, 1, 53 – 83.*

Royden, L. H. & Horváth, F. (eds.), 1988: The Pannonian Basin. A study In Basin Evolution. *Memoir (Amer. Assoc. Petrol. Geol.), 45, 1 – 394.*

Salaj, J., Began, A., Hanáček, J., Mello, J., Kullman, E., Čechová, A. & Šucha, P., 1987: Vysvetlivky ku geologickej mape Myjavskej pahorkatiny, Brezovských a Čachtických

Karpát 1 : 50 000. *Bratislava, Geol. Úst. D. Štúra, 181 p. (In Slovak.)*
Schmid, S. M., Bernouli, D., Fügenchuh, B., Matenco, L., Schefer, S., Schuster, R., Tischler, M. & Ustaszewski, K., 2008: The Alpine-Carpathian-Dinaridic orogenic system: correlation and evolution of tectonic units. *Swiss J. Geosci., 101, 139 – 183.*
Slávik, J., 1976: Zemplinikum – možná nová tektonická jednotka centrálnych Karpát. *Geol. Práce, Spr., 65, 7 – 19. (In Slovak with English summary.)*
Šefara, J., Bielik, M., Vozár, J., Katona, M., Szalaiová, V., Vozárová, A., Šimonová, B., Pánisová, J., Schmidt, S. & Götze, H., 2017: 3D density modelling of Gemeric granites of the Western Carpathians. *Geol. Carpath., 68, 3, 177 – 192.*
Šimon, L. & Maglay, J., 2005: Datovanie sedimentov podložia lávového prúdu vulkánu Putikov vrch metódou opticky stimulovanej luminiscencie. *Miner. Slov., 37, 279 – 281. (In Slovak with English summary.)*
Teťák, F. (ed.), Kováčik, M., Pešková, I., Nagy, A., Buček, S., Maglay, J., Vlačiky, M., Laurinc, D., Žecová, K., Zlinská, A., Liščák, P., Marcin, D., Žilka, A., Kucharič, Ľ., Gluch, A. & Baláž, P., 2016: Vysvetlivky ku geologickej mape regiónu Biela Orava 1 : 50 000. *Bratislava, Št. Geol. Úst. D. Štúra, 217 p. (In Slovak with English summary.)*
Uher, P., Kohút, M., Ondrejka, M., Konečný, P. & Siman, P., 2014: Monazite-(Ce) in Hercynian granites and pegmatites of the Bratislava Massif, Western Carpathians: compositional variations and Th-U-Pb electron-microprobe dating. *Acta Geol. Slov., 6, 2, 215 – 231.*
Uhlig, V., 1903: Tektonische Kartenskizze der Karpaten. Mafsstab 1 : 1 500.000. *Leipzig, Wagner & Debes.*
Vass, D., 2002: Litostratigrafia Západných Karpát: neogén a budínsky paleogén. *Bratislava, Št. Geol. Úst. D. Štúra, 1 – 202. (In Slovak with English summary.)*
Vass, D., Töröková, I. & Elečko, M., 2001: Čiernolúcke vrstvy – vrchná krieda v podloží Rimavskej kotliny: litologická a petrografická charakteristika. *Geol. Práce, Spr., 105, 23 – 27. (In Slovak with English summary.)*
Vozárová, A. & Vozár, J., 1988: Late Paleozoic in the West Carpathians. *Bratislava, Geol. Úst. D. Štúra, 314 p.*
Vozárová, A. & Vozár, J., 1979: Nižnobocianske a malužinské súvrstvie – nové litostratigrafické jednotky v mladšom paleozoiku hronika. *Miner. Slov, 11, 5, 477 – 478. (In Slovak with English summary.)*
Vozárová, A., 1993: Variscan metamorphism and crustal evolution in the Gemericum. *Západ. Karpaty, Sér. Mineral. Petrogr. Geochém. Metalogen., 16, 55 – 117. (In Slovak.)*
Vozárová, A., 1996: Tectono-sedimentary evolution of Late Paleozoic basins based on interpretation of lithostratigraphic data (Western Carpathians; Slovakia). *Slovak Geol. Mag., 3-4, 251 – 271.*
Vozárová, A., Konečný, P., Šarinová, K. & Vozár, J., 2014: Ordovician and Cretaceous tectonothermal history of the Southern Gemericum Unit from microprobe monazite geochronology (Western Carpathians, Slovakia). *Int. J. Earth Sci., 103, 4, 1 005 – 1 022.*
Wagreich, M. & Marschalko, R. ,1995: Late Cretaceous to Early Tertiary palaeogeography of the Western Carpathians (Slovakia) and the Eastern Alps (Austria): implications from heavy mineral data. *Geol. Rdsch., 84, 1, 187 – 199.*
Wolska, A., Bąk, K. & Bąk, M., 2016: Siliciclastic input into Upper Cenomanian synorogenic sediments of the High-Tatric Unit, Central Western Carpathians (Tatra Mountains); petrography, geochemistry and provenance. *Geol. Quart., 60, 4, 919 – 934.*
Zoubek, V., 1957: Hranice gemerid s veporidami. *Geol. Práce, Zoš., 46, 38 – 43. (In Czech.)*

Prehľad geologickej stavby Slovenska

Územie Slovenska tvorí pásmové pohorie Západných Karpát vyklenuté na sever a severný okraj Panónskej nížiny (obr. 1). Geologická stavba Západných Karpát je výsledkom alpínskej orogenézy, pričom deformácia postupovala od vnútorných častí dnešného oblúka smerom na sever. Vnútorné (interné) Západné Karpaty (IZK) vznikali hlavne v období kriedy a Vonkajšie (externé) Západné Karpaty (EZK) v období neogénu (obr. 2). Za hlavné tektonické jednotky EZK môžeme zo severu na juh a zdola nahor považovať flyšové pásmo tvorené krosnianskym a magurským systémom príkrovov a štruktúru bradlového pásma, ktorá je zároveň deliacim elementom medzi EZK a IZK (obr. 1). V rámci IZK sú prítomné tektonické jednotky spodnej skupiny príkrovov (váhikum a tatrikum), strednej skupiny príkrovov (veporikum, fatrikum a hronikum) a vrchnej skupiny príkrovov (gemerikum, meliatikum, turnaikum a silicikum). Tatrikum, veporikum a gemerikum vzhľadom na prítomnosť paleozoického kryštalinického podložia sa považujú za celokôrové tektonické jednotky. Ostatné tektonické jednotky tvoria pripovrchové príkrovy (obr. 2). Horninové súbory vrchnej kriedy (koňak – mástricht) a kenozoika sa v rámci IZK tradične považujú za popríkrovové útvary, no pri vonkajšom okraji IZK sú často zvrásnené spoločne so svojím podložím (obr. 2). Medzi charakteristické popríkrovové štruktúry IZK patria: 1. paleogénne sedimenty podtatranskej skupiny, transgresívne prekrývajúce príkrovy IZK a dosahujúce vo východnej časti územie hrúbku niekoľko tisíc metrov (obr. 17); 2. štruktúry horských chrbtov a depresií jadrových pohorí predstavujúce prechodnú zónu medzi IZK a severnou časťou Podunajskej, resp. Panónskej panvy (obr. 7 a 18); 3. miocénny až kvartérny vulkanizmus, obzvlášť rozsiahly na strednom a východnom Slovensku (obr. 18).

Doručené / Received: 30. 4. 2019
Prijaté na publikovanie / Accepted: 4. 6. 2019

Mineralia Slovaca, Web ISSN 1338-3523, ISSN 0369-2086
51 (2019), 61 – 78,

Mineralogy and geochronology of calc-alkaline lamprophyres from the Nízke Tatry Mts. crystalline complex (Western Carpathians)

JÁN SPIŠIAK[1], LUCIA VETRÁKOVÁ[1], TOMÁŠ MIKUŠ[2], DAVID CHEW[3], ŠTEFAN FERENC[1], VIERA ŠIMONOVÁ[1] and PAVOL SIMAN[2]

[1] Matej Bel University, Faculty of Natural Sciences, Tajovského 40, SK-97401 Banská Bystrica, Slovak Republic; jan.spisiak@umb.sk
[2] Slovak Academy of Sciences, Earth Science Institute, Dúbravská cesta 9, SK-840 05 Bratislava, Slovak Republic
[3] University of Dublin, Trinity College Dublin, College Green, Dublin 2, Ireland

Abstract: The examined Late Paleozoic calc-alkaline dyke rocks occur within the Nízke Tatry Mts. crystalline complex (Kumštová valley and Jarabá village). Their mineral composition is quite simple – the main mafic minerals are clinopyroxene, amphibole and biotite, and the felsic minerals are alkaline feldspar, plagioclase and quartz. They show a rather high degree of alteration. According to their mineralogical composition, the studied rocks correspond to calc-alkaline lamprophyres having revealed and age of 259. 0 ± 2.8 Ma.

Key words: mineralogy, geochemistry, U-Pb dating, lamprophyres, Nízke Tatry Mts.

Graphical abstract

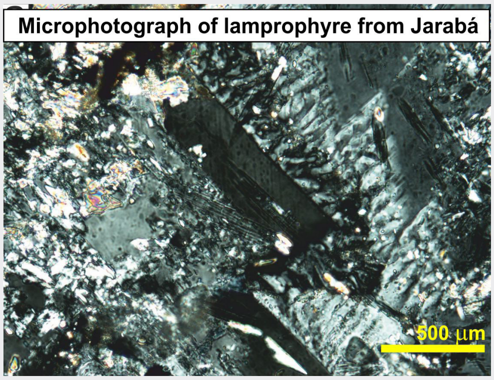

Highlights

- Studied lamprophyre rocks from southern slopes of the Nízke Tatry Mts. are classified as kersantites and spessartites.
- Similarity of their mineral and chemical composition with Permian volcanics of the Hronicum and revealed age 259.0 ± 2.8 Ma point to a possible co-magmatism of these rocks.

Introduction

Lamprophyres represent the dyke rocks, whose mineral composition, structure and chemical composition are different from plutonic and volcanic rocks. Within the Western Carpathian Tatricum and Veporicum crystalline basement, the calc-alkaline dykes occur in the Malé Karpaty Mts., Strážovské vrchy Mts., Malá Fatra Mts., Nízke Tatry Mts. and Veporic Kohút zone. They form a heterogeneous rock group usually classified as quartz porphyrites or lamprophyres (Hovorka, 1967). In the crystalline basement, the dyke rocks were firstly reported by Kamenický (1962) and Krist (1967) in the area of Jarabá and Mýto pod Ďumbierom villages and subsequently described in more details by Hovorka (1967). In the Central Europe, the calc-alkaline lamprophyres typically occur within the granite/granitoid, gneissic and gabbroic rocks – they are represented by minettes, kersantites and spessartites in the Krupka locality, Krušné hory Mts. (Czech Republic; Štemprok et al., 2014; Ulrich et al., 1993), spessartites in Lusatia (Germany; Abdelfadil et al., 2013), kersantites and spessartites in the Erzgebirge (Germany; Seifert, 2008), and in the Sudetes (Poland) with the occurrences of all types of these rocks (Awdankiewicz, 2007). In the French Massif Central, calc-alkaline lamprophyres are represented by kersantites and minettes (Turpin et al., 1988). The age of calc-alkaline lamprophyres from Central Europe is Late-Variscan: French Massif Central (290-315 Ma), Lusatia (ca 330 Ma), Erzgebirge (300-330 Ma), Sudetes (ca 300 Ma) and the Black Forest (314-332 Ma; Hegner et al., 1998). The different extent of enrichment of Late-Variscan lamprophyres in different domains of Central Europe reflects the regional heterogeneous effect of the Variscan orogeny. In this paper, we pay special attention to the chemical composition and the age of the examined minerals.

Geological position

Dykes of calc-alkaline lamprophyres are rather rare in the Western Carpathians. In the eastern part of the Nízke Tatry Mts., lamprophyres occur in several localities (Kamenický, 1962; Krist, 1967). We have focused our research on two best outcropped localities from the wider surroundings of the Jarabá village (Fig. 1). One dyke is cropping out at the mouth of the Kumštová dolina valley to the Jarabá–Čertovica road (N 48° 54′ 19″, E 19° 42′ 14″). The outcrop is located on the left side of the valley. The dyke is 60 – 80 cm thick and is made up of fine-grained kersantite. The host rocks are formed by banded and augen textures (prevailingly mylonitized with abundant amphibolite lenses). The second dyke is cropping out near the village of Jarabá. It is an abandoned quarry approximately in the middle of the village, on the left bank of the brook, on the western slope of the Mlynárska hill (1051.5; N 48° 53′ 25″, E 19° 41′ 39″). The dyke body is uncovered here in a length of about 20 m. It is cropping out in a thickness of at least 5 m. The host rocks are diaphtorized biotite gneisses. The rims of the body are finer grained. Coarse grained kersantite is cropping out in the southern part of the quarry. The lamprophyres are rather highly altered.

Analytical methods

The 18 thin sections were studied with a NIKON Eclipse LV 100N microscope. Silicates and apatites were studied using electron microprobe JEOL JXA 8530FE at Earth Sciences Institute of the Slovak Academy of Sciences in Banská Bystrica under the following conditions for silicates: accelerating voltage 15 kV, probe current 20 nA, beam diameter 3-8 µm, ZAF correction, counting time 10 s on peak, 5 s on background. The used standards, X-ray lines and D.L. (in ppm) were: Ca(Kα, 25) – diopside, K (Kα, 44) – orthoclase, P (Kα, 41) – apatite, F (Kα, 167) – fluorite, Na (Kα, 43) – albite, Mg (Kα, 41) – diopside, Al (Kα, 42) – albite, Si (Kα, 63) – quartz, Ba (Lα, 72) – barite, Fe (Kα, 52) – hematite, Cr (Kα, 113) – Cr_2O_3, Mn (Kα, 59) – rhodonite, Ti (Kα, 130) – rutile, Cl (Kα, 12) – tugtupite, Sr (Lα, 71) – celestite. Following conditions were used for apatites: accelerating voltage 15 kV, probe current 20nA and beam diameter 5 µm and ZAF matrix correction. The EPMA was calibrated by the natural and synthetic standards. Used standards, X-ray lines, crystal and D.L. (in ppm) are: Ca (Kα, PETL, 24-62) - diopside, K (Kα, PETL, 20-48) – orthoclase, Th (Mα, PETL, 41-75) – thorianite, Pb (Mβ, PETL, 65-138) – crocoite, Cl (Kα, PETL, 11-12) – tugtupite, P (Kα, PETL, 56-85) – apatite, S (Kα, PETL, 27-47) – barite, Y – (Lα, PETL, 59-122) – YPO_4, F (Kα, LDE1, 103-273) – fluorite, Na (Kα, TAP, 46-78) – albite, Sr (Lα, TAP, 38-201) – celestite, Si (Kα, TAP, 50-125) – orthoclase, Al (Kα, TAP, 37-100) – albite, Mg (Kα, TAP, 37-87) – diopside, Sm (Lβ, LIFH, 62-274) – $SmPO_4$, Pr (Lβ, LIFH, 121-235) – $PrPO_4$, Nd (Lα, LIFH, 62-123) – $NdPO_4$, Ce (Lα, LIFH, 65-129) – $CePO_4$, La (Lα, LIFH, 72-139) – $LaPO_4$, Fe (Kα, LIF, 94-333) – hematite, Mn (Kα, LIF, 79-238) – rhodonite, Ti (Kα, LIF, 133-333) – rutile, Ba (Lα, LIF, 242-674) – barite.

Apatite crystals were separated using standard techniques. Apatite U-Pb data were acquired using a Photon Machines Analyte Exite 193 nm ArF Excimer laser-ablation system coupled to a Thermo Scientific iCAP Qc at the Department of Geology, Trinity College Dublin. Twenty-eight isotopes (^{31}P, ^{35}Cl, ^{43}Ca, ^{55}Mn, ^{86}Sr, ^{89}Y, ^{139}La, ^{140}Ce, ^{141}Pr, ^{146}Nd, ^{147}Sm, ^{153}Eu, ^{157}Gd, ^{159}Tb, ^{163}Dy, ^{165}Ho, ^{166}Er, ^{169}Tm, ^{172}Yb, ^{175}Lu, ^{200}Hg, ^{204}Pb, ^{206}Pb, ^{207}Pb, ^{208}Pb, ^{232}Th, ^{238}U and mass ($^{248/232}Th\,^{16}O$) were acquired using a 50 µm laser spot, a 4 Hz laser repetition rate and a fluence of 3.31 J/cm^2. A ca 1 cm sized crystal of Madagascar apatite, which has yielded a weighted average ID-TIMS concordia age of 473.5± 0.7 Ma (Thomson et al., 2012; Cochrane et al., 2014), was used as a primary apatite reference material in this study. McClure Mountain syenite apatite (the rock from which the $^{40}Ar/^{39}Ar$ hornblende standard MMhb is derived) was used as a secondary standard. McClure Mountain syenite has moderate but reasonably consistent U and Th contents (~23 ppm and 71 ppm – Chew & Donelick, 2012) and its thermal history, crystallization age (weighted mean $^{207}Pb/^{235}U$ age of 523.51 ± 2.09 Ma) and initial Pb isotopic composition ($^{206}Pb/^{204}Pb$ = 17.54 ± 0.24; $^{207}Pb/^{204}Pb$= 15.47 ± 0.04) are known from high-precision TIMS analyses (Schoene & Bowring, 2006). Durango apatite was also analysed in this study as a secondary standard. Durango apatite is a distinctive yellow-green fluorapatite widely used as a mineral standard in apatite fission-track and (U-Th)/He dating and apatite electron micro-probe analyses. It is found in the form of large crystals within an open pit iron mine at Cerro de Mercado, Durango, Mexico. The apatite formed between the eruptions of two major ignimbrites, yielding a sanidine-anorthoclase ^{40}Ar-^{39}Ar age of 31.44 ± 0.18 Ma (McDowell et al., 2005). NIST 612 standard glass was used as the apatite trace element concentration reference material. The raw isotope data were reduced using the "VisualAge" data reduction scheme of Petrus & Kamber (2012) within the freeware IOLITE package of Paton et al. (2011). User-defined time intervals are established for the baseline correction procedure to calculate session-wide baseline-corrected values for each isotope. The time-resolved fractionation response of individual standard analyses is then characterized using a user-specified down-hole correction model (such as an exponential curve, a linear fit or a smoothed cubic spline). The data reduction scheme then fits this appropriate sessionwide "model" U-Th-Pb fractionation curve to the time-resolved standard data and the unknowns. Sample-standard bracketing is applied after the correction of down-hole fractiona-

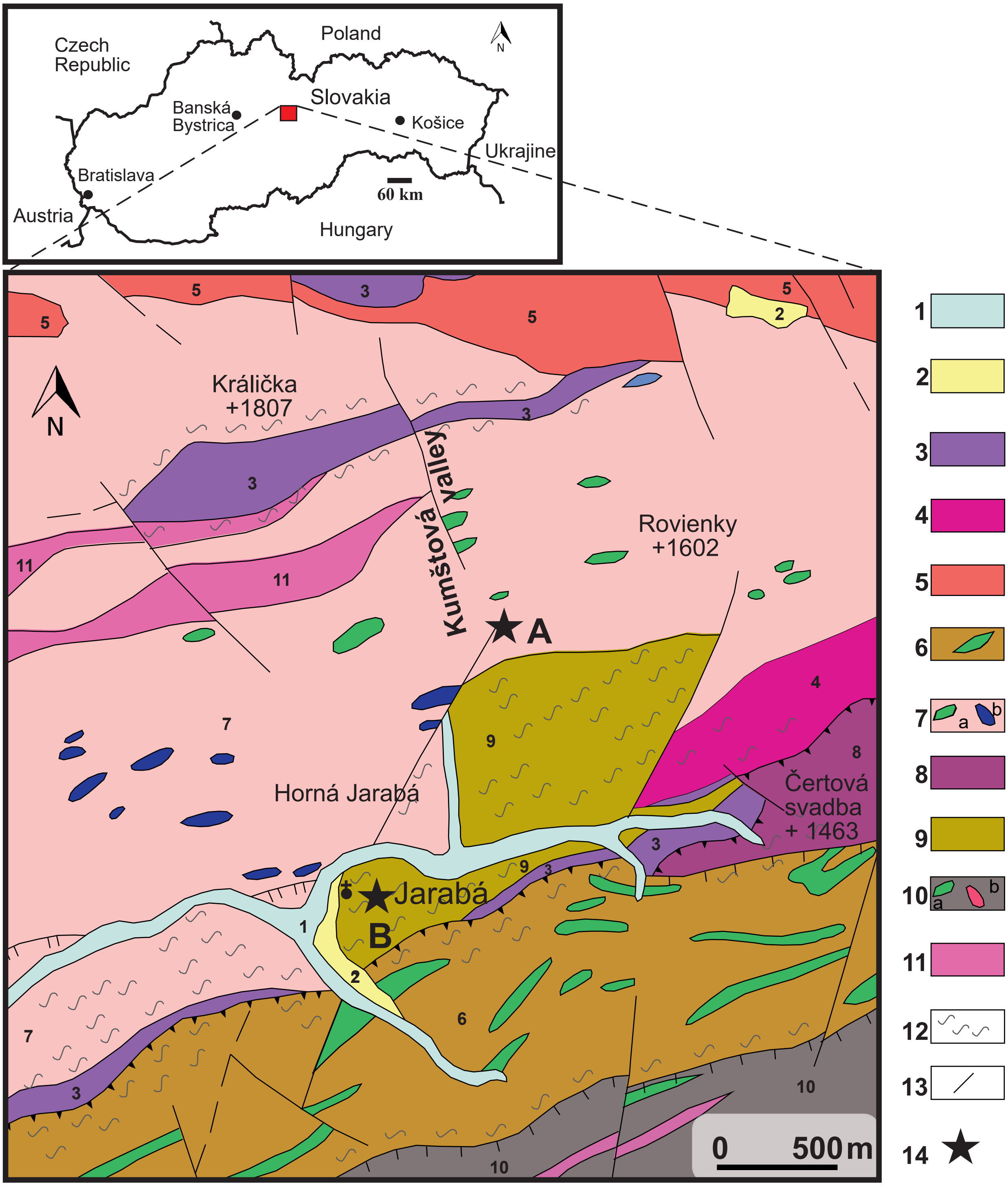

Fig. 1. Geological map of a part of the Nízke Tatry Mts. (Digital geological map of the Slovak Republic at scale 1 : 50 000 [online]. State Geological Institute of Dionýz Štúr, Bratislava, 2013). Legend: Quaternary: 1 – fluvial sediments, 2 – deluvial sediments; Early Triassic: 3 – Lúžňa Formation; Late Paleozoic: 4 – biotite granodiorites to tonalites (Ďumbier type), 5 – biotite and two-mica granites (Králička type); Early Paleozoic: 6 – garnet-muscovite-biotite paragneisses, mica schist gneisses to mica schists with rock body of amphibolites, 7 – biotite and muscovite-biotite gneisses with banded structure with rock body of: a – amphibolites, b – porphyrites, lamprophyres; 8 – K-feldspar-plagioclase gneisses and synkinematic, banded migmatites, 9 – biotite paragneisses, 10 – chlorite-sericite phyllites with rock body of (a) metamorphites of volcanics and volcaniclastics of basic composition, (b) metamorphites of volcanics and volcaniclastics of rhyodacitic and dacitic composition, 11 – orthogneisses (Struhár type). 12 – mylonite zones, 13 – fault lines, 14 – samples (A = Kum-1, 2, 3; B = Jar-1, 2, 3, 4).

tion to account for long-term drift in isotopic or elemental ratios by normalizing all ratios to those of the U-Pb reference standards. Common Pb in the apatite standards was corrected using the ^{207}Pb-based correction method using a modified version of the VisualAge DRS that accounts for the presence of variable common Pb in the primary standard materials (Chew et al., 2014). Over the course of two months of analyses, McClure Mountain apatite (^{207}Pb/^{235}U TIMS age of 523.51 ± 1.47 Ma, (Schoene & Bowring, 2006) yielded a U-Pb Tera-Wasserburg concordia lower intercept age of 524.5 ± 3.7 Ma with an MSWD = 0.72. The lower intercept was anchored using a ^{207}Pb/^{206}Pb value of 0.88198, derived from an apatite ID-TIMS total U-Pb isochron (Schoene & Bowring, 2006).

The structural formulas of clinopyroxenes, biotites and feldspars were recalculated using the Mineral Formulae Recalculation. The mineral recalculation is accessible on the (web:https://serc.carleton.edu/research_education/equilibria/mineralformulaerecalculation.html). The structural formulas of amphiboles were recalculated using the Amphibole Classification (Locock, https://github.com/AndrewLocock/Amphibole/releases/tag/1.9.3).

Mineralogy and petrology

Lamprophyre rocks from the Jarabá wider surroundings are grey-black in colour, have a fine-grained to aphanitic groundmass and medium to fine-grained texture. In coarser grained varieties, thin lamellae of clinopyroxene, and/or amphibole can be observed. The mineral composition of the rocks in two localities is different in modal abundance of dark minerals (especially biotite, amphibole and pyroxene), biotite is prevailing in the Kumštová dolina valley, whereas in Jarabá it is mostly clinopyroxene and amphibole. The modal composition of the rocks is also reflected in their classification. Based on IUGS classification (LeMaitre et al., 2002; Ondrejka et al., 2015), the examined dyke rocks from the Nízke Tatry Mts. belong to kersantite (Kumštová dolina; plagioclase > K-feldspar, biotite > amphibole and clinopyroxe), and/or spessartite (Jarabá, plagioclase > K-feldspar, amphibole and clinopyroxene). Besides primary minerals (clinopyroxene, amphibole, biotite, feldspar and quartz), the lamprophyres under study often contain also secondary minerals (chlorite, epidote and carbonates). From ore minerals there are dominating magnetite, Fe-Ti rutile, hematite and pyrite, and in accessory amounts there occur apatite and zircon. The rocks are characteristic with strongly altered primary minerals, notably clinopyroxene, amphibole, biotite as well as plagioclase.

Clinopyroxenes represent the main rock forming minerals (Tab. 1). They were observed only in the Jarabá locality. They are often enclosing amphiboles (Fig. 2a, b) and based on Morimoto et al. (1988) classification, their chemical composition corresponds to augite (Fig. 3).

Several types of amphiboles occur in examined rocks. All they are strongly altered – chloritized (Fig. 2a, b). There are frequent occurrences of older (lighter) amphiboles with a high FeO, Na_2O and a low MgO and CaO contents enclosed by younger (darker) amphiboles with a lower FeO and Na_2O and a higher MgO and CaO contents (Fig.4a, Tab. 2). Generally, the studied amphiboles are characteristic for a low TiO_2 content. Based on IMA classification (Hawthorne et al., 2012), the amphiboles can be classified as Ca-amphiboles, tremolites (Fig. 5). From the composition and occurrences of the amphiboles it is very likely that their current composition was strongly influenced by alteration processes and the composition of the primary amphiboles, co-existing with clinopyroxenes, was different. In the Kumštová dolina valley, there were found only pseudomorphoses after amphiboles mostly filled with chlorite.

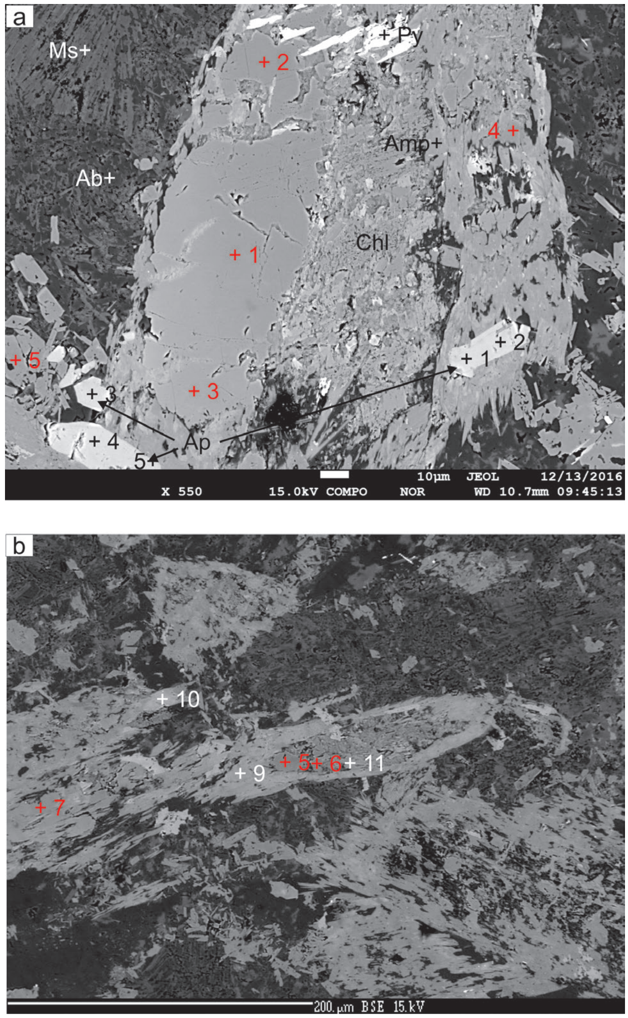

Fig. 2. Back scattered electron (BSE) images of lamprophyre, Ab - albite, Amp - amphibole, Ap - apatite, Ms – muscovite, Py – pyrite, Chl - chlorite. The numbers in figures correspond to those in Table 1 and Table 6. Locality: Jarabá.

Tab. 1.
Selected analyses of clinopyroxenes.

Sample	**JAR-1**							
Figure	**Fig. 2a**	**Fig. 2a**	**Fig. 2a**	**Fig. 2a**	**Fig. 2b**	**Fig. 2b**	**Fig. 2b**	**Fig. 2b**
N. anal.	**1**	**2**	**3**	**4**	**5**	**6**	**7**	**8**
SiO_2	51.63	51.54	51.61	52.63	51.26	51.01	50.07	50.96
TiO_2	1.30	1.34	0.90	1.16	1.14	1.04	1.39	1.12
Al_2O_3	2.39	2.67	2.01	2.35	2.23	2.06	2.27	2.33
Cr_2O_3	0.11	0.00	0.01	0.00	0.05	0.05	0.00	0.03
FeO*	10.87	9.41	13.48	10.09	9.91	10.08	12.89	10.91
MnO	0.31	0.26	0.32	0.25	0.25	0.28	0.37	0.29
MgO	13.65	14.18	12.31	14.31	14.86	14.88	13.48	15.17
CaO	19.24	19.70	18.95	18.51	19.60	19.66	18.80	18.86
Na_2O	0.13	0.15	0.11	0.15	0.35	0.24	0.28	0.22
K_2O	0.00	0.00	0.00	0.00	0.02	0.05	0.04	0.01
Sum	99.64	99.24	99.70	99.45	99.68	99.35	99.57	99.90
Formula based on 6 oxygens								
Si	1.947	1.939	1.965	2.052	1.914	1.913	1.895	1.902
Ti	0.037	0.038	0.026	0.032	0.032	0.029	0.040	0.031
Al	0.106	0.118	0.090	0.100	0.098	0.091	0.101	0.102
Cr	0.003	0.000	0.000	0.000	0.001	0.001	0.000	0.001
Fe^{3+}	0.000	0.000	0.000	0.000	0.033	0.039	0.049	0.046
Fe^{2+}	0.343	0.296	0.429	0.306	0.276	0.277	0.359	0.294
Mn	0.010	0.008	0.010	0.008	0.008	0.009	0.012	0.009
Mg	0.767	0.795	0.699	0.773	0.827	0.832	0.761	0.844
Ca	0.777	0.794	0.773	0.719	0.784	0.790	0.763	0.754
Na	0.010	0.011	0.008	0.010	0.025	0.017	0.021	0.016
X (Wol) %	41.179	42.114	40.664	39.978	40.824	40.761	39.481	38.900
X (En) %	40.664	42.177	36.762	43.010	43.065	42.926	39.389	43.536
X (Fs) %	18.157	15.709	22.574	17.012	16.111	16.313	21.129	17.564

FeO* total Fe as FeO

Tab. 2.
Selected analyses of amphiboles.

Sample	**JAR-1**								
Figure	**Fig. 2b**	**Fig. 2b**	**Fig. 2b**	**Fig. 4a**	**Fig. 4a**	**Fig. 4a**	**Fig. 4a**	**Fig. 4a**	**Fig. 4a**
N. anal.	**9**	**10**	**11**	**12**	**13**	**14**	**15**	**16**	**17**
SiO_2	48.89	48.75	49.85	48.68	48.49	49.25	49.68	50.05	50.71
TiO_2	0.11	0.12	0.28	0.15	0.18	0.09	0.05	0.00	0.05
Al_2O_3	4.09	3.07	3.64	2.02	2.18	1.50	3.26	2.75	3.15
Cr_2O_3	0.01	0.00	0.03	0.00	0.01	0.02	0.00	0.01	0.00
FeO*	22.13	24.26	19.04	32.35	32.20	31.86	23.35	24.42	23.03
MnO	0.31	0.69	0.22	0.61	0.62	0.75	0.34	0.42	0.39
MgO	8.30	9.12	10.89	3.47	3.48	3.87	8.21	7.60	8.33
CaO	12.03	8.03	10.88	9.38	9.34	9.59	12.03	11.85	11.89
Na_2O	0.50	1.25	0.26	0.94	0.87	0.76	0.32	0.28	0.17
K_2O	0.28	0.29	0.94	0.22	0.24	0.27	0.28	0.24	0.64
Sum	96.67	95.67	96.03	97.82	97.62	97.96	97.50	97.62	98.35

Tab. 2 – continuation.

Sample	JAR-1								
Figure	**Fig. 2b**	**Fig. 2b**	**Fig. 2b**	**Fig. 4a**	**Fig. 4a**	**Fig. 4a**	**Fig. 4a**	**Fig. 4a**	**Fig. 4a**
N. anal.	**9**	**10**	**11**	**12**	**13**	**14**	**15**	**16**	**17**
Formula based on 24 (OH.F.Cl.O)									
Si	7.489	7.532	7.569	7.673	7.659	7.745	7.555	7.636	7.649
Al^{IV}	0.511	0.468	0.431	0.327	0.341	0.255	0.445	0.364	0.351
Al^{VI}	0.228	0.091	0.221	0.049	0.065	0.023	0.139	0.130	0.208
Ti	0.013	0.013	0.032	0.018	0.022	0.011	0.006	0.000	0.005
Fe^{3+}	0.081	0.400	0.024	0.291	0.272	0.235	0.188	0.172	0.036
Fe^{2+}	2.755	2.734	2.393	3.974	3.982	3.955	2.781	2.944	2.869
Mn	0.040	0.090	0.028	0.081	0.083	0.100	0.018	0.030	0.042
Mg	1.896	2.102	2.464	0.815	0.820	0.907	1.861	1.728	1.873
Ca	1.975	1.328	1.770	1.583	1.580	1.615	1.961	1.936	1.921
Na	0.149	0.374	0.077	0.286	0.267	0.232	0.094	0.084	0.050
K	0.055	0.058	0.182	0.045	0.048	0.054	0.054	0.046	0.123

FeO* total Fe as FeO

Tab. 3.
Selected analyses of biotites.

Sample	KUM-1			KUM-2			
Figure	**Fig. 4b**	**Fig. 4b**	**Fig. 4b**				
N. anal.	**1**	**2**	**3**	**4**	**5**	**6**	**7**
SiO_2	36.83	35.03	36.18	36.27	36.89	35.83	36.48
TiO_2	4.14	3.36	4.00	4.67	3.65	3.49	4.02
Al_2O_3	12.29	13.37	12.91	12.29	12.39	14.34	13.07
Cr_2O_3	0.02	0.00	0.00	0.00	0.02	0.00	0.00
FeO*	23.61	25.22	24.21	25.12	24.50	23.68	23.55
MnO	0.11	0.16	0.14	0.12	0.15	0.08	0.21
MgO	9.02	10.79	9.39	8.06	9.23	9.61	9.44
CaO	0.10	0.24	0.04	0.06	0.07	0.07	0.08
Na_2O	0.03	0.12	0.06	0.13	0.08	0.03	0.04
K_2O	8.94	6.62	8.30	8.98	8.68	7.76	8.12
Sum	95.10	94.90	95.23	95.71	95.66	94.89	95.01
Formula based on 24 oxygens							
Si	5.755	5.479	5.647	5.685	5.745	5.513	5.604
Al^{IV}	2.245	2.465	2.353	2.271	2.255	2.487	2.367
Al^{VI}	0.019	0.000	0.022	0.000	0.019	0.114	0.000
Ti	0.487	0.395	0.469	0.551	0.428	0.404	0.464
Fe	3.086	3.299	3.160	3.293	3.191	3.047	3.025
Mn	0.015	0.022	0.018	0.016	0.020	0.011	0.027
Mg	2.102	2.516	2.185	1.884	2.142	2.204	2.162
Ca	0.017	0.040	0.006	0.010	0.012	0.011	0.013
Na	0.010	0.036	0.019	0.041	0.025	0.009	0.011
K	1.782	1.320	1.652	1.795	1.725	1.524	1.591
Al total	2.263	2.465	2.376	2.271	2.274	2.601	2.367
Fe/Fe+Mg	0.595	0.567	0.591	0.636	0.598	0.580	0.583

FeO* total Fe as FeO

Tab. 4.
Selected analyses of plagioclases.

Sample	KUM-2		KUM-1					JAR-1
Figure	Fig. 8a	Fig. 8a	Fig. 8b	Fig. 8b	Fig. 8b	Fig. 8b	Fig. 8b	
N. anal.	1	2	3	4	5	6	7	8
SiO_2	59.83	55.20	54.92	64.58	56.25	58.12	58.09	66.51
TiO_2	0.00	0.00	0.00	0.00	0.00	0.00	0.00	0.07
Al_2O_3	24.91	27.64	27.45	21.27	26.74	25.63	24.94	20.70
Cr_2O_3	0.00	0.00	0.00	0.00	0.00	0.00	0.00	0.05
FeO*	0.34	0.40	0.38	0.14	0.44	0.35	0.31	0.12
MnO	0.00	0.00	0.00	0.00	0.00	0.00	0.00	0.08
MgO	0.00	0.06	0.00	0.00	0.03	0.00	0.03	0.00
CaO	7.31	11.09	11.18	3.63	9.90	8.65	9.28	1.18
Na_2O	6.53	4.75	4.79	8.14	5.44	5.91	5.82	10.32
K_2O	1.05	0.53	0.53	1.59	0.65	0.81	0.74	0.18
Sum	99.98	99.68	99.25	99.36	99.45	99.47	99.21	99.19
Formula based on 8 oxygens								
Si	2.688	2.513	2.507	2.897	2.553	2.633	2.641	2.952
Ti	0.000	0.000	0.000	0.000	0.000	0.000	0.000	0.002
Al	1.318	1.482	1.477	1.124	1.430	1.368	1.337	1.083
Cr	0.000	0.000	0.000	0.000	0.000	0.000	0.000	0.002
Fe^{3+}	0.000	0.000	0.000	0.000	0.000	0.000	0.000	0.000
Fe^{2+}	0.013	0.015	0.015	0.005	0.017	0.013	0.012	0.004
Mn	0.000	0.000	0.000	0.000	0.000	0.000	0.000	0.003
Mg	0.000	0.000	0.000	0.000	0.002	0.000	0.002	0.000
Ca	0.352	0.541	0.547	0.174	0.481	0.420	0.452	0.056
Ba	0.000	0.000	0.000	0.000	0.000	0.000	0.000	0.000
Na	0.569	0.419	0.424	0.708	0.479	0.519	0.513	0.888
K	0.060	0.031	0.031	0.091	0.038	0.047	0.043	0.010
X (An) %	35.874	54.585	54.592	17.923	48.250	42.591	44.846	5.880
X (Ab) %	57.991	42.308	42.326	72.730	47.978	52.660	50.896	93.053
X (Or) %	6.135	3.106	3.082	9.348	3.772	4.749	4.258	1.068

FeO* total Fe as FeO

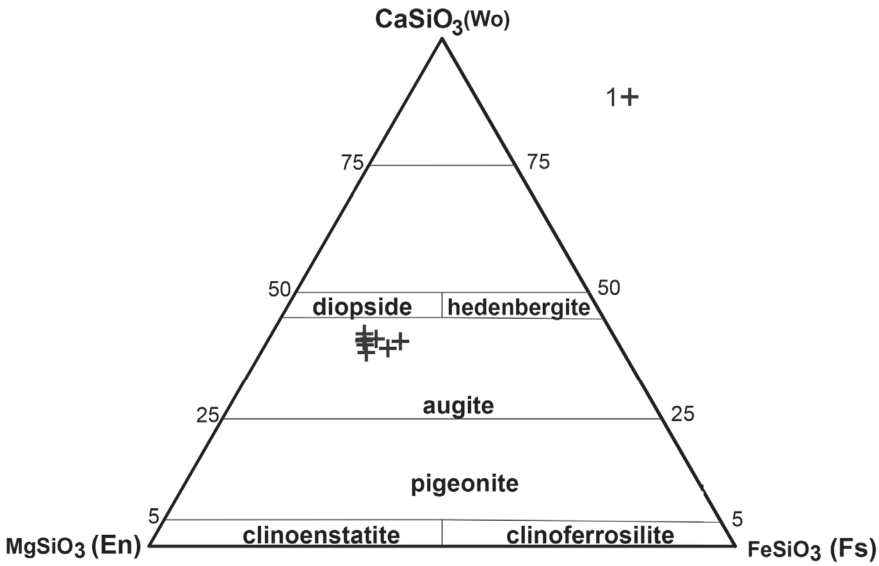

Fig. 3. The classification diagram of pyroxenes, according Morimoto et al. (1988), 1 – clinopyroxene from Jarabá.

Tab. 5.
Selected analyses of K-feldspars.

Sample	JAR-1			KUM- 2		KUM- 1			JAR-1		
Figure	Fig. 4a	Fig. 4a	Fig. 4a	Fig. 8a	Fig. 8a	Fig. 8b	Fig. 8b	Fig. 8b	Fig. 8c	Fig. 8c	Fig. 8c
N. anal.	1	2	3	4	5	6	7	8	9	10	11
SiO_2	59.81	61.19	64.18	62.78	64.63	64.86	64.75	64.10	61.83	62.50	64.05
TiO_2	0.00	0.00	0.00	0.00	0.00	0.00	0.00	0.00	0.00	0.00	0.00
Al_2O_3	20.48	20.01	19.22	20.15	19.47	19.82	18.77	18.73	19.02	18.94	18.67
Cr_2O_3	0.00	0.00	0.00	0.00	0.00	0.00	0.00	0.00	0.02	0.10	0.00
BaO	5.46	3.67	0.03	1.63	0.10	0.00	0.03	0.00	2.52	2.25	0.04
FeO*	0.25	0.20	0.23	0.21	0.09	0.08	0.11	0.20	0.03	0.04	0.09
MnO	0.00	0.00	0.00	0.00	0.00	0.00	0.00	0.00	0.00	0.04	0.00
MgO	0.00	0.00	0.00	0.00	0.00	0.00	0.00	0.00	0.00	0.00	0.00
CaO	0.06	0.06	0.03	0.47	0.44	0.45	0.07	0.10	0.00	0.00	0.21
Na_2O	0.46	0.29	0.29	1.84	3.30	3.72	0.42	0.55	0.21	0.20	0.19
K_2O	14.08	14.79	16.29	12.88	11.50	10.70	15.55	15.45	15.42	15.79	16.53
Sum	100.60	100.22	100.26	99.96	99.52	99.62	99.69	99.12	99.05	99.85	99.79
Formula based on 8 oxygens											
Si	2.902	2.930	2.961	2.928	2.960	2.959	3.007	2.990	2.963	2.965	2.971
Ti	0.000	0.000	0.000	0.000	0.000	0.000	0.000	0.000	0.000	0.000	0.000
Al	1.171	1.129	1.045	1.107	1.051	1.065	1.027	1.029	1.074	1.059	1.020
Fe	0.010	0.008	0.009	0.008	0.003	0.003	0.004	0.008	0.001	0.002	0.004
Mn	0.000	0.000	0.000	0.000	0.000	0.000	0.000	0.000	0.000	0.001	0.000
Mg	0.000	0.000	0.000	0.000	0.000	0.000	0.000	0.000	0.000	0.000	0.000
Ca	0.003	0.003	0.001	0.023	0.022	0.022	0.004	0.005	0.000	0.000	0.011
Na	0.043	0.027	0.026	0.166	0.292	0.329	0.037	0.049	0.019	0.019	0.017
K	0.871	0.903	0.958	0.766	0.672	0.622	0.921	0.919	0.942	0.955	0.978
X(An) %	0.345	0.339	0.145	2.450	2.194	2.244	0.379	0.517	0.000	0.000	1.062
X(Ab) %	4.708	2.880	2.631	17.414	29.665	33.808	3.885	5.086	1.989	1.914	1.685
X(Or) %	94.947	96.782	97.224	80.136	68.141	63.947	95.736	94.397	97.990	98.086	97.253

FeO* total Fe as FeO

Similar to amphibole, biotite is strongly chloritized. High TiO_2 contents prove its magmatic origin, and at the same time, lower contents of K_2O in analyses point to a high secondary alteration. Biotite is a dominant mineral in kersantites from the Kumštová dolina valley. In Jarabá, only rarely there were found tiny, strongly altered biotites. On the basis of chemical composition (Tab. 3, Fig. 6), we include the studied dark micas into the group of annite (Rieder et al., 1998). We also used a discrimination diagram for biotites from different types of geotectonic environments (Fig. 7; Abdel-Rahman, 1993). In the diagram, the biotites fall within the group of biotites from calc-alkaline rocks, on the boundary with alkaline rocks.

From the felsic minerals, the plagioclase and alkaline feldspar are dominant for the lamprophyric rocks studied. Plagioclases significantly predominate over alkaline feldspars. They are strongly sericitized and often contain albite lamellae. Plagioclases are typical with their zonal structure – their central parts are more basic (An_{36-55}) than the rims (An_{18}) (Tab. 4, Figs. 8 and 9). In the case of alkaline feldspars, in addition to the varying amounts of sodium (Na_2O content up to 3.72%), an increased BaO content is obser-

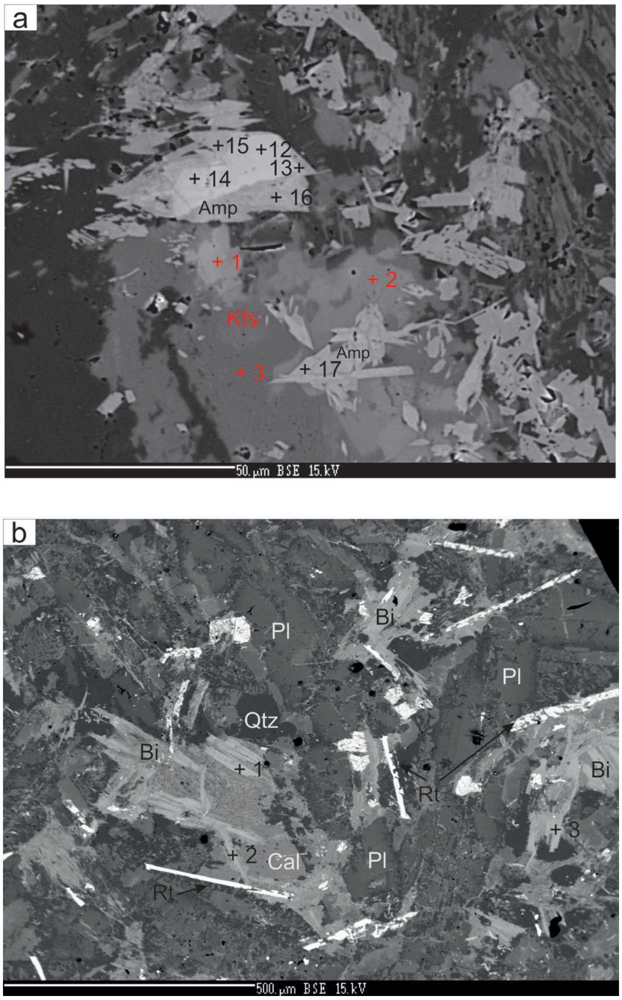

Fig. 4. Back scattered electron (BSE) images of lamprophyre; Pl – plagioclases, Cal – calcite, Qtz – quartz, Rt – rutile, Bt – biotite, Kfs – K-feldspar; the numbers in figures correspond to those in Table 2 and Table 3.

ved. In some cases, the content of BaO is relatively high (5.46 wt.%, Tab. 5). Barium feldspar forms central parts of the grains and the marginal parts are formed by pure potassium feldspar (Figs. 4a and 8c). Quartz in the studied rocks is mostly irregularly restricted, allotriomorphic and often undulous. It is often overgrown with other minerals, especially K-feldspars (Fig. 10). We did not observe xenoliths of individual minerals or fragments of surrounding rocks in the rocks, as was observed in the case of lamprophyres from the Malá Fatra Mts. region (Spišiak et al., 2018).

Apatite is a common and very important accessory mineral in a wide range of igneous rocks. In the rocks studied, apatite occurs as microphenocrysts and in the groundmass it is a very common phase crystallizing at an early stage. It is mostly present in the form of needles (closed in quartz and albite; Fig. 11), or less commonly in the form of short-column shapes (Fig. 2a). The composition of apatite is optically and chemically homogeneous. Fluorine is the dominant anion present in the apatites (Tab. 6) and its content is about 4.0 wt.%. Such high F contents are typical of apatite from lamprophyres with orogenic affinities (e.g., Krmíček et al., 2011; Tappe et al., 2006; Pandey et al., 2017). The content of Cl is very low. Sr content in apatites (Tab. 7) varies around 1500 ppm, which is lower than in orogenic and anorogenic lamprophyres (e.g. Mitchell and Bergman, 1991; Chakhmouradian et al., 2002). In general, Sr content in apatites decreases with magmatic differentiation (e.g. Belousova et al., 2002; Chu et al., 2009). On the contrary, the REE concentration in apatite increases during the evolution from primitive to more-evolved rocks (Ladenburger et al., 2016). REE contents in the studied apatites are rather high (Tab. 7), with a significant enrichment in LREE against HREE. The chondrite-normalized REE curve (Fig. 12) has a sloping course in the direction of decreasing HREE content, and

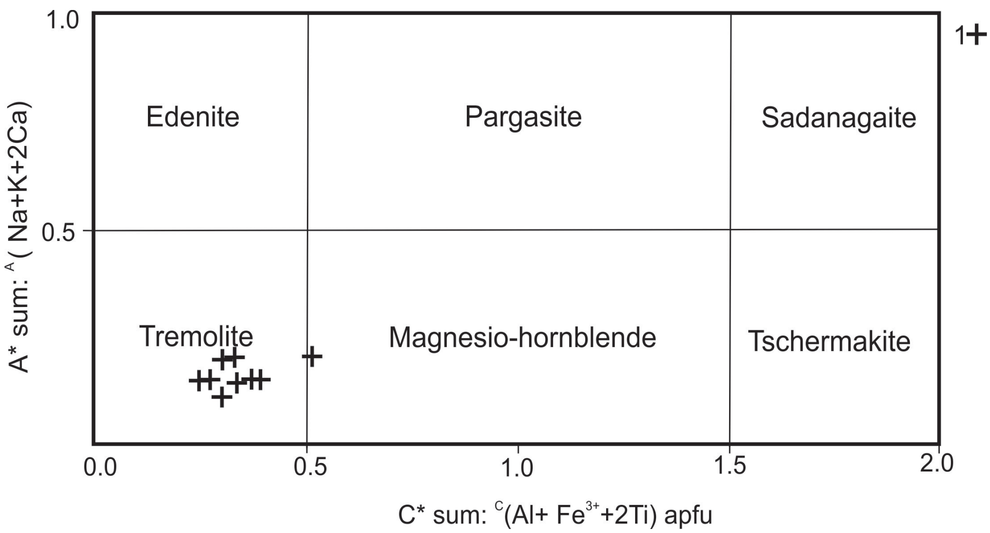

Fig. 5. The classification diagram of amphiboles, according Hawthorne et al. (2012) 1 – amphiboles from Jarabá.

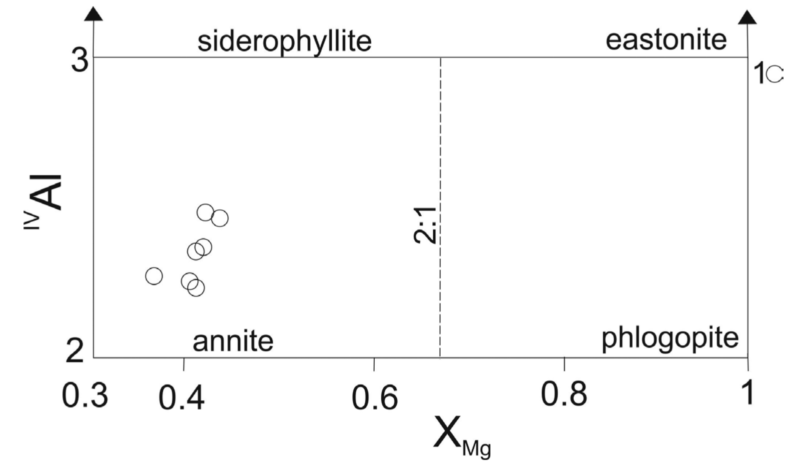

Fig. 6. Classification diagram of studied micas. End-members names according to Rieder et al. (1998), 1 – biotites from Kumštová Valley.

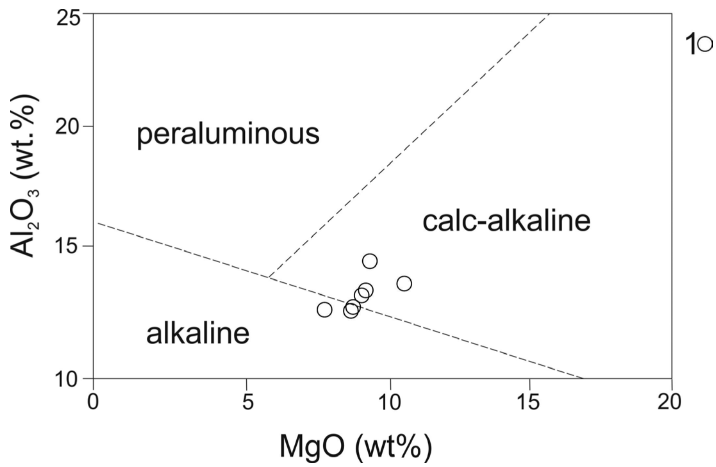

Fig. 7. Position of studied mica in the classification diagram of Abdel-Rahman (1993) for micas from different magmatic series. 1 – biotites from Kumštová Valley.

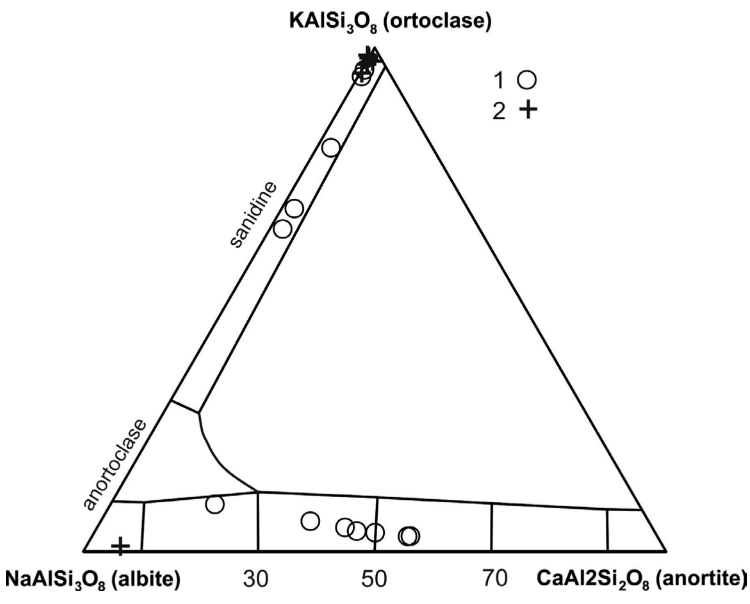

Fig. 9. The classification diagram of feldspars. 1 – Kumštová valley, 2 – Jarabá.

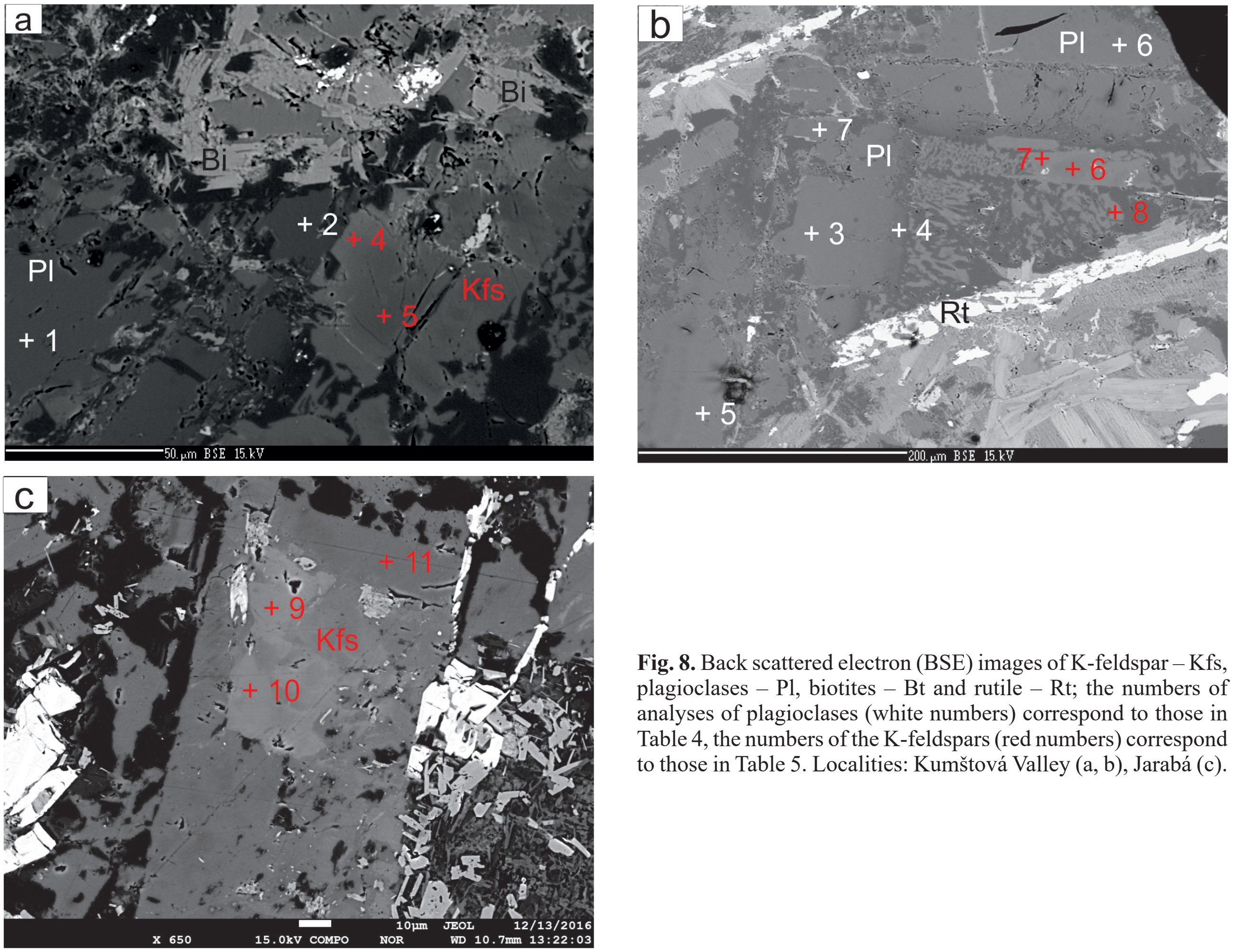

Fig. 8. Back scattered electron (BSE) images of K-feldspar – Kfs, plagioclases – Pl, biotites – Bt and rutile – Rt; the numbers of analyses of plagioclases (white numbers) correspond to those in Table 4, the numbers of the K-feldspars (red numbers) correspond to those in Table 5. Localities: Kumštová Valley (a, b), Jarabá (c).

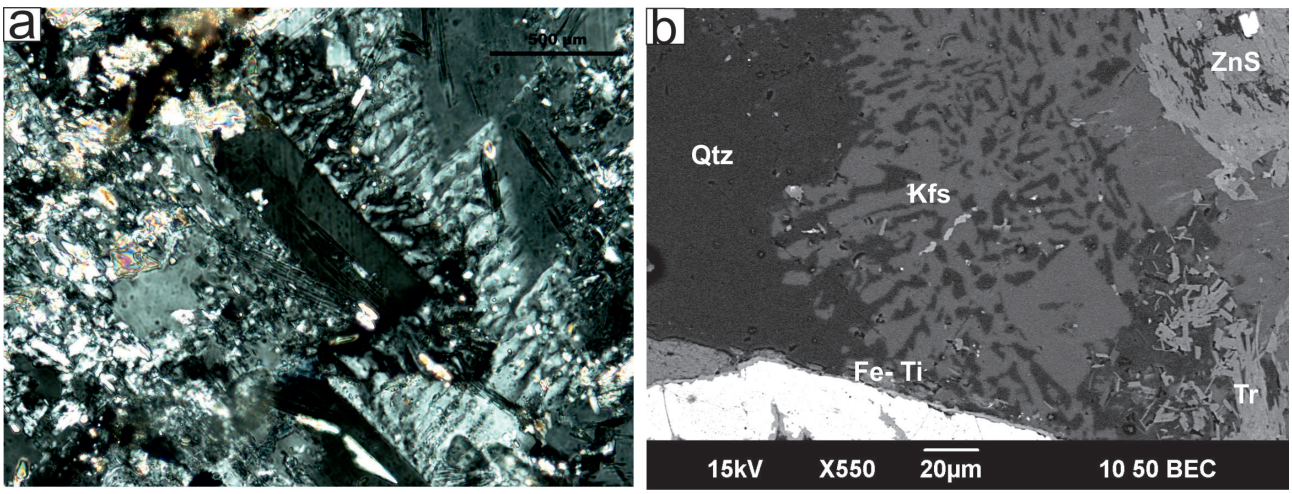

Fig. 10. a – Photomicrograph of lamprophyre; crossed polaroids. b – Back scattered electron (BSE) images of lamprophyres; Kfs – K-feldspar, Qtz – quartz, Tr – tremolite. Locality: Jarabá.

Tab. 6.
The selected microprobe analyses of apatites.

Sample	JAR-1				
Figure	**Fig. 2a**	**Fig. 2a**	**Fig. 2a**	**Fig. 2a**	**Fig. 2a**
N. anal.	**1**	**2**	**3**	**4**	**5**
SiO_2	0.21	0.18	0.19	0.14	0.13
TiO_2	0.02	0.08	0.07	0.03	0.00
Al_2O_3	0.02	0.02	0.02	0.01	0.03
FeO	0.70	0.55	0.73	0.58	0.53
MnO	0.05	0.03	0.07	0.07	0.00
CaO	52.78	52.35	52.87	52.79	52.90
MgO	0.10	0.05	0.06	0.03	0.07
SrO	0.11	0.09	0.15	0.15	0.11
BaO	0.00	0.10	0.03	0.00	0.03
PbO	0.01	0.00	0.00	0.03	0.00
Na_2O	0.00	0.00	0.00	0.00	0.05
K_2O	0.01	0.02	0.03	0.03	0.07
P_2O_5	40.89	41.35	41.09	41.62	41.34
F	3.99	4.01	3.92	3.33	3.19
SO_3	0.02	0.00	0.00	0.01	0.02
ThO_2	0.00	0.00	0.03	0.00	0.01
Y_2O_3	0.28	0.18	0.24	0.27	0.24
Sm_2O_3	0.11	0.01	0.06	0.06	0.07
Pr_2O_3	0.04	0.13	0.06	0.08	0.02
Nd_2O_3	0.36	0.34	0.30	0.30	0.20
Ce_2O_3	0.48	0.41	0.47	0.44	0.37
La_2O_3	0.21	0.17	0.19	0.11	0.16
Total	**100.38**	**100.07**	**100.55**	**100.07**	**99.52**

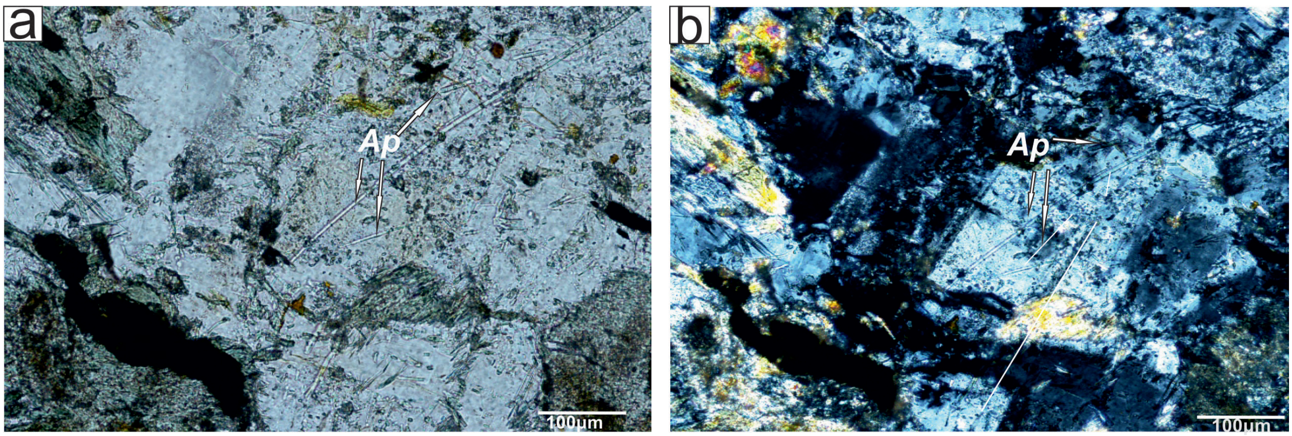

Fig. 11. a – The microphotography of apatite shape (closed in quartz and albite) in lamprophyres, parallel polaroids; b – crossed polaroids. Locality: Jarabá.

Tab. 7.
Representative apatite La-ICP-MS analyses of REE. Y. Pb. Th and U

Sample	JAR-1																					
N. anal.	1	2	3	4	5	6	7	8	9	10	11	12	13	14	15	16	17	18	19	20	21	22
La	1309	1327	1303	1297	1307	1282	1299	1289	1289	1299	1301	1275	1307	1313	1281	1268	1257	1270	1255	1298	1303	1277
Ce	2753	2800	2748	2764	2803	2760	2768	2757	2726	2815	2697	2745	2754	2754	2773	2691	2703	2711	2674	2743	2809	2744
Pr	357.4	362.9	354.8	355.9	363	353.1	361	359	349.3	360.7	356	355.6	357.8	356	360.9	351	350.7	351	349.2	357.3	357	348.9
Nd	1438	1444	1431	1441	1453	1420	1450	1447	1421	1455	1439	1421	1446	1445	1443	1412	1411	1415	1378	1441	1448	1407
Sm	234.9	236.1	231.8	233.2	237.3	230.7	233.3	233.8	229.6	236.5	230.3	229.8	234.3	232.4	232.3	228.2	229.1	226.1	223	228.9	233.6	223.9
Eu	43.14	43.35	42.79	43.82	43.53	42.73	42.69	42.69	42.17	43.12	43.16	42.64	42.96	43.77	42.85	42.4	41.85	41.57	41.17	42.7	42.75	42.12
Gd	174.4	175.9	176.3	175.2	176	172.6	177.9	176.1	173.3	175.1	172.7	172.3	174.1	175.4	175.8	172.1	170.8	167.2	166.2	175.8	178	172.1
Tb	21.52	21.82	21.51	21.72	21.84	21.44	21.74	21.38	21.3	21.69	21.44	21.42	21.5	21.71	21.79	20.94	21.07	20.8	20.6	21.41	21.53	21.23
Dy	121.3	123.1	121.4	122.4	123	121.7	122.5	121.8	119.8	123.3	120.9	121.9	121.6	122.2	122.7	121.4	119.7	117.6	117.7	122.3	122.8	119.7
Ho	21.48	22.13	22	21.79	22.21	21.7	22.12	21.68	21.5	22.12	21.96	21.73	21.98	21.84	22.11	21.46	21.28	21.14	21.09	21.59	22.2	21.34
Er	54.65	55.92	55.5	54.75	55.69	55.2	55.9	55.25	54.47	55.38	54.7	54.75	54.5	55.61	55.29	54.38	53.73	53.66	53.25	54.92	55.84	53.9
Tm	6.86	6.91	6.82	6.82	6.93	6.91	6.87	6.87	6.88	6.88	6.78	6.76	6.88	6.95	6.95	6.77	6.68	6.64	6.63	6.78	6.85	6.62
Yb	39.26	40.28	40.08	38.37	39.01	38.85	39.51	40.19	39	39.59	38.98	39.16	39.28	39.46	39.19	38.79	38.36	38.14	38.32	38.97	39.85	38.4
Lu	5.181	5.28	5.207	5.29	5.32	5.23	5.296	5.337	5.25	5.35	5.29	5.332	5.33	5.202	5.17	5.098	5.15	5.066	5.02	5.296	5.268	5.127
Y	562.5	569.2	566.1	560.7	569.3	562	563.2	557.8	560.3	573.7	559.4	562.6	563.8	561.5	569.9	552.2	558.3	555.7	551.8	568.2	571.9	562.3
Sr	1553	1553	1561	1535	1550	1551	1541	1535	1552	1550	1556	1550	1559	1557	1552	1545	1529	1534	1522	1534	1540	1540
Pb	0.71	0.99	0.72	0.75	0.85	0.53	0.42	0.73	0.65	0.92	0.63	0.8	0.75	1.29	0.6	0.4	0.44	0.45	0.64	0.95	1.16	1.17
Th	23.87	24.7	23.21	24.21	24.79	23.24	24.26	23.93	22.44	25.14	23.93	24.08	23.54	24.51	24.09	23.76	23.05	23.32	22.57	24.23	25.43	22.79
U	11.65	11.96	11.18	11.61	11.83	11.23	11.72	11.69	10.97	12.09	11.58	11.53	11.47	11.62	11.55	11.44	11.23	11.32	10.92	11.48	11.79	11.06
LREE	6309.84	6389.25	6287.69	6310.12	6382.83	6261.13	6331.89	6304.59	6230.37	6384.42	6239.16	6241.34	6316.16	6319.57	6308.85	6164.70	6163.45	6181.87	6086.57	6286.70	6371.35	6215.02
HREE	270.25	275.44	272.52	271.14	274.00	271.03	273.94	272.51	268.20	274.31	270.05	271.05	271.07	272.97	273.20	268.84	265.97	263.05	262.61	271.27	274.34	266.32
LREE/HREE	23.35	23.20	23.07	23.27	23.30	23.10	23.11	23.14	23.23	23.27	23.10	23.03	23.30	23.15	23.09	22.93	23.17	23.50	23.18	23.18	23.22	23.34
Ce/Ce*	0.96	0.96	0.96	0.97	0.97	0.98	0.96	0.97	0.97	0.98	0.94	0.97	0.96	0.96	0.97	0.96	0.97	0.97	0.96	0.96	0.98	0.98
Eu/Eu*	0.62	0.62	0.62	0.63	0.62	0.63	0.61	0.62	0.62	0.62	0.63	0.63	0.62	0.63	0.62	0.63	0.62	0.62	0.62	0.62	0.61	0.63
(La/Yb)N	22.65	22.38	22.08	22.96	22.76	22.42	22.33	21.79	22.45	22.29	22.67	22.12	22.60	22.60	22.21	22.21	22.26	22.62	22.25	22.63	22.21	22.59
(La/Sm)N	3.48	3.51	3.51	3.47	3.44	3.47	3.48	3.44	3.51	3.43	3.53	3.46	3.48	3.53	3.44	3.47	3.43	3.51	3.51	3.54	3.48	3.56

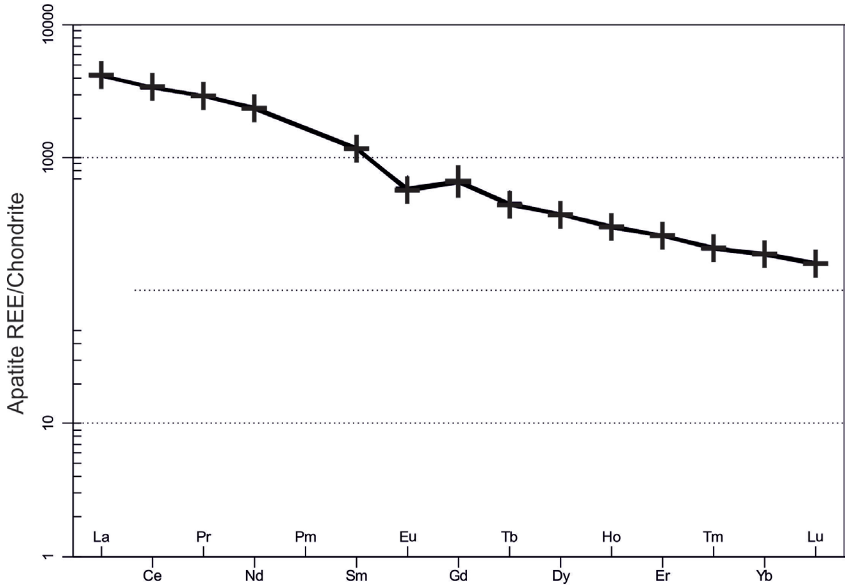

Fig. 12. Chondrite-normalized pattern for studied apatite. Chondrite values are from McDonough & Sun (1995).

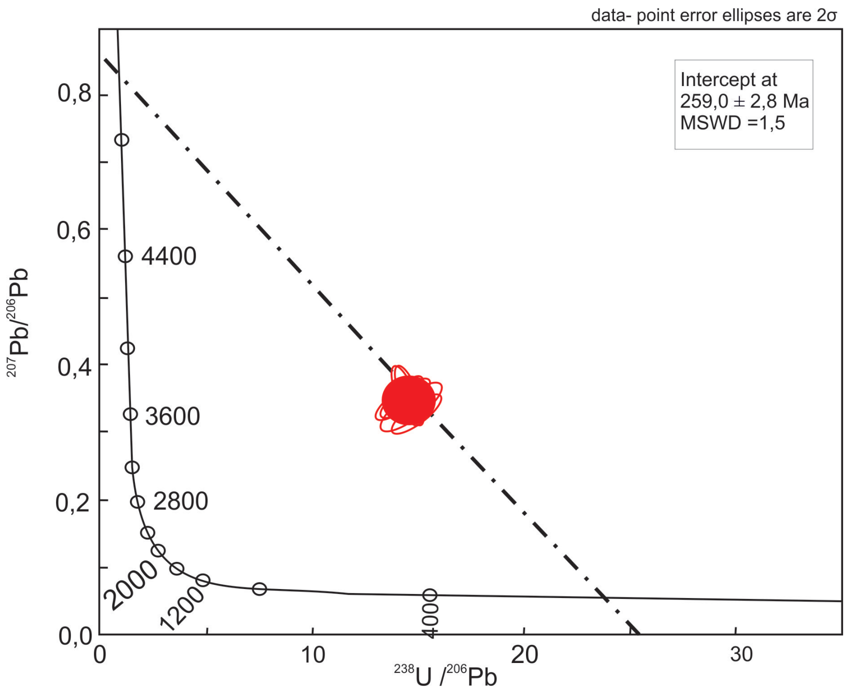

Fig. 14. The LA ICP MS analysis of apatites from the Jarabá locality.

a rather significant negative Eu anomaly can be observed. A similar course can be observed with the chondrite-normalized REE curve of bulk rocks. The contents of REE, F and Sr are similar to those found in apatites from the Frankenwald kersantites in Germany (Seifert, 2005). From secondary minerals, the chlorite, epidote and carbonates are the most common. From opaque minerals, the following association of mineral phases was found: magnetite, ilmenite (unspecified Fe-Ti oxides), rutile, hematite and pyrite. Some younger minerals (Fe-Ti oxides, hematite) supersede older mineral phases (magnetite) in the process of magmatic autohydrothermal processes (Fig. 13).

Geochronology of lamprophyres

The age of the lamprophyre rocks studied has not been precisely determined so far and their expected age classification was based on their outcropping (in crystalline rocks, they do not penetrate through the surrounding Mesozoic complexes) and the degree of alteration. In general, their age was considered as Late Paleozoic. Apatite was also used to determine the age of the rocks from Jarabá, with the aid of U/Th-Pb dating (LA ICP-MS, University of Dublin). The detected age of the rocks is 259.0 ± 2.8 Ma (Fig. 14), which stratigraphically corresponds to the

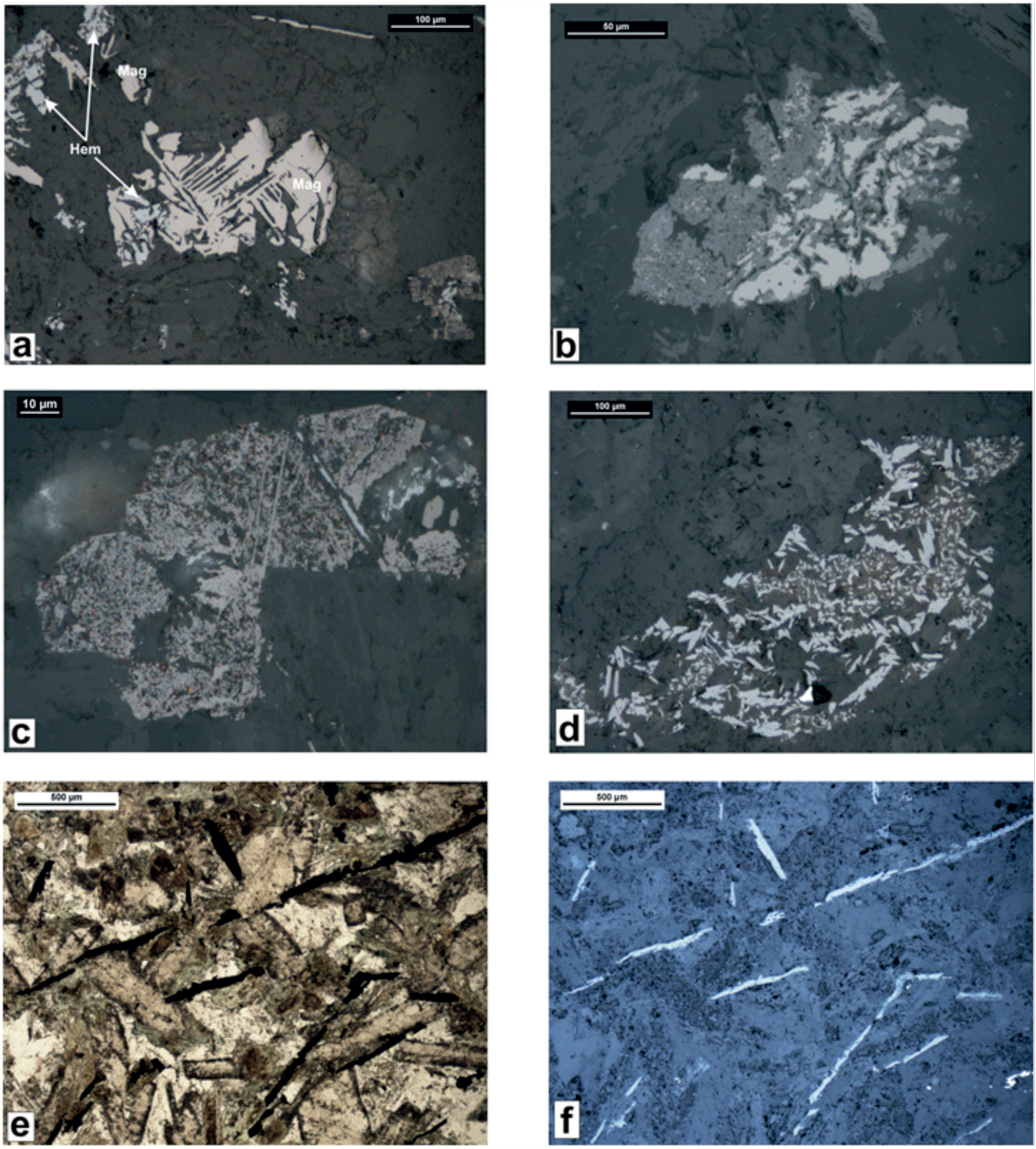

Fig. 13. The microphotography of opaque minerals: a – Disintegrated magnetite grain (Mag) pressed with hematite (Hem) and Fe-Ti oxides (dark grey) in locality of Kumštová Valley, reflected light 1N. b – Relics of magnetite (Mag) form in Fe-Ti oxides (dark-grey), locality: Jarabá, reflected light, 1N. c – Leucoxenized grain of Fe-Ti oxides decomposed into mixture of rutile (Rt) and hematite (Hem) in locality Kumštová Valley, reflected light, 1N. d – Phantom rutile (Rt) after the original Fe-Ti oxide grain, light grain is pyrite (Py) in locality Kumštová Valley, reflected light, 1N. e – Fe-Ti oxides (black) forming strips in lamprophyre from the locality of Jarabá, transmitted light, 1N. f – Detto as in part e – Fe-Ti oxides (white) from the locality of Jarabá, reflected light, 1N.

Permian. Similar ages were also found in the lamprophyre rocks of the Považský Inovec Mts. (Pelech et al., 2017), the Malá Fatra Mts. (Spišiak et al., 2018) and the Permian volcanics of the Hronicum (Malužiná Fm.; Vozár et al., 2015).

Conclusion

Based on the mineral composition, the studied lamprophyre rocks from the southern slopes of the Nízke Tatry Mts. can be characterized as kersantites and spessartites. Lamprophyres occur within the sequence of metamorphic crystalline rocks (muscovite-biotite paragneisses) and are strongly altered. From mafic minerals, mainly clinopyroxenes, amphiboles and biotites occur in the rocks. Clinopyroxenes, by their composition, correspond to augite. Amphiboles can be classified as Ca-amphiboles – tremolites. However, their composition is strongly influenced by alteration processes. Biotites are characterized by a high content of TiO_2, indicating their magmatic origin. The felsic minerals are represented by feldspar and quartz. Among the feldspars, there are plagioclases and K-feldspars. Plagioclases have a basicity from labradorite to albite and predominate over K-feldspar. Alkaline feldspars have, in addition to various amounts of sodium (Na_2O content up to 3.72 %), often also increased contents of Ba. In some cases (BaO = 5.46 %) we can already consider the barium feldspars – hyalophane. Apatites and zircons are present in accessory amounts. Apatite corresponds to fluorine dominant type (F 4.0 wt.%), which is characteristic for orogenic calc-alkaline lamprophyre. Apatite has a high content of REE, with a significant enrichment of LREE. Secondary minerals include chlorite, epidote and carbonates. Ore minerals are represented by magnetite, ilmenite, hematite and pyrite. Based on the mineral composition of the rocks, the studied lamprophyres belong to calc-alkaline type – it well corresponds to their geochemical composition (calc-alkaline lamprophyre with affinity for orogenic – subduction related types; Spišiak et al., 2017; Vetráková & Spišiak, 2018).

The age of the studied lamprophyre rocks was determined by LA ICP-MS analysis of apatites to 259.0 ± 2.8 Ma, stratigraphically corresponding to the Permian and being in agreement with their geological position. The similarity of their mineral and chemical composition with Permian volcanics of the Hronicum and identical age point to a possible co-magmatism of these rocks.

Acknowledgements

This research was supported by grants VEGA 1/0650/15, 1/0237/18 and APVV 15-0050. We appreciate the critical reviews by Marian Putiš and anonymous reviewer who helped to improve the manuscript.

References

Abdelfadil, K. H., Romer, R. L., Seifert, T. H. & Lobst, R., 2013: Calc-alkaline lamprophyres from Lusatia (Germany) – evidence for a repeatedly enriched mantle source. *Chem. Geol., 353, 230 – 245.*

Abdel-Rahman, A. M., 1993: Nature of biotites from alkaline, calcalkaline, and peraluminous magmas. *J. Petrol., 35, 525 – 541.*

Awdankiewicz, M., 2007: Late Palaeozoic lamprophyres and associated mafic subvolcanic rocks of the Sudetes (SW Poland): petrology, geochemistry and petrogenesis. *Geol. Sudet., 39, 11 – 97.*

Belousova, E. A., Griffin, W. L., O'Reilly, S. Y. & Fisher, N. I., 2002: Apatite as an indicator mineral for mineral exploration: trace-element composition and their relationship to host rock type. *J. Geochem. Explor., 76, 45 – 69.*

Chakhmouradian, A., Reguir, E. P. & Mitchell, R. H., 2002: Strontium-apatite: New occurrences, and the extent of Sr-for-Co substitution in apatite-group minerals. *Canad. Mineralogist, 40, 121 – 136.*

Chew, D. M. & Donelick, R. A., 2012: Combined apatite fission track and U-Pb dating by LA-ICP MS and future trends in apatite provenance analysis. In: Sylvester P. (Ed.): Quantitative mineralogy and microanalysis of sediments and sedimentary rocks. *Mineral. Assoc. Canada*, 219 – 248.

Chew, D., Petrus, J. A. & Kamber, B. S., 2014: U-Pb LA-ICP MS dating using accessory mineral standards with variable common Pb. *Chem. Geol., 363, 185 – 199.*

Chu, M. F., Wang, K. L., Griffin, W. L., Chung, S. L., O'Reilly, S. Y., Pearson, N. J. & Ilzuka, Y., 2009: Apatite composition: Tracing petrogenetic processes in Transhimalayan granitoids. *J. Petrol., 50, 1 829 – 185.*

Cochrane, R., Spikings, R. A., Chew, D., Wotzlaw J. F., Chiaradia, M., Tyrrell, S., Schaltegger, U. & Van der Lelij, R., 2014: High temperature (>350 °C) thermochronology and mechanisms of Pb loss in apatite. *Geochim. cosmochim. Acta, 127, 39 – 56.*

Geologická mapa Slovenska M 1 : 50 000 [online]. Bratislava, Št. Geol. Úst. D. Štúra, 2013. Available on the internet: http://apl.geology.sk/gm50js.

Hawthorne, C. F., Oberti, R., Harlow, G. E., Maresch,V. W., Martin, F. R., Schumacher C. J. & Welch, D. M., 2012: Nomenclature of the amphibole supergroup. *Amer. Mineralogist, 97, 2 031 – 2 048.*

Hegner, E., Kölbl-Ebert, M. & Loeschke, J., 1998: Postcollisional Variscan lamprophyres (Black Forest, Germany), $^{40}Ar/^{39}Ar$ phlogopite dating, Nd, Pb, Sr isotope and trace element characteristics. *Lithos, 45, 395 – 411.*

Hovorka, D., 1967: Porphyres and lamprophyres from tatraveporide crystalline complexes. *Sbor. geol. Vied, 8, 51 – 78.*

Kamenický, J., 1962: Geological-petrographic conditions of kersantite of the Nízke Tatry Mts. *Geol. Práce, Zpr., 24.*

Krist, E., 1967: Geological-petrographic conditions of spessartite-kersantite dyke in the Nízke Tatry Mts. *Acta. geol. geogr. Univ. Comen., Geol., 12, 63 – 73.*

Krmíček, L., Cempírek, J., Havlín, A., Přichystal, A., Houzar, S., Krmíčková, M. & Gadas, P., 2011: Mineralogy and petrogenesis of a Ba-Ti-Zr-rich peralkaline dyke from Šebkovice (Czech Republic): recognition of the most lamproitic Variscan intrusion. *Lithos, 121, 74 – 86.*

Ladenburger, S., Marks, **M. A. W.**, Upton, B., Hill, P., Wenzel, T. & Markl, G., 2016: Compositional variation of apatite from rift-related alkaline igneous rocks of the Gardar Province, South Greenland. *Amer. Mineralogist, 101, 612 – 626.*

Le Maitre, R. W., Streckeisen, A., Zanettin, B., Le Bas, M. J., Bonin, B., Bateman, P., Bellieni G., Dudek, A., Efremova, S., Keller, J., Lameyre, J., Sabine, P. A., Schmidt, R., Sorensen, H. & Wolley, A. R., 2002: Igneous rocks a classification and Glossary of Terms. Recommendationas of the International Union of Geological Sciences. Subcommision on the Systematics of Igneous Rocks. *Cambridge University Press, 236 pp.*

Macdonough, W. F. & Sun, S. S., 1995*:* Composition of the Earth. *Chem. Geol., 120, 228.*

McDowell, F.W., McIntosh, W. C. & Farley, K. A., 2005: A precise ^{40}Ar-^{39}Ar reference age for the Durango apatite (U-Th)/He and fission-track dating standard. *Chem. Geol., 214, 249 – 263.*

Mitchell, R. H. & Bergman, S. C., 1991: Petrology of Lamproites. *New York, Plenum. Press, 1 – 447.*

Morimoto, N., Fabries, J., Ferguson, A. K., Ginzburg, I. V., Ross, M., Seifert, F. A., Zussman, J., Aoki, K. & Gottardi, G., 1988: Nomenclature of pyroxenes. *Amer. Mineralogist, 73, 1 123 – 1 133.*

Ondrejka, M., Huraiová, M., Petrík, I., Kohút, M., Spišiak, J., Šarinová, K., Konečný, V. & Vančová, I., 2015: Klasifikácia a nomenklatúra magmatických hornín. *Miner. Slov., 47, 97 – 112.*

Pandey, R., Chalapathi Rao, N. V., Dhote, P., Pandit, D., Choudhary, A. K., Sahoo, S. & Lehmann, B., 2017: Rift-associated ultramafic lamprophyre (damtjernite) from the middle part of the Lower Cretaceous (125 Ma) succession of Kutch, northwestern India: Tectonomagmatic implications. *Geosci. Front., 1 – 20.*

Paton, C., Hellstrom, J., Paul, B., Woodhead, J. & Hergt, J., 2011: Iolite: freeware for the visualisation and processing of mass spectrometric data. *J. Anal. At. Spectrom., 26, 2 508 – 2 518.*

Pelech, O., Vozárová, A., Uher, P., Petrík, I., Plašienka, D., Šarinová, K. & Rodionov, N., 2017: Late Permian volcanic dykes in the crystalline basement of the Považský Inovec Mts. (Western Carpathians): U-Th-Pb zircon SHRIMP and monazite chemical dating. *Geol. Carpath., 68, 6, 530 – 542.*

Petrus, J. A. & Kamber, B. S., 2012: Vizual age: A novel approach to laser ablation ICP-MS U-Pb geochronology data reduction. *Geostand. Geoanalytical. Res., 36, 247 – 270.*

Plank, T. & Langmuir, C. H., 1998: The chemical composition of subducting sediment and its consequences for the crust and mantle. *Chem. Geol., 145, 325 – 394.*

Rieder, M., Cavazzini, G., D'Yakonov, Y. S., Frank-Kamenetskii V. A., Gottardi, G., Guggenheim, S., Koval, P. V., Müller, G., Neiva, A. M. R., Radoslovich, E. W., Robert, J. L., Sassi, F. P., Takeda, H., Weiss, Z. & Wones, D. R., 1998: Nomenclature of micas. *Canad. Mineralogist, 36, 905 – 912.*

Schoene, B. & Bowring, S. A., 2006: U-Pb systematics of the McClure Mountain syenite: thermochronological constraints on the age of the ^{40}Ar/^{39}Ar standard MMhb. *Contr. Mineral. Petrology, 151, 5, 615 – 630.*

Seifert, T., 2008: Metallogeny and Petrogenesis of Lamprophyres in the Mid-European Variscides. *Amsterdam, IOS Press Millpress, 1 – 303.*

Seifert, W., 2005: REE-, Zr-, and Th-rich titanite and associated accessory minerals from a kersantite. *Mineral. Petrol., 84, 129 – 146.*

Spišiak, J., Vetráková, L., Chew, D., Ferenc, Š., Šimonová, V. & Prokešová, R., 2017: Calc-alkaline laprophyres from Nízke Tatry Mts. *13th Workshop of Alpine Geological Studies. Serbia, 100 pp.*

Spišiak, J., Vetráková, L., Chew, D., Ferenc, Š., Mikuš, T., Šimonová, V. & Bačík, P., 2018: Petrology and dating of the Permian lamprophyres from the Malá Fatra Mts. (Western Carpathians, Slovakia). *Geol. Carpath., 69, 5, 453 – 466.*

Štemprok, M., Dolejš, D. & Holub, F. V., 2014: Late Variscan calc–alkaline lamprophyres in the Krupka ore district, Eastern Krušné Hory/Erzgebirge: their relationship to Sn-W mineralization. *J. Geosci., 59, 41 – 68.*

Tappe, S., Foley, S. F., Jenner, G. A., Heaman, L. M., Kjarsgaard, B. A., Romer, R. L., Stracke, A., Joyce, N. & Hoefs, J., 2006: Genesis of ultramafic lamprophyres and carbonatites at Aillik Bay, Labrador: a consequence of incipient lithospheric thinning beneath the North Atlantic Craton. *J. Petrology, 47, 1 261 – 1 315.*

Thomson, S. N., Gehrels, G. E., Ruiz, J. & Buchwaldt, R., 2012: Routine low-damage apatite U-Pb dating using laser ablation-multicollector-ICPMS. *Geochem. Geophys. Geosyst*., 13, 2, 23.

Turpin, L., Velde, D. & Pinte, G., 1988: Geochemical comparison between minettes and kersantites from the western European Hercynian orogen: trace element and Pb-Sr-Nd isotope constraints on their origin. *Earth. planet. Sci. Lett., 87, 73 – 86.*

Ulrych, J., Pivec, E., Zak, K., Bendl, J. & Bosak, P., 1993: Alkaline and ultramafic carbonate lamprophyres in central Bohemian carboniferous basins, Czech Republic. *Mineral. Petrol., 48, 65 – 81.*

Vetráková, L. & Spišiak, J., 2018: Geochemistry and geochronology of calc-alkaline lamprophyres, Central Slovakia/Western Carpathians. *Joint 5th Central-European Mineralogical Conference and 7th Mineral Sciences in the Carpathians Conference, 112 pp.*

Vozár, J., Spišiak, J., Vozárová, A., Bazarník, J. & Kráľ, J., 2015: Geochemistry and Sr, Nd isotopic composition of the Hronic Upper Paleozoic basic rocks (Western Carpathians, Slovakia). *Geol. Carpath., 66, 3 – 17.*

Mineralógia a geochronológia vápenato-alkalických lamprofýrov z Nízkych Tatier (tatrikum, Západné Karpaty)

Lamprofýry sú dajkové horniny, ktoré sú minerálnym zložením, štruktúrou a do určitej miery aj chemickým zložením odlišné od intruzívnych a efuzívnych hornín. Ide o tmavozelené porfyrické horniny s jemnozrnnou až afanitickou základnou hmotou. V kryštaliniku Nízkych Tatier bolo opísaných viacero telies týchto bázických žilných hornín (Kamenický, 1962; Hovorka, 1967; Krist, 1967). Pri štúdiu sme sa zamerali na relatívne najčerstvejšie typy hornín z dvoch lokalít: z oblasti Jarabá – Mýto pod Ďumbierom; 1 – odkryv pri ústí Kumštovej doliny nad hlavnou cestou na Čertovicu, N 48° 54′ 19″, E 19° 42′ 14″; 2 – starší opustený lom zhruba v strede dediny Jarabá na ľavej strane potoka, N 48° 53′ 25″, E 19°, 41′ 39″. Telesá žilných hornín na lokalite Jarabá a Kumštová dolina ležia v rulách (staršie paleozoikum). Študované lamprofýrové horniny z Nízkych Tatier na základe klasifikácie IUGS (Le Maitre et al., 2002; Ondrejka et al., 2015) zaraďujeme na lokalite Kumštová dolina ku kersantitom a na lokalite Jarabá k spessartitom. Minerálne zloženie tvoria primárne (mafické a felzitické), sekundárne a opakové minerály. Z mafických minerálov sa v horninách vyskytujú hlavne klinopyroxény, amfiboly a biotity. Z felzitických minerálov sú prítomné živce a kremeň. Klinopyroxény svojím zložením zodpovedajú augitom (Morimoto et al., 1988), amfiboly Ca-amfibolom, tremolitom (Hawthorne et al., 2012). Ich koexistencia s klinopyroxénmi je však nejasná a sú pravdepodobne mladšie. Pre biotity je charakteristický vysoký obsah TiO_2, čo poukazuje na ich magmatický pôvod. Zo skupiny živcov sa vyskytujú plagioklasy aj draselné živce. Plagioklasy majú bazicitu zodpovedajúcu labradoritu a po okrajoch ich zatláča mladší albit. Alkalické živce okrem rôzneho zastúpenia sodíka (obsah Na_2O do 3,72 %) majú často aj zvýšený obsah Ba. V niektorých prípadoch (BaO = 5,46 hm. %) už môžeme hovoriť o bárnatých živcoch. Zo sekundárnych minerálov sú zastúpené chlorit, epidot a karbonáty. Z rudných minerálov sa zistila nasledujúca asociácia opakových minerálnych fáz: magnetit, ilmenit (resp. nešpecifikované Fe-Ti oxidy), rutil, hematit a pyrit. Vek študovaných lamprofýrových hornín bol stanovený LA ICP-MS analýzou apatitov a je 259,0 ± 2,8 Ma.

Doručené / Received: 1. 4. 2019
Prijaté na publikovanie / Accepted: 4. 6. 2019

Mineralia Slovaca, Web ISSN 1338-3523, ISSN 0369-2086
51 (2019), 79 – 101

Prieskum ochrannej funkcie zóny aerácie nad Krásnohorskou jaskyňou (Silická planina) pomocou stopovacích skúšok

PETER MALÍK[1], JAROMÍR ŠVASTA[1], BRANISLAV MÁŠA[2], FRANTIŠEK BOTTLIK[1], NATÁLIA BAHNOVÁ[1] a ALEXANDRA VASILENKOVÁ[1]

[1] Štátny geologický ústav Dionýza Štúra, oddelenie hydrogeológie a geotermálnej energie, Mlynská dolina 1, 817 04 Bratislava 11
[2] HES-Comgeo, spol. s r. o., Kostiviarska cesta 4, 974 01 Banská Bystrica;

Survey of protective function of the aeration zone above the Krásnohorská jaskyňa Cave (Silická planina Plateau) using tracing tests

Abstract: Four tracer experiments were performed on the surface of the Silická planina karstic Plateau in the period of October 2016 – April 2017. The aim was to verify the natural protection function of the 185 – 250 m thick unsaturated zone above the underground hydrologic system of the Krásnohorská jaskyňa Cave. The cave is situated on the northern rim of the Silická planina Plateau along the underground stream that appears on the land surface as the Buzgó karstic spring. No perennial swallow hole/ponor exists here to feed the underground, the tracers were injected into the dug pits artificially excavated on the bottoms of four major sinkoles in the area. Dye tracers of sodium naphtionate, fluorescein and sulphorhodamine B were injected into the sinkoholes marked as (A), (B) and (C) on the 26th October 2016. Later, on 14th November 2016 bacteriophages H40/1 suspension was injected to the last (D) sinkhole. Six submergible flow-through field fluorometers GGUN-FL30 were used for tracer detection at 5 points of the Krásnohorská jaskyňa Cave underground hydrologic system (Marikino jazero Lake, two smaller tributaries – left under the Veľká sieň Hall and right in the Abonyiho dóm Dome and Buzgó spring outlet) and at the Eveteš spring, exploited as drinking water source. Capsules filled with activated carbon were installed at 5 smaller springs in the area. Signals recorded at sorption material were weak and ambiguous, but fluorimeters' data showed reliable results. While sulphorhodamine and bacteriophages from the (C) and (D) sinkholes were not detected in the whole period of observations, naphtionate injected at (A) site appeared in several consecutive peaks of various strength at every monitoring point within the cave, but also in the 4.8 km distanced spring of Eveteš. Fluorescein from the (B) sinkhole appeared in quite a low concertation only at two side tributaries (both left and right) of the main underground stream. Recorded travel times were from 3.3 to 36.3 days, flow velocities recorded by GGUN-FL30 fluorometers were ranging between 1.9 and 1443.2 m/day (0.002 – 1.670 cm/second), recorded maximal concentrations at individual monitoring sites were within the range of 0.24 – 121.71 ppb. Based on these results, area to west and southwest from the cave system is supposed to have relatively good natural protective function, while the area eastwards represent a naturally weakly protected place. If possibly hit by potential pollution, its quick spreading and appearance at quite distanced places can be expected.

Key words: sinkholes, vulnerability, trace experiments, fluorescein, naphtionate, sulphorhodamine, bacteriophages H40/1, Silická planina Plateau, Krásnohorská jaskyňa Cave (Slovakia)

Kľúčové slová: závrty, zraniteľnosť, stopovacie skúšky, fluoresceín, naftionát, sulforodamín, bakteriofágy H40/1, Silická planina, Krásnohorská jaskyňa

Graphical abstract

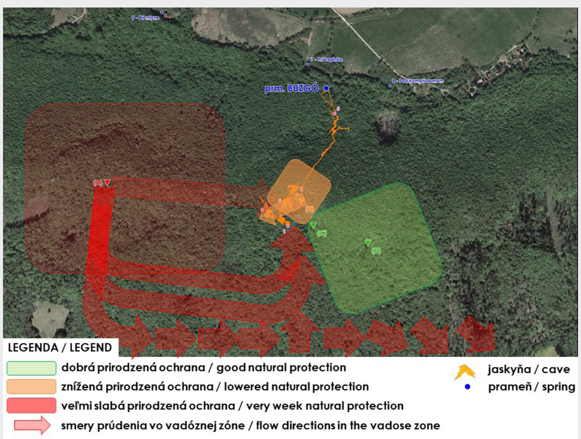

Highlights

- dye tracers verified the natural protection function of the 185 – 250 m thick unsaturated zone above the Krásnohorská jaskyňa Cave system
- four tracers injected into manually excavated dug holes in the sinkholes' bottoms
- bacteriophages H40/1 were also used, but without success
- environmentally sensitive area delineated west from the cave system, relatively good natural protective function is on the east

Úvod

Ochrana zdrojov podzemnej vody v krasovom prostredí predstavuje kľúčový problém zachovania významného množstva pitnej vody sústredeného v takomto type kolektorov. Vápence a dolomity, na ktoré sa táto voda viaže, dokážu sústrediť do malých vývěrových oblastí ekonomicky významnú výdatnosť, ktorá v súčasnosti predstavuje takmer 54 % celkovej spotreby vody na Slovensku (Malík et al., 2018). Kvalita vody v krasovom prostredí vo veľkej miere závisí od spôsobu prepojenia podzemného hydrologického systému s povrchom (Zwahlen – ed., 2004), jeho správne ohraničenie zas determinuje bilanciu množstva vody obiehajúcej v podzemí. V rokoch 2012 až 2018 pracovníci Štátneho geologického ústavu Dionýza Štúra v rámci projektu LIFE+ KRASCAVE realizovali množstvo výskumných aktivít v oblasti Krásnohorskej jaskyne. Medzi inými sa v roku 2016 realizovali stopovacie skúšky. Ich cieľom bolo overiť prirodzenú ochrannú funkciu, ktorú podzemnému hydrologickému systému poskytuje horninové nadložie nad jaskyňou. Hrúbka tohto nadložia – vadóznej zóny nad jaskyňou – je medzi dnami závrtov v oblasti a úrovňou podzemného hydrologického systému Krásnohorskej jaskyne 185 až 240 m. Stopovacie skúšky realizované v októbri a novembri 2016 a trvajúce až do jarných mesiacov 2017 boli zamerané na testovanie citlivosti vody Krásnohorskej jaskyne na potenciálnu kontamináciu prítomnú na bezprostredne blízkom povrchu Silickej planiny. Metodika ich realizácie bola odlišná, než je obvyklé pri speleologických alebo vodohospodárskych prieskumoch v krasových oblastiach. V prípade našich stopovacích skúšok bola predmetom testovania rýchlosť prepojenia s podzemím dna závrtov, resp. krasových jám, ktoré signalizujú prirodzený úbytok horninovej hmoty smerom do podzemia, a tým aj blízkosť komunikačných ciest, prostredníctvom ktorých je tento odnos hmoty sprostredkúvaný. Cieľom prác bolo overenie priestorovej distribúcie vzájomných prepojení a rýchlosti postupu prúdenia podzemnej vody do podzemného hydrologického systému Krásnohorskej jaskyne, prípadne do podzemnej vody v jej okolí z bezprostredného nadložia tvoreného povrchom severnej časti Silickej planiny.

Charakteristika skúmaného územia

Krásnohorská jaskyňa a jej podzemný hydrologický systém predstavujú unikátny súbor fenoménov vytváraných podzemnou vodou. Jeho jedinečnosť spočíva najmä v mimoriadnej kumulácii sintrových foriem previazaných na činnosť vody, ktorá pri svojom sústredenom výstupe z podzemia vytvára mohutný krasový prameň Buzgó. Jaskyňa je tak prirodzene predmetom mnohých odborných štúdií, do ktorých zapadá aj naša práca. Terminálnym prejavom podzemného hydrologického systému Krásnohorskej jaskyne je krasový prameň Buzgó, v ktorom spomínaná voda v katastri obce Krásnohorská Dlhá Lúka vystupuje na povrch. Prirodzený výstup krasovej podzemnej vody v prameni Buzgó bol známy už od nepamäti, no jaskynný systém Krásnohorskej jaskyne, ktorý sa za ním nachádza, bol objavený až po namáhavom speleologickom prieskume v rokoch 1954 až 1964 (Stankovič a Cílek – red., 2005). Krásnohorská jaskyňa, ktorú v lete 1964 objavili rožňavskí jaskyniari (Roda, 1964; Skřivánek, 1965; Roda, 1966; Stankovič a Horváth, 2004), má v súčasnosti známu dĺžku 1 550 m, pričom aktívny vodný tok v podzemí sleduje približne jednu tretinu tejto dĺžky. Jaskyňa v sebe ukrýva mohutný stalagnát vysoký 32,6 m a Kvapeľ rožňavských jaskyniarov vážiaci približne 2 000 t, ktorý bol v čase svojho objavu považovaný za najväčší sintrový útvar na svete (Roda, 1966). Podľa Gaála (in Stankovič a Cílek – red., 2005) je severná časť Krásnohorskej jaskyne vytvorená v strednotriasových gutensteinských dolomitoch a dolomitových vápencoch, jej zadné (najjužnejšie) časti sú situované už v mladších, steinalmských vápencoch tektonickej jednotky silicika (Mello et al., 1997). Hlavnou osou podzemného hydrologického systému Krásnohorskej jaskyne je vodný tok objavujúci sa v Suťovom dóme, prechádzajúci Marikiným jazerom a Sifónom potápačov, pričom na svojej zhruba 400 m dlhej ďalšej ceste priberá len dva významnejšie prítoky – ľavostranný v priestoroch pod Veľkou sieňou (od Heliktitového dómu) a pravostranný v Abonyiho dóme. Výdatnosť oboch prítokov je približne rovnaká a ani jedna z nich zvyčajne nepresahuje 2,0 l . s^{-1}, takže ich podiel na celkovom prietokovom množstve podzemného vodného toku pretekajúceho jaskyňou je menej ako 10 % (Bajtoš et al., 2017). Je zaujímavé, že prítok vody, recentne dotujúcej tvorbu Kvapľa rožňavských jaskyniarov, je veľmi malý, len okolo 0,02 až 0,04 l . s^{-1}. Možno ho pozorovať ako ľavostranný prítok v Chodbe perál asi 35 m pod vyššie sa nachádzajúcim prítokom pod Veľkou sieňou (od Heliktitového dómu). V tejto práci je označený ako miesto presakovania zo Siene obrov, v suchých obdobiach úplne zaniká. Ani detailné rezistivimetrické a termometrické merania podzemného vodného toku v jaskyni (Malík et al., 2011) neoverili existenciu iných viditeľných či skrytých prítokov do hlavného podzemného toku v jaskyni až po úroveň Sifónu potápačov, resp. Marikinho jazera. Za Marikiným jazerom pokračuje tok v podzemí sifónom Marikinho jazera dlhým 120 m a hlbokým 28 m, potom ešte 250 m v sérii troch dómov, kde za ďalším sifónom dlhým 15 m priteká voda spod závalu do jazera v poslednom známom Suťovom dóme (Stankovič a Cílek – red., 2005). Vývěr vody na povrch v krasovom prameni Buzgó je sprostredkúvaný Výstupným sifónom dlhým približne 40 m. Výstup krasovej podzemnej vody je tu podmienený existenciou poklesnutého bloku strednotriasových karbonátov so šírkou

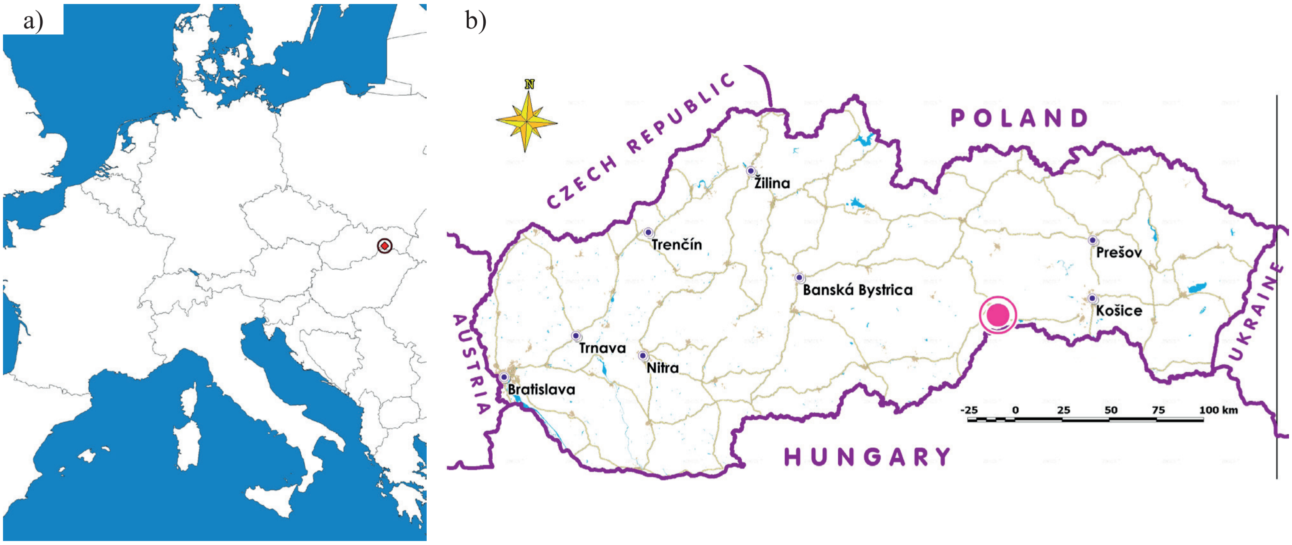

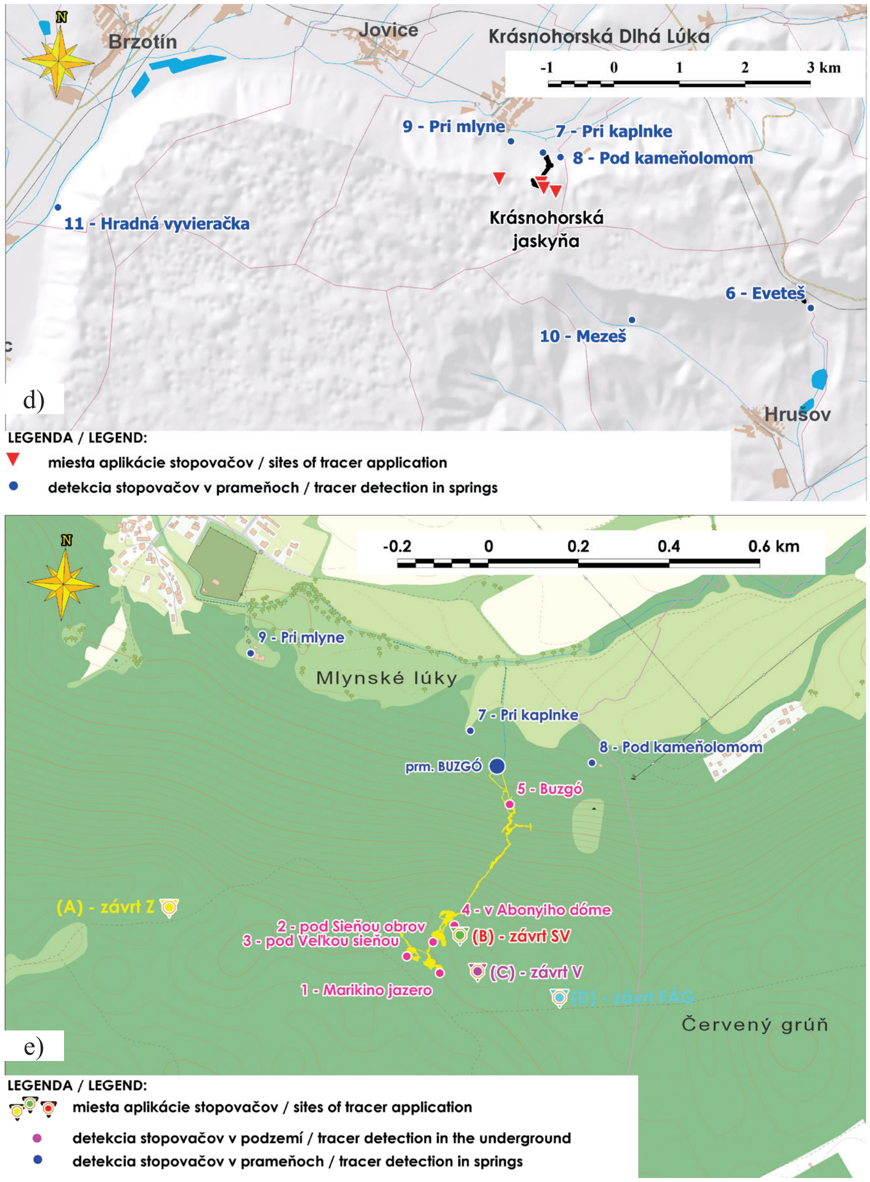

Obr. 1. Lokalizácia skúmanej oblasti: a) v rámci Európy, b) na území Slovenska. Polohy miest aplikácie a miest detekcie stopovacích látok: c) v oblasti severnej časti Silickej planiny, d) vnútri podzemného hydrologického systému Krásnohorskej jaskyne.

Fig. 1. Location of the investigated area in: a) Europe, b) on the territory of Slovak Republic. Situation of tracer injection sites: c) in the northern part of the Silická planina Plateau, d) inside the underground hydrologic system of the Krásnohorská jaskyňa Cave.

približne 800 m, kde sa táto voda dostáva do priameho kontaktu s aluviálnymi náplavmi toku Čremošnej.

Hydrogeologický vrt RHV-4, ktorý bol v minulosti (Orvan a Vrábľová, 1986) v rámci rozsiahleho vyhľadávacieho hydrogeologického prieskumu v oblasti Silickej planiny realizovaný v blízkosti vstupu do Krásnohorskej jaskyne, overil, že málo priepustné podložie spodnotriasových sinských vrstiev je tu poklesnuté ešte asi 80 m pod úrovňou toku Čremošnej. V uvedenom 800 m koridore vystupuje krasová podzemná voda ešte v ďalších dvoch menších prameňoch Pod kameňolomom a Pri kaplnke (Malík et al., 2014a, b). Smerom na východ aj na západ od nich sú potom severné svahy Silickej planiny budované spodnotriasovými sinskými vrstvami (Mello et al., 1996). Samotný krasový prameň Buzgó má za celé doteraz pozorované obdobie priemernú výdatnosť 55,1 l . s^{-1}. Je jedným z najdlhšie pozorovaných prameňov na území Slovenska. Pozorovania Slovenského hydrometeorologického ústavu (SHMÚ) tu s dvomi menšími prestávkami v rokoch 1966 – 1967 a 2010 prebiehajú od roku 1958. Najvyššia výdatnosť, 1 355,8 l . s^{-1}, tu bola zaznamenaná 10. augusta 2002, minimálna výdatnosť, 5,3 l . s^{-1}, bola registrovaná počas viacerých dní vo februári 1987. Teplota vody prameňa je relatívne stála, okolo 9,3 °C, namerané hodnoty za uvedené obdobie pozorovania sa však pohybovali od 5,3 do 12,2 °C.

Mimoriadna príťažlivosť jedinečných prírodných fenoménov nachádzajúcich sa v oblasti severných svahov Silickej planiny, a najmä v podzemí Krásnohorskej jaskyne, už desaťročia podnecuje mnohé výskumné aktivity v tejto oblasti. Okrem uvedených už skôr publikovaných prác (ich dobrý prehľad poskytuje sumarizujúca publikácia Stankovič a Cílek – red., 2005) to bolo vypracovanie podrobnej geologickej mapy tejto oblasti v mierke 1 : 5 000 (Kronome a Boorová, 2016). Jej autori spresnili hranice jednotlivých litostratigrafických členov v príslušnej oblasti Silickej planiny (Mello et al., 1996), pričom však pomocou získaných výbrusov rozlíšili aj stratigraficky mladšie horizonty v rozsahu až po mladší trias (karn – norik, azda až rét). Pukliny sv.-jz. smeru, viditeľné aj v Krásnohorskej jaskyni, však odvodzujú z gravitačných svahových pohybov (rozsadlín). Ich smer je následne daný najmä morfologicky určeným smerom gravitačne nestabilného okraja planiny. Podľa týchto autorov aj samotné založenie Krásnohorskej jaskyne je na takejto gravitačnej svahovej skalnej rozsadline. Chemické a izotopové zloženie vody v systéme Krásnohorskej jaskyne skúmala v rámci svojej dizertačnej práce Gavuliaková (2016), výsledky boli publikované aj v práci Gavuliaková et al. (2015). V širšej perspektíve bolo izotopové a chemické zloženie vody jaskyne v kontexte celej Silickej planiny opísané v práci Fľaková et al. (2018). Geochemický model tvorby chemického zloženia vody v časti podzemného hydrologického systému zostavili Bajtoš et al. (2017). Kováčová et al. (2017) publikovali výsledky meraní obsahu CO_2 a niektorých mikroklimatických parametrov v dĺžkovom profile Krásnohorskej jaskyne počas letného režimu prúdenia vzduchu. V nedávnom období v tejto oblasti prebiehal rozsiahly inžinierskogeologický a hydrogeologický prieskum pre cestný tunel projektovaný popod priesmyk Soroška, realizovaný pracovníkmi spoločnosti DPP Žilina (Grenčíková et al., 2018; Szabó et al., 2018).

Z pohľadu výsledkov prác uvedených v tejto práci sú najrelevantnejšie výsledky stopovacích skúšok realizovaných v tejto oblasti v minulosti. V rámci nich boli overené prepojenia podzemného hydrologického systému Krásnohorskej jaskyne s občasne sa ponárajúcou vodou v oblasti studne Rakaťa (Roda, 1967; Erdös, 1995) a studne Žedem (Roda et al., 1986). Z pohľadu autochtónnosti/alochtonity vôd však tieto vody pochádzajú len z najbližšieho povrchu Silickej planiny a možno teda konštatovať, že jaskyňa je v podstate dotovaná autochtónnymi vodami, infiltrujúcimi do hĺbky Silickej planiny najmä po jarnom topení snehu alebo po výdatných zrážkach. Je však zjavné, že rýchlosť prepojenia jej podzemného hydrologického systému s povrchom je veľmi rozdielna, rovnako, ako sú na povrchu Silickej planiny nerovnomerne distribuované oblasti, z ktorých môže byť potenciálny kontaminant mimoriadne rýchlo prenesený do vody Krásnohorskej jaskyne. Preto v rámci možností, ktoré nám poskytoval projekt LIFE+ KRASCAVE podporovaný Európskou komisiou, zameraný na ochranu podzemného ekosystému Krásnohorskej jaskyne, sme sa pokúsili realizovať v danej oblasti viacero stopovacích skúšok. Pri ich realizácii sme sa snažili využiť jednak bakteriofágy H40/1 osvedčené v minulosti (Haviarová, 2008, 2014, 2016; Haviarová a Pristaš, 2008, 2010, 2013, 2018; Haviarová et al., 2009a, b), jednak farbiace stopovacie látky aplikované v nízkej koncentrácii, detegovateľné citlivými prietokovými fluorimetrami inštalovanými priamo na miestach potenciálnych prepojení.

Metodika realizovaných prác

Spôsob realizácie stopovacích skúšok úlohy vyplýval z cieľa prác, ktorým bolo overenie priestorovej distribúcie vzájomných prepojení a rýchlosti postupu prúdenia podzemnej vody z bezprostredného nadložia tvoreného povrchom severnej časti Silickej planiny do podzemného hydrologického systému Krásnohorskej jaskyne, prípadne do podzemnej vody v jej okolí. V rámci toho sa realizovali technické, monitorovacie, analytické a vyhodnocovacie práce. Situovanie celého skúmaného územia v rámci jeho širšieho nadregionálneho zaradenia, ako aj miest aplikácie stopovačov je na obrázku 1. Selekcia relevantných závrtov na povrchu Silickej planiny prebehla v koordinácii s dodávateľom technickej časti prác spoločnosťou HES –

COMGEO, spol. s r. o. (obrázok 2, tabuľka 1). Stopovacím skúškam predchádzal povoľovací proces, ktorý zahŕňal vyjadrenia Východoslovenskej vodárenskej spoločnosti pôsobiacej v regióne, Slovenského vodohospodárskeho podniku, Regionálneho úradu verejného zdravotníctva so sídlom v Rožňave a odboru starostlivosti o životné prostredie Okresného úradu Rožňava, resp. oddelenia ochrany prírody a vybraných zložiek životného prostredia kraja odboru starostlivosti o životné prostredie Okresného úradu v sídle (Košického) kraja.

Technické práce sa začali najprv terénnymi úpravami na dne závrtu – išlo o vytvorenie injektážneho priestoru s rozmermi zhruba 1,0 x 1,0 m do hĺbky 1,0 m. Následne sa do dna takto vyhĺbenej jamy vyhĺbilo niekoľko infiltračných sond, v rámci možností ručným vrtákom (obr. 3). Nasledovala príprava stopovacích roztokov v dostatočnom objeme (rozpustenie stopovačov v pracovnom objeme zhruba 200 l; obr. 4), resp. rýchla príprava fágovej suspenzie po jej transporte v chladenom priestore (obr. 5). Na zatláčanie stopovacej látky do prostredia bolo potrebné zabezpečiť dostatočné množstvo vody v objeme asi 2 až 5 m^3 do každého testovaného závrtu (obr. 6 a 7). Voda použitá na zatláčanie pochádzala z prameňa Buzgó (Krásnohorská Dlhá Lúka). Dôležitým a zároveň náročným prvkom technických prác bola preprava zatláčacej vody na miesto aplikácie (dná závrtov na povrchu Silickej planiny).

Obr. 2. Miesta aplikácie stopovacích látok – dná závrtov na povrchu Silickej planiny nad Krásnohorskou jaskyňou: závrt (A) západne od priemetu polohy Marikinho jazera (a) a závrt (C) východne od Marikinho jazera (b).

Fig. 2. Sites of tracers injection – sinkhole bottoms on the Silická planina Plateau surface above the Krásnohorská jaskyňa Cave: sinkhole (A) west from the Marikino jazero Lake vertical projection on the surface (a) and sinkhole (C) east from the Marikino jazero Lake (b).

Monitorovacie práce sa vykonávali na 11 stanovištiach a spočívali v meraniach pomocou poľných prietokových fluorimetrov – kontinuálnych meračov prítomnosti stopovačov v prostredí – s časovým krokom 15 minút a sorpčného zachytávania stopovačov do indikačných kapsúl indikujúcich prítomnosť stopovačov na monitorovacom mieste. Boli použité prietokové fluorimetre GGUN-FL30 švajčiarskej výroby (Piérre-André Schnegg, Neuchâtel, Switzerland; obr. 8). Tento fluorimeter je možné použiť na kontinuálne merania počas stopovacích testov s použitím fluoresceínových farbív, ako je uranín, rodamín, sulforodamín, tinopál, naftionát a pod., pričom je možné použiť súčasne až tri vhodne vybrané (navzájom sa neprekrývajúce vlnovou dĺžkou) indikátory. Kontinuálne, resp. v nastavenom časovom intervale snímaná voda preteká optickou bunkou fluorimetra, ktorou je sklenená trubica s valcovým prierezom. Optický systém pozostáva zo štyroch svetelných zdrojov a troch fotografických detektorov, ktoré sú namontované na štyroch kolmých osiach v dvoch úrovniach. Každá z osí je vybavená budiacimi a detekčnými filtrami a objektívmi. Budiace svetlá sa zapínajú a vypínajú postupne, merajú sa tri nezávislé reakcie a zakalenie vody (turbidita). V každom meracom cykle sa zaznamenáva aj vyrovnávacie napätie z predzosilňovačov (tmavý signál). Fluorimetrická sonda je napojená na analógovo-digitálny prevodník slúžiaci na konvertovanie fluorimetrických signálov na unipolárne 24-bitové údaje (rozlíšenie údajov je 1 : 16 000 000). Najväčší merateľný signál má veľkosť 2 500 mV a intenzita najmenšieho signálu je preto 0,000 156 25 mV. Práve v tomto vysokom rozlíšení signálu tkvie výhoda použitia poľného prietokového fluorimetra, keď je možné v teréne aplikovať podstatne menšie množstvo stopovacích látok pri zachovaní schopnosti ich zaznamenania. Zaznamenané údaje sa zasielajú do záznamníka cez kábel, štandardne dlhý 15 m (môže byť aj dlhší), so 4 vodičmi. Box dátového záznamníka (obr. 8b) obsahuje jednu alebo dve chránené olovené batérie a potrebné obvody na zaznamenávanie údajov. V rámci uvedených prác bolo využitých 6 poľných prietokových fluorimetrov (obr. 9) pri nastavení časového záznamu na 15-minútový interval snímacej frekvencie (tab. 2).

Ďalšie miesta potenciálneho objavenia stopovačov boli vybavené indikačnými kapsulami (obr. 10, tab. 2). Indikačné absorpčné kapsuly slúžili len na indikáciu prítomnosti stopovačov. Kapsuly vyhotovené z plastu neohrozujúceho zdravie a náplne sorpčného materiálu vhodného na kontakt s potravinami sa v pravidelných intervaloch kontrolovali a náplne sa vymieňali. Ako sorpčný materiál bolo použité granulované aktívne uhlie NORIT® typu PK 3-5 s plochou efektívneho povrchu 875 m^2/gram. Po odobratí sa náplne rozrušovali ultrazvukom, lúhovali v etanolovom kúpeli a výluh sa následne semikvantitatívne analyzoval na prítomnosť farbív pomocou luminiscenčného spektrofotometra Perkin Elmer. Interval kontroly bol vytvorený na základe predpokladaných disperzných vlastností horninového prostredia a bol stanovený na dňové intervaly v prvých dňoch od aplikácie a následne na týždňové až dvojtýždňové intervaly v priebehu piatich mesiacov.

V rámci starostlivosti o monitorovaciu sieť (spolu 11 stanovíšť, pozri tab. 2) prebiehala pravidelná údržba prístrojovej techniky, výmena náplní indikačných kapsúl, údržba a čistenie miest uloženia meracích prístrojov a kapsúl. Následné analytické a vyhodnocovacie práce spočívali v analýzach sorpčných náplní indikačných kapsúl na prítomnosť sledovaných stopovačov, spracovaní zaznamenaných údajov z kontinuálnych meračov a terénnych meraní a napokon v záverečnom spracovaní výsledkov tabuľkovou a grafickou formou.

Pri výbere stopovacích látok boli zohľadnené technologické možnosti realizátora, charakteristiky horninového prostredia, a najmä vlastnosti jednotlivých stopovačov s ohľadom na ochranu zdravia obyvateľstva a životného prostredia. Ako stopovacie látky sa použili farbivá fluoresceín (zelený, UN1170, čiastočne rozpustený denaturovaným 96 % etanolom K10L), sulforodamín B (farbivo červenej farby) a naftionát sodný (bezfarebný). Štvrtou použitou stopovacou látkou (miesto aplikácie D v tab. 1) bola fágová suspenzia bakteriofágov H40/1 (Pronk et al., 2006a, b; Gillmann, 2007; Kallies et al., 2017; Pristaš, 2017), takže naraz boli v krátkom čase aplikované až 4 stopovače. Na túto stopovaciu skúšku sa použilo 8 litrov fágovej suspenzie bakteriofágov H40/1 s početnosťou fágov 2 x 10^8 na mililiter kubický suspenzie, pripravenej doc. RNDr. Petrom Pristašom, CSc., vedúcim oddelenia genetiky mikroorganizmov v Ústave fyziológie hospodárskych zvierat SAV (ÚFHZ SAV) v Košiciach. Hostiteľským kmeňom tohto bakteriofága je pôvodom morská baktéria *Pseudoalteromonas gracilis*. Bakteriofág H40/1 i baktéria *Pseudoalteromonas gracilis* použité pri stopovacom experimente boli darom od Dr. Zopfiho z Université de Neuchâtel (Švajčiarsko). Baktérie *Pseudoalteromonas gracilis* sa kultivovali v médiu SWB (*Sea Water Broth*) v zložení *Bacto Tryptone Peptone* (*Becton Dickinson*, 211 699) 5 g/l, *yeast extract* (Merck, 211 699) 1 g/l a morská soľ 24,75 g/l. Ako tuhé kultivačné médium sa používalo to isté médium s prídavkom 15 g agaru (*Becton Dickinson*) na liter média. Po pridaní všetkých zložiek sa pH média upravilo na 7,1 až 7,2, médium sa naplnilo do vhodných nádob a 20 minút sterilizovalo pri teplote 121 °C. Baktérie *Pseudoalteromonas gracilis* v glycerínovej konzerve, dlhodobo uschovávanej pri teplote –70 °C, sa vysiali na povrch platne s médiom SWA (*Sea Water Agar*) a inkubovali sa počas 24 hodín pri izbovej teplote. Individuálne kolónie sa sterilne odpichli a inokulovali sa do 20 mililitrov média SWA. Narastené kultúry sa udržiavali pri teplote 4 °C. Príprava fágovej suspenzie prebiehala tak, že sa 4 l média SWB inokulovali 4 ml nočnej kultúry *Pseudoalteromonas gracilis* a 4 ml fágovej suspenzie bakteriofágov H40/1. Takto pripravená zmes sa 24 hodín inkubovala pri izbovej teplote za výdatnej aerácie. Výsledná početnosť fágov v takto pripravenej suspenzii je zvyčajne 10^{10} fágových častíc v mililitri suspenzie. Táto suspenzia sa aplikovala 14. 11. 2016 v čase do 12 hodín od jej prevzatia na ÚFHZ SAV Košice a následne sa odoberali vzorky vody na 11 vybraných odberných miestach.

Obr. 3. Úprava miest aplikácie stopovacích látok na dnách závrtov: a) hĺbenie jamy v závrte (D), b) navŕtavanie dna jamy zemným vrtákom v závrte (D).

Fig. 3. Preparation tracers application sites on the sinkhole bottoms: a) pit digging in the (D) sinkhole, b) drilling the bottom of the pit by simple earth drill in the (D) sinkhole.

Po aplikácii roztoku stopovacej látky sa predpokladala jeho významná disperzia a difúzia v podzemnej vode krasovo-puklinového zvodnenca, spojená s mnohonásobným zriedením. Pri uvedenom objeme použitých stopovačov a odhadovanom objeme akumulácie podzemnej vody rádovo v jednotkách tisícov kubických metrov sa predpokladala koncentrácia riedenia rádovo v stovkách mikrogramov, resp. fágových častíc. Miesta a čas aplikácie stopovacích látok sú prehľadne uvedené v tabuľke 1.

Detekcia stopovacích látok sa vykonávala na miestach prirodzeného odvodňovania triasových karbonátov Silickej planiny. Boli vybrané 4 prítoky vody vnútri Krásnohorskej jaskyne – pravostranný prítok v Abonyiho dóme, ľavostranný prítok pod Veľkou sieňou (od Heliktitového dómu), miesto presakovania zo Siene obrov a výtok z Marikinho jazera pod Sifónom potápačov. Samostatne sme pozorovali celkový odtok vody z Krásnohorskej jaskyne ako krasový prameň Buzgó. V sieti pozorovaní boli aj 2 pramenné záchyty vzdialenejších vodárenských zdrojov (VZ): VZ Eveteš a VZ Mezeš v katastri obce Hrušov. Z vodárensky nezachytených pramenných výverov sa sledovali 4 pramene – prameň Pri kaplnke (Krásnohorská Dlhá Lúka), Pod kameňolomom (Krásnohorská Dlhá Lúka), prameň Pri mlyne (Krásnohorská Dlhá Lúka)

Tab. 1
Miesta aplikácie stopovačov, použitý typ a množstvo stopovača, dátum a čas jeho aplikácie na povrchu Silickej planiny.

Tab. 1
Sites of tracers injection, applied tracer type and its amount, date and time of its application on the surface of the Silická planina Plateu.

Označenie miesta aplikácie	Miesto aplikácie	Druh použitého stopovača	Množstvo použitého stopovača/objem zatláčacej vody	Dátum aplikácie a čas jej trvania
(A) závrt Z	závrt západne od Marikinho jazera; relatívna hĺbka 7 m, rozmery zhruba 60 × 50 m E 20,577 376°, N 48,614 533°	naftionát sodný	998,53 g/3 m^3 vody	26. 10. 2016 15.50 – 17.00
(B) závrt SV	závrt sv. od Marikinho jazera; relatívna hĺbka 15 m, rozmery zhruba 100 × 70 m E 20,586 298°, N 48,614 409°	fluoresceín	1 014,86 g/2 m^3 vody	26. 10. 2016 10.30 – 11.50
(C) závrt V	závrt východne od Marikinho jazera; relatívna hĺbka 15 m, rozmery zhruba 125 × 100 m E 20,586 799°, N 48,613 737°	sulforodamín B	1 010,36 g/3 m^3 vody	26. 10. 2016 12.14 – 14.00
(D) závrt FÁG	závrt vjv. od Marikinho jazera; relatívna hĺbka 22 m, rozmery zhruba 70 × 50 m E 20,589 2°, N 48,613 2°	fágová suspenzia bakteriofágov H40/1	8 000 ml/5 m^3 vody	14. 11. 2016 12.30 – 14.20

Obr. 4. Zapúšťanie stopovacej látky sulforodamín B na dne závrtu (C) (a), zatláčanie fluoresceínu na dne závrtu (B) dodatočným množstvom 2 m^3 čistej vody (b).

Fig. 4. Injection of sulphorhodamin B dye tracer in the (C) sinkhole bottom (a), acceleration of the fluorescein dye in the (B) sinkhole bottom by adding additional 2 m^3 of clean water (b).

a Hradná vyvieračka (Brzotín). Na týchto miestach boli inštalované poľné prietokové fluorimetre ako kontinuálne detekčné prístroje v počte 6 kusov a/alebo indikačné absorpčné kapsuly. Zároveň sa odoberali vzorky vody na prítomnosť bakteriofágov H04/1. Celkový prehľad použitej indikačnej metódy na každom monitorovanom mieste je špecifikovaný v tab. 2.

Vzorky vody na detekciu bakteriofágov H40/1 sa postupne odoberali a doručovali do ÚFHZ SAV v Košiciach, kde boli spracované do 24 hodín po doručení. Pri analýze výskytu bakteriofágov v odoberaných vzorkách sa na analýzu výskytu bakteriofágových častíc použil 1 ml vzorky. K vzorke sa pridalo 100 µl vzorky čerstvej kultúry *Pseudoalteromonas gracilis* (OD_{600} = 0,2) a zmes sa 15 minút inkubovala pri izbovej teplote. Po tomto čase sa rovnomerne naniesla na povrch kultivačnej platne s médiom SWA a prekryla sa 4 ml „soft" SWA agaru (médium SWB s prídavkom 6 g agaru na jeden liter média). Po stuhnutí média sa platne 24 hodín inkubovali pri izbovej teplote. Prítomnosť fágov sa prejavila ako jasne viditeľné zóny zjasnenia (plaky) na súvislej vrstve rastúcich baktérií. Počet fágových častíc sa stanovil vizuálne na základe počtu plakov, t. j. zón bez rastu indikátorovej kultúry *P. gracilis*. Všetky experimenty sa opakovali minimálne dva razy. Pri každej analýze sa použil kmeň *P. gracilis* bez pridania bakteriofágov ako negatívna kontrola a ten istý kmeň s pridaním 10^3 fágových častíc H40/1 ako pozitívna kontrola (Pristaš, 2017).

Presné miesta inštalácie boli v rámci každej etapy stopovacích skúšok spresnené na základe miestnej obhliadky lokality a technicko-bezpečnostných možností inštalácie. Prehľadne sú uvedené v tab. 2 a na obr. 1.

Vlastný priebeh stopovacích skúšok sa realizoval v nasledujúcich postupných krokoch:

1. umiestnenie kontinuálnych meračov (detekčných prístrojov) a indikačných kapsúl na určené miesta pred aplikáciou, resp. minimálne do jednej hodiny od aplikácie stopovačov. Inštalácia sa realizovala s minimálnym zásahom do okolitého prostredia. Fluorimeter, resp. kapsula sa umiestnili na určené monitorovacie miesto a zabezpečili sa proti odplaveniu zafixovaním pomocou inertného materiálu prítomného v okolí (skaly, štrk);

2. vytvorenie injektážneho priestoru s rozmermi zhruba 1,0 x 1,0 m do hĺbky 1,0 m – terénne úpravy na dne závrtu, do dna takto vyhĺbenej jamy bolo vyhĺbených

Tab. 2
Miesta inštalácie zariadení na indikovanie stopovacích látok aplikovaných do jednotlivých závrtov na povrchu Silickej planiny nad Krásnohorskou jaskyňou.

Tab. 2
Sites of tracer measuring devices installations for tracers applied to the sinkholes on the surface of the Silická planina Plateau above the Krásnohorská jaskyňa Cave.

Č.	Miesto detekcie	Použitý detektor	Č.	Miesto detekcie	Použitý detektor
1	výtok z Marikinho jazera (Krásnohorská jaskyňa)	prietokový fluorimeter	7	prameň Pri kaplnke (Krásnohorská Dlhá Lúka) N 48,618 482° E 20,586 127	indikačná kapsula
2	miesto presakovania zo Siene obrov (Krásnohorská jaskyňa)	prietokový fluorimeter	8	prameň Pod kameňolomom (Krásnohorská Dlhá Lúka) N 48,617 661° E 20,589 708°	indikačná kapsula
3	ľavostranný prítok pod Veľkou sieňou od Heliktitového dómu (Krásnohorská jaskyňa)	prietokový fluorimeter	9	prameň Pri mlyne (Krásnohorská Dlhá Lúka) N 48,619 836° E 20,579 599°	indikačná kapsula
4	pravostranný prítok v Abonyiho dóme (Krásnohorská jaskyňa)	prietokový fluorimeter	10	prameň Mezeš, VZ (Hrušov) N 48,595 371° E 20,607 126 1°	indikačná kapsula
5	prameň Buzgó, výstupný sifón (Krásnohorská Dlhá Lúka) N 48,618 043° E 20,587 435°	prietokový fluorimeter	11	prameň Hradná vyvieračka (Brzotín) N 48,607 541° E 20,486 957°	indikačná kapsula
6	prameň Eveteš, VZ (Hrušov) N 48,599 159° E 20,643 091°	prietokový fluorimeter			

Obr. 5. Suspenzia bakteriofágov H40/1 po preprave na lokalitu (a), aplikácia fágovej suspenzie do jamy vyhĺbenej na dne závrtu (D) 14. 11. 2016 (b).

Fig. 5. Suspension of bacteriophages H40/1 after its transportation to the application site (a), application of the phage suspension in the dug pit in the (D) sinkhole bottom on the 14. 11. 2016 (b).

Obr. 6. Preprava čistej vody používanej na hydraulické zatlačenie stopovacej látky do horninového prostredia (a), hydraulické dotláčanie stopovacej látky (b).

Fig. 6. Transport of clean water used for hydraulic pushing of the tracer into the rock environment (a), hydraulic pushing of the tracer (b).

Obr. 7. Prívod čistej vody použitej na hydraulické zatlačenie stopovacej látky do horninového prostredia hadicou ku dnu závrtu (a), stopovač naftionát sodný v jame vyhĺbenej na dne závrtu (A) (b).

Fig. 7. Clean water supply through the hose to the bottom of the sinkhole for hydraulic pushing of the tracer into the rock environment (a), sodium naphtionate tracer in the dug pit of the (A) sinkhole (b).

niekoľko infiltračných sond, v rámci možností ručným vrtákom;

3. dovoz zdravotne neškodnej (pitnej) vody v objeme 2 až 5 m^3 pre každý stopovač na jeho hydraulické zatlačenie do horninového prostredia;
4. príprava zásobného roztoku stopovacej látky (objem zhruba 200 l);
5. inštalácia infiltračného potrubia na aplikáciu stopovača pod terénom;
6. „predinjektáž“ pomocnej vody (zhruba 0,5 m^3) na zmáčanie suchých komunikačných ciest a tým zabránenie viazania farbiacej látky do prostredia pri vyrovnávaní vlhkosti prostredia (lepší prienik stopovača do prostredia);
7. aplikácia príslušného zásobného roztoku stopovača, zhruba 200 l, s podporou ďalšieho množstva pomocnej vody v objeme 1 m^3;
8. injektáž zatláčacej vody (1,5 až 4,5 m^3) na zlepšenie mobility stopovača v krasovo-puklinovom prostredí. Kvôli dôkladnému vypláchnutiu použitého zariadenia bola aplikácia zatláčacej vody zabezpečená prietokom cez zásobné nádrže a infiltračné potrubie;
9. pravidelný monitoring detekčných miest v dňových a týždňových intervaloch v závislosti od klimatických a hydrologických podmienok a priebežných výsledkov v období piatich mesiacov (do 11. 4. 2017); zber zaznamenaných údajov, odber kontrolných vzoriek vody a výmena náplní indikačných kapsúl;
10. demontáž kontinuálnych meračov (prietokových fluorimetrov) a indikačných kapsúl, uvedenie pozorovacích miest do pôvodného stavu;
11. analýzy sorpčných náplní indikačných kapsúl, analýza vzoriek vody na prítomnosť bakteriofágov H40/1, spracovanie zaznamenaných údajov z kontinuálnych meračov;
12. spracovanie výsledkov.

Výsledky a diskusia

Celoplošné kontinuálne sledovanie prítomnosti stopovacích látok vo vode sa začalo 25. 10. 2016 o 12.00 hod., prietokové fluorimetre pracovali s časovým krokom 15 minút. Toto monitorovanie sa skončilo 5. 4. 2017 po viac ako 23 týždňoch pozorovaní (162 dní po zapustení stopovačov). Následne boli záznamy z meracích prístrojov – prietokových fluorimetrov – dekódované a transformované. Výsledky pozorovaní prítomnosti stopovacích látok na indikačných miestach pomocou prietokových fluorimetrov sú uvedené v tab. 3.

Na všetkých šiestich indikačných miestach, kde boli inštalované prietokové fluorimetre (tab. 2 a 3), bol zaznamenaný signál stopovacej látky naftionát sodný, ktorá bola aplikovaná v závrte (A) západne od Marikinho jazera. Počas celého obdobia sledovania zároveň nebol zaznamenaný signál stopovacej látky sulforodamín B, aplikovanej v závrte (C) východne od Marikinho jazera. Signál pozitívnej reakcie (prítomnosti stopovacej látky vo vode) na fluoresceín, ktorý bol injektovaný do dna závrtu (B) sv. od Marikinho jazera, bol zaznamenaný len vo veľmi slabej intenzite v oboch bočných prítokoch v Krásnohorskej jaskyni – ľavostrannom prítoku pod Veľkou sieňou od Heliktitového dómu aj pravostrannom prítoku v Abonyiho dóme, na iných miestach však nie.

Bakteriofágy H40/1, ktoré boli aplikované s časovým sklzom takmer troch týždňov od zapúšťania farbiacich stopovačov do závrtu (D) vjv. od Marikinho jazera, neboli – podobne ako farbivo sulforodamín B – na žiadnom z monitorovaných miest v žiadnom zo série 16 až 25 odberov realizovaných na 11 monitorovacích miestach (tab. 4). Spolu sa teda vykonalo a následne analyzovalo 223 odberov, všetky bez preukázania prítomnosti bakteriofágov vo vzorke (Pristaš, 2017).

Výsledky získané po spracovaní sorpčných náplní indikačných kapsúl z aktívneho uhlia preukázali prítomnosť dvoch stopovačov na rozdielnych sledovaných miestach vo veľmi nízkej intenzite. Naftionát sodný, aplikovaný v závrte (A) západne od Marikinho jazera, sa objavil vo vode prameňa Pod kameňolomom (označenie miesta indikácie: 8), ako aj vo vode prameňa Mezeš (10).

Zatiaľ čo prítomnosť naftionátu v prameni Pod kameňolomom bola zaznamenaná už pri prvom odbere sorpčnej náplne 14. 11. 2016, teda 19 dní po jeho aplikovaní, a pretrvávala až do odberu 5. 1. 2017 (52 dní po aplikácii), v prípade vodárenského zdroja Mezeš to bolo iba počas neskoršieho a kratšieho obdobia. Naftionát tu bol zaznamenaný len v odberoch z 21. 11. 2016 a 28. 11. 2016, teda 7 až 14 dní po jeho uvedení do horninového prostredia na povrchu Silickej planiny v závrte Z (A). Väčším prekvapením je ale indikovanie fluoresceínu vo vode prameňa Hradná vyvieračka pri Brzotíne (11) v rovnakom čase, teda 7 až 14 dní po jeho vypustení do dna závrtu (B) sv. od Marikinho jazera. Ide tu o podstatne väčšiu vzdialenosť, 7,57 km vzdušnou čiarou, na rozdiel od 2,95 km medzi závrtom Z (A) a prameňom Mezeš. V prvom prípade (fluoresceín v prameni Hradná vyvieračka) by bola nepravá rýchlosť prúdenia (pri prepočte vzdušnou vzdialenosťou miest aplikácie a indikovania) v rozsahu medzi 540,7 a 1 081,4 m/deň (0,63 – 1,25 cm/s). V prípade prameňa Mezeš a závrtu (A) by bola nepravá rýchlosť prúdenia 210,7 až 421,4 m/deň (0,24 až 0,49 cm/s).

Prítomnosť stopovačov nebola vizuálne zaznamenaná na žiadnom z miest detekcie počas celého priebehu monitoringu. S výnimkou výpadku meraní na prietokovom

Tab. 3
Výsledky pozorovaní prítomnosti stopovacích látok na indikačných miestach pomocou prietokových fluorimetrov počas stopovacích skúšok v období 25. 10. 2016 – 5. 4. 2017.
Tab. 3
Results of tracer observations at indication sites using flow-through fluorometers during tracing tests in the period 25. 10. 2016 – 5. 4. 2017.

Miesto detekcie (výrobné číslo fluorimetra)	Stopovacia látka	Dátum a čas prvej indikácie stopovača	Dátum a čas vrcholnej detekcie stopovača	Maximálna koncentrácia stopovača [ppb]	Poznámka
1 – výtok z Marikinho jazera (914)	naftionát sodný	6. 11. 2016 16.45	21. 11. 2016 6.00	61,82	jediný signál
	sulforodamín B	– – –	– – –	– – –	nedetegovaný
	fluoresceín	– – –	– – –	– – –	nedetegovaný
2 – ľavostranný prítok pod Veľkou sieňou (737)	naftionát sodný	8. 11. 2016 17.00	9. 11. 2016 15.30	56,3	jediný signál
	sulforodamín B	– – –	– – –	– – –	nedetegovaný
	fluoresceín	17. 11. 2016 07.15	1. 12. 2016 17.30	0,68	jediný signál
3 – miesto presakovania zo Siene obrov (309)	naftionát sodný	7. 11. 2016 02.00	19. 11. 2016 01.15	0,68	jediný signál
	sulforodamín B	– – –	– – –	– – –	nedetegovaný
	fluoresceín	– – –	– – –	– – –	nedetegovaný
4 – pravostranný prítok V Abonyiho dóme (736)	naftionát sodný	8. 11. 2016 00.00	8. 11. 2016 22.30	32,96	jediný signál
	sulforodamín B	– – –	– – –	– – –	nedetegovaný
	fluoresceín	6. 11. 2016 19.15	8. 11. 2016 14.30	0,24	jediný signál
5 – prameň Buzgó (310)	naftionát sodný	27. 10. 2016 06.00 30. 10. 2016 06.00 6. 11. 2016 17.15	28. 10. 2016 06.00 3. 11. 2016 06.00 21. 11. 2016 07.00	166,00 124,96 58,30	prvý signál druhý signál tretí signál
	sulforodamín B	– – –	– – –	– – –	nedetegovaný
	fluoresceín	– – –	– – –	– – –	nedetegovaný
6 – prameň Eveteš, VZ[1] (738)	naftionát sodný	27. 10. 2016 08.15 6. 11. 2016 09.00	29. 10. 2016 23.45 7. 11. 2016 18.30	107,73 121,71	prvý signál druhý signál
	sulforodamín B	– – –	– – –	– – –	nedetegovaný
	fluoresceín	– – –	– – –	– – –	nedetegovaný

Pozn.: [1]VZ – vodárenský zdroj

Obr. 8. Použitie kontinuálne pracujúceho poľného prietokového fluorimetra GGUN-FL30 – detailná ukážka detekčnej časti (a) a pamäťovej časti zariadenia slúžiaceho na zber údajov (b).

Fig. 8. The use of continuously measuring field fluorometer GGUN-FL30 – detail of its detection part (a) and data memory part (b).

Obr. 9. Terénny zber výsledkov z poľného prietokového fluorimetra GGUN-FL30 vnútri Krásnohorskej jaskyne.

Fig. 9. Data collection from the flow-through field fluorometer GGUN-FL30 inside the Krásnohorská jaskyňa Cave.

Obr. 10. Poľný prietokový fluorimeter GGUN-FL30 inštalovaný vnútri vodárenského zdroja – krasového prameňa Eveteš v Hrušove (a), detailný pohľad na kapsulu so sorpčnou látkou, použitú na detekčných miestach 7 až 11 v rámci opisovaných stopovacích skúšok (b).

Fig. 10. Flow-through field fluorometer GGUN-FL30 inside the drinking water source of Eveteš karstic spring (a), capsule with sorption agent, as applied on sites 7 to 11 (b).

fluorimetri č. 914 na výtoku z Marikinho jazera (monitorovací bod č. 1) počas prvých 10 dní meraní po injektáži farbiacich stopovačov, ostatné kontinuálne merače pracovali počas celého monitoringu bez vážnych porúch a prerušení.

Spracovanie sorpčných náplní sa robilo semikvantitatívnou metódou, ktorá neumožňuje stanoviť koncentráciu stopovacích látok vo vode. Indikuje sa len ich prítomnosť v určitom časovom intervale, ktorý je definovaný frekvenciou výmeny sorpčných náplní. Naše výsledky preukázali prítomnosť dvoch stopovačov na troch sledovaných miestach (tab. 5) vo veľmi nízkej (+) intenzite. Okrem vody prameňov Pod kameňolomom, Mezeš a Hradná vyvieračka, kde sa v určitom úseku monitorovacieho obdobia zaznamenali stopovače naftionát sodný, resp. fluorescеín, sa zistili aj dve miesta detekcie, ktoré vykazovali úplnú negativitu – neprítomnosť žiadnej z aplikovaných stopovacích látok. Išlo o prameň Pri kaplnke (7) a prameň Pri mlyne (9). Počas analýz vzoriek získaných z aktívneho uhlia sa však zaznamenala veľmi nízka hladina prítomnosti stopovačov, čo výrazne sťažovalo detekciu ich prítomnosti a spôsobilo nutnosť výkonu opakovaných analýz vzoriek. Ani uvedené tri prepojenia (tab. 5) teda nemožno považovať sa overenie miest s úplnou pozitivitou vo vzťahu k aplikovaným stopovačom. Výsledky získané zo spracovania sorpčných náplní treba skôr považovať za indície možných prepojení.

Pri stopovacej látke sulforodamín B aplikovanej v závrte (C) východne od Marikinho jazera ani pri bakteriofágoch H40/1 aplikovaných do závrtu (D) vjv. od Marikinho jazera sa nezistili nijaké reakcie na žiadnom z jedenástich miest ich detekcie. Tieto miesta možno považovať za miesta s lepšou prirodzenou ochrannou funkciou proti potenciálnemu znečisteniu.

Naopak, za lokalitu s vysokým stupňom aktívneho podzemného prepojenia s jednotlivými časťami podzemného hydrologického systému Krásnohorskej jaskyne možno považovať závrt (A) západne od Marikinho jazera. Okrem uvedených nálezov aplikovaného naftionátu sodného v prameňoch Pod kameňolomom (8) a Mezeš (10) bol naftionát sodný indikovaný prietokovými fluorimetrami na všetkých nimi monitorovaných miestach, a to v značnej intenzite, danej maximálnou indikovanou koncentráciou stopovača (tab. 6). Tá sa pohybovala od 0,68 ppb vo vode presakovanej zo Siene obrov až do 107,73 ppb, zistených prekvapujúco už po vyše 3 dňoch v prameni Eveteš nad obcou Hrušov vzdialenom 4,8 km. Vo vode tohto prameňa bol zaznamenaný aj príchod druhého, ešte intenzívnejšieho signálu s intenzitou 121,71 ppb po 12,1 dňoch. Vzhľadom na silu signálu a rýchlosť jeho prenosu je potrebné v oblasti medzi závrtom (A) západne od Marikinho jazera a prameňom Eveteš predpokladať existenciu dvoch vzájomne oddelených, ale v obidvoch prípadoch veľmi aktívnych obehových ciest vo vadóznej zóne pod polohovo relevantným povrchom Silickej planiny. Nepravá rýchlosť prúdenia je v tomto prípade 1 443,2 m/deň (1,67 cm/s) v prípade predpokladaného „rýchlostne aktívnejšieho kanála“ nenasýtenej zóny a 396,8 m/deň (0,46 cm/s) v prípade druhého „kanála“, pri ktorom zas možno predpokladať nižšiu mieru disperzie a prenos vyššej koncentrácie aj v prípade kontaminantov, nielen stopovacích látok.

Najvyššia úroveň zachyteného signálu sa podľa očakávania prejavila vo vode krasového prameňa Buzgó, kde dosiahla pri príchode dvoch po sebe idúcich signálov (1,6 dňa a 7,6 dňa) po injektáži naftionátu sodného do závrtu (A) úroveň 166,0 ppb pri prvom, skoršom signáli a 125,0 ppb pri druhom signáli prichádzajúcom šesť dní po ňom. Aj v tomto prípade môžeme hovoriť o dvoch vzájomne oddelených aktívnych obehových cestách vody vo vadóznej zóne. Pretože uvedené monitorované miesto spája v sebe vody prechádzajúce monitorovanými miestami 1 až 4 (hlavným výtokom z Marikinho jazera či tromi nižšie sa nachádzajúcimi prítokmi), predpokladáme, že signál sa objavil vo vode Marikinho jazera, kde bol v danom čase nefunkčný fluorimeter. Pri výpočte nepravej rýchlosti prúdenia je potrebné počítať so vzájomnou vzdušnou vzdialenosťou Marikinho jazera a závrtu (A) 613 m, pri ktorej je potom v prípade aktívnejšieho kanála nepravá rýchlosť 385,5 m/deň (0,45 cm/s) a v prípade druhého 80,8 m/deň (0,09 cm/s). S týmto („prvým“ naftionátovým) maximom zisteným vo vode prameňa Buzgó a predpokladaným vo vode Marikinho jazera súvisí zrejme aj prítomnosť naftionátu sodného v prameni Pod kameňolomom indikovaná sorpčnými kapsulami (dva odbery s pozitívnym výsledkom, zachytávajúce časový interval 18. 11. až 28. 11. 2016; tab. 5). Podľa systematického monitorovania chemického zloženia vody oboch týchto zdrojov v rámci projektu KRASCAVE (Malík et al., 2019) sú ich kvalitatívne vlastnosti veľmi podobné a možno medzi nimi očakávať významný súvis.

Po čase, keď sa zistil chybný záznam fluorimetra č. 914 inštalovaného v Sifóne potápačov (kde je prirodzená cesta odvodňovania Marikinho jazera) a došlo k náprave meraní, bol 6. 11. 2016 v čase od 16.45 detegovaný nástup ďalšieho, v poradí už tretieho signálu, ktorý dosiahol najvyššiu intenzitu až 21. 11. 2016 okolo 6.00 hod. Z toho vyplýva, že išlo o značne rozptýlený príchod stopovača signalizujúci značný stupeň disperzie, hoci úroveň vrcholovej koncentrácie bola až 61,8 ppb. Pri zjednodušenom chápaní by sme k tomuto tretiemu signálu priradili nepravú rýchlosť 23,9 m/deň (0,028 cm/s), no v tomto prípade evidentne ide o pomalý nárast stopovača rozptýleného v horninovom prostredí. Oveľa intenzívnejší bol koncentračný nárast v prípade dvoch väčších prítokov v Krásnohorskej jaskyni – ľavostranného prítoku pod Veľkou sieňou (od Heliktitového dómu; č. 2 v tab. 2) a pravostranného prítoku v Abonyiho dóme (č. 4). V oboch prípadoch sa zaznamenal časový rozdiel medzi prvou indikáciou stopovača a jeho najvyššou hodnotou 22.30 hod. (0,94 dňa), v prítoku v Abonyiho dóme však bola prvá indikácia stopovača zaznamenaná o 17 hodín skôr a takisto bola v čase posunutá aj najvyššia zistená hodnota. V oboch prípadoch však išlo o časový posun od injektáže naftionátu sodného do závrtu (A) v rozmedzí 13 až 14 dní. Zaujímavosťou je, že stopovač bol zaznamenaný skôr vo vzdialenejšom pravostrannom prítoku v Abonyiho dóme (č. 4) na „opačnej“, východnej strane Krásnohorskej jaskyne. Preto je v prípade prítoku pod Veľkou sieňou (2) hodnota nepravej rýchlosti menšia (38,2 m/deň, resp. 0,044 cm/s), v prípade prítoku v Abonyiho dóme o 25 % väčšia (47,4 m/deň, resp. 0,055 cm/s). Uvedené signály boli zaznamenané aj na fluorimetri č. 310 na monitorovacom mieste 5 – prameň Buzgó. Napokon bolo po vyše troch týždňoch zachytené maximum signálu stopovacej látky naftionát sodný aj v mieste presakovania zo Siene obrov, teda vo vode, ktorá sa podieľa na vytváraní gigantického, 32,6 m vysokého Kvapľa rožňavských jaskyniarov nachádzajúceho sa v tejto sieni. Toto maximum však bolo mimoriadne nízke (len 0,68 ppb), a tak nebol tento signál ani rozlíšený v rámci kontinuálnych meraní na prietokovom fluorimetri č. 310 priamo nad prameňom Buzgó, na monitorovacom mieste 5. Podobne ako v prípade tretieho signálu vo vode Marikinho jazera, aj tu išlo o veľmi pomalý nárast – prvá indikácia stopovača bola registrovaná 7. 11. 2016 o 2.00 hod. a maximum nastalo až o 12 dní neskôr (19. 11. 2016 o 1.15 hod.). Časovo sa oba signály (tento z prítoku zo Siene obrov a tretí z Marikinho jazera) veľmi podobajú, jednak časom tranzitu (23,39, resp. 25,59 dňa) a časom svojho nástupu, jednak časom dosiahnutia maxima (tab. 6). Môžeme preto predpokladať, že uvedené miesta nachádzajúce sa v zadných, vzdialenejších častiach Krásnohorskej jaskyne boli zasiahnuté rozptýleným mrakom naftionátu sodného zo závrtu (A), keď predtým bol cez Marikino jazero transportovaný stopovač vstupujúci koncentrovane do iných miest podzemného hydrologického systému Krásnohorskej jaskyne. Zároveň tieto miesta neboli zasiahnuté stopovačom, ktorý sa v trocha menej koncentrovanej forme objavil v dvoch väčších prítokoch – v ľavostrannom pod Veľkou sieňou (od Heliktitového dómu), ako aj pravostrannom v Abonyiho dóme (č. 2 a 4).

Pri stopovacom fluoresceíne, ktorý bol aplikovaný do závrtu (B) nachádzajúceho sa sv. od Marikinho jazera, bol fluorimetrami zaznamenaný len slabý signál. Je však zaujímavé, že zasiahol len bezprostredne najbližšie monitorovacie miesta – ľavostranný prítok pod Veľkou sieňou (od Heliktitového dómu; č. 2 v tab. 2) a pravostranný prítok v Abonyiho dóme (č. 4) – a na iných miestach podzemného hydrologického systému Krásnohorskej jaskyne fluoresceín nebol detegovaný. Nebolo to tak ani v prípade monitorovacieho bodu č. 5 nad prameňom Buzgó. Vysvetľujeme si to príliš veľkým zriedením stopovača, ktorý mal mimoriadne nízku koncentráciu už v spomínaných prítokoch. Vo vode pravostranného prítoku v Abonyiho dóme to bolo len 0,24 ppb a vo vode ľavostranného prítoku pod Veľkou sieňou 0,68 ppb. Aj čas tranzitu fluoresceínu tu však bol napriek mimoriadne malej vzdialenosti pomerne dlhý – príchod maxima bol zaznamenaný po vyše 13, resp. vyše 36 dňoch (tab. 6), pritom vzdušnou čiarou je vzdialenosť týchto monitorovacích mieste 25, resp. 126 m od dna závrtu – závrt (B) sa prakticky nachádza priamo nad priestormi Krásnohorskej jaskyne. Nepravá rýchlosť odvodená z týchto hodnôt (1,9 m/deň, resp. 0,002 cm/s v prítoku č. 4 v Abonyiho dóme a 3,5 m/deň, resp. 0,004 cm/s v prítoku č. 3 pod Veľkou sieňou od Heliktitového dómu) je najnižšia, aká bola zistená počas nami analyzovaných stopovacích skúšok. V prípade monitorovacieho bodu č. 3 možno navyše konštatovať pomerne veľkú disperziu stopovacieho farbiva v horninovom prostredí, keď čas od záznamu prvej indikácie po záznam najvyššej koncentrácie stopovača tu bol až 14,4 dňa (v bližšom monitorovacom bode č. 4 len 1,8 dňa). Z nízkych hodnôt zistenej koncentrácie, veľmi dlhého tranzitného času a malej rýchlosti tranzitu vyplýva, že horninové prostredie v oblasti pod závrtom (B) sv. od Marikinho jazera v smere ku Krásnohorskej jaskyni poskytuje vcelku dobrú prirodzenú ochranu pred potenciálne prenikajúcim znečistením vďaka svojim hydrofyzikálnym vlastnostiam alebo značnému objemu vody v zóne epikrasu, ktorým stopovač nestačil preniknúť. O to zaujímavejšia je potom detekcia stôp fluoresceínu na aktívnom uhlí sorpčných kapsúl situovaných vo vode prameňa Hradná vyvieračka pri Brzotíne (tab. 5) v čase medzi 18. 11. a 28. 11. 2016. V tomto prípade by pri vzájomnej vzdialenosti oboch bodov bola nepravá rýchlosť v rozmedzí približne 220 až 320 m/deň, resp. 0,258 až 0,369 cm/s.

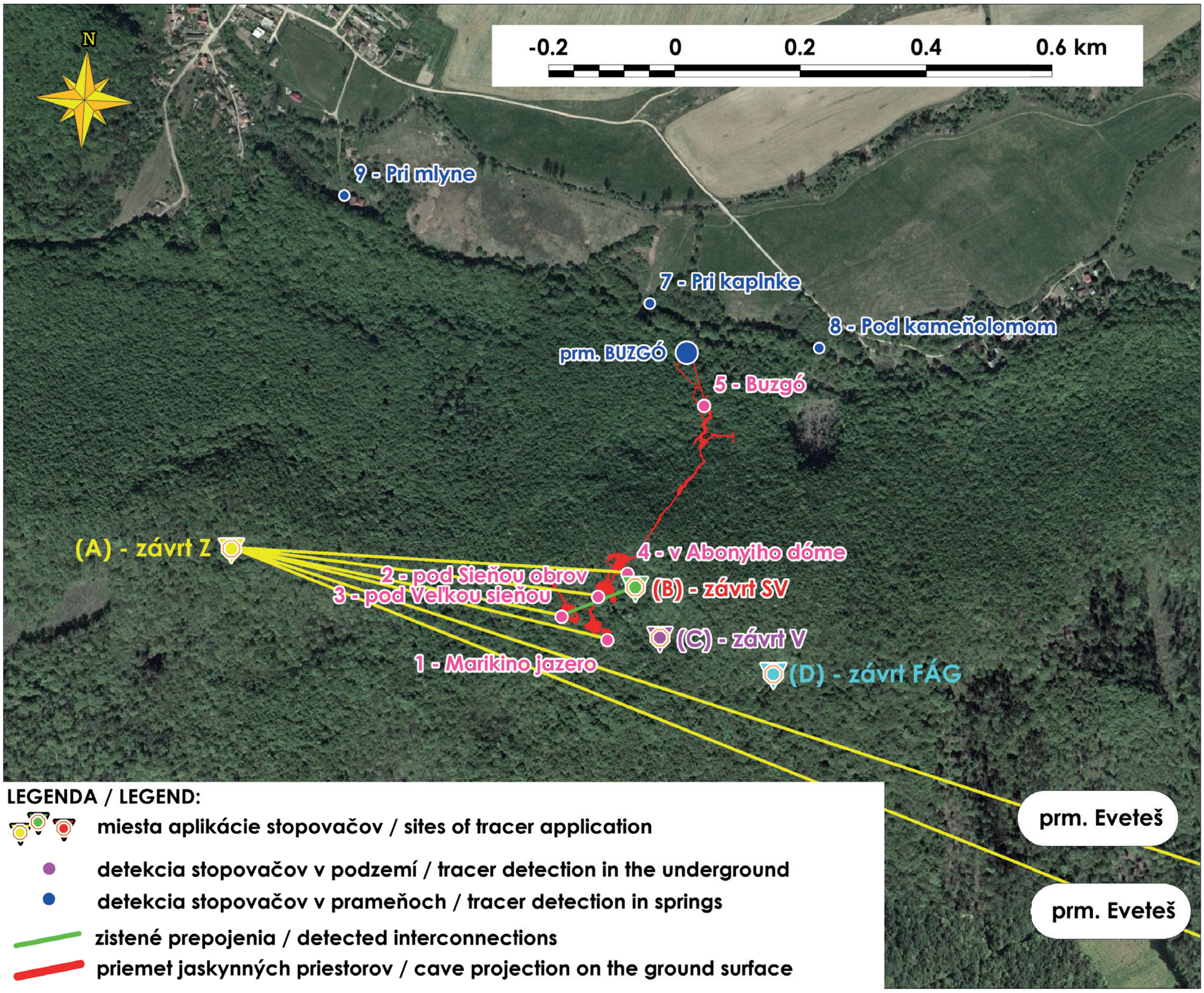

Obr. 11. Výsledky stopovacích skúšok podľa údajov zaznamenaných prietokovými ponornými fluorimetrami GGUN-FL30 – detail bezprostrednej oblasti Krásnohorskej jaskyne.

Fig. 11. Results of tracer tests according to the data recorded by GGUN-FL30 flow-through submergible fluorometers – detail for the nearest area of the Krásnohorská jaskyňa Cave.

Stopovacia látka by sa však zjavne od závrtu (B), kde bola injektovaná, musela šíriť spočiatku južným smerom (mimo oblasti Krásnohorskej jaskyne, kde sa vyskytla len v zanedbateľnej koncentrácii približne v rovnakom čase) a až následne v smere na západ, takže jej rýchlosť by mala byť ešte vyššia.

Vlhkostné pomery v skúmanej oblasti Silickej planiny boli v období realizácie stopovacích skúšok nadnormálne: pre zrážkomernú stanicu SHMÚ 55 180 Silica (505 m n. m.) je charakteristický zrážkový úhrn za mesiac október 57 mm, októbrový zrážkový úhrn v roku 2016 však bol v takmer dvojnásobnej výške, 112 mm. Výrazné tu boli zrážky v dňoch 3. 10. 2016 (28,0 mm), a najmä 21. 10. 2016 (27,2 mm), ktoré prispeli k saturácii pôdy dostatočným množstvom vlahy pred samotnou aplikáciou stopovačov 26. 10. 2016. Mesiac november 2016 so zaznamenaným úhrnom 52,0 mm bol potom vlhkostne priemerný, pretože priemerné novembrové úhrny na stanici Silica dosahujú 52 mm. Väčšina denných úhrnov neprekročila 3,0 mm, s výnimkou dvoch výrazných daždových dní 5. 11. 2016 (18,4 mm) a 6. 11. 2016 (17,8 mm). Je zrejmé, že uvedený zrážkový impulz v tomto období do veľkej miery aktivoval prenos stopovačov, pretože väčšina prvých indikácií stopovačov bola zaznamenaná až po 5. novembri 2016. Naopak, december 2016 s úhrnom 1,3 mm bol v stanici Silica mimoriadne suchý, keďže úhrny tu zvyčajne dosahujú 40 mm. V uvedenom období nedošlo na povrchu Silickej planiny k akumulácii snehových zrážok, a teda ani k ich topeniu. Priemerný zrážkový úhrn v stanici Silica za 44-ročné obdobie 1973 – 2017 je 707 mm.

Výsledky prepojení jednotlivých miest aplikácie a indikácie stopovacích látok sú zhrnuté v tab. 3 až 6, znázornené sú aj na obr. 11 a 12.

Záver

V období na prelome rokov 2016 a 2017 v oblasti východnej časti Silickej planiny v rámci predpokladaného rozsahu podzemného hydrologického systému Krásnohorskej jaskyne sa realizovali štyri stopovacie skúšky na testovanie citlivosti vody Krásnohorskej jaskyne na potenciálnu kontamináciu prítomnú na bezprostredne blízkom povrchu Silickej planiny. Farbiace stopovacie látky boli aplikované do horninového prostredia 26. októbra 2016

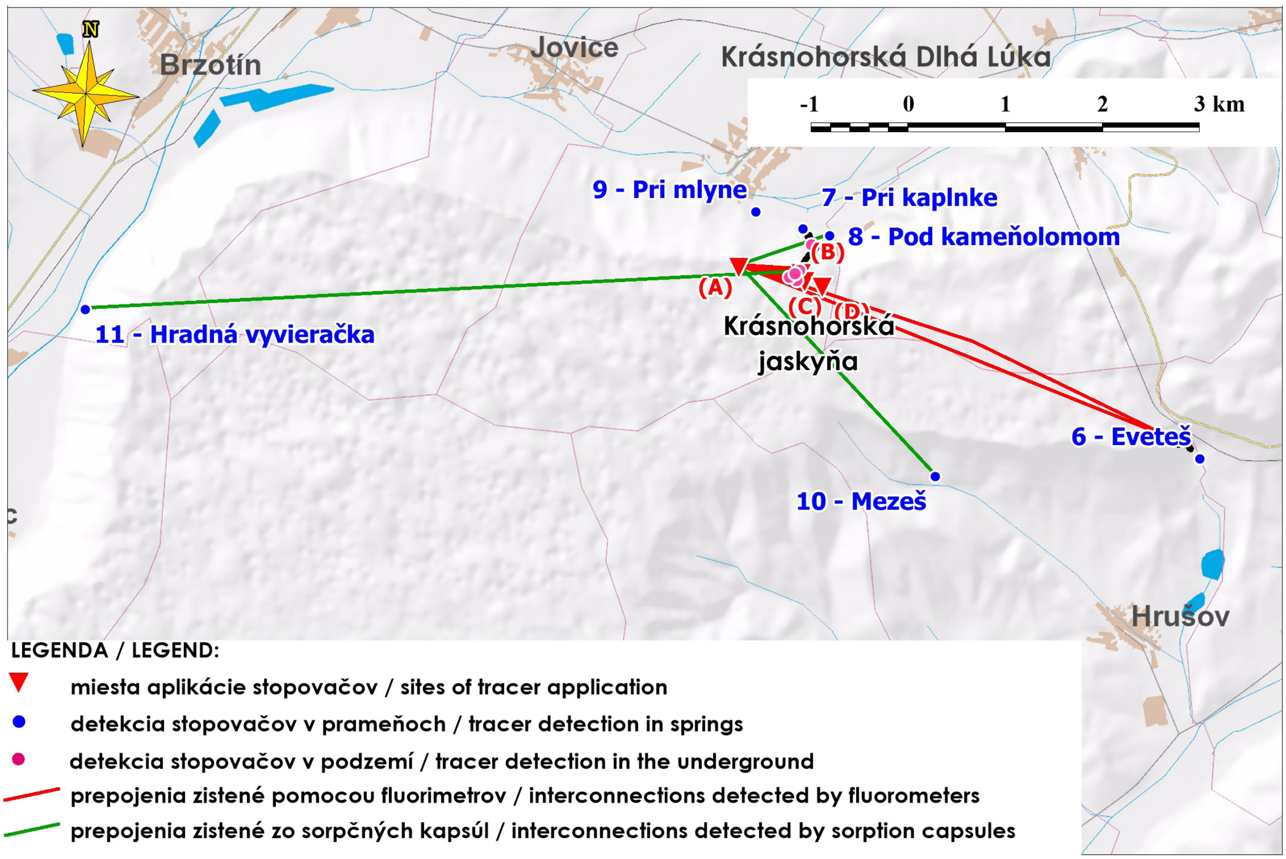

Obr. 12. Výsledky stopovacích skúšok v širšej oblasti Krásnohorskej jaskyne podľa údajov zaznamenaných prietokovými ponornými fluorimetrami GGUN-FL30 a aktívnym uhlím v sorpčných kapsulách.
Fig. 12. Results of tracer tests in the broader area of the Krásnohorská jaskyňa Cave according to the data recorded by GGUN-FL30 flow-through submergible fluorometers and activated carbon in the capsules.

Tab. 4
Počty plakov detegované v jednotlivých vzorkách počas stopovacej skúšky s použitím bakteriofágov H40/1 v závrte (D) vjv. od Marikinho jazera v období 14. 11. 2016 až 11. 04. 2017.

Tab. 4
Presence of plaques detected in individual samples taken in the period 14. 11. 2016 – 11. 04. 2017, during tracer test using H40/1 bacteriophages in the (D) sinkhole ESE from the Marikino jazero Lake.

Dátum	1 – výtok z Marikinho jazera	2 – presakovanie zo Siene obrov	3 – ľavostranný prítok pod Veľkou sieňou od Heliktitového dómu	4 – pravostranný prítok v Abonyiho dóme	5 – prameň Buzgó	6 – prameň Eveteš, VZ (Hrušov)	7 – prameň Pri kaplnke	8 – prameň Pod kameňolomom	9 – prameň Pri mlyne	10 – prameň Mezeš (Hrušov)	11 – prameň Hradná vyvieračka (Brzotín)
14. 11. 2016 14.30	0/0	0/0	0/0	0/0	0/0		0/0	0/0	0/0		
14. 11. 2016 18.00					0/0		0/0	0/0	0/0		
14. 11. 2016 22.15					0/0		0/0	0/0	0/0		
15. 11. 2016 02.15	0/0	0/0	0/0	0/0	0/0		0/0	0/0	0/0		
15. 11. 2016 06.00					0/0		0/0	0/0	0/0		
15. 11. 2016 10.00					0/0		0/0	0/0	0/0		
15. 11. 2016 15.00	0/0	0/0	0/0	0/0	0/0	0/0	0/0	0/0	0/0	0/0	0/0
15. 11. 2016 22.00					0/0		0/0	0/0	0/0		
16. 11. 2016 02.30	0/0	0/0	0/0								
16. 11. 2016 06.15					0/0		0/0	0/0	0/0		
16. 11. 2016 14.00	0/0	0/0	0/0	0/0	0/0	0/0	0/0	0/0	0/0	0/0	0/0
16. 11. 2016 22.20					0/0		0/0	0/0	0/0		
17. 11. 2016 02.15	0/0	0/0	0/0	0/0	0/0	0/0	0/0	0/0	0/0	0/0	0/0
17. 11. 2016 06.15	0/0	0/0	0/0	0/0	0/0	0/0	0/0	0/0	0/0	0/0	0/0
17. 11. 2016 14.00	0/0	0/0	0/0	0/0	0/0	0/0	0/0	0/0	0/0	0/0	0/0
17. 11. 2016 22.15	0/0	0/0	0/0	0/0	0/0	0/0	0/0	0/0	0/0	0/0	0/0
18. 11. 2016 14.00	0/0	0/0	0/0	0/0	0/0	0/0	0/0	0/0	0/0	0/0	0/0
19. 11. 2016 14.00	0/0	0/0	0/0	0/0	0/0	0/0	0/0	0/0	0/0	0/0	0/0
20. 11. 2016 14.00	0/0	0/0	0/0	0/0	0/0	0/0	0/0	0/0	0/0	0/0	0/0
21. 11. 2016 14.00	0/0	0/0	0/0	0/0	0/0	0/0	0/0	0/0	0/0	0/0	0/0
28. 11. 2016 13.00	0/0	0/0	0/0	0/0	0/0	0/0	0/0	0/0	0/0	0/0	0/0
5. 12. 2016 12.00	0/0	0/0	0/0	0/0	0/0	0/0	0/0	0/0	0/0	0/0	0/0
5. 1. 2017 12.00	0/0	0/0	0/0	0/0	0/0	0/0	0/0	0/0	0/0	0/0	0/0
5. 2. 2017 12.00	0/0	0/0	0/0	0/0	0/0	0/0	0/0	0/0	0/0	0/0	0/0
28. 2. 2017 12.00	0/0	0/0	0/0	0/0	0/0	0/0	0/0	0/0	0/0	0/0	0/0
10. 4. 2017 12.00	0/0	0/0	0/0	0/0		0/0			0/0	0/0	0/0
11. 4. 2017 12.00					0/0		0/0	0/0			

Tab. 5
Prítomnosť stopovačov zistená na sorpčnom materiáli v indikačných kapsulách na vybraných miestach, čísla miest detekcie zodpovedajú tab. 2. Detegované farbivá: Ns – naftionát sodný, Fl – fluoresceín.

Tab. 5
Presence of tracers detected on sorption material in indicator capsules at selected detection sites, markings of tracer detection sites correspond to Tab. 2. Detected dye tracers: Ns – sodium naphtionate, Fl – fluorescein.

Dátum	7 – prameň Pri kaplnke	8 – prameň Pod kameňolomom	9 – prameň Pri mlyne	10 – prameň Mezeš (Hrušov)	11 – prameň Hradná vyvieračka (Brzotín)
14. 11. 2016 12.00	– – –	Ns +	– – –	– – –	– – –
16. 11. 2016 12.00	– – –	Ns +	– – –	– – –	– – –
18. 11. 2016 12.00	– – –	Ns +	– – –	– – –	– – –
18. 11. 2016 12.00	– – –	Ns +	– – –	– – –	– – –
21. 11. 2016 12.00	– – –	Ns +	– – –	Ns +	Fl +
28. 11. 2016 12.00	– – –	Ns +	– – –	Ns +	Fl +
5. 12. 2016 12.00	– – –	Ns +	– – –	– – –	– – –
5. 1. 2017 12.00	– – –	Ns +	– – –	– – –	– – –
5. 2. 2017 12.00	– – –	– – –	– – –	– – –	– – –
5. 3. 2017 12.00	– – –	– – –	– – –	– – –	– – –
5. 4. 2017 12.00	– – –	– – –	– – –	– – –	– – –

Pozn.: Intenzita signálu: + veľmi nízka, ++ nízka, +++ stredná, ++++ zvýšená, +++++ vysoká

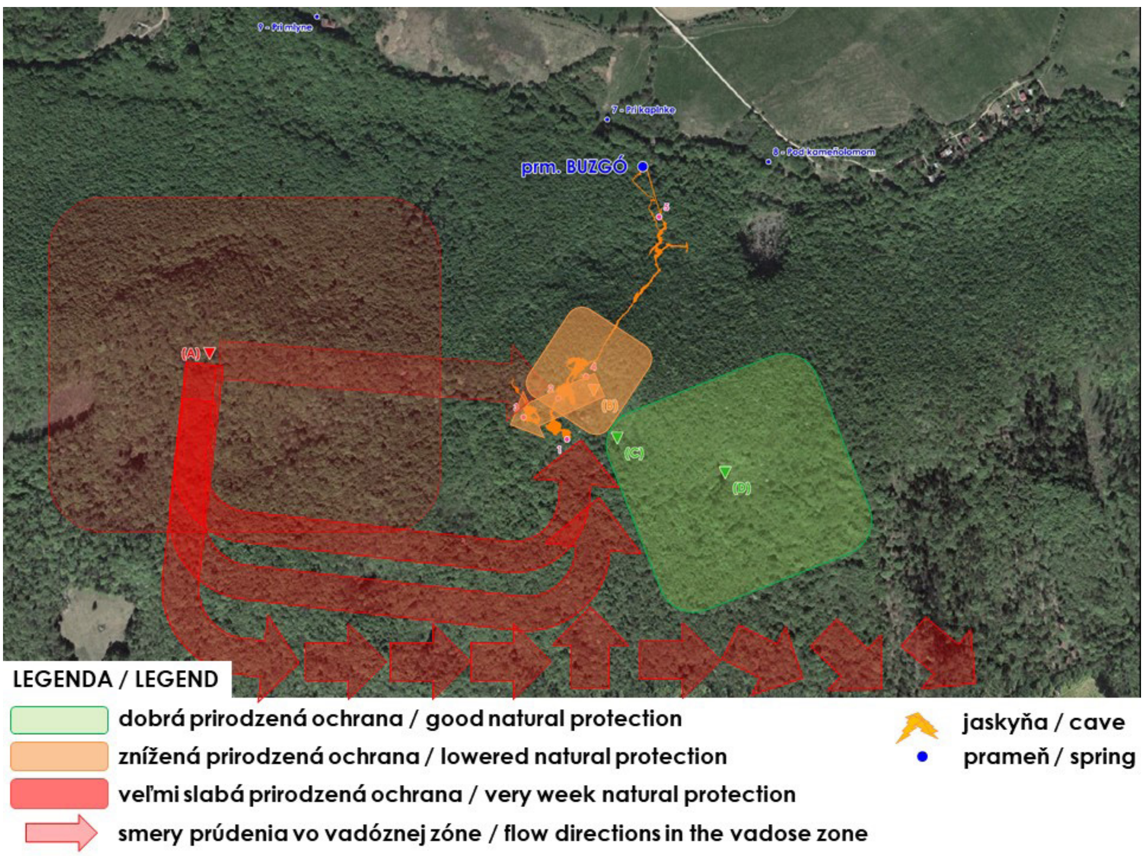

Obr. 13. Prirodzená ochranná funkcia horninového prostredia nad Krásnohorskou jaskyňou.
Fig. 13. Natural protection function of the rock environment above the Krásnohorská jaskyňa Cave.

Tab. 6
Sumarizácia výsledkov stopovacích skúšok podľa záznamov z prietokových fluorimetrov GGUN-FL30, označenia miest aplikácie zodpovedajú tab. 1 a čísla miest detekcie tab. 2.

Tab. 6
Summary of tracer tests results according to data taken from GGUN-FL30 field fluorometers, markings od tracer aplications correspond to Tab. 1 and markings of tracer detection sites correspond to Tab. 2.

Miesto aplikácie stopovača	Miesto indikovania stopovača	Druh stopovača	Vzdialenosť [m]	Maximálna indikovaná koncentrácia stopovača	Čas tranzitu [deň]	Rýchlosť tranzitu koncentračného maxima [m/deň]	Rýchlosť tranzitu koncentračného maxima [cm/s]	Dátum a čas zapustenia stopovača	Dátum a čas prvej indikácie stopovača	Dátum a čas najvyššej koncentrácie stopovača
(A) závrt Z	1 – výtok z Marikinho jazera	naftionát sodný	613	61,82	25,59	23,9	0,028	26. 10. 2016 15.50	6. 11. 2016 16.45	21. 11. 2016 06.00
(A) závrt Z	2 – ľavostranný prítok pod Veľkou sieňou od Heliktitového dómu	naftionát sodný	534	56,30	13,99	38,2	0,044	26. 10. 2016 15.50	8. 11. 2016 17.00	9. 11. 2016 15.30
(A) závrt Z	3 – miesto presakovania zo Siene obrov	naftionát sodný	586	0,68	23,39	25,1	0,029	26. 10. 2016 15.50	7. 11. 2016 02.00	19. 11. 2016 01.15
(A) závrt Z	4 – pravostranný prítok v Abonyiho dóme	naftionát sodný	629	32,96	13,28	47,4	0,055	26. 10. 2016 15.50	8. 11. 2016 00.00	8. 11. 2016 22.30
(A) závrt Z	5 – prameň Buzgó	naftionát sodný	783	166,00	1,59	492,4	0,570	26. 10. 2016 15.50	27. 10. 2016 06.00	28. 10. 2016 06.00
(A) závrt Z	5 – prameň Buzgó	naftionát sodný	783	124,96	7,59	103,2	0,119	26. 10. 2016 15.50	30. 10. 2016 06.00	3. 11. 2016 06.00
(A) závrt Z	5 – prameň Buzgó	naftionát sodný	783	58,30	25,63	30,5	0,035	26. 10. 2016 15.50	6. 11. 2016 17.15	21. 11. 2016 07.00
(A) závrt Z	6 – prameň Eveteš, VZ (Hrušov)	naftionát sodný	4 806	107,73	3,33	1 443,2	1,670	26. 10. 2016 15.50	27. 10. 2016 08.15	29. 10. 2016 23.45
(A) závrt Z	6 – prameň Eveteš, VZ (Hrušov)	naftionát sodný	4 806	121,71	12,11	396,8	0,459	26. 10. 2016 15.50	6. 11. 2016 09.00	7. 11. 2016 18.30
(B) závrt SV	2 – ľavostranný prítok pod Veľkou sieňou od Heliktitového dómu	fluoresceín	126	0,68	36,29	3,5	0,004	26. 10. 2016 10.30	17. 11. 2016 07.15	1. 12. 2016 17.30
(B) závrt SV	4 – pravostranný prítok v Abonyiho dóme	fluoresceín	25	0,24	13,17	1,9	0,002	26. 10. 2016 10.30	6. 11. 2016 19.15	8. 11. 2016 14.30

v troch závrtoch, resp. krasových jamách: (A) závrt západne od vertikálneho priemetu Marikinho jazera na povrch Silickej planiny – naftionát sodný, (B) závrt sv. od Marikinho jazera – fluoresceín, (C) závrt východne od Marikinho jazera – sulforodamín B. Fágová suspenzia bakteriofágov H40/1 sa pre technologické ťažkosti prípravy jej dostatočného množstva a koncentrácie aplikovala až neskôr, a to 14. novembra 2016 do miesta aplikácie (D) – závrtu vjv. od Marikinho jazera. Po aplikácii stopovačov sa realizoval ich monitoring na 11 pozorovacích miestach v trvaní zhruba päť mesiacov. V šiestich prípadoch boli použité poľné prietokové fluorimetre GGUN-FL30 s kontinuálnym meraním koncentrácie použitých farbív a na ostatných miestach indikačné kapsuly so sorpčnou látkou. Na tých istých miestach sa odoberali aj vzorky vody na detekciu bakteriofágov H04/1, ktoré sa následne doručili do Ústavu fyziológie hospodárskych zvierat SAV v Košiciach, kde sa do 24 hodín po doručení spracúvali.

Detekcia stopovacích látok sa vykonávala na 5 miestach vnútri podzemného hydrologického systému Krásnohorskej jaskyne (1 – výtok z Marikinho jazera pod Sifónom potápačov, 2 – miesto presakovania zo Siene obrov, 3 – ľavostranný prítok pod Veľkou sieňou od Heliktitového dómu, 4 – pravostranný prítok v Abonyiho dóme, 5 – celkový odtok vody z Krásnohorskej jaskyne v krasovom prameni Buzgó), kde boli inštalované fluorimetre GGUN-FL30. Tento prístroj bol inštalovaný aj vo vodárensky zachytenom prameni Eveteš nad obcou Hrušov. Na ďalších prameňoch boli inštalované kapsuly so sorpčným materiálom (aktívne uhlie), ktorý sa v pravidelných intervaloch vymieňal a následne analyzoval. Takto bolo sledovaných päť menších prameňov: Pri kaplnke (Krásnohorská Dlhá Lúka), Pod kameňolomom (Krásnohorská Dlhá Lúka), Pri mlyne (Krásnohorská Dlhá Lúka), Hradná vyvieračka (Brzotín) a prameň Mezeš (Hrušov). Posledný z nich sa využíva aj ako vodárenský zdroj pre obec Hrušov.

Počas celého obdobia sledovania nebol zaznamenaný signál stopovacej látky sulforodamín B, aplikovanej v závrte (C) východne od Marikinho jazera. Takisto nebola zaznamenaná prítomnosť bakteriofágov H40/1 aplikovaných do závrtu (D) vjv. od Marikinho jazera ani v jednej z 223 odobraných a analyzovaných vzoriek. Oba závrty sa nachádzajú južne, resp. jv. od Krásnohorskej jaskyne. Predpokladáme, že v týchto miestach poskytuje povrch Silickej planiny pre Krásnohorskú jaskyňu a jej podzemný hydrologický systém vcelku dobrú prirodzenú ochranu pred potenciálne prenikajúcim znečistením.

Výsledky získané po spracovaní sorpčných náplní indikačných kapsúl z aktívneho uhlia preukázali prítomnosť dvoch stopovačov na rozdielnych sledovaných miestach vo veľmi nízkej intenzite. Naftionát sodný, aplikovaný v závrte (A) západne od Marikinho jazera, sa objavil vo vode prameňa Pod kameňolomom (označenie miesta indikácie: 8), ako aj vo vode prameňa Mezeš (10). Fluoresceín aplikovaný do závrtu (B) bol zas detegovaný v dvoch sorpčných náplniach v prameni Hradná vyvieračka (11) pri Brzotíne. Neprítomnosť stopovacích látok sa zistila v prameni Pri kaplnke (7) a prameni Pri mlyne (9). Výsledky získané pomocou sorpčných náplní však treba skôr považovať za indície možných prepojení. Dôvodom je veľmi nízka hladina prítomnosti stopovačov, ktorá sa tu zistila.

Veľmi dobrú charakteristiku spôsobu šírenia stopovacích látok poskytli prietokové fluorimetre GGUN-FL30 švajčiarskeho výrobcu. Zistená nepravá rýchlosť (stanovená podľa vzdušnej vzdialenosti miest aplikácie a indikovania) sa tu pohybovala od 1,9 do 1 443,2 m/deň (0,002 až 1,670 cm/s), čas tranzitu bol od 3,3 do 36,3 dňa s mediánovou hodnotou 13,6 dňa. Miesta indikovania stopovačov boli vzdialené od 25 do 4 806 m vzdušnou čiarou a maximálna indikovaná koncentrácia stopovacej látky sa v individuálnych prípadoch pohybovala od 0,24 do 127,71 ppb.

Najrýchlejšie a zároveň najintenzívnejšie šírenie stopovacej látky sa zistilo v prípade naftionátu sodného, ktorý bol aplikovaný na dne závrtu (A) západne od Krásnohorskej jaskyne. Tento stopovač už v priebehu 1,59 dňa dosiahol Marikino jazero (1), v dôsledku krátkodobého výpadku fluorimetra však bol indikovaný na celkovom výtoku z jaskyne. Na ďalších troch miestach prítokov v jaskyni sa však v rámci tohto prvého a najintenzívnejšieho signálu (166,0 ppb nad prameňom Buzgó; 5) už nezistil. Vzápätí sa v sile 107,73 ppb už po 3,33 dňoch od injektáže objavil naftionát vo vode prameňa Eveteš (6), po 7,59 dňoch opäť v prameni Buzgó (124,96 ppb) a po 12,11 dňoch bolo 7. 11. 2016 o 18.30 zaznamenané maximum druhého signálu aj v prameni Eveteš. Uvedené štyri prípady boli zároveň najintenzívnejším prejavom tohto stopovača, ktorý sa až následne po 13,28 dňoch objavil v pravostrannom prítoku v Abonyiho dóme (4) pri sile signálu 32,96 ppb a po 13,99 dňoch v ľavostrannom prítoku pod Veľkou sieňou (56,30 ppb). Vzhľadom na silu signálu a rýchlosť jeho prenosu je teda potrebné v oblasti medzi závrtom (A) a prameňom Eveteš predpokladať existenciu dvoch vzájomne oddelených, ale v obidvoch prípadoch veľmi aktívnych obehových ciest vo vadóznej zóne pod polohovo relevantným povrchom Silickej planiny. Nepravá rýchlosť prúdenia je tu 1 443,2 m/deň (1,67 cm/s) v prípade predpokladaného „rýchlostne aktívnejšieho kanála“ nenasýtenej zóny a 396,8 m/deň (0,46 cm/s) v prípade druhého „kanála“, pri ktorom zas možno predpokladať nižšiu mieru disperzie a prenos vyššej koncentrácie nielen stopovacích látok, ale aj kontaminantov. Obdobné cesty vo vadóznej zóne možno očakávať aj v smere do oblasti južne od Marikinho jazera (tu možno rátať s nepravou rýchlosťou 385,5 m/deň, čiže 0,45 cm/s a 80,8 m/deň, resp. 0,09 cm/s). Smerom k prítokom pod Veľkou sieňou (2) a v Abonyiho dóme (4) sa potom zjavne dostáva samostatná vetva prúdenia od závrtu (A), ktorá zároveň nezasahuje oblasť nad Marikiným jazerom, ale ani nad Sieňou obrov. Do týchto posledných sa potom dostala ešte tretia „naftionátová“ vlna s posunom 25,59 dňa v Marikinom jazere (1) a 23,39 dňa v prítoku v Sieni obrov (3). Kým signál zaznamenaný pod Sieňou obrov bol len slabučký (0,68 ppb), vo výtoku z Marikinho jazera to bolo až 61,82 ppb. Tento signál už nebol zachytený ani v prameni Eveteš, ani na inom mieste Krásnohorskej jaskyne, s výnimkou odtoku v prameni Buzgó (5). Vo vadóznej zóne medzi oblasťou južne od Marikinho jazera a závrtom (A) zjavne existuje ešte tretia diskrétna cesta potenciálneho šírenia kontaminantu, tentoraz však s vyšším stupňom jeho disperzie (časový rozdiel medzi prvou indikáciou stopovača a jeho maximom tu bol najvyšší, až 14,55 dňa).

V prípade fluoresceínu aplikovaného v závrte (B) nachádzajúcom sa sv. od Marikinho jazera sa fluorimetrami zaznamenala len slabá prítomnosť stopovača, ktorá po 13,17 dňoch zasiahla pravostranný prítok v Abonyiho dóme (4) v sile signálu iba 0,24 ppb a po 36,29 dňoch a s intenzitou 0,68 ppb aj ľavostranný prítok pod Veľkou sieňou (2). Išlo teda len o bezprostredne najbližšie monitorovacie miesta od miesta aplikácie fluoresceínu, pretože na iných miestach podzemného hydrologického systému Krásnohorskej jaskyne nebol tento stopovač detegovaný.

Z nízkych hodnôt zistenej koncentrácie, veľmi dlhého tranzitného času a malej rýchlosti tranzitu vyplýva, že horninové prostredie v oblasti pod závrtom (B) sv. od Marikinho jazera je v smere ku Krásnohorskej jaskyni buď slabo skrasovatené, alebo v dôsledku veľkého objemu vody akumulovanej v epikrasovej zóne poskytuje vcelku dobrú prirodzenú ochranu pred potenciálne prenikajúcim znečistením (obr. 13). Najrizikovejšou oblasťou z hľadiska potenciálneho ohrozenia podzemného hydrologického systému Krásnohorskej jaskyne je oblasť závrtu (A). Z týchto miest možno na základe získaných výsledkov predpokladať rýchle šírenie potenciálnej kontaminácie, a to nielen do Krásnohorskej jaskyne, ale aj krasového prameňa Eveteš nad obcou Hrušov. Pre existenciu vzájomne oddelených krasových obehových ciest vo vadóznej zóne tu zároveň možno očakávať príchod znečistenia vo viacerých vlnách, s rôznou mierou jeho zriedenia v dôsledku jeho rôznej disperzie v horninovom prostredí.

Poďakovanie

Výsledky uvedené v práci boli získané vďaka projektu LIFE+ 11 ENV SK 1023 *Zavedenie trvalo udržateľného využívania podzemnej vody v podzemnom krasovom systéme Krásnohorskej jaskyne* (akronym KRASCAVE), ktorý realizoval Štátny geologický ústav Dionýza Štúra (ŠGÚDŠ) ako koordinujúci projektový partner a OZ ENVI Slovakia ako pridružený projektový partner s podporou finančného nástroja LIFE+ Európskej komisie a príspevku Ministerstva životného prostredia Slovenskej republiky. Spracovanie týchto výsledkov sa mohlo vykonávať ako súčasť projektu aplikovaného výskumu a vývoja s názvom *Výskum zraniteľnosti podzemných vôd pre manažment trvalo udržateľného využívania podzemných vôd v BSK* s ITMS kódom projektu 26240220059, ktorý v rokoch 2010 až 2014 riešil ŠGÚDŠ na základe podpory Agentúry Ministerstva školstva, vedy, výskumu a športu SR pre štrukturálne fondy EÚ (ASFEU, v súčasnosti Výskumná agentúra). Podporujeme výskumné aktivity na Slovensku. Projekt je spolufinancovaný zo zdrojov Európskej únie.

Literatúra / References

Bajtoš, P., Malík, P., Repková, R. & Máša, B., 2017: Geochemické modelovanie tvorby chemického zloženia vody Krásnohorskej jaskyne v Slovenskom krase. *Miner. Slov., 49, 1, 73 – 94.*

Erdös, M., 1995: Jaskyne, priepasti a vyvieračky severnej časti Silickej planiny. *Slov. Kras, 33, 115 – 127.*

Fľaková, R., Gavuliaková, B., Haviarová, D. & Ženišová, Z., 2018: Izotopový výskum krasových vôd Silickej planiny. *Bratislava, Slovenská asociácia hydrogeológov, ISBN 978-80-972651-2-0, 126 s.*

Gavuliaková, B., 2016: Štúdium krasových vôd metódami izotopovej geológie. Dizertačná práca. *Manuskript. Bratislava, Univerzita Komenského v Bratislave, 190 s.*

Gavuliaková, B., Fľaková, R., Ženišová, Z., Haviarová, D. & Grolmusová, Z., 2015: Chemické a izotopové zloženie vôd v systéme Krásnohorskej jaskyne. *Podzemná voda, 21, 2, 118 – 136.*

Gillmann, A., 2007. Etude du comportement des substances particulaires et solubles dans le systeme karstique de la source de la Noiraigue. *Travail de diplôme. Université de Neuchâtel, Centre d'hydrogéologie, 89 s.*

Grenčíková, A., Bučová, J., Gaži, P., Mitter, P., Moravanský, D., Szabó, S., Smoleňák, J., Majerčák, J., Gažúr, J., Lukács, M., Copláková, J., Sklenárová, D., Otruba, M., Heglas, D., Hajčík, J., Šáli, J., Andrisková, O., Vlček, M., Flimmel, J., Komoň, J. & Záhorec, P., 2018: Rýchlostná cesta R2 Rožňava – Jablonov nad Turňou. Záverečná správa, DPP Žilina. *Manuskript. Bratislava, archív Št. Geol. Úst. D. Štúra, 230 s.*

Haviarová, D., 2008: Nové poznatky k hydrografii jaskyne Štefanová (Nízke Tatry, Demänovská dolina). *Aragonit, 13, 2, 20 – 23.*

Haviarová, D., 2014: Smery prúdenia ponorných autochtónnych vôd z bočných krasových doliniek na pravej strane Demänovskej doliny. *Aragonit, 19, 1 – 2, 15 – 20.*

Haviarová, D., 2016: Výsledky nových stopovacích skúšok na lokalite Priepadlá (Važecký kras). *Aragonit, 21, 1 – 2, 22 – 28.*

Haviarová, D. & Pristaš, P., 2008: Najnovšie výsledky stopovacích skúšok z povodia Brestovskej jaskyne. *Slov. Kras, 46, 1, 81 – 86.*

Haviarová, D. & Pristaš, P., 2010: Výsledky nových stopovacích skúšok ponorových jaskýň v Demänovskej doline vo vzťahu k Demänovskej jaskyni slobody. *Aragonit, 15, 2, 76 – 82.*

Haviarová, D. & Pristaš, P., 2013: Riešenie otázky komunikácie povrchových vôd Studeného potoka s podzemným tokom v Brestovskej jaskyni. *Aragonit, 18, 1, 17 – 21.*

Haviarová, D. & Pristaš, P., 2018: Stopovacie skúšky v okolí Ponickej jaskyne (Zvolenská pahorkatina, Ponický kras). *Aragonit, 13, 1 – 2, 3 – 8.*

Haviarová, D., Pristaš, P. & Stankovič, J., 2009a: Nové poznatky o smeroch prúdenia krasových vôd Plešivskej planiny. *Aragonit, 14, 1, 27 – 31.*

Haviarová, D., Tulis, J. & Pristaš, P., 2009b: Nové poznatky k odvodňovaniu jaskynného systému Stratenskej jaskyne. *Slov. Kras, 47, 2, 217 – 230.*

Kallies, R., Kiesel, B., Schmidt, M., Kacza, J., Ghanem, N., Narr, A., Zopfi, J., Wick, L. Y., Hackermüller, J., Harms, H. & Chatzinotas, A., 2017: Complete genome sequence of Pseudoalteromonas phage vB_PspS-H40/1 (formerly H40/1) that infects Pseudoalteromonas sp. strain H40 and is used as biological tracer in hydrological transport studies. *Stand Genomic Sci., 12, 20.*

Kováčová, E., Malík, P., Švasta, J., Bahnová, N., Pažická, A., Bajtoš, P. & Grolmusová, Z., 2017: Priestorové zmeny distribúcie mikroklimatických parametrov počas letného režimu prúdenia vzduchu v Krásnohorskej jaskyni. *Slov. Kras – Acta Carsol. Slov., 55, 1, 81 – 102.*

Kronome, B. & Boorová, D., 2016: Geologická stavba Silickej planiny pri Krásnohorskej Dlhej Lúke. *Geol. Práce, Spr., 129, 55 – 78.*

Malík, P., Gregor, M., Švasta, J. & Haviarová, D., 2011: Interpretácia meraní teploty a mernej elektrickej vodivosti v profile podzemného toku Krásnohorskej jaskyne. *Slov. Kras, 49, 1, 41 – 56.*

Malík, P., Gregor, M., Bottlik, F. & Švasta, J., 2014a: Kvantitatívna charakteristika prirodzených výstupov podzemnej vody v oblasti Krásnohorskej Dlhej Lúky. *In: Fľaková, R. & Ženišová, Z. (red.): Zborník 17. slovenskej hydrogeologickej konferencie Nové výzvy v oblasti ochrany vôd, Piešťany, 14. – 17. 10. 2014. Bratislava, Slovenská asociácia hydrogeológov, 65 – 68.*

Malík, P., Gregor, M., Černák, R., Bottlik, F., Šutarová, B. & Otruba, M., 2014b: Stupeň skrasovatenia horninového prostredia severného okraja Silickej planiny na základe analýzy výtokových čiar. *Podzemná voda, 20, 2, 128 – 141.*

Malík, P., Bahnová, N., Bajtoš, P., Bottlik, F., Gregor, M., Michalko, J., Švasta, J. & Vasilenková, A., 2018: Projekt LIFE+ KRASCAVE. Laická správa. *Bratislava, Št. Geol. Úst. D. Štúra, ISB N 978-80-8174-033-6, 48 s.*

Malík, P., Michalko, J., Pažická, A., Máša, B. & Stankovič, J., 2019: Detailed water quality monitoring at various points of the Krásnohorská Cave system (Slovakia). Chapter 23. *In: Bertrand, C., Denimal, S., Steinmann, M. & Renard, P. (eds.): EuroKarst 2018, Besançon: Advances in Karst Science. Springer, Cham, Switzerland, 199 – 212. DOI: https://doi.org/10.1007/978-3-030-14015-1_23.*

Mello, J. (red.), Elečko, M., Pristaš, J., Reichwalder, P., Snopko, L., Vass, D., Vozárová, A., Gaál, Ľ., Hanzel, V., Hók, J., Kováč, P., Slavkay, M. & Steiner, A., 1996: Geologická mapa Slovenského krasu 1 : 50 000. *Bratislava, Ministerstvo život. prostr. Slovak. rep., GS SR*.

Mello, J. (red.), Elečko, M., Pristaš, J., Reichwalder, P., Snopko, L., Vass, D., Vozárová, A., Gaál, Ľ., Hanzel, V., Hók, J., Kováč, P., Slavkay, M. & Steiner, A.. 1997: Vysvetlivky ku geologickej mape Slovenského krasu 1 : 50 000. *Bratislava, GS SR, Vyd. D. Štúra, 255 s.*

Orvan, J. & Vrábľová, M., 1986: Rožňava – Horný vrch, predbežný hydrogeologický prieskum. *Manuskript. Bratislava, Št. Geol. Úst. D. Štúra, 69 s.*

Pristaš, P., 2017. Záverečná správa o výsledku analýzy výskytu bakteriofága H40/1 vo vzorkách vody počas stopovacej skúšky v priestore Krásnohorskej jaskyne. Záverečná správa. *Manuskript. Bratislava, archív Št. Geol. Úst. D. Štúra, 11 s.*

Pronk, M., Goldscheider, N. & Zopfi, J., 2006a: Dynamics and interaction of organic carbon, turbidity and bacteria in a karst aquifer system. *Hydrogeol. J., 14, 473 – 484.*

Pronk, M., Goldscheider, N. & Zopfi, J., 2006b: Monitoring of organic carbon, natural particles and bacteria in a deep karst system, Yverdon-les-Bains, Switzerland. Proc. 8th Conference on Limestone Hydrogeology, Neuchâtel (Switzerland) 21 – 23 sep. 2006. *Presses universitaires de Franche-Comté, Besançon, France, 215 – 219.*

Roda, Š., 1964: Jaskyňa Buzgó. *Krásy Slovenska, 41, 10, Bratislava, 382 – 386.*

Roda, Š., 1966: Je najvyšší na svete? *Krásy Slovenska, 43, 7, 258 – 259.*

Roda, Š., 1967: Výskum občasného toku „Studňa Rákoťa“ na Silickej planine farbením fluoresceínom. *Zbor. Východoslov. Múz. (Košice), Sér. A, VIII, 69 – 71.*

Roda, Š., Roda, Š., ml. & Ščuka, J., 1986: Aplikácia fraktálnej analýzy na interpretáciu stopovacích skúšok. *Slov. Kras, 24, 61 – 75.*

Skřivánek, F., 1965: Objev jeskyně Buzgó v Jihoslovenském krasu. *Čs. Kras, 16, 139 s.*

Stankovič, J. & Horváth, P., 2004: Jaskyne Slovenského krasu v živote Viliama Rozložníka. *Rožňava, Speleoklub MINOTAURUS, 193 s.*

Stankovič, J., Cílek, V. (red.), Bruthans, J., Cílek, V., Gaál, Ľ., Kovács, Á., Rozložník, M., Stankovič, J., Schmelzová, R., Zeman, O., Kováč, Ľ., Mock, A., Ľuptáčik, P., Hudec, I., Nováková, A., Košel, V. & Fenďa, P., 2005: Krásnohorská jaskyňa Buzgó. *Rožňava, Speleoklub Minotaurus, Region. rozvoj. Agentúra, 150 s.*

Szabó, S., Copláková, J., Soták, J., Majerčák, J., Otruba, M., Moravanský, D., Mitter, P., Gaži, P., Bučová, J., Grenčíková, A. & Malík, P., 2018: Engineering-geological, geotechnical and hydrogeological parameters of the Soroška tunnel rock sequences. *Miner. Slov., 50, 2, 101 – 124.*

Zwahlen, F. (ed.), 2004: Vulnerability and risk mapping for the protection of carbonate (karst) aquifers. COST Action 620 Final Report. *Luxembourg, Office Offic. Publ. Europ. Commun., XVIII, 297 s.*

Survey of protective function of the aeration zone above the Krásnohorská jaskyňa Cave (Silická planina Plateau) using tracing tests

Four tracing tests verifying the pollution sensitivity of water circulation inside the underground hydrological system of the Krásnohorská jaskyňa Cave were performed in the area of the eastern part of the Silická planina Plateau in 2016/2017 (October 2016 – April 2017). Dye tracers of sulphorhodamine B, fluorescein and sodium naphtionate were injected into the pits manually dug in the bottoms of sinkholes / dolines / surface karst depression on the 26th October 2016. The aim of this testing was the verification of the natural protection function of the vadose zone above the cave system. Taking into account the vertical distance of the underground stream in the cave (310 – 315 m a.s.l.) and the levels of the sinkholes' bottoms in the area (500 – 550 m a.s.l.), the thickness of the vadose zone was between 185 and 240 m. Sodium naphtionate was applied in the (A) sinkhole located west of the vertical projection of the Marikino jazero Lake to the Plateau surface, sulphorhodamince B was used in the (B) sinkhole SE of the Marikino jazero Lake and fluorescein was injected into the (C) sinkhole eastwards of the Marikino jazero Lake surface projection. Suspension of H40/1 bacteriophages was applied only 19 days later (on 14th November 2016) into the (D) sinkhole eastwards of the Marikino jazero Lake, due to its slow preparation process and relatively small abundance of bacteriophages in the prepared suspension (2 x 10^8 per 1 mm^3 of suspension). After the injection of these tracers, water monitoring was carried out at 11 observation points for about five months. GGUN-FL30 flow-through filed fluorometers were used in six cases, indication capsules with activated carbon sorbent were used at the remaining monitoring sites. Samples for bacteriophages H40/1 detection were taken at the same locations and subsequently delivered to the Slovak Academy of Sciences Institute of Animal Physiology in Košice, where they were processed within 24 hours after delivery.

Tracer detection was carried out at 5 sites inside the underground hydrological system of the Krásnohorská jaskyňa Cave: 1 – water outlet from the Marikino jazero Lake under the Sifón potápačov (Divers' Siphon); 2 – seepage from the Sieň obrov; 3 – left-hand tributary under the Veľká sieň Hall, from the Heliktitový dóm Dome, 4 – right-hand tributary in the Abonyiho dóm Dome; 5 – total water outflow from the Krásnohorská jaskyňa Cave in the Buzgó karst spring. GGUN-FL30 field flow-through fluorometers were installed here. This device was also installed in the karstic spring of Eveteš above the Hrušov municipality, exploited as drinking water source. Capsules with sorption material (activated carbon) were installed on other springs and exchanged at regular intervals. Five smaller karstic springs were monitored in this way: Pri kaplnke, Pod kameňolomom, Pri mlyne (all three springs located in the Krásnohorská Dlhá Lúka municipality), Hradná vyvieračka (Brzotín) and Mezeš spring (Hrušov). The last one is also used as drinking water supply for the village of Hrušov.

In the whole period of tracing experiment, no response of the sulphorhodamine B dye tracer, applied in the (C) sinkhole, was observed. Also, the presence of bacteriophages H40/1 applied to the (D) sinkhole was not recorded in any of, in neither of the 223 samples. Both sinkholes are located south, respectively southeast of the Krásnohorská jaskyňa Cave. Therefore we can assume that in these places the surface of the Silická planina Plateau provides relatively good natural protection against potential pollution for the Krásnohorská jaskyňa Cave and its underground hydrological system.

The results obtained from activated carbon (charcoal) after processing the sorption fillings of indicator capsules showed the presence of two tracers at different monitored sites at very low intensities. Sodium naphthionate, applied in the sinkhole (A) appeared in the waters of the Pod kameňolomom spring (site marking: 8) as well as in the waters of Mezeš spring (10). Fluorescein applied to the (B) sinkhole was detected in two sorption cartridges in the Hradná vyvieračka spring (11) near Brzotín. The tracers were totally absent in analyses of charcoal taken at Pri kaplnke (7) and Pri Mlyne springs (9). However, the results obtained by activated carbon analyses should rather be considered as indicative of possible interconnections as the signal intensity was mostly very low.

The most reliable results were achieved by continuously measuring flow-trough fluorometers GGUN-FL30 records. The detected apparent velocities (determined by the air distance of the application and indication sites) ranged from 1.9 to 1443.2 m/day (0.002 to 1.670 cm/s), the recorded transit time was from 3.3 to 36.3 days, with median value of 13.6 days. The tracer indication sites were at a direct distance range of 25 to 4,806 m. The maximal indicated tracer concentration in the individual breakthrough curves was ranging from 0.24 ppb to 127.71 ppb (median: 44.63 ppb).

The fastest and most intensive tracer spreading was found for sodium naphthionate, which was applied at the bottom of sink (A). This dye tracer has already reached Marikino jazero Lake (marked as 1) in 1.59 days. Due to a short-term, ten days lasting failure of the fluorimeter at site 1, this peak has been indicated on the total cave discharge (5 – Buzgó monitoring site). As this first strong

(166.0 ppb at Buzgó site, No. 5) and quick peak was not detected in the other three tributary sites in the cave, it has to be directly linked to the main karst water stream appearing at 1 – Marikino jazero Lake monitoring site. However, after 3.33 days of injection, naphthionate appeared in waters of 6 – Eveteš spring, in the peak concentration of 107.73 ppb. After 7.59 days the second naphtionate peak appeared again in 5 – Buzgó spring (124.96 ppb) and after 12.11 days (on November 7, 2016 at 6:30 pm) the second naphtionate peak with higher (121.71 ppb) intensity arrived to the spring of Eveteš (6). These four cases were also the most intense manifestation of the naphtionate dye tracer, which, after 13.28 days, appeared also in the right-hand tributary of the Abonyiho dóm Dome (4) at a peak concentration of 32.96 ppb and after 13.99 days in the left-hand tributary below the Veľká sieň Hall (56.30 ppb). Thus, taking into account the peak concentration and its transmission rate, it is necessary to assume that in the area between the sinkhole (A) and the Eveteš spring the existence of two mutually separated but very active water circulation pathways present in the vadose zone below the relevant surface of the Silická planina Plateau. The apparent flow velocity in this case is 1443.2 m/day (1.67 cm/s) for the anticipated "faster active conduit" of the unsaturated zone and 396.8 m/day (0.46 cm/s) for the second conduit. In the second case, lower dispersion rates and higher concentrations can be expected even in the case of potential contaminants, not just dye tracers.

Similar underground pathways in the vadose zone can also be expected in the area south of Marikino jazero Lake (site 1; fictive velocities of 385.5 m/day or 0.45 cm/s and 80.8 m/day or 0.09 cm/s can be envisaged in two independent unsaturated channels). Towards the tributaries below the Veľká sieň Hall (2) and in the Abonyiho dóm Dome (4), a third separate flow branch from the sinkhole (A) can be expected, which at the same time does not interfere with the area above (south from) the Marikino jazero Lake (1), or over the Sieň obrov site (3). The "third naphthionate" peak wave with a shift of then reached the site 1 of Marikino jazero Lake with time shift of 25.59 days and the Sieň obrov (3) within 23.39 days. While the peak recorded under the Sieň obrov (3) was only weak (0.68 ppb), it was up to 61.82 ppb in the outlet from the Marikino jazero Lake (1), and this peak was no longer recorded either in the Eveteš spring (6) or elsewhere in the Krásnohorská jaskyňa Cave except for the outlet of the whole hydrologic system in the Buzgó spring (6). Obviously, in the vadose zone between the area south of the Marikino jazero Lake and the sinkhole (A) a third discrete path for potential contaminant propagation exists, but with substantially higher degree of its dispersion (the time difference between the first tracer indication and its maximum was 14.55 days).

Only a weak response was detected by two fluorimeters for fluorescein dye tracer applied in the (B) sinkhole. Fluorescein peak of maximal 0.24 ppb concentration after 13.17 days reached the right-hand tributary in the Abonyiho dóm Dome (4), and only after 36.29 days, with an intensity of maximal peak concentration only 0.68 ppb, a left-hand tributary below the Veľká sieň Hall (2). These sites represent the closest monitoring points to the (B) application site, and fluorescein was not detected at other places in the whole underground hydrological system of the Krásnohorská jaskyňa Cave.

Rock environment in the area around the (B) sinkhole northeast of Marikino jazero Lake provides good natural protection against potential pollution propagation (Figure 13), as indicated by low levels of detected concentrations, very long transit times and low apparent velocities of transit. The sinkhole (A) area, on the other hand represents the most risky area in terms of potential threats to the Krásnohorská jaskyňa Cave underground hydrological system. Rapid spreading of potential contamination can be expected from these sites, not only towards the Krásnohorská jaskyňa Cave, but also to the Eveteš karst spring (6; Hrušov municipality). Pollution arrival in several waves, in various degrees of dilution due to its different dispersion in the rock environment can be expected here due to the existence of distinct karst circulation pathways in the vadose zone.

Doručené / Received: 15. 4. 2019
Prijaté na publikovanie / Accepted: 4. 6. 2019

Mineralia Slovaca, Web ISSN 1338-3523, ISSN 0369-2086
51 (2019), 102 – 108, © Authors 2019. CC BY 4.0

Intensification of dehydration processes of lead-zinc concentrates by ultraflocculation

AZAMAT YESSENGAZIYEV[1,2], NESIPBAY TUSSUPBAYEV[1] and SALTANAT BILYALOVA[1]

[1]Institute of Metallurgy and Beneficiation JSC, 29/133 Shevchenko str., 050010, Almaty, Kazakhstan
[2]Satbayev University, 22 Satpayev str., 050000, Almaty, Kazakhstan; esengazyev@yandex.ru

Abstract: The influence of the "UltraflockTester" device on the process of lead-zinc concentrate dehydration was investigated. The results of the comparison of the effectiveness of the flocculating action of various polyacrylamides with respect to the object of the study showed the advantage of a non-ionic copolymer of the "N100" brand in the amount of 21-24 g/t. The optimal dewatering parameters were set: the gradient of the velocity of the medium was 1300–1500 s^{-1}, the filtration rate was 0.44 m/s, the moisture content of the cake was 24 %. The use of ultraflocculation treatment allowed to intensify the processes of thickening the products with a high content of finely dispersed size classes. Obviously, the use of ultraflocculation equipment will significantly reduce the turbidity of the discharge, reduce the delivered dose of flocculant, and improve the filtration properties of the cake. As a result, it significantly increases the productivity and reduces the production costs of the enterprise.

Key words: UltraflockTester, flocculation, flocculants, collective concentrate, thickening, filtration, concentration.

Graphical abstract

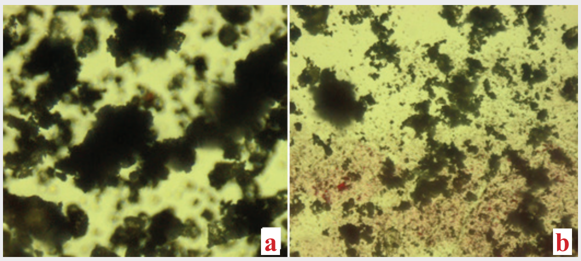

Highlights

- The flocculating ability of copolymers to form aggregates of fine minerals was tested and optimized.
- Optical analysis of two types of non-ionic flocculants shows the advantage of the N100 (a - in Graphical abstract) flocculant over N300 (b).
- The use of ultraflocculation treatment allowed to intensify the processes of thickening products with a high content of fine-grained size classes.

Introduction

In the ore dressing processes of non-ferrous and rare metals, a large number of concentrated technogenic suspensions are formed and they are separated by condensation in radial thickeners. In order to accelerate the process of sedimentation of particles in the dispersed phase, a solution of flocculant is added to the suspension before being fed into the thickener, designed to bind individual particles into relatively large quickly deposited floccules. Since the flocculant molecules, in most cases, are fairly large polymer formations with a molecular weight of about 10-20 million, their transition requires a fairly long time from the initial solution to the suspension, uniform distribution in the dispersion medium and adsorption on the surface of suspended particles.

To reduce significantly the processing time, it is necessary to use the ultraflocculation method, which results not only in the rapid and uniform distribution of flocculant molecules in the suspension and their adsorption on the surface of the particles, but also the formation of large and dense floccules. An important advantage of ultrafloccular processing is that it provides the integration of large and small particles directly in the process of floc formation, i.e. before they enter the thickener, which, in fact, ensures their rapid sedimentation and a high degree of clarification of the aqueous phase.

Typically, the process of thickening the beneficiation products with flocculants occurs in a laminar mode, wherein in order to improve flocculating activity, flocculants must be selected with a high molecular weight and heavily charged macromolecules. The principle of ultraflocculation allows the flocculation to reduce the time by about 100 times and to increase its efficiency. This result is achieved due to the short-term treatment of the suspension in a strongly inhomogeneous hydrodynamic field formed in a cylindrical flocculator.

Due to the need to improve the technical indicators of the processing plants on the background of the complexity of the composition of processed ores, the importance of preparatory operations increases and they accompany the main ore dressing processes.

Various products of beneficiation are subjected to condensation: middlings are condensed to remove the water before their further processing, concentrates - before filtration, and tails - to obtain recycled water and reduce volumes of tailing dumps.

Regarding the above stated principles, in this work we have conducted studies to improve the process of thickening and dehydrating of industrial suspension - a collective concentrate of lead-zinc ore from the Shalkiya deposit using the ultraflocculation method.

Earlier studies related to flocculation

The research by Bauman (2013, 2015) deals with the problem of choosing a radial thickener for mining and processing, metallurgical and other industries. The purpose of the article is to briefly present a methodology for the rapid assessment of the manufacturability of radial thickeners in the design of thickening and water circulation schemes using reagents. The design parameters and the principle of operation of the radial thickener are considered, the features of the thickening process are described by giving the necessary information for the design and selection of the apparatus. The selection criteria are analysed for this type of equipment. Difficulties arising in the selection of radial thickeners for a particular process are described, associated both with the abundance of their names and some terminological uncertainty, and the lack of specific methodologies for evaluating their adaptability. It is noted that the use of coagulants and flocculants in the thickening process requires appropriate approaches to the choice of equipment and technology management.

In Yeremeyev's and Yevmenova's (2006) research, the effect of several anionic flocculants was investigated on the degree of clarification of sludge waters during the thickening of the flotation tailings of coal slimes of two coal preparation plants. A polymer flocculant is proposed, which is effective in settling sludge in both mechanical and column flotation.

The work by Lavrinenko et al. (2012) presents the results of flocculation and flotation of fine particles of pyrrhotite in the presence of a hydrophobic styrene-butadiene copolymer and a partially hydrophobic polyoxyethylene with a molecular weight of 4 million. Polyoxyethylene has a weaker effect on flocculation and flotation of pyrrhotite slurry particles.

On pulps prepared from lead-zinc ores, the process of flocculation of thin slimes of classes was studied by Kapralov et al. (2011). There was determined that the speed of flocculation of solid particles by aluminosilicate flocculant depends on the flow rate, the added flocculant and the amount of slime fraction. It was established that at the optimal amount of flocculant, which provides the highest rate of the thickening process of slime, the added amount is equal to 1.0 mg SiO_2 /g.

The work by Novak et al. (2010) about PF "Raspadskaya" considers on the processing of coal sludge by the method of selective flocculation, describing the technological scheme of processing coal slimes. The efficiency of the process of selective flocculation is shown in comparison with the flotation for coal brand CF at the Raspadskaya coal mine.

In study by Peng et al. (2016) the flotation of bituminous coal with the addition of polyethylene oxide PEO was considered. PEO was found to degrade flotation performance in tap water but significantly improves flotation in sodium hexametaphosphate solution. In vitro sedimentation experiments, floc observation and analysis of zeta potential have shown that sodium hexametaphosphate interferes with the flocculation of kaolinite by enabling the selective flocculation of coal.

The data of comparative studies of industrial flocculants are presented by Nikanorov et al. (2013), including the polyacrylamide and flocculants of the Besfloc brand, aiming to intensify the processes of thickening the flotation slurries of gold-bearing minerals. The possibility of industrial replacement of polyacrylamide (basic reagent) with flocculants of the Besfloc brand (K-4000, K-4020, K-4032, K-4041, K-4043, and K-4045) manufactured in South Korea was considered as they are the closest in activity to the base reagent, as well as the choice of the optimal dosage of each of the flocculants studied for gold in the gold extraction plant of Sovrudnik LLC. The results of optimizing presents the cost of flocculants. A graphical representation of the dynamics of sedimentation of the pulp for various flocculants is given. Besfloc K-4020 in amount of 5 g/t, K-4034, and K-4046 - 3 g/t are recommended for industrial trials.

The experiments by Mandrov et al. (2013) and Moyakhe et al. (2017) show that binary flocculant in the form of a composition similar to block copolymers of partially hydrolyzed polyacrylamide (PAA) and amidoimide polymer (AIP) effectively thickens the carbon-clay dispersions, and can be successfully used for clarification of the process water.

In monograph by Bogdanova & Revnivtseva (eds.; 1983) and Yeremeyev's (2008) work the factors affecting the thickening and the influence of clay particles on the deposition process are described. The process of thickening, proceeding under the action of gravity, is influenced by the mineralogical and granulometric composition of the material, the shape of the particles, the pH of the pulp, the design of the thickener, etc.

Currently, there are many studied methods of intensifying the process of thickening: improvement of the design of equipment for thickening; selection of the optimal type and flow rate of flocculant; systems of stabilization of the quality of raw materials, a.o.

Principles of ultraflocculation

In our studies, in order to intensify the process of condensation of beneficiation products, the so-called ultraflocculation treatment of the investigated suspensions was applied. The ultraflocculation differs from classical flocculation using the modes of hydrodynamic processing of suspensions, where the average shear rate (medium velocity gradient) reaches several thousand revolving seconds. The use of such strongly inhomogeneous hydrodynamic fields allows, within a few seconds, not only to achieve a uniform distribution of macromolecules of the flocculant in the suspension volume and on the surface of flocculent particles, but also to form larger and more compact flakes. In addition, this approach can significantly reduce processing time, as well as flocculant consumption (Rulyov et al., 2005, 2006).

Experimental works and discussion of results

In our work, samples of Kemira brand acrylamide copolymers – non-ionic polyacrylamides (N100, N300) and ionic anionic (A150, A150A) and cationic (C455, C456) types – were used.

Anionic flocculants are copolymers of acrylamide with sodium acrylate with a molecular weight of about $14 \cdot 10^6$ and an anion charge of 53–63 %. The molecular weight of the non-ionic polyacrylamide is also about $14 \cdot 10^6$. Cationic flocculants (copolymers of acrylamide with methyl chloride dimethylamino-propyl-acrylamide) have a molecular weight of about $9 \cdot 10^6$ and cation charge of 27–39 %.

For performing laboratory studies to improve the process of thickening the beneficiation products, suspension samples were prepared from a lead-zinc collective concentrate of the Shalkiya (CCS) deposit.

Tab. 1
Particle size and elemental composition of the bulk concentrate

Size classes, mm	Content %	Material composition	Content %
+0.1	2.24	Zn	4.83
-0.1+0.074	5.15	Pb	16.75
-0.074+0.044	13.46	Fe	6.55
-0.044+0	79.15	SiO_2	34.11
		$S_{общ.}$	15.95
		other	21.81
Total:	100	Total:	100

The granulometric analysis of the bulk concentrate indicates that 79.15 % is represented by a class minus 44 microns. The content of the upper size class plus 0.1 mm is insignificant and amounts to about 2.24 %. It should be noted that due to the significant amount of this class in the sample, the flocculation and sedimentation processes are complicated. In our work, we deliberately chose this type of model suspension, with the intention of testing the actual effectiveness of the ultraflocculation treatment.

At the initial stage of the study, suspensions were prepared from a CCS with a ratio of 150 g per liter of water. For better wettability of the sample, the prepared suspensions were pre-mixed with an overhead stirrer before the ultraflocculation treatment. Also, pre-selected doses and volume of the studied flocculants prepared solutions. Preparation of the flocculant solution took place at a temperature of 60–70 °C on a magnetic stirrer for 1 hour.

As an intensifier of dehydration, we used the original UltraflockTester device (Fig. 1) created by the Ukrainian company "Turboflotservice", including a mini-flocculator, as well as an optoelectronic mechanism for fixing the efficiency of flocculation according to the average floc size and water clarification. By means of this device, it is possible not only to establish the optimal type and dosage of the flocculant but also to fix the optimum mode of hydrodynamic processing of a particular suspension.

Fig. 1. UltraflocTester-2010.

The investigated sample of the suspension and the prepared flocculant solution through the pump on the device continuously passed through the ultraflocculator, in which they were mixed and processed in a hydrodynamic flow for 5 seconds. At the output of the device, the processed sample, passing through the optical sensor, was analysed and the flocculation flow efficiency was determined. The principle of operation of the optical sensor was to recognize fluctuations in the strength of the flow of the sample after processing. Data from the optoelectronic mechanism appeared on the instrument panel in the form of a numerical value (from 1 to 99).

The control panel of UltraflockTester (with a constant pulp consumption of 1 cm^3/s) was able to change the dosage of the flocculant, just by changing the rate of rotation of the rotor of the device it was possible to adjust the intensity of the hydrodynamic processing of the suspension (average gradient of the velocity of the medium was from 150 to 4 000 s^{-1}).

The results of the effectiveness comparison of the flocculating effect of the non-ionic, cationic and anionic polyacrylamides with respect to the lead-zinc collective concentrate showed the advantage of the non-ionic copolymer. Of the study, the most preferred is the flocculant "N-100" of non-ionic type. It was noticeable that the selected flocculant allows obtaining significantly better flocculating effect compared to other used flocculants. The applied flocculant N300 of non-ionic type and the flocculant C496 of cationic origin are equally effective with respect to the sample. Cationic flocculant C458 showed weak activity, at the same time, the anionic flocculants A150 and A150A did not have a flocculating effect on the sample under study. It is worth noting that the object of laboratory research were mainly sulfides of lead, zinc, iron and rock-forming mineral components. Obviously, the non-ionic flocculant N100 has a higher molecular weight and a suitable molecular structure for the flocculation of the pulp under study.

According to the data of the laboratory experiment on ultrafloccular processing of the sample, graphic dependences of the flocculation efficiency on their consumption were constructed (Fig. 2).

The optimum consumption of the most effectively used reagents flocculant "N100" was 21–24 g/t. Other flocculants at the same dosage showed lower productivity. At this expense, the high purity of the plums and the highest density of the condensed product were ensured. The increase in flocculant consumption led to a decrease in density, which is explained by the formation of very large floccules, which formed very porous and friable sediment. The results of the study showed that the consumption of the reagent 21–24 g/t is optimal and allows to get the highest density of the condensed material.

During comparative laboratory testing, the sedimentation properties (Fig. 3) of the samples after ultrafloccular processing were also assessed. Testing to determine the deposition rate was carried out in a 250 ml cylinder. Samples treated with various flocculants with added amount of 24 g/t were selected for experiments in cylinders. Due to the worst efficiency in relation to the pulp from the collective concentrate, anionic flocculants A150 and A150A were not used in these experiments. During the tests in the cylinders, the flocculant "N100" also showed the best results in the sedimentation rate and purity of the drain. Based on measurements of the particle deposition rate, deposition curves were plotted, shown in Fig. 3, allowing selecting the preferred type of flocculant.

As noted above, the main feature of the used apparatus was the ability to process the sample in the hydrodynamic model. From the obtained data, a graph of the dependence of the flocculation efficiency of the suspension on the velocity gradient of the medium was constructed (Fig. 4). It was determined that for a CCS suspension, the concentration of which is 24 g/l, the optimum value of the velocity gradient of the medium lies in the range of 1300–1500 s^{-1}.

The condensed product was filtered on a Buchner funnel using a vacuum pump at a vacuum of 0.02 MPa and the duration of the process was recorded.

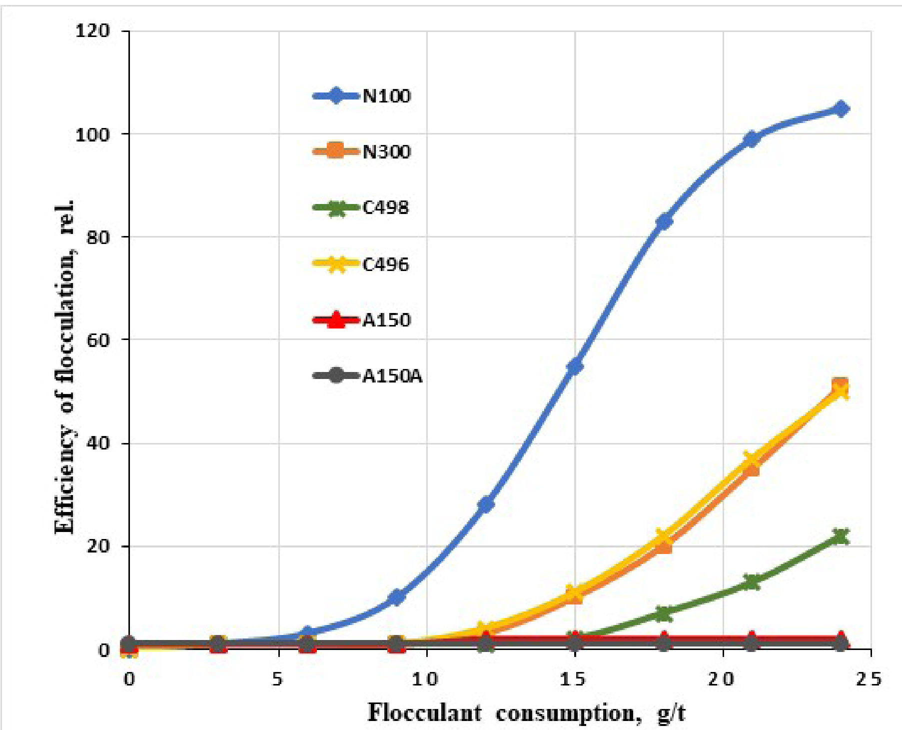

Fig. 2. Dependence of the efficiency of ultrafloccular treatment on the flocculant consumption: suspension concentration 150 g/l; medium velocity gradient – 1500 s^{-1}; processing time – 5 s.

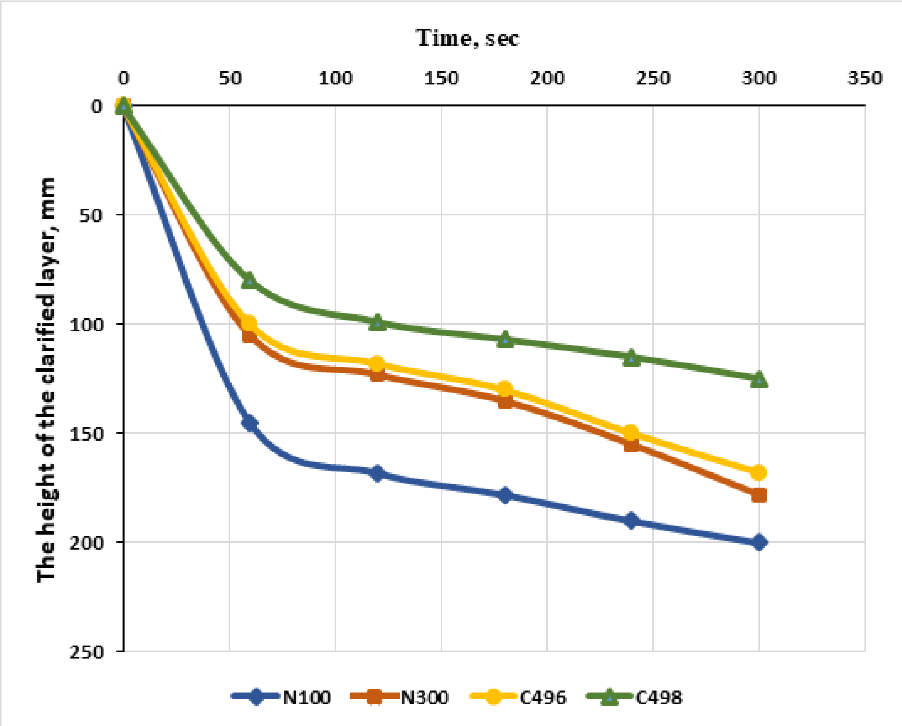

Fig. 3. Dependences of the time of pulp deposition after ultrafloccular processing.

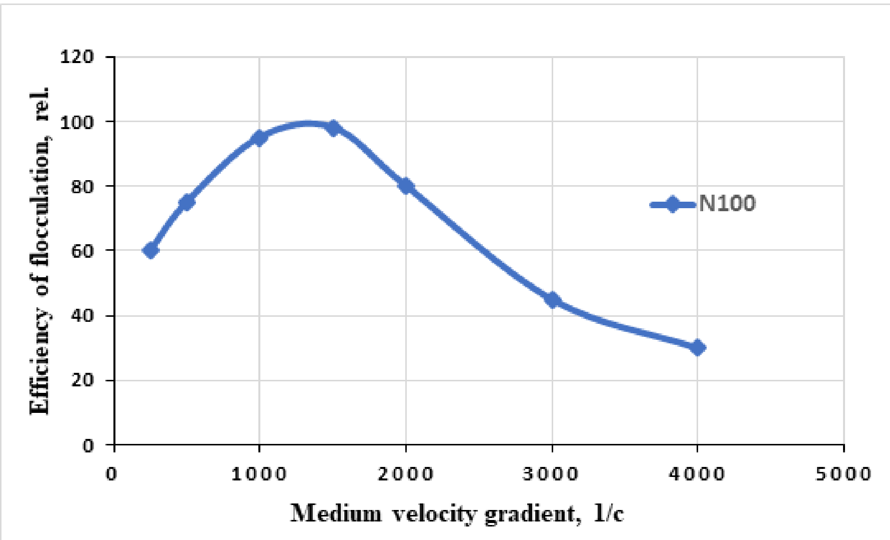

Fig. 4. Dependence of the efficiency of ultrafloccular treatment on the velocity gradient of the medium: suspension concentration 150 g/l; processing time - 5s; flocculant "N100"; flocculant consumption 24 g/t.

Fig. 5. Micrographs of CCS suspension after treatment with N100 (a) and N300 (b).

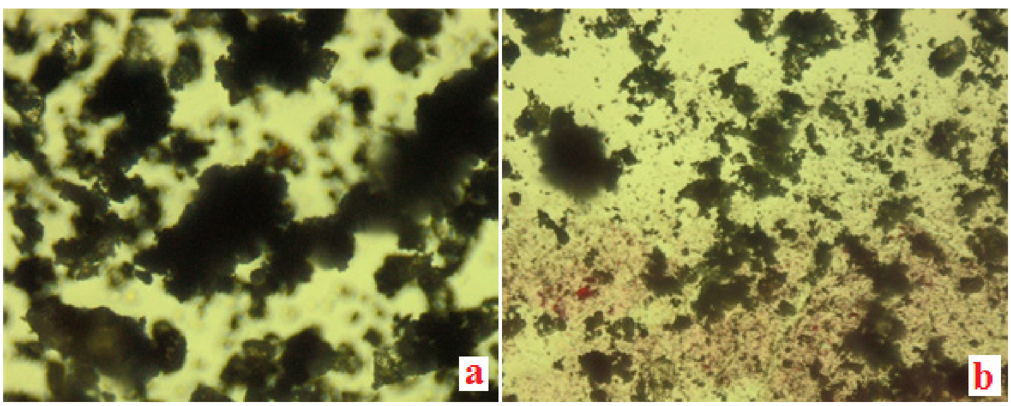

The filtration rate can be represented as the volume of filtrate that passes per unit of time through a unit of filter surface:

$$W = \frac{dV}{Sd\tau}$$

where W – filtration rate, m/s; V – filtrate volume, m³, S – filtration area, m², τ – filtration time, s.

At the end of filtration, the cake was weighted and dried, after which it was weighted again, the humidity of the cake was determined by the difference in weight before after drying:

$$T = \frac{q_1 - q_2}{q_1} \cdot 100$$

where q_1 and q_2 represent the mass of wet and dry cake, g.

Tab. 2
Indicators of thickening and dewatering of the pulps after ultraflocking.

Flocculant	Flocculant consumption, g/t	Flocculation efficiency	Filtration rate, m/s	The moisture content of the filtered cake, %
A150	24	2	0.331741	28.14371
A150A	24	1	0.331741	27.54491
C496	24	50	0.398089	24.8503
C498	24	22	0.361899	24.73054
N100	24	105	0.442321	23.9521
N300	24	51	0.408297	24.01198

Samples of the suspension after treatment with flocculants N100 and N300 were examined in transmitted light on an Olympus microscope at 40x magnification and photographed. Comparison of the photographs of the samples (Fig. 5), with an enlargement of the particles of the concentrate, allows to evaluate the effectiveness of the flocculating effect of two samples of flocculants.

Conclusion

The pulp from lead-zinc bulk concentrate studied in operation contains difficultly precipitated small and dissimilar fractions. In turn, these factors complicate the process of dehydration of this pulp.

As our research revealed, with the selected flocculant N100, after ultrafloccular processing, the following optimal parameters of thickening and dehydrating the industrial CCS suspension were obtained:

- Flocculant consumption 21–24 g/t
- The velocity gradient of the medium 1 300–1 500 s^{-1}
- Filtration speed 0.44 m/s
- The humidity of the filtered cake 24 %.

The use of ultraflocculation treatment allowed to intensify significantly the processes of thickening products with a high content of fine-grained size classes. Obviously, the use of ultraflocculation equipment will significantly reduce the turbidity of the discharge, reduce the delivered dose of flocculant, and improve the filtration properties of the cake. As a result, it significantly increases the productivity and reduces the production costs of the enterprise.

Acknowledgement

Authors express their thanks to Ľubomír Tuček (Slovakia) and two other anonymous reviewers, who increased the quality of original manuscript.

References

Bauman, A. V., 2013: Kriterii vybora radial'nogo sgustitelya dlya protsessov sgushcheniya i vodooborota. *Obogashch. rud, 4, 40 – 43.*

Bauman, A. V., 2015: Sgushhenie i vodooborot na predpriyatiyax cvetnoj metallurgii. *Sbornik dokladov VII Mezhdunarodnogo Kongressa «Cvetnye metally i mineraly», 791 – 795.*

Bogdanova, O. S. & Revnivtseva, V. I. (eds.), 1983: Spetsial'nyye i vspomogatel'nyye protsessy, ispytaniya obogatimosti, kontrol' i avtomatika. *Spravochnik po obogashcheniyu rud.* 2-ye izd., pererab. i dop. *Nedra,1 – 376.*

Kapralov, V. I., Telkov, Sh. A. & Almagambetova, S. T., 2011: Ispol'zovaniye alyumosilikatnogo flokulyanta v protsessakh obesshlamlivaniya tonkovkraplennykh svintsovo-tsinkovykh rud Kazakhstana. *Vest. Kaz. NU, 4, 133 – 136.*

Lavrinenko, A. A., Glukhova, N. I. & Lapin, Ye. V., 2012: Primeneniye flokulyantov dlya intensifikatsii flotatsii tonkikh chastits pirrotina. *Gornyy informatsionno-analiticheskiy byull.*, *9, 167 – 170.*

Moyakhe, D. M., Campbell, Q. P. & Fosso-Kankeu, E., 2017: The effect of flocculant type on settling properties of fine coal tailings. *9th Inter. Conference on Advances in Science, Engineering, Technology & Waste Management*, *105 – 108.*

Novak, V. I., Dolmatov, V. I. & Kozlov, V. A., 2010: Selektivnaya flokulyatsiya ugol'nogo shlama na OF «Raspadskaya». *Gornyy informatsionno-analiticheskiy byull. (nauchno--tekhn. zhurnal), 5, 48 – 51.*

Nikanorov, A. V. Mineyeva, T. S. & Fedorov, S. N., 2013: Sravnitelnye issledovania promyslennych flokuljantov. *Sovremennyye problemy nauki i obrazovaniya. 1, 1 – 7.*

Mandrov, G. A., Klishin, V. I. & Patrakov, Y. F., 2013: Sedimentation of coal-clay dispersions with a binary polymeric flocculant (short communication). *Solid Fuel Chem.*, *47, 1, 56 – 58.*

Peng, Y., Liang, L. & Xia, W., 2016: Coal flotation improvement through hydrophobic flocculation induced by polyethylene oxide. *XVIII International Coal Preparation Congress*, *1 003 – 1 008*.

Rulyov, N. N., Korolyov, B. Y. & Kovalchuk, N. M., 2006: Application of ultraflocculation for improving fine coal concentrate dewatering. *Coal Prepar.*, *26, 1, 17 – 32*.

Rulyov, N. N., Dontsova, T. A. & Korolyov, V. J., 2005: Ultra-flocculation of diluted fine disperse suspensions. *Mineral Process. Extractive Metallurgy Rev.*, *26, 1, 203 – 217*.

Yeremeyev, D. N., 2012: Osvetleniye shlamovykh vod i sgushcheniye otkhodov flotatsii ugol'nykh shlamov s primeneniyem polimernykh flokulyantov. *Voda: khimiya i ekologiya*, *2, 63 – 66*.

Yevmenova, G. L., 2006: Kompleksnoye ispol'zovaniye flokulyantov dlya ochistki shlamovykh vod ugleobogashcheniya. *Vest. Kuzbas. gosud. tekhn. univ.*, *53 – 57*.

Intenzifikácia dehydratačných procesov v oloveno-zinkových koncentrátoch ultraflokuláciou

Článok prezentuje výsledky výskumu zameraného na zlepšenie procesu zahusťovania a dehydratácie priemyselnej suspenzie – koncentrátu oloveno-zinkovej rudy – v prípadovej štúdii z ložiska Šalkija v Kazachstane (*Shalkiya deposit*) s využitím metódy ultraflokulácie.

Ultraflokulácia sa líši od klasickej flokulácie hydrodynamickým pôsobením na suspenziu, pričom rotácia miešadla dosahuje až niekoľko tisíc otáčok za sekundu. Umožňuje to už v priebehu niekoľkých sekúnd dosiahnuť rovnomerné rozdelenie makromolekúl vločkovacieho činidla v rámci celého objemu suspenzie, a tiež aj na povrchu rozptýlených častíc v suspenzii. Vedie to k vytvoreniu väčších a kompaktnejších vločiek (obr. 5). Použitie ultraflokulácie prispieva k skráteniu flokulačného procesu a zníženiu spotreby flokulantu (Rulyov et al., 2005, 2006).

Účinnosť rôznych flokulačných činidiel v procese dehydratácie koncentrátu olova a zinku bola skúmaná využitím zariadenia UltraflockTester (obr. 1 – 4). Najlepšie výsledky boli dosiahnuté neiónovým kopolymérom N100 pri dávkovaní 21 – 24 g/t. Pri aplikovaní ďalších optimalizovaných parametrov dehydratácie – rýchlosti otáčok miešadla 1 300 – 1 500/s a rýchlosti filtrácie 0,44 m/s – bol dosiahnutý obsah vlhkosti vo filtračnom koláči 24 %.

Použitie metodiky ultraflokulácie umožnilo zintenzívniť procesy zahusťovania produktov s vysokým obsahom jemne rozptýlených častíc rôznych veľkostných tried. Je zrejmé, že aplikácia ultraflokulácie významne zníži zakalenie výtoku, zníži potrebnú dávku flokulantu a zlepší vlastnosti filtračného koláča. Prispeje to k zvýšeniu produktivity extrakcie úžitkových zložiek z rôznych roztokov a v konečnom dôsledku k zníženiu finančných nákladov na technologický proces.

Doručené / Received: 22. 5. 2019
Prijaté na publikovanie / Accepted: 4. 6. 2019

Inštrukcie autorom

Etika publikovania, záväzná pri publikovaní v časopise Mineralia Slovaca: *www.geology.sk/mineralia* položka *Publikačná etika*

1. Geovedný časopis Mineralia Slovaca publikuje scientometricky hodnotné recenzované pôvodné vedecké články s vysokým citačným potenciálom. V úvode príspevku musí autor jasne deklarovať, čím konkrétnym je jeho príspevok prínosný pre rozvoj geovied. Rešeršné štúdie sa publikujú len ojedinele.

2. Články na publikovanie (manuskripty) sa do redakcie zasielajú poštou (dva vytlačené exempláre a CD so všetkými súbormi v editovateľnej podobe) alebo e-mailom (editovateľné súbory a kompletná verzia vo formáte PDF).

3. Súčasne s článkom je potrebné redakcii poslať autorské vyhlásenie o originalite textu a obrázkov. Kópie obrázkov z iných publikácií musia byť legalizované získaním práva na publikovanie. Vyhlásenie musí obsahovať meno autora (autorov), akademický titul a trvalé bydlisko.

4. Rozsah manuskriptu na publikovanie je najviac 25 rukopisných strán (MS Word, Times New Roman, veľkosť písmen 12 bodov, riadkovanie 1,5) vrátane literatúry, obrázkov a vysvetliviek. V prípade veľkého odborného prínosu sú v ojedinelých prípadoch povolené aj dlhšie články.

5. Články sú publikované v angličtine alebo v slovenčine. Články v slovenčine musia obsahovať anglický preklad názvu, abstraktu, kľúčových slov, resumé a popisov k obrázkom a tabuľkám. Články písané v angličtine musia obsahovať slovenské resumé.

Text

1. Abstrakt stručne sumarizuje článok. Môže mať najviac 200 slov a nemá obsahovať citácie. Počet kľúčových slov je maximálne 6. Text má mať úvod, charakteristiku (stav) skúmaného problému, použitú metodiku, nové zistenia, ich interpretáciu, diskusiu, záver a zoznam literatúry. Východiskové údaje musia byť zreteľne odlíšené od interpretácií. V texte musia byť odvolávky na všetky použité obrázky a tabuľky.

2. Hierarchiu nadpisov v texte je potrebné vyznačiť ceruzkou na ľavom okraji strany manuskriptu: 1 – najvyššia, 2 – nižšia, 3 – najnižšia.

3. V texte sa uprednostňuje citácia v zátvorke, napr. (Dubčák, 1987; Hrubý et al., 1988), pred formou ... podľa Dubčáka (1987).

4. Pozícia obrázkov a tabuliek v texte sa označí. Nie je vhodné, aby text v editore MS Word obsahoval vložené obrázky, ale náhľadová verzia v pdf ich má obsahovať.

5. Grécke písmená treba identifikovať na ľavom okraji slovom (napr. sigma). Potrebné je odlišovať pomlčku od spojovníka. Symboly, matematické značky, názvy skamenelín a pod., ktoré sa majú vysádzať kurzívou, autor v rukopise podčiarkne vlnovkou.

Obrázky a tabuľky

1. Ilustrácie a tabuľky vysokej kvality bývajú publikované buď **na šírku stĺpca (81 mm), alebo strany (170 mm).** Optimálna veľkosť písma a čísiel v publikovaných obrázkoch je 2 mm. Články v slovenčine musia mať popisy v obrázkoch a tabuľkách v slovenčine, záhlavie tabuliek a texty pod obrázkami a tabuľkami sú v slovenčine a angličtine. Články v angličtine majú všetky texty v angličtine. **Maximálny rozmer ilustrácie a tabuľky vytlačený v časopise je 170 x 230 mm.** Väčšie (skladané) ilustrácie sú publikované len v ojedinelých prípadoch.

2. Pri počítačovej tvorbe obrázkov odporúčame používať programy s vektorovým zobrazením (Corel Draw, Adobe Illustrator a pod.). Čiary tzv. vlasovej hrúbky, softvérová alebo rastrová výplň plôch (napr. v Corel Draw) nie sú prípustné. Výplne v obrázkoch musia pozostávať zo samostatne vysádzaných objektov.

3. Ilustrácie vrátane fotografií musia obsahovať **grafickú mierku** v centimetrovej či metrovej škále, prípadne sa rozmer zobrazených objektov vyjadrí v popise obrázka. Mapy a profily musia mať aj **azimutálnu orientáciu** a jednotné vysvetlivky, ktoré sa uvedú pri prvom obrázku. Zoskupené obrázky, napr. fotografie a diagramy, sa uvádzajú ako jeden obrázok s jednotlivými časťami označenými písmenami (a, b, c atď.).

4. Pri zasielaní fotografií vo forme počítačových súborov (formáty JPG alebo TIF) sa požaduje rozlíšenie minimálne 600 DPI. Publikovanie farebných ilustrácií môže byť spoplatnené.

Literatúra

1. Minimálne 50 % citácií musí reprezentovať publikácie od roku 2000. V zozname literatúry sa v abecednom poradí uvádza len literatúra citovaná v danom článku.

2. Spôsob uvádzania literatúry v zozname literatúry

Knižná publikácia: Gazda, L. & Čech, M., 1988: Paleozoikum medzevského príkrovu. *Bratislava, Alfa, 155 s.*

Časopis: Vrba, P., 1989: Strižné zóny v metapelitoch. *Miner. Slov., 21, 135 – 142.*

Zborník: Návesný, D., 1987: Vysokodraselné ryolity. *In: Romanov, V. (ed.): Stratiformné ložiská gemerika. Špec. publ. Košice, Slov. geol. spol., 203 – 215.*

Manuskript: Radvanský, F., Slivka, B., Viktor, J. & Srnka, T., 1985: Žilné ložiská jedľoveckého príkrovu gemerika. Záverečná správa z úlohy SGR-geofyzika. *Manuskript. Spišská Nová Ves, archív Št. Geol. Úst. D. Štúra, 28 s.*

3. Pri článku viac ako dvoch autorov sa v texte cituje iba prvý autor s dodatkom et al., ale v zozname literatúry sa uvádzajú všetci.

Instructions to authors

Publication ethics, being obligatory for publishing in the journal Mineralia Slovaca: *www.geology.sk/mineralia* item *Publication ethics*

1. Geoscientific journal Mineralia Slovaca publishes scientometrically valuable original peer-reviewed scientific articles with a high citation potential. In the introduction of each article the author(s) must clearly declare, which innovative data the paper brings for the development of geosciences. The retrieval studies are published only exceptionally.

2. The articles for publishing (manuscripts) must be sent to Editorial Office by post (two printed copies and CD with editable files), or by e-mail (editable files plus complete preview version in PDF format).

3. Simultaneously with the article the Editorial Office must receive the author´s proclamation that no part of the manuscript was already published and figures and tables are original as well. Copied illustrations from other publications must contain a copyright.

4. The extent of the manuscript for publishing is limited to 25 manuscript pages (MS Word, 12 points Times New Roman, line spacing 1.5) including figures, tables, explanations and references. In the case of contribution with a high scientific value, the longer manuscripts for publishing are exceptionally permitted.

5. Articles can be published in Slovak or English languages. The title, abstract, key words, shortened text (resumé), as well as description to figures and tables in Slovak articles are published also in English. Articles published in English contain Slovak resumé.

Text

1. Abstract briefly summarizing the article is limited to 200 words, no references are allowed. The maximum number of key words is 6. Text of the article has to contain the introduction, characterization (state) of investigated problem, applied methodology, obtained new data, discussion, conclusion and references. The obtained data must be distinctly separated from interpretations. All applied figures and tables must be referred in the text.

2. The hierarchy of headings in the manuscript must be indicated by a pencil note: 1 – highest level, 2 – lower, 3 – lowermost level.

3. The references in the text prefer parentheses, e.g. (Dubčák, 1987; Hrubý et al., 1988). The form "according to Dubčák (1987)" should be used only exceptionally.

4. Position of figures and tables must be indicated in the manuscript. Editable text of manuscript sent to editorial office must be without figures and tables, though the preview PDF has to contain them in a correct position.

5. Greek letter in the text must be identified at the left margin of the text (e.g. sigma). The text should strictly distinguish the dash from hyphen. Symbols, mathematic signs, names of fossils, etc., which should be printed in italics, must be underlined by the wavy line in the manuscript.

Figures and tables

1. The high quality figures and tables can be published either in **maximum width of column (81 mm) or page (170 mm).** The optimum size of letters and numbers in the camera-ready figure is 2 mm. Articles published in Slovak contain the Slovak descriptions in figures and tables, the tables headings and descriptions beneath figures and tables are in Slovak and English. English articles contain all texts in English. **Maximum dimension of figures and tables in the journal is 170 x 230 mm. Larger (fanfolded)** illustrations are published only exceptionally.

2. For figures drawing the editorial office recommends the vector graphics editors (Corel Draw, Adobe Illustrator, etc.). The very thin lines (hair lines), the pre-defined software or raster fillings of polygons (e.g. in Corel Draw) are not allowed. The filling must consist from separately set objects.

3. Each illustration including photographs must contain graphic (metric) scale, eventually the dimensions of visualized objects have to be stated in the describing text to figure. Maps and profiles must contain also the azimuth orientation, their detail explanations are stated at the first figure. Grouped figures, e.g. photographs and diagrams, are compiled as one figure with separate parts designated by letters (a, b, c, etc.).

4. The photographs sent as JPG of TIF files are required for having minimum 600 DPI resolution. Publishing of colour illustrations can be charged by a fee.

References

1. Minimum 50 % of referred works must represent contemporary publications after 2000. The references in alphanumeric order encompass only literature cited in the article.

2. Examples of referring:

Book: Gazda, L. & Čech, M., 1988: Paleozoic of the Medzev nappe. *Bratislava, Alfa, 155 p.*

Journal: Vrba, P., 1989: Shear zones in the metapelite complexes. *Miner. Slov., 21, 135–142.*

Anniversary volume: Návesný, D., 1987: High-potassium rhyolites. *In: Romanov, V. (ed.): Stratiform deposits of Gemericum. Spec. publ. Košice, Slov. geol. soc., 203–215.*

Manuscript: Radvanský, F., Slivka, B., Viktor, J. & Srnka, T., 1985: Vein deposits of the Jedľovec nappe of Gemericum. Final report from the project SGR-geophysics. *Manuscript. Spišská Nová Ves, Archive Št. Geol. Úst. D. Štúra, 28 p.*

3. The article with more than two authors is referred by the name of the first author with the amendment et al., but the list of references contains names of all authors.

Ďalšie informácie/Further information: mineralia.slovaca@geology.sk; zoltan.nemeth@geology.sk

OBSAH – CONTENT

Indexed / Abstracted / Accessed by SCOPUS and EBSCO
Indexované / abstraktované / sprístupňované databázami SCOPUS a EBSCO

www.geology.sk/mineralia